Canadian Journal of
pure&applied
sciences
an International Journal

The Canadian Journal of Pure and Applied Sciences (CJPAS-ISSN 1715-9997) is a peer reviewed multi-disciplinary specialist journal aimed at promoting research worldwide in Agricultural Sciences, Biological Sciences, Chemical Sciences, Computer and Mathematical Sciences, Engineering, Environmental Sciences, Medicine and Physics (all subjects).

Every effort is made by the editors, board of editorial advisors and publishers to see that no inaccurate or misleading data, opinions, or statements appear in this journal, they wish to make clear that data and opinions appearing in the articles are the sole responsibility of the contributor concerned. The CJPAS accept no responsibility for the misleading data, opinion or statements.

CJPAS is indexed by: Ulrich's Periodicals Directory, Scirus, CiteSeerX, Index Copernicus, Google Scholar, Yahoo, CABI, Chemical Abstracts, Zoological Records, Biblioteca Central, The Intute Consortium. CJPAS has received Index Copernicus Journals Evaluation for 2009 = 4.98

CANADIAN JOURNAL OF PURE AND APPLIED SCIENCES

Board of Editorial Advisors

CONTENTS

SHORT COMMUNICATIONS

Canadian Journal of
pure&applied
sciences

A REVIEW ON THE EFFECTS OF SOME SELECTED PYRETHROIDS AND RELATED AGROCHEMICALS ON AQUATIC VERTEBRATE BIODIVERSITY

*Sara FM Ali, Ben HH Shieh, Zeyad Alehaideb, MZ Khan, Alvin Louie, Noor Fageh and Francis CP Law
Department of Biological Sciences, Simon Fraser University
8888 University Drive, Burnaby, BC V5A 1S6 Canada

ABSTRACT

Pollution in the aquatic ecosystem by pesticides, their metabolites and by-products is considered critical in the conservation of biodiversity and natural resources. Several studies have reported the toxicological issues and adverse effects of pesticides in aquatic biodiversity. After the development of the field ecotoxicology, researchers have expanded their studies towards the effects of pesticides in aquatic ecosystems. Pesticides containing chemicals such as Pyrethroids, cypermethrin, deltamethrin, cyphenothrin and other related compounds have been shown to cause adverse effects on the development, behaviour and mortality of different species of fish, birds, amphibians and aquatic mammals. This review article summarizes the adverse impact of the use of pesticides and related agrochemicals in populations of aquatic, amphibian and avian species.

Keywords: Aquatic biodiversity, pesticides, pyrethroid, cypermethrin, deltamethrin.

INTRODUCTION

The term "biodiversity" is a contracted version of "biological diversity". The conventional view on Biological Diversity defines biodiversity as "the variability among living organisms from all sources including, *inter alia*, terrestrial, marine and other aquatic ecosystems and the ecological complexes of which they are a part; this includes diversity within species, between species, and of ecosystems" (Lloyed, 2010). Aquatic ecosystems provide a habitat for phytoplankton, zooplankton, aquatic plants, insects as well as many vertebrates such as fish, water birds, amphibians and aquatic mammals. In addition, aquatic ecosystems are also an important source of food and medicines while also providing an area for recreational and commercial purposes.

There are many factors that can affect and change biodiversity within aquatic ecosystems. Aquatic biodiversity may decrease due to habitat destruction, fragmentation, pollution or the introduction of an invasive species. In many countries, anthropogenic activities have lead to aquatic organisms being at a higher risk for extinction compared to terrestrial mammals and birds.

Aquatic organisms may be exposed to pesticides through the consumption of contaminated food and water, breathing in pesticide residues or through the absorption of pesticides through their skin. This is a cause for concern as predators (i.e. birds) may be acutely poisoned by eating animals that have been exposed to pesticides. Pesticides are a major factor affecting aquatic biodiversity

along with habitat loss and climate change. They can have adverse effects in the short term by directly affecting the organisms, or long-term effects by causing changes in habitat and the food chain. In Canada, losses among 62 imperilled species were significantly more related to rates of pesticide use and species loss was highest in areas with intensive agriculture (Gibbs *et al.,* 2009).

Many pesticides affect the nervous system of animals, which can interfere with their ability to survive. The contamination of the environment by toxic substances is linked with both agriculture and industrialization. Toxic substances are introduced into aquatic ecosystems from discharges and leaks of industrial products, as well as agricultural runoff. Aquatic ecosystems are important in that there is a continuous exchange of pesticides between land, sediment water interface, air-water interface, and aquatic organisms.

The indiscriminate use of pesticides is considered one of the important factors that change the environment by causing imbalances in the ecosystem, especially in biota of the aquatic system (Sancho *et al*., 1998).

Many agro and related chemicals are found in aquatic ecosystems and have the potential to affect the natural communities within. Among the agrochemicals, pesticides may cause major problems because they are specifically formulated to kill living organisms and are intentionally released into the environment. Impacts of agriculture on aquatic biodiversity may result from many sources, including channelization, removal or alteration of riparian vegetation, dredging, and inputs of contaminants,

* Corresponding author email: saraa@sfu.ca

including sediment, nitrate, phosphate, and pesticides (Brown *et al*., 2007).

Globally, excessive loss of food crops to insects or other pests may contribute to possible starvation, and use of pesticides seems to have a favourable cost-benefit relationship (Murphy, 1986). It is commonly believed that there is a continuous increase in the use of pesticides, thus it is a major factor affecting biological diversity, along with habitat loss.

Many biochemical and physiological changes in aquatic organisms are caused by pesticides which influence the activities of several enzymes (Khan and Law, 2005). Several pesticides are toxic to amphibians, fish, birds and mammals. Normally, pesticides accumulating in the food chain, particularly those which cause endocrine disruption, pose a long-term risk to mammals, birds, amphibians, and fish. One-third of the 6,000 amphibian species found worldwide are at risk. Besides habitat loss, overexploitation and introduced species**,** amphibians are also affected by the pollution of surface waters with fertilisers and pesticides from agriculture (IUCN, 2011). Amphibians have shown vulnerability to agrochemicals that are cholinesterase inhibitors (Wang and Murphy, 1982; Khan *et al*., 2006).

Agricultural activity may intensify the infection of frogs by harmful nematodes (King *et al*., 2008). Aquatic ecosystems have deteriorated over time as anthropogenic activities encroach in water, once primarily the realm of biodiversity (Khan and Yasmeen, 2005).

Several pesticides, such as pyrethroid insecticides, are toxic to most aquatic organisms including aquatic vertebrates. It is evident that pesticides cause major loss in global fish production (Rand, 1995). Many pesticides interfere with the physiological processes of living organisms, and can be passed from one organism to another in the food chain. Therefore, many adverse environmental effects may result from the indiscriminate use of pesticides. Several agrochemicals such as organophosphates, organochlorines and carbamates may cause morphological changes to fish sex organs, which leads to the inhibition of steroid hormone synthesis and delayed oocyte development (Kim, 1998; Khan and Law, 2005).

Pyrethrins and pyrethroids are pesticides included in over 3,500 registered products used for controlling pests (US EPA, 2010). Pyrethroids are used widely as insecticides both in households and in agriculture. They are known to alter the normal function of insect nerves by interfering with the kinetics of voltage-sensitive sodium channels (Soderlund *et al*., 2002). Pyrethrins are natural pesticides produced from *inter alia* pyrethrum, whereas pyrethroids are structurally very similar compounds rendered

photostable by many substituent groups like bromine and chlorine on the basic structure (Bryan *et al*., 1993).

Field and lab investigations have proved that pyrethroids are highly toxic to a number of non-target organisms such as freshwater fish, amphibians and other aquatic organisms; even at very low concentrations (Oudou *et al*., 2004). Non-target species such as aquatic animals are extremely sensitive to the neurotoxic effects of these pesticides when they enter surface water-courses (Philip *et al*., 1995).

Bradbury and Coats (1989) reviewed the adverse effects of pyrethroids in different species of fish and stated a 96 hour cypermethrin toxicity (LC_{50}; μg/l) of 0.9–1.1 to Carp (*Cyprinus carpio*); 1.2 to Brown Trout (*Salmo trutta*); 0.5 to Rainbow Trout (*S. gairdneri*); 0.4 to *Scardinius erythropthalmus* and 2.2 to *Tilapia nilotica*.

The aim of this review is to summarize the effects of pyrethroids and related agrochemicals on aquatic biodiversity and give the picture of their detrimental effects on the environment and biodiversity.

Effects on Fish
The balance of an aquatic ecosystem may be disturbed or altered under the effects of pesticides. Many pesticides indirectly influence fish by affecting their food supply and/or deteriorating the aquatic habitat. Thus the growth and survival of fish is greatly disturbed by use of pesticides in or near a body of water (Ewing, 1999).

There are three ways in which fish and other aquatic creatures are exposed to pesticides: oral, by drinking/feeding on pesticide-contaminated water/prey; dermal, by absorption of pesticides through skin in contaminated water; and inhalation, by up taking contaminants through the gills during respiration (Johnson and Finley, l980).

Fish are chronically exposed to a variety of pesticides in their natural environment. Many of these chemicals also have the potential to accumulate in their tissues. Several studies have shown that most fish sampled from the agricultural areas contained detectable levels of pesticides. In particular, high levels were detected in fish from the Los Angeles and San Diego harbours, parts of the San Francisco Bay, and the Sacramento and San Joaquin Rivers (US EPA, 1992).

Pyrethroids are metabolized and eliminated at a significantly slower rate in fish when compared to birds and mammals. This may explain the higher toxicity of pyrethroids in fish when compared to other animals (Bradbury and Coats, 1989). Laboratory investigations have proved that pyrethroids are absorbed at a high rate by gills and these factors into the vulnerability of fish to

aqueous pyrethroid. Fish also metabolizes and eliminates these chemicals at a very low rate. The half-lives are greater than 48 hours for the elimination of several pyrethroids by trout, whereas the half-lives of the same compounds are between 6-12 hours in birds and mammals (Bradbury and Coats, 1989).

Fish are deficient in the enzymes that hydrolyze pyrethroids. Metabolism of deltamethrin, cypermethrin or cyhalothrin is largely oxidative in fish, whereas in rats/mice the main reaction is the ester cleavage by carboxyesterase (Demoute, 1989).

Deltamethrin may also disturb phosphate and calcium homeostasis which may impact the reproductive state of the fish (Srivastav *et al.*, 1997).

Fish primarily metabolize pyrethroids by oxidative degradation, with ester hydrolysis being a secondary reaction. Glickman *et al.* (1981) and Glickman and Lech (1981) reported that the oxidation and hydrolysis of permethrin in *Oncorhynchus mykiss* tissues were comparatively slower than in mammalian tissues. Mulla *et al.* (1978) reported the permethrin toxicity in 48 hours with LC_{50} of 0.005, 0.006, and 0.097 mg/L for adult Desert pupfish (*Cyprinodon macularius*), Rainbow trout (*Oncorhynchus mykiss*), and Western mosquitofish (*Gambusia affinis*), respectively.

Deltamethrin is a pyrethroid widely used in agricultural areas. Koprucu and Aydin (2004) investigated the effects of deltamethrin on embryos and larvae of *Cyprinus carpio* and reported that the number of dead embryos significantly increased in response to deltamethrin concentrations of 0.005, 0.05, 0.5, 5, 25, and 50 μg L^{-1} (*p*<0.05 for each cases). While dose–response decreases in hatching success were recorded as 75.2, 64.6, 47.4, 26.0, 14.4, and 9.0%, respectively. Exposure to the lowest concentration of deltamethrin (0.005 μg L^{-1}) resulted in significantly reduced numbers of dead larvae when compared to the higher concentrations (*p*<0.05)**?** Based on experimental results, deltamethrin may affect the development and reproduction of *Cyprinus carpio*. Therefore, deltamethrin must not be used in agricultural areas near the aquatic ecosystems.

Exposure to deltamethrin at a concentration of 2mg/l caused an inhibitory effect on the monooxygenase system of the Carp liver (*Cyprinus carpio* L.), whereas a faster metabolism of deltamethrin occurred when the Carp liver was exposed to a low concentration of 0.2 mg/l. The faster metabolism was due to an induction of hepatic microsomal cytochrome P450-dependent monooxygenases (Dee´ r *et al.*, 1996).

Viran *et al.* (2003) conducted a study on deltamethrin's effects on behavioural responses of the fish *Poecilia reticulate* for 8 consecutive hours and then every 12 hours during the acute toxicity tests. Exposure to the lowest concentration of 1.00 mg/l had close to normal behaviour response, while less general activity and loss of equilibrium was observed at the highest concentration of 4mg/l when compared to the control group. The changes in behavioural response started an hour after the dosing of deltamethrin in all concentrations tested.

The exposure of deltamethrin to freshwater fish, *Channa punctatus* showed a significant (*P*<0.01) decrease in the activity of all organs. The decreased activity observed was 45% in liver, 43% in kidney and 33% in gills. A significant (*P*<0.01–0.001) increase was recorded in the activities of Glutathione S-transferase (GST) and Glutathione Peroxidase (GPx) in the liver and kidney, while there was a significant decrease (*P*<0.001) in the activities of GST and GPx in the gills (Sayeed *et al.*, 2003).

Cypermethrin is extremely toxic to bees (WHO, 1992) and vertebrates, with fish being the most sensitive of all vertebrates (Edwards *et al.*, 1986). Several studies have already shown the LC_{50} of between 0.93 and 21.4 μg/l in many fish species (Carriquiriborde *et al.*, 2007; Polat *et al.*, 2002; Stephenson, 1982).

Cypermethrin is toxic to the freshwater fish *Colisa fasciatus*. Sub-lethal doses of cypermethrin altered the total protein, free amino acids, nucleic acids (DNA and RNA) and enzymes LDH, SDH and AChE in the fish (Singh *et al.*, 2010). Smith and Stratton (1986) compiled the adverse effects of cis-cypermethrin on fish species as follows (exposure time and LC_{50} in μg/l): Rainbow trout (*S. gairdneri*) 96-h 6.0, Atlantic salmon (*Salmo salar*) 96-h 2.0, Mosquito fish (*Gambusia affinis*) 24-h 9.0 and 48-h 8.0; Desert pupfish (*Cyprinodon macularius*) 24-h 10.0 and 48-h 6.0.

Alpha-cypermethrin is extremely toxic to fish and aquatic invertebrates but is non-toxic to birds. It is metabolized and eliminated slower in fish as compared to mammals and birds (Sarikaya, 2009).

Some Threatened Fish Species

The Atlantic Sturgeon (*Acipenser sturio*) (Fig. 1) was formerly found to inhabit areas in the North Sea, north-eastern Atlantic and Mediterranean coasts of Europe and the Black Sea. Due to pollution and river regulations, there has been degradation and destruction of many of their spawning sites. In the last three generations, the population has declined by 90% and has become extinct in most of its former areas. Currently in the Garonne River, France, the last remaining population is still declining (Kottelat *et al.*, 2009).

Fig. 1. Atlantic Sturgeon (*Acipenser sturio*).

Populations of fish *Tilapia busumana* (Fig. 2) from Ghana are presently declining due to agricultural practise, leaching of pesticides and other agrochemicals (Entsua-Mensah and Lalèyè, 2006).

Fig. 2. *Tilapia busumana.*

Sahara Aphanius (*Aphanius saourensis*) (Fig. 3) is a species Endemic to Algeria. Due to water pollution and other threats this species has been listed as Critically Endangered (Azeroual, 2007).

Fig. 3. Sahara Aphanius (*Aphanius saourensis*).

Effects on Amphibians
Amphibians are an important part of aquatic ecosystems and are the good indicator of environmental stress (Blaustein, 1994; Blaustein and Wake, 1995). They have contact with water as larvae and both with water and land as an adult. Thus, they are exposed to the stressors in both aquatic and terrestrial environments (Blaustein and Wake, 1990; Vitt, *et al*., 1990; Khan *et al*., 2009). Out of 6285 amphibians species, 1895 are in danger of extinction, this makes them the most threatened group of species known to date (IUCN, 2011).

Pesticides can affect frogs and other amphibians in different ways, as they destroy the natural biotic balance in agricultural fields' and reduce the diversity and abundance of biodiversity with cascading effects at higher trophic levels (Larson *et al.*, 1997; Khan and Ghazala, 2008). Pesticides can affect their behaviour and reduce their growth rates (Bishop, 1992; Carey and Bryant, 1995; Alford and Richards, 1999). Under the effects of pesticides, many frogs and toads grow extra legs and eyes and do not survive to adulthood (Kegley *et al*., 1997).

Amphibians are known to be vulnerable to pesticides that are cholinesterase inhibitors. Several studies have reported that some pesticides reduce cholinesterase (ChE) activity in the frogs; *Rana tigrina* (Khan *et al.*, 2002a,b and 2003a) and *Rana cyanophlyctis* (Khan *et al.*, 2003b,c,d ; Khan and Yasmeen, 2005; Khan *et al.*, 2006; Khan *et al.*, 2007). There is some indication that field application of these pesticides may be deleterious to amphibians (Jolly *et al.*, 1978; Thybaud, 1990; Berril *et al.*, 1993; Materna *et al*., 1995). In 1992, World Health Organization (WHO) recognized that cypermethrin is an alpha-cyano pyrethroid, whose primary target site in the vertebrate nervous system is the sodium channel of the nerve membrane. The behavioural response of twisting, writhing, and non-coordinated swimming in amphibians is an indication of cyano pyrethroid poisoning (Berril *et al*., 1993; Greulich and Pflugmacher, 2003).

Khan *et al*. (2003c) studied the induced effects of lambda cyhalothrin on *Rana cyanophlyctis* and reported that this pesticide decreased cholinesterase levels up to 46.3% in liver, 57.1% in kidney and 50.7% in brain. In another study, Khan and Ghazala (2009) investigated the effects of beta cypermethrin on frogs and reported that the ChE activity decreased to 30.0% in the liver ($F_{2,6}=13.28$, $P=0.006$), up to 40.0% in the kidney ($F_{2,6}=6.80$, $P=0.029$) and to 44.44% in the brain, ($F_{2,6}=22.99$, $P=0.002$). In another study, Khan *et al*. (2003b), compared the effects of both lambda cyhalothrin and permethrin on cholinesterase in *R. cyanophlyctis* and *R. tigrina* and reported that amphibians in general are sensitive. *R. cyanophlyctis* is more sensitive to these chemicals than *R. tigrina,* and lambda cyhalothrin is most toxic among the pesticides tested.

Berrill *et al*. (2009) subjected embryos and larvae of three species of the *Rana* genus of frogs *(R. sylvatica, R. pipiens, R. Clamitans),* the toad *(Bufo americanus)* and salamander *(Ambystoma maculatum)* to one or both of the

pyrethroid fenvalerate and permethrin. Concentrations of 0.01ppm to 2ppm were used and subjects were exposed for 22 or 96 hours. No significant mortality of embryos or larvae occurred during or following the exposure to these pyrethroids. Nevertheless, tadpoles showed delayed growth following the exposure. Affected tadpoles and larvae responded to prodding by twisting abnormally instead of darting away. These effects (slower growth and abnormal behaviour) may result in higher risk to predation.

Some Threatened Amphibian Species
In South Africa, Pickersgill's Reed Frog (*Hyperolius pickersgilli*) (Fig. 4) is an Endemic species. Due to habitat destruction, agricultural activities and pollutants such as pesticides, it has been listed as a Critically Endangered Species (SA-Frog, 2010).

Fig. 4. Pickersgill's Reed Frog (*Hyperolius pickersgilli*).

In addition, the population of Spotted Snout-burrowe**r**s (*Hemisus guttatus*) (Fig. 5) in South Africa is also facing habitat loss and agrochemical pollution threats (SA-Frog, 2010). A recent study (Khan *et al.*, 2010) indicated that three species of frog are at risk due to pesticide contamination. Tiger Frog (*Hoplobatrachus tigerinus*) (Fig. 6) found in Taiwan, throughout Southern China and the other mainland countries of South East Asia throughout most of the Indian Subcontinent, Northward to Nepal and Pakistan; Indian Burrowing Frog (*Tomopterna breviceps*) is distributed throughout India, West of the Ganges Delta and Nepal, Bangladesh, Myanmar, Sri Lanka and Pakistan, and Indian Cricket Frog (*Limnonectes limnocharis*) found in Southern Japan and the Riu-Kiu Islands through the Philippines and the Island of Indonesia East-Central China West to Nepal and Kashmir and Pakistan are now listed as Threatened Species in the Thatta districts of Sindh province due to the effects of agricultural pesticides and habitat destruction.

Fig. 5. Spotted Snout-burrower (*Hemisus guttatus*).

Fig. 6. Tiger Frog (*Hoplobatrachus tigerinus*).

Effects on Aquatic Mammals and
Some Threatened Aquatic Mammalian Species
Many cases of adverse impact of pesticides affecting dolphins have been reported. Dolphins accumulate high concentrations of organic pollutants because they have a low activity of drug-metabolizing enzymes (Tanabe *et al.*, 1997). River dolphins are one of world's Threatened Species (Akhtar *et al.*, 2009). Critically Endangered Yangtze River Dolphin (*Lipotes vexillifer*) in China (Fig. 7), and 1331 remaining *Platanista minor* dolphins of the Indus River in Pakistan (Fig. 8) are already close to extinction (Perrin *et al.*, 1989; Reeves *et al.*, 1991; Reeves and Chaudhry, 1998; Khan, 2006).

Fig. 7. Yangtze River Dolphin (*Lipotes vexillifer*).

Fig. 8. Indus River Dolphin (*Platanista minor*).

In Bangladesh, the extensive use of fertilizers and pesticides for the ''green revolution'' has created major water-quality problems. The Ganges River Dolphin (*Platanista gangetica*) inhabits the Ganges, Meghana, Brahmaputra and Karnaphuli rivers and their tributaries in India (Fig. 9), Bangaladesh, Nepal and Bhutan (Lal Mohan, 1989). A recent study has shown that Ganges River Dolphins or susu (*Platanista gangetica*) are unable to metabolize the chemicals found in pesticides (Kannan *et al.*, 1994).

Fig. 9. Ganges River dolphin, *Platanista gangetica.*
 (source: http://euteachers.net/cms/index1.php).

Another freshwater Gray Dolphin (*Sotalia fluviatilis*) is considered to be the world's only exclusive freshwater delphinid (Fig. 10). It inhabits the Amazon drainage as far inland as southern Peru, south eastern Colombia and eastern Ecuador and is facing some threats including pollution (Secchi, 2010).

Fig. 10. Gray Dolphin (*Sotalia fluviatilis*). (source: www.iucnredlist.org).

Effects on Birds
Reduction in the population levels of several bird species has been linked to exposure to pesticides through ingestion and/or absorption (Mineau *et al*. 2005; Ortego *et al*. 2007).

Fig. 11. Baikal Teal (*Anas Formosa*). (source: BirdLife International, 2011).

Fig. 12. Marbled Teal. (*Marmaronetta angustirostris*) (source: BirdLife International, 2011).

Synthetic pyrethroids have a relatively low acute toxicity in birds but can destroy a bird's food supply. Waterfowl that feed on aquatic insects and insectivorous birds are especially vulnerable to pyrethroids (Mueller-Beilschmidt, 1990).

Egrets and herons are at the top of the aquatic food webs, and thus particularly susceptible to pollutant bioaccumulation (De Lucca-Abbot *et al.,* 2001). However in the case of cypermethrin, the birds are affected without being exposed directly to the pesticides. This usually occurs when pesticides are applied to birds' food sources such as bugs/insects and rodents. Some studies have indicated that the growth of young birds can be stunted in areas where insecticides have been used heavily, resulting in insect populations too low to meet young birds' protein growth demands (Facemire, 1991).

Cypermethrin has shown no toxicity to birds. The acute oral LD_{50} in mallard ducks is greater than 4,640 mg/kg. The dietary LC_{50} is > 20,000ppm for mallards and Bobwhite Quail. No adverse reproductive effects have been observed in mallards or Bobwhite Quails given 50 ppm, the highest dose tested (US EPA, 1989). Cypermethrin is used in killing insect larvae which are normally eaten by birds, thus birds are indirectly affected by this compound as their food source is affected. A study on Blue Tits' (*Parus caeruleus*) nesting success showed a

100% mortality of caterpillars (eaten by Blue Tits) after an aerial application of cypermethrin in an oak forest. An increase in nestling fatality, a decrease in successful nests and a decrease in weight of the surviving nestling was observed when exposure to cypermethrin coincided with egg hatching and early nestling stage (Pascual and Peris, 1992).

Some Threatened Bird Species
In China and South Korea, birds were indirectly affected by poisoned grain and pollution from agricultural and household wastes. The Baikal Teal (*Anas Formosa*) (Fig. 11) is now listed as a threatened bird species. This bird breeds in eastern Siberia, Russia and is found mainly on passage in Mongolia and North Korea. It winters mainly in Japan and South Korea (BirdLife International, 2011). Another species, the Marbled Teal (*Marmaronetta angustirostris*) (Fig. 12) found in Russia, Uzbekistan, Turkmenistan, Tajikistan, Kazakhstan, Afghanistan, China, Iraq and winters in Iran, Pakistan and north-west India is also listed as a threatened species due to agricultural and industrial pollution (BirdLife International, 2011).

CONCLUSION

Pesticides have harmful effects on species biodiversity. These compounds can have adverse effects either directly or indirectly on the normal life cycles of animals and their habitats. Different species of fish, amphibians, birds and aquatic mammals have been listed as endangered because of chronic exposure to pyrethroids and other related agrochemicals. Measures can be taken to lower the level of exposure to animals and their habitat. Flow of energy is disturbed when any level of the food chain/web is affected by compounds such as pesticides and other agrochemicals. This can lead to widespread adverse effects causing an imbalance in the ecosystem.

REFERENCES

Alford, RA. and Richards, SJ. 1999. Global Amphibian Declines: A Problem in Applied Ecology. Annu. Rev. Ecol. Syst. 30:133-165.

Azeroual, A. 2007. *Aphanius saourensis*. In: IUCN 2010. IUCN Red List of Threatened Species. Version 2010.4.

Akhtar, MW., Sengupt, D. and Chowdhury, A. 2009. Impact of pesticides use in agriculture: their benefits and hazards. Interdisc Toxicol. 2(1):1-12.

Bradbury, SP. and Coats, JR. 1989. Toxicokinetics and toxicodynamics of pyrethroid insecticides in fish. Environmental Toxicology and Chemistry. 8(5):373-380.

Bradbury, SP. and Coats, JR. 1989. Comparative toxicology of the pyrethroid insecticides. Rev. Environ. Contam. Toxicol. 108:133-177.

Blaustein, AR. and Wake, DB. 1990. Declining amphibian populations: a global phenomenon? Trends in Ecol. Evol. 5:203-4.

Bishop, CA. 1992. The effects of pesticides on amphibians and the implications for determining causes of declines in amphibian populations. In Declines in Canadian Amphibian Populations: Designing a National monitoring Strategy. Canadian Wildlife Service. Occas. Pap. No. 76:67-70.

Berril, M., Bertram, S., Wilson, A., Louis, S,, Brigham, D. and Stromberg, C. 1993. Lethal and sub-lethal impacts of pyrethroid insecticides on amphibian embryos and tadpoles. Environ. Toxicol. Chem. 12:525-539.

Bryan, B., Marrs, T. and Turner, P. 1993. General and Applied Toxicology (vol. 2). Macmillan Publishers Ltd., New York, USA.

Berril, M., Bertram, S., Wilson, A., Louis, S., Brigham, D. and Stromberg, C. 1993. Lethal and sublethal impact of pyrethroid insecticides on amphibian embryos and tadpoles. Environ Toxicol Chem. 12:525-539.

Blaustein, AR. 1994. Chicken Little or Nero's fiddle? A perspective on declining amphibian populations. Herpetologica. 50:85-97.

Blaustein, AR. and Wake, DB. 1995. The puzzle of declining amphibian populations. Sci. Am. 272:52-57.

Brown, CD., Holmes, C., Williams, R., Beulke, S., Beinum, W., Pemberton, E. and Wells, C. 2007. How does crop type influence risk from pesticides to the aquatic environment? Environmental Toxicology and Chemistry. 26(9):1818-1826.

Berrill, M., Bertram, S., Wilson, A., Louis, S., Brigham, D. and Stromberg, C. 2009. Lethal and sublethal impacts of pyrethroid insecticides on amphibian embryos and tadpoles. 12(3):525-539.

BirdLife International. 2011. IUCN Red List for birds. http://www.birdlife.org

Carey, C. and Bryant, CJ. 1995. Possible inter-relationships among environmental toxicants, amphibian development, and decline of amphibian populations. Environ. Health Perspec. 103(4):13-17.

Carriquiriborde, P., Diaz, J., Mugni, H., Bonetto, C. and Ronco, EA. 2007. Impact of cypermethrin on stream fish populations under fielduse in biotech-soybean production. Chemosphere. 68:613-621.

Demoute, JP. 1989. A brief review of the environmental fate and metabolism of Pyrethroids. Pest. Sci. 27:375-385.

Dee´r, KA., Banka, L., Nemcsok, J. and Abraham, M. 1996. Effects of deltamethrin on hepatic microsomal cytochrome P450-dependent monooxygenases in carp. J. Environ. Sci. Health. B 31 (3):637-644.

De Lucca-Abbott, SB., Wong, BSF., Peakall, DB., Lam PKS., Young, L., Lam, MHW. and Richardson, BJ. 2001. Review of effects of water pollution on the breeding success of waterbirds, with particular reference to ardeids in Hong-Kong. Ecotoxicology. 10:327-349.

Edwards, R., Millburn, P. and Hutson, DH. 1986. Comparative toxicity of cis-cypermetrhrin in Rainbow trout, frog, mouse and quail. Toxicol Appl Pharmacol. 84:512-522.

Ewing, RD. 1999. Diminishing Returns: Salmon Decline and Pesticides. Biotech Research and Consulting, Inc., Corvallis, OR. pp 55.

Entsua-Mensah, M. and Lalèyè, P. 2006. *Tilapia busumana*. In: IUCN 2010. IUCN Red List of Threatened Species. Version 2010.4. <www.iucnredlist.org>

Facemire, FC. 1991. Impact of agricultural chemicals on wetland habitats and associated biota with special reference to migratory birds. B 780, SDSU, Brookings, SD. pp 65.

Glickman, AH., Hamid, AAR., Rickert, DE. and Lech, JJ. 1981. Elimination and metabolism of permethrin isomers in rainbow trout. Toxicol. Appl. Pharmacol. 57:88-98.

Glickman, AH. and Lech, JJ. 1981. Hydrolysis of permethrin, a pyrethroid insecticide, by rainbow trout and mouse tissues in vitro: A comparative study. Toxicol. Appl. Pharmacol. 60:186-192.

Greulich, K. and Pflugmacher, S. 2003. Differences in susceptibility of various life stages on amphibians to pesticide exposure. Aquat Toxicol. 65:329-336.

Gibbs, KE., Mackey, RL. and Currie, DJ. 2009. Human land use, agriculture, pesticides and losses of imperiled species. Diversity and Distributions. 15(2):242-253.

IUCN. 2011. Why is biodiversity in crisis? www.iucn.org

Johnson, W. and Finley, MT. l980. Handbook of Acute Toxicity of Chemicals to Fish and Aquatic Invertebrates. US Fish and Wildlife Service Publication 137. Washington, DC, USA.

Jolly, AL. Jr., Avault, JW. Jr., Koonce, KL. and Graves, JB. 1978. Acute toxicity of Permethrin to several aquatic animals. Trans. Am. Fish Soc. 107:825-827.

Kannan, K., S. Tanabe, and R. Tatsukawa. 1994. Biodegradation capacity and residue pattern of organochlorine in the Ganges river dolphins from India. Toxicological and Environmental Chemistry. 42:249-261.

Kegley, S., Neumeister, L. and Martin, T. 1997. Disrupting the Balance: Ecological Impacts of Pesticides in California. Pesticide Action Network, USA. pp 99

Kim, DE. 1998. Endocrine disruption in fish. Kluwer Academic Publishers, London. IUCN. The Asian amphibian crisis. http://www.iucn.org/about/union/secretariat/offices/asia/regional_activities/asian_amphibian_crisis/

Khan, MZ., Fatima, F. and Ahmad, I. 2002[a]. Effect of Cypermethrin on Protein Contents in Lizard *Calotes versicolor* in comparison to that in Frog *Rana tigrina.* Online Journal of Biological Sciences. 2(12):780-781.

Khan, MZ., Shah, EZ., Ahmed, I. and Fatima, F. 2002[b]. Effects of agricultural pesticides permethrin (pyrethroid) on protein contents in kidney and liver of lizard species *Calotes versicolor* in comparison to that in frog *Rana tigrina*. Bull. of Pure & App. Sc. 21A (2):93-97.

Khan, MZ., Tabassum, R., Naqvi, SNH., Shah, EZ., Tabassum, F., Ahmad, I., Fatima, F. and Khan, MF. 2003[a]. Effect of Cypermethrin and Permethrin on Cholinesterase Activity and Protein Contents in *Rana tigrina* (Amphibia).Turk. J. Zool. 27: 243-246.

Khan, MZ., Nazia, M., Fatima, F., Rahila, T. and Gabol, K. 2003[b]. Comparison of the effect of Lamda cyhalothrin with permethrin on cholinesterase activity in *Rana cyanophlyctis* and *Rana tigrina (*Ranidae: amphibian). Bull. of Pure & App. Sc. 22A (1):43-49.

Khan, MZ., Maria, Z. and Fatima, F. 2003[c]. Effect of Lamda Cyhalothrin (Pyrethroid) and Monocrotophos (Organophosphate) on Cholinesterase activity in liver, kidney and brain of *Rana cyanophlyctis.* Korean J. Biol. Sciences. 7(2):165-168.

Khan, MZ., Fatima, F., Mahmood, N. and Yasmeen, G. 2003[d]. Comparison of Cholinesterase activity in the brain tissue of lizard *Calotes versicolor* with that of frog *Rana cyanophlyctis* under the effect of Cypermethrin, Lamda Cyhalothrin, Malathion and Monocrotophos. Bulletin of Pure and Applied Sciences. 22 A (2):105-112.

Khan, MZ. and Yasmeen, G. 2005. Pesticide dependent cholinesterase activity in brain of *Rana cyanophlyctis* (amphibian). J Exp. Zool. India. 8 (1):135-140.

Khan, MZ. and Law, FCP. 2005. Adverse Effects of Pesticides and related Chemicals on Enzyme and Hormone Systems of Fish, Amphibians and Reptiles. Proc. Pakistan Acad. Sci. 42(4):315-323.

Khan, MZ. 2006. Current Status and Biodiversity of Indus Dolphin Reserve and Indus Delta Wetlands (Ramsar Sites). Proc. 9th International River Symposium, Brisbane, Australia. 1-26.

Khan, MZ., Yasmeen, G. and Hamid, S. 2006. Effect of Sundaphos (Organophasphate) and beta-cypermethrin (Synthetic Pyrethroid) on Cholinesterase Activity in Liver and Kidney of *Euphlyctis cyanophlyctic*. Hamadryad. 30(1&2):176-180.

Khan, MZ., Rais, M. and Yasmeen, G. 2007. Inhibitory effects on cholinesterase activity produced by the two

different pesticides on brain, liver and kidney of *Euphlyctis cyanophlyctis*. J. Exp. Zool. India.10(1):89-93.

Khan, MZ. and Yasmeen, G. 2008. Effects of Sandaphose and beta-cypermethrin on Cholinesterase and Alkaline Phosphatase activity in liver, kidney and brain of Euphlyctis cyanophlyctis. CJPAS. 2(3):511-519.

Khan, MZ. and Yasmeen, G. 2009. A study on the induced effect of beta-cypermethrin on skin of *Euphlyctis cyanophlyctis*. CJPAS. 3(3):937-941.

Khan, MZ., Nazia M., Ghalib, SA., Hussain, B., Saima, S, Shahnaz, P. and Darakhshan, A. 2010. Impact of Habitat Destruction on the Population of Amphibans with Reference to Current Status of Frogs and Toads in Karachi and Thatta, Sindh. Canadian Journal of Pure and Applied Sciences. 4(3):1257-1265.

King, KC., Gendron, AD., McLaughlin JD., Giroux, I., Brousseau, P., Cyr, D., Ruby, SM., Fournier, M. and Marcogliese, DJ. 2008. Short-term seasonal changes in parasite community structure in Northern Leopard froglets (*Rana pipiens*) inhabiting agricultural wetlands. J Parasitol. 94(1): 13-22.

Koprucu, K. and Aydin, R. 2004. The toxic effects of pyrethroid deltamethrin on the common carp (*Cyprinus carpio* L.) embryos and larvae. Pesticide Biochemistry and Physiology. 80(1):47-53.

Kottelat, M., Gesner, J., Williot, P., Rochard, E. and Freyhof, J. 2009. *Acipenser sturio*. In: IUCN 2010. IUCN Red List of Threatened Species. Version 2010.4. <www.iucnredlist

Lal Mohan, RS. 1989. Conservation and management of the Ganges river dolphin, *Platanista gangetica* in India. In: Biology and Conservation of the River Dolphin. Eds. Perrin, WF., Brownell, RL. Jr., Zhou, K. and Liu, J. Occasional papers of the IUCN Species Survival Commission (SSC). 3:64-69.

Larson, SJ., Capel, PD. and Majewski, MS. 1997. Pesticides in surface waters: Distribution, Trends, and Governing Factors. Ann Arbor, Inc., USA.

Lloyed, J. 2010. Encyclopedia of Earth. Biodiversity. (Washington, DC, USA. Environmental Information Coalition, National Council for Science and the Environment). Retrieved April 26, 2011.

Mulla, MS., Navvab-Gojrati, HA. and Darwazeh, JA. 1978. Toxicity of mosquito larvicidal pyrethroids to four species of freshwater fishes. Environ. Entomol. 7:428-430.

Murphy, SD. 1986. Toxic effects of pesticides. In: Klassen CD et al. Eds. Casarett and Doull's Toxicology, The Basic Science of Poisons (3rd ed.). New York. pp. 519-581.

Mueller-Beilschmidt, D. 1990. Toxicology and environmental fate of synthetic pyrethroids. J. Pesticide Reform. 10(3):32-36.

Materna, EJ., Rabeni, CF. and La Point, TW. 1995. Effects of synthetic pyrethroid insecticides, esfenvalerate, on larval leopard frogs (*Rana* spp.) Environ. Toxicol. Chem. 14:613-622.

Mineau, P., Downes, CM., Kirk, DA., Bayne, E. and Csizy, M. 2005. Patterns of bird species abundance in relation to granular insecticide use in the Canadian prairies. Ecoscience. 12(2):267-278. doi:10.2980/i1195-6860-12-2-267.1.

Oudou, HC., Alonso, RM. and Bruun, HC. 2004. Voltammetric behaviour of the synthetic pyrethroid lambda-cyhalothrin and its determination in soil and well water. Anal. Chim. Acta. 523(1):69-74.

Ortego, J., Aparicio, JM., Munoz, A. and Bonal, R. 2007. Malathion applied at standard rates reduces fledgling condition and adult male survival in a wild lesser kestrel population. Anim. Conserv. 10(3):312-319. oi:10.1111/j.1469-1795.2007.00114.x.

Perrin, WF., Brownell, RL Jr., Kaiya, Z. and Jiankang, L. 1989. Biology and conservation ofthe river dolphins. In: Proceedings of the Workshop on Biology and Conservation of the Platanistoid Dolphins. Eds. Perrin, WF., Brownell, RL Jr., Kaiya, Z. and Jiankang, Wuhan, L. China.

Pascual, JA. and Peris, SJ. 1992. Effects of forest spraying with two application rates of cypermethrin on food supply and on breeding success of the Blue Tit (*Parus caeruleus*). Environ. Toxicol. Chem. 11:1271-1280.

Philip, GH., Reddy, PM. and Sridevi, G. 1995. Cypermethrin-induced in vivo alterations in the carbohydrate-matabolism of freshwater fish, *Labeo rohita*. Ecotoxicol. Environ. Safety. 31(2):173-178.

Polat, H., Erkoc¸ FU., Viran, R. and Koçak, O. 2002. Investigation of acute toxicity of beta-cypermethrin on guppies Poecilia reticulata. Chemosphere. 49(1):39-44.

Reeves, RR., Chaudhry, AA. and Khalid, U. 1991. Competing for water on the Indus plain: Is there a future for Pakistans River Dolphins? Environ Conserv. 18:341-350.

Reeves, RR. and Chaudhry, AA. 1998. Status of the Indus River Dolphin *Platanista minor*. Oryx. 32:35-44.

Rand, GM. 1995. Fundamentals of Aquatic Toxicology: Effects, Environmental Fate and Risk Assessment. 2nd ed. Washington, DC, USA.

Stephenson, RR. 1982. Aquatic toxicology of cypermethrin. I. Acute toxicology to some freshwater fish

and invertebrates in laboratory tests. Aquat Toxicol. 2:175-185.

Smith, TM. and Stratton, GW. 1986. Effects of synthetic pyrethroid insecticides on nontarget organisms. Res. Rev. 97:93-119.

Srivastav, AK., Srivastava, SK. and Srivastav, SK. 1997. Impact of deltamethrin on serum calcium and inorganic phosphate of freshwater catfish, Heteropneustes fossilis. Bull. Environ. Contam. Toxicol. 59(5):841-846.

Sancho, E., Fernando, MD., Lleó, C. and Andreu-Moliner, E. 1998. Pesticide toxicokinetics in fish: Accumulation and Elimination. Ecotoxicol. Environ. Saf. 41(3): 245-250.

Soderlund, DM., Clark, JM., Sheets, LP., Mullin, LS., Piccirillo, VJ., Sargent, D., Stevens, JT. and Weiner, ML. 2002. Mechanisms of pyrethroid neurotoxicity: Implications for cumulative risk assessment Toxicology. 171(1):3-59.

Sayeed, I., Parvez, S., Pandey, S., Bin-Hafeez, B., Haque, R. and Raisuddin, S. 2003. Oxidative stress biomarkers of exposure to deltamethrin in freshwater fish, *Channa punctatus* Bloch. Ecotoxicology and Environmental Saftey. 56(2):295-301.

Sarıkaya, R. 2009. Investigation of Acute Toxicity of Alpha-Cypermethrin on Adult Nile Tilapia (*Oreochromis niloticus* L.). Turkish Journal of Fisheries and Aquatic Sciences. 9:85-89.

Singh, SK., Singh, Sunil Kumar S. and Yadave, RP. 2010. Toxicological and Biochemical Alterations of Cypermethrin (Synthetic Pyrethroids) Against Freshwater Teleost Fish *Colisa fasciatus* at Different Season. World Journal of Zoology. 5 (1):25-32.

Secchi, E. 2010. *Sotalia fluviatilis*. In: IUCN 2010. IUCN Red List of Threatened Species. Version 2010.4. <www.iucnredlist.org>. Downloaded on 27 April 2011.

South African Frog Re-assessment Group (SA-FRoG) and IUCN SSC Amphibian Specialist Group 2010. *Hemisus guttatus*. In: IUCN 2010. IUCN Red List of Threatened Species. Version 2010.4. <www.iucnredlist.org>.

South African Frog Re-assessment Group (SA-FRoG) and IUCN SSC Amphibian Specialist Group 2010. *Hyperolius pickersgilli*. In: IUCN 2010. IUCN Red List of Threatened Species. Version 2010.4. <www.iucnredlist.org>.

Tanabe, S., Senthilkumar, K., Kannan, K. and Subramanian, AN. 1997. Accumulation features of polychlorinated biphenyls and organochlorine pesticides in resident and migratory birds from south India. Arch Environ Contam Toxicol. 34(4):387-397.

Thybaud, E. 1990. Acute toxicity and bioconcentration of lindane and deltamethrin in tadpoles of *Rana temporaria* and the mosquito fish *Gambusia affinis*. Hydrobiologia. 190:137-146.

US Environmental Protection Agency. 1992. Pesticide Fact Sheet Number 199: Cypermethrin. US EPA, Office of Pesticide Programs. Washington, DC, USA.

US EPA. 2010. National Study of Chemical Residues in Fish, Volume I and II. Environmental Protection Agency, Washington,   DC. http://www.epa.gov/oppsrrd1/reevaluation/pyrethroids-pyrethrins.html

Viran, R., Erkoç, FÜ., Polat, H. and Koçak, O. 2003. Investigation of acute toxicity of deltamethrin on guppies(*Poecilia reticulata*). Ecotoxicology and Environmental Safety. 55(1): 82-85.

Vitt, LJ., Caldwell, JP., Wilbur, HM. and Smith, DC. 1990. Amphibians as harbingers of decay. Bio Sci. 40:418-18.

Wang, C. and Murphy, SD. 1982. Kinetic analysis of species to organophosphate insecticides. Toxicology and Applied Pharmacology. 66 (3):409-419.

World Health Organization. 1992. Alpha-cypermethrin. Environmental Health Criteria.

Zitko, V., Mcleese, DW., Metcafe, CD. and Carson, WG. 1979. Toxicity of permethrin, decamethrin, and realted pyrethroids to salmaon and lobster. Bull. Environ. Contam. Toxicol. 21(3):336-343.

Canadian Journal of
pure&applied
sciences

IN VITRO KINETICS OF STAPHYLOCOCCAL DEATH IN THE STEM BARK EXTRACTS OF *JATROPHA CURCAS* LINN (EUPHORBIACEAE)

Amos Olusegun Abioye [1, 2], *Solayide A Adesida[3], Solomon B Bamiro[4] and Ese Okpako[1]
[1]Department of Pharmaceutics and Pharmaceutical Technology, Faculty of Pharmacy, University of Lagos
[2]Leicester School of Pharmacy, Faculty of Health and Life Sciences
DeMontfort University, The Gateway, Leicester LE1 9BH, United Kingdom
[3]Molecular Biology and Biotechnology Division, Nigerian Institute of Medical Research, Yaba, Nigeria
[4]Microbiology and Endocrinology Research Laboratory, Department of Obstetrics and Gynaecology
College of Medicine, University of Lagos, Nigeria

ABSTRACT

Medicinal plants present a promising option in the treatment of infectious diseases. Although literature is replete of the traditional utilization of *Jatropha curcas* for healing various ailments, scientific studies validating its phytochemotherapeutic properties are limited. In this study, both aqueous and methanol extracts of *Jatropha curcas* were tested against thirteen clinical staphylococcal isolates including Methicillin Resistant *Staphylococcus aureus* (MRSA) using agar diffusion and microdilution techniques. Nineteen commonly used antibiotics were employed as control drugs and to determine the resistance profiles of the organisms. Bactericidal activity was evaluated by the time-kill assay. The susceptibility patterns of all the staphylococcal isolates tested were similar in aqueous and methanol extracts. The methanol extract (100mg/ml) demonstrated inhibitory activity against *Staphylococcus haemolyticus*, which was resistant to ciprofloxacin, tetracycline and erythromycin. The MIC and MBC of the methanol extract ranged between 0.5 and 8mg/ml and between 4 and 128mg/ml respectively while that of aqueous extract ranged between 1 and 8mg/ml and between 4 and 128mg/ml respectively. The MRSA strain was sensitive to the methanol extract but resistant to twelve of the 20 antibiotics studied. Within the first 2.5h and 5h of incubation with the methanol extract, the MRSA isolate declined by $1.7\log_{10}$ and $2.3\log_{10}$ respectively while incubation with ciprofloxacin declined the growth by $3\log_{10}$ and $4\log_{10}$ respectively. The methanol extract exhibited the highest killing rates of 13.88×10^5 cell/h against *S. haemolyticus*. The lowest killing rate, 1.86×10^5 cell/h, was against MRSA. 1×10^6 of the resistant staphylococcal cells was completely inhibited within 8hrs and there was no growth after 7 days. The methanol stem extract of *Jatropha curcas* exhibited enhanced bactericidal activity against staphylococcal strains and could be indicated for the empiric treatment of staphylococcal infections. Toxicity studies may need to be carried out to authenticate its use.

Keywords: *In-vitro* kinetics, *Jatropha curcas*, *Staphylococci*, stem bark, resistance profile, time-kill assay.

INTRODUCTION

Resistance to commonly available and affordable antibiotics is particularly a major concern in the management of bacterial infections, especially in resource poor countries (Morton, 1980). Among the numerous bacterial infections, those caused by *Staphylococcus* are of great public health importance. These gram-positive spherical bacteria have been described as one of the most versatile human pathogens due to their ability of acquiring resistance to virtually all known antibiotics. The genus is divided into two broad groups; known as coagulase positive staphylococci and mainly represented by *S. aureus* which has emerged over the past several decades as a leading cause of hospital – and community – acquired infections. The second group, coagulase negative staphylococci are very diverse and are implicated in various infectious processes especially in immuno-

compromised individuals and those with implant devices such as shunts and catheters (Akinkunmi and Lamikanra, 2010). The emergence of multi-drug resistance in *staphylococci* has led to substantial morbidity and mortality rates all over the world.

One of the important approaches to solving the problem of drug resistance has been to seek structurally novel antibiotics that have entirely different mechanisms of action from the currently used agents. Nature has been a source of medicinal agents for thousands of years and an impressive number of modern drugs have been isolated from plants used in the practices of traditional medicine (Gragg and Newman, 2001). Plant-based therapy plays an essential role in healthcare and it has been estimated by WHO that 80% of the world's inhabitants rely mainly on traditional medicines for their primary health care (Farnsworth *et al*., 1985). In the US alone, use of herbal products increased 380% between 1990 and 1997 (Eisenberg *et al*., 1998). In other parts of the world

---

*Corresponding author email: adesidasola@yahoo.com

traditional utilization of medicinal plants for healing is extremely frequent. The primary benefits of using plant-derived medicines include their desirable safety profile and a more affordable acquisition cost (Iwu, 1993; Nebedum *et al*., 2009).

Several ethnopharmacological claims have been made regarding *Jatropha curcas* (physic nut), a member of the family Euphorbiaceae. The extracts of *Jatropha curcas* have wide traditional uses for treating inflammatory conditions, toothaches, warts, gum-bleeding, piles, rashes, wounds, ulcers, allergies, burns, leucodema, scabies, tumors and small-pox (Morton, 1980; Elewude, 1986). The chemical constituents of the bark and leaves of *Jatropha curcas* are glycosides, phytostrerols, flavonoids, steroidal saponins, and tannins while the latex portion of the plant contains proteolytic enzymes and essential oils (Morton, 1980)

Although, traditional utilization of *Jatropha curcas* for healing various ailments is evident in Nigeria, well designed studies validating its phytochemotherapeutic properties are limited. Nevertheless, previous studies in our laboratory have shown that the latex of the plant has potent hemostatic, antimicrobial and wound healing effects (Odusote *et al*., 1996, 1999). In addition, preliminary studies using the stem bark extract of the plant show potent antimicrobial activity against different species of staphylococci including methicillin-resistant strains. Consequently, we present this detailed study to investigate the kinetics of antistaphylococcal activities of the bark extract. Our emphasis is on staphylococci because of their high infection rate, great capability for developing resistance and the recent increased recognition of their community acquired infections.

MATERIALS AND METHODS

Plant collection and identification

Jatropha curcas plant materials (stem bark) were collected from a sub-tropical forest reserve in Ogbomoso, Oyo State, Southwest, Nigeria. The plant was identified and authenticated by Professor Olowokudejo, Department of Botany and Microbiology, University of Lagos, Akoka and a voucher specimen was deposited in the departmental herbarium for reference.

Preparation of Plant Extract
Fresh stem bark samples were thoroughly rinsed with purified water and dried in a hot-air oven (Vindon Ltd, England) at 40°C for 6 days (to avoid thermal degradation of the active principle at higher temperatures) and crushed into powder using a Tornado Mill (Pennwalt Corporation, Pennsylvania, US). Water extract was prepared by soaking 500g of the bark powder in 1L sterile de-ionized distilled water for 24hrs at 4°C. The mixture was then centrifuged at 2000rpm for 10min at 4°C. The supernatant

was then filtered through a 0.45μm membrane with the aid of a suction pressure and freeze-dried (Modulyo Freeze Dryer, England). The methanol extract was prepared by Soxhlet extraction of 500g of the bark powder with methanol for 10hrs. The solvent was removed under reduced pressure at 45°C to give a crude extract. The crude extract was further dried in a vacuum dessicator over anhydrous copper sulphate. Our preliminary study has shown that the maximum solubility of either extract is about 400mg/mL at room temperature (26 ± 2.0^{o}C). Concentrations (400, 200, 100, 50, 25, 12.5, 6.25, 3.125mg/ml) of aqueous and methanol extracts were serially prepared for immediate use in the susceptibility screening.

Bacterial Isolates
Staphylococcal isolates were obtained from the Microbiology Laboratory of Lagos University Teaching Hospital (LUTH), Idi-Araba, Lagos, and the Nigerian Institute of Medical Research (NIMR), Lagos. The isolates consisted of a control strain methicillin sensitive *S. aureus* ATCC 25923), two clinical isolates of methicillin sensitive *S. aureus (w-388 and w-415),* a clinical isolate of methicillin resistant *S. aureus (GS4)* and nine clinical isolates of coagulase-negative staphylococci *(S. haemolyticus, S. sciuri, S. warneri, S. chromogens, S. cohnii* (strains SU-1 and SC-2)*, S. epidermidis, S. lugdunensis* and *S. xylosus).* Preliminary identification was achieved by colony morphology, Gram-staining, catalase and tube coagulase tests and speciation was done using API kit (BioMerieux, France) according to manufacturers' recommendations.

Preliminary Phytochemical Screening
Solvent extracts were tested for phytochemical components by the simple experiments described by Sofowora (1984). 0.5g of each extract was stirred with 5ml of 1% hydrochloric acid on a steam bath. 1ml of the filtrate was treated with a few drops of Mayer's reagent and Dragendorff's reagent respectively to detect the presence of alkaloids. Other qualitative assay methods were used to detect the presence of tannins, phlobatannins, cardiac glycosides, saponins, anthraquinones, flavonoids, saponins and reducing sugars (Sofowora, 1984).

Antimicrobial Susceptibility Testing
The identified staphylococcal isolates were subjected to susceptibility testing using the disk diffusion technique as recommended by CLSI (2006a) guidelines. All isolates were grown on Mueller-Hinton (MH) agar plates (Hi-Media, India) and suspended in MH broth prior to use for the antimicrobial susceptibility test and adjusted to 0.5 MacFarland. The following antimicrobial agents were tested: amoxicillin (25μg); cloxacillin (5μg); tetracycline (30μg); erythromycin (15μg); cotrimoxazole (25μg); cefuroxime (30μg); cefotaxime (30μg); ceftazidime

(30μg); chloramphenicol (30μg); amoxicillin/clavulanic acid (30μg); teicoplanin (30μg); ciprofloxacin (5μg); ofloxacillin (5μg); gentamycin (10μg); penicillin (10 units); amikacin (30μg); vancomycin (30μg); piperacillin-tazobactam (110μg). Resistance to methicillin was determined by placing a 1μg oxacillin disk (oxoid) on Muller Hinton agar without NaCl and incubated for 24hrs at 35°C. Methicillin Resistance was confirmed using CLSI (2006a) published guidelines for the agar screen test.

Screening of extract for antibacterial activities
Eight concentrations of each extract (400, 200, 100, 50, 25, 12.5, 6.25, 3.125 mg/ml) were prepared and antimicrobial effects of each concentration determined using both the agar-well diffusion and calibrated paper disk technique (Perez *et al.*, 1990; Abioye *et al.*, 2004). The plates were incubated at 37°C for 18 – 24hrs in Isotemp incubator (Fisher Scientific Co., USA). Respective proper controls of solvent extracts, and control antibiotic – (ciprofloxacin) were maintained. All assays were performed in triplicate and the antimicrobial activity of each plant extract was recorded as the mean diameter of resulting inhibition zones of growth measured in millimeters.

Minimum inhibitory concentration (MIC) and Minimum bactericidal concentration (MBC)
The MIC and MBC of the extracts against the *S. aureus* strains were determined by the micro-broth dilution method according to the CLSI (2006b) guidelines, using Muller-Hinton broth. The inoculum suspension was prepared from 8h broth cultures and adjusted to obtain 0.5 McFarland turbidity standards. Two fold serial dilutions of the extract were tested to obtain the MIC. The bacterial suspensions were incubated for 24hrs at 37°C. The uninoculated tubes containing growth medium or growth medium and extract were maintained as controls.

Time-Kill Analysis
In vitro killing rates of the *Jatropha curcas* methanol and aqueous extracts and ciprofloxacin were investigated respectively against two highly resistant staphylococcal isolates at a concentration twice the MIC. Inocula were standardized and diluted to 10^6 cfu/ml in fresh Mueller Hinton broth. 1ml volume of freshly prepared extract (methanol or aqueous) or ciprofloxacin at 20 times the final concentration were added to 19ml of broth in 50ml reaction vials while one vial contained only 20ml fresh broth and the organism without the extract or antibiotic (control). The vials were shaken properly and incubated at 37°C. Viable counts at time 0, 0.5, 1.0, 2.5, 5.0, and 10 hours were determined using 6% Tween 80 as the quenching system (Miles *et al.*, 1938). The growth inhibition percentage (1%) of the bacterial strains was calculated according to the following formula:

$$I\% = \frac{N_0 - N_t}{N_0} \times 100$$

where N_0 is the initial number of organisms and N_t is the number of organisms remaining at time t. The extract concentration required to produce 50% (EC_{50}) of the maximal zone of inhibition was obtained by interpolation of concentration-inhibition curves while the time required to reduce the microbial population to 50% (T_{50}) was determined from the survivor – time curves by regression analysis.

Statistical Analysis
All parameters measured were expressed as mean ± standard deviation. Differences between mean values were analyzed by a student t-test at 5% level of significance. $P < 0.05$ was considered to be statistically significant. Data on viable cell count were log-transformed and presented graphically using Microsoft Excel 2003 statistical software.

RESULTS

Phytochemical characteristics of the stem bark extracts of *Jatropha curcas* indicated the presence of soluble carbohydrates, cardiac glycosides, saponins, tannins and free flavonoids while starch, alkaloids and anthraquinones were not detected. The result of the antimicrobial resistance profile of the staphylococcal strains determined with nineteen antibiotics is presented on table 1. Methicillin resistant *S. aureus* (MRSA G-4) was resistant to all the antibiotics tested. *Staphylococcus scuiri* was resistant to 11 of the 19 antibiotics. All the strains studied were also susceptible to ciprofloxacin except MRSA-GS4, *S. cohnii* (strain SU-1) and *S. haemolyticus*. *Staphylococcus aureus* (ATCC 25923) was sensitive to all antibiotics and extracts except amoxicillin, penicillin, ceftazidine and cefotaxime, while *S. warneri* was resistant to cloxacillin only. Two clinical strains of *S. aureus* were resistant to penicillin, amoxicillin, cloxacillin, cotrimoxazole, ceftazidime, cefotaxime, tetracycline and chloramphenicol. The result of antibacterial susceptibility patterns of the stem bark extracts on various strains of staphylococci used in this study is presented in table 2.

10 of the 13 (76.92%) staphylococcal strains studied were susceptible to ciprofloxacin, the control drug. While 4 out of the 13 (30.77%) strains used in this study were resistant to ciprofloxacin, both methanol and aqueous extracts of the stem bark of *Jatropha curcas* inhibited all the tested strains with measurable zones of inhibition. The inhibitory activity of *Jatropha curcas* extracts was more pronounced against *S. haemolyticus* (zone diameter: 27.9 ± 1.14mm). MRSA-GS4 was more sensitive to both the aqeous and methanolic extracts (zone diameter: 13.3 ± 0.82 and 14.5 ± 0.98mm respectively) than ciprofloxacin (10.0 ± 0.58mm). The activity of aqueous extract was not

Table 1. Antibiotic Resistance Profiles of *Staphylococcus* strains used in this study.

Staphylococcus Strains	Antibiotic Resistance
Staphylococcus chromogens	None
Staphylococcus aureus (ATCC 25923)	AMX, PEN, CAZ, CTZ
Staphylococcus aureus (MSSA W-388)	AMX, PEN, CXC, COT, CAZ, CTZ
Staphylococcus aureus (MSSA W-415)	AMX, PEN, TET, COT, CHL, CAZ
Staphylococcus aureus (MRSA G4)	OXA, AMX, PEN, CXC, CAZ, CTZ, TET, ERY, CIP, COT, CHL, AMC, CXM, OFX, GEN, TZP, VAN, AMK, TEC
Staphylococcus warneri	CXC
Staphylococcus haemolyticus	TET, ERY, CIP, CAZ, CTZ
Staphylococcus scuiri	OXA, AMX, CXC, TET, ERY, COT, CHL, AUG, CXM, CAZ, CTZ
Staphylococcus cohnii (SC-2)	AMX, CAZ, TET, PEN
Staphylococcus cohnii (SU-1)	AMX, PEN
Staphylococcus epidermidis	AMX, PEN
Staphylococcus lugdunensis	CAZ, CTZ, AMX, AMC, TET, OFX, PEN, COT, CXC, ERY
Staphylococcus xylosus	CAZ, AMX, CIP, PEN

AMX = Amoxicillin; CXC = Cloxacillin; TET = Tetracycline; ERY = Erythromycin; COT = Cotrimoxazole; CXM = Cefuroxime; CHL = Chloramphenicol; AMC = Amoxicillin/Clavulanic acid; CIP = Ciprofloxacin; OFX = Ofloxacin; GEN = Gentamicin; OXA = Oxacillin; PEN = Penicillin; TZP = Piperazilin/Tazobactam; VAN= Vancomycin; AMK = Amikacin; TEC = Teicoplanin; CAZ = Ceftazidime; CTZ = Cefotaxime

Table 2. Antistapylococcal Susceptibility Pattern of Plant Extract of *Jatropha curcas*.

Microorganisms	Mean Diameter of zone of inhibition in mm (mean ± s.d.)				
	Methanol Extract		Aqueous Extract		*Ciprofloxacin Standard (5μg/ml)* Disc Diffusion
S. aureus ATCC25923	21.6 ± 1.19*	22.4 ± 1.23*	18.1 ± 0.71*	18.2 ± 1.01*	33.9 ± 0.81
S. aureus (MSSA-W388)	21.8 ± 1.12	22.6 ± 1.15	21.1 ± 0.67	21.2 ± 1.00	20.4 ± 0.55
S. aureus (MSSA-W415)	19.1 ± 1.11**	19.2 ± 0.94**	19.8 ± 0.62**	19.1 ± 0.78**	25.5 ± 1.32
S. aureus (MRSA-GS4)	14.3 ± 1.21**	14.5 ± 0.98**	13.1 ± 0.67**	13.3 ± 0.82**	10.0 ± 0.58
S. haemolyticus	27.5 ± 1.26*	27.9 ± 1.14*	25.7 ± 0.98*	25.0 ± 0.83*	10.0 ± 1.02
S. sciuri	19.5 ± 0.66**	19.8 ± 0.86**	17.0 ± 0.54**	17 4 ± 0.70**	16.6 ± 0.60
S. warneri	22.1 ± 0.30*	22.6 ± 0.44*	20.2 ± 0.36*	20.5 ± 0.40*	32.4 ± 0.90
S. chromogens	19.5 ± 0.66*	19.8 ± 0.86*	16.0 ± 0.54*	16 4 ± 0.70*	30.6 ± 0.60
S. cohnii (SC-2)	19.6 ± 1.03**	20.1 ± 1.28**	18.2 ± 0.81**	18.5 ± 1.37**	24.0 ± 2.08
S. cohnii (SU-1)	23.1 ± 0.96*	24.0 ± 1.04*	22.0 ± 0.77*	22.8 ± 0.84*	12.0 ± 1.12
S. epidermidis	18.7 ± 2.02*	19.6 ± 0.99*	17.9 ± 0.66*	18 2 ± 0.58*	27.6 ± 2.67
S. lugdunensis	20.5 ± 1.98	21.2 ± 0.88	18.0 ± 1.29	19.0 ± 1.06	21.5 ± 1.59
S. xylosus	22.0 ± 0.77	22.7 ± 1.35	20.2 ± 1.09	21 6 ± 1.28	23.0 ± 0.89

Values of inhibitory zone diameter were expressed as mean ± sd for *Jatropha curcas* extract (100mg/ml) and compared to ciprofloxacin (5 µg/ml). *Statistically significant (p < 0.05), ** (p< 0.01) compared to the value of ciprofloxacin

statistically different from the methanol extract (P>0.05, n=13) (Table 2). The 100mg/ml concentrations of both extracts have similar activity to 5μg/ml ciprofloxacin against methicillin sensitive strains of *S. aureus* (W-388 and W-415).

Table 3 shows the MICs and MBCs of *Jatropha curcas* extracts. The mean MIC of the extracts ranged from 0.5mg/ml for *S. haemolyticus* to 8.0mg/ml for MRSA-GS4 compared to a range of 0.125μg/ml (*S. aureus* ATCC25923, *S. warneri*, *S. chromogens*) to 8.0μg/ml (MRSA, *S. haemolyticus*) for ciprofloxacin. The MBC of the extracts also ranged from 4.0 to 128mg/ml while that of ciprofloxacin ranged from 0.125 to 16.0μg/ml.

The extracts exhibited lower killing rates compared to the control drug - ciprofloxacin (P>0.05, n=13) (Table 4). Methanol extract exhibited the highest killing rate of 13.88×10^5 cfu/h against *S. haemolyticus* and the least rate of 1.86×10^5 cfu/h against MRSA. Within the first 2.5 and 5.0hrs of incubation with the extract most strains declined by 1.7 to $5\log_{10}$ (methanol extract) and 1.0 to $3.8\log_{10}$ (aqueous extract) while ciprofloxacin declined by 3 to $6\log_{10}$. The antistaphylococcal activities of the extracts and ciprofloxacin are concentration dependent (Table 5). The yield value of each antimicrobial agent on the concentration axis indicates the tolerability potentials of the representative strains (Figs. 1-4). The activity of

Table 3. Minimum Inhibitory and Bactericidal Concentration of Extract of *Jatropha curcas* against Staphylococcal Isolates.

Microorganisms	Mean MIC and MBC of *Jatropha curcas* (mg/ml) and Ciprofloxacin (µg/ml) (mean ± s.d)					
	Methanol Extract		*Aqueous Extract*		*Ciprofloxacin*	
	MIC	MBC	MIC	MBC	MIC	MBC
S. aureus ATCC25923	1.0 ± 0.09	4.0 ± 0.03	2.00 ± 0.06	16.0 ± 0.58	0.125 ± 0.001	0.125± 0.010
*S. aureus (*MSSA-W388)	1.0 ± 0.12	8.0 ± 0.25	2.0 ± 0.07	16.0 ± 0.80	0.5 ± 0.003	0.5± 0.002
*S. aureus (*MSSA-W415)	1.0 ± 1.21	8.0 ± 3.94	2.0 ± 3.02	16.0 ± 4.73	0.5 ± 0.009	1.0± 0.006
*S. aureus (*MRSA-GS4)	8.0 ± 1.28	128.0 ± 1.92	4.0 ± 1.97	16.0 ± 4.82	8.0 ± 0.003	16.0± 0.007
S. haemolyticus	0.5 ± 0.26	2.0 ± 1.04	1.0 ± .2.98	4.0 ± 3.03	8.0 ± 0.004	16.0± 0.004
S. sciuri	1.0 ± 2.60	16 ± 3.85	4.0 ± 1.89	128 ± 5.38	2.0± 0.001	4.0± 0.005
S. warneri	1.0 ± 3.30	8.0 ± 3.44	8.0 ±2.36	8.0 ± 2.40	0.125± 0.003	0.125± 0.006
S. chromogens	2.0 ± 0.64	16.0 ± 0.46	8.0 ± 3.04	16.0 ± 4.70	0.125 ± 0.001	0.125 ± 0.001
S. cohnii (SC-2)	2.0 ± 0.28	16.0 ± 1.05	8.0 ± 2.17	16.0 ± 2.61	4.0± 0.007	4.0± 0.002
S. cohnii (SU-1)	1.0 ± 0.19	8.0 ± 1.67	8.0 ± 0.96	8.0 ± 1.29	0.5 ± 0.003	2.0± 0.006
S. epidermidis	1.0 ± 0.90	8.0 ± 2.24	8.0 ± 2.32	8.0 ± 1.96	0.125± 0.001	0.5± 0.005
S. lugdunensis	2.0 ± 0.63	32.0 ± 2.60	8.0 ±2.82	64.0 ± 4.36	0.125± 0.002	0.5± 0.001
S. xylosus	2.0 ± 0.39	16.0 ± 1.88	8.0 ± 2.08	16.0 ± 1.09	0.5 ± 0.006	2.0± 0.007

Table 4. Rate of Killing / Log Decrease in Colony Forming Units (cfu) At 2 x MIC of *Jatropha curcas* against Representative Staphylococcal strains.

Microorganism	*J. curcas* Extract		Ciprofloxacin
	Aqueous	Methanolic	
S. aureus (ATCC 25923)			
Killing Rate x10^5 cfu/h	4.74 ± 0.62*	5.79 ± 0.39*	13.80 ± 0.
Log$_{10}$ decrease (cfu/ml)			
2.5h	3.0 ± 0.16*	4.0 ± 0.21*	5.8 ± 0.32
5.0h	3.8 ± 0.19**	5.0 ± 0.24*	6.4 ± 0.51
10.0h	4.6 ± 0.40**	5.6 ± 0.36*	7.1 ± 0.48
S. aureus (MSSA-W388)			
Killing Rate x10^5 cfu/h	2.20 ± 0.09***	2.76 ± 0.16***	6.60 ± 0.20
Log$_{10}$ decrease (cfu/ml)			
2.5h	1.2 ± 0.10***	2.2 ± 0.22**	4.0 ± 0.25
5.0h	1.6 ± 0.20***	2.8 ± 0.31**	4.6 ± 0.17
10.0h	2.0 ± 0.17***	3.2 ± 0.26**	6.0 ± 0.21
*S. aureus (*MRSA-GS4)			
Killing Rate x10^5 cfu/h	1.78 ± 0.20**	1.86 ± 0.21**	1.38 ± 0.29
Log$_{10}$ decrease (cfu/ml)			
2.5h	1.0 ± 0.09**	1.7 ± 0.24**	3.0 ± 0.30
5.0h	1.5 ± 0.26**	2.3 ± 0.19**	4.1 ± 0.24
10.0h	1.9 ± 0.18***	3.0 ± 0.17**	6.0 ± 0.48
S. haemolyticus			
Killing Rate x10^5 cfu/h	2.34 ± 0.40**	13.88 ± 0.41**	1.51 ± 0.28
Log$_{10}$ decrease (cfu/ml)			
2.5h	2.6 ± 0.22**	3.0 ± 0.26*	5.0 ± 0.23
5.0h	3.4 ± 0.32*	4.2 ± 0.14*	5.8 ± 0.30
10.0h	4.0 ± 0.24*	5.3 ± 0.32*	6.4 ± 0.22

p-Value is *statistically significant ($p < 0.05$), ** ($p < 0.01$) and *** ($p < 0.001$) compared to the value of ciprofloxacin

both extracts against *S. haemolyticus* was greater than ciprofloxacin by a factor of 1.5 (Figs. 1 and 2).

DISCUSSION

In this study, we investigated the antistaphylococcal activity of *Jatropha curcas* bark extracts in order to provide an *in vitro* basis for its use as natural antimicrobial agents. The sensitivity of all staphylococcal strains to *Jatropha curcas* extracts implies that the intrinsic bio-substances in the extract are naïve to the various drug resistance potential of the isolates. The MIC and the MBC results of the extracts against staphylococcal strains suggest that the activity of the

Table 5. Comparative Effect o*f Jatropha curcas* extract on the growth of *Staphylococcus* strains at 2 x MIC.

| Microorganism | Control | *Jatropha curcas* Extract | | | | | | Ciprofloxacin | | |
| | | Aqueous | | | Methanol | | | | | |
	Rate of Growth $(x10^6 cfu/h)$	Rate of Kill $(x10^6 cfu/h)$	T_{50} (hr)	EC_{50} (mg/ ml)	Rate of Kill $(x10^6 cfu/h)$	T_{50} (hr)	EC_{50} (mg/ ml)	Rate of Kill $(x10^6 cfu/h)$	T_{50} (hr)	EC_{50} (μg/ ml)
Staphylococcus aureus (ATCC 25923)	2.75 ± 0.10	4.74 ± 0.57	2.00 ±0.15	1.59 ± 0.09	3.79± 1.00	1.76 ± 0.10	0.32 ± 0.06	13.80 ± 1.96	1.20 ± 0.07	0.05 ± 0.01
Staphylococcus aureus (MSSA W-388)	2.09± 0.24	2.04 ± 0.36	2.22 ±0.34	0.75 ± 0.22	2.19± 0.66	2.13 ± 0.19	0.60 ± 0.08	2.82 ± 0.16	1.80 ± 0.20	0.39 ± 0.13
Staphylococcus aureus (MRSA G-4)	2.69 ± 0.29	1.78 ± 0.30	2.62 ±0.33	0.54 ± 0.07	1.86 ±0.09	2.34 ± 0.56	0.14 ± 0.02	1.38 ± 0.05	3.19 ± 0.27	7.55 ± 1.05
Staphylococcus haemolyticus	2.88 ± 0.17	2.34 ± 0.66	1.77 ±0.09	0.40 ± 0.06	13.88 ± 1.16	1.19 ± 0.17	0.15 ± 0.04	1.51 ± 0.23	2.56 ± 0.31	7.20 ± 0.71
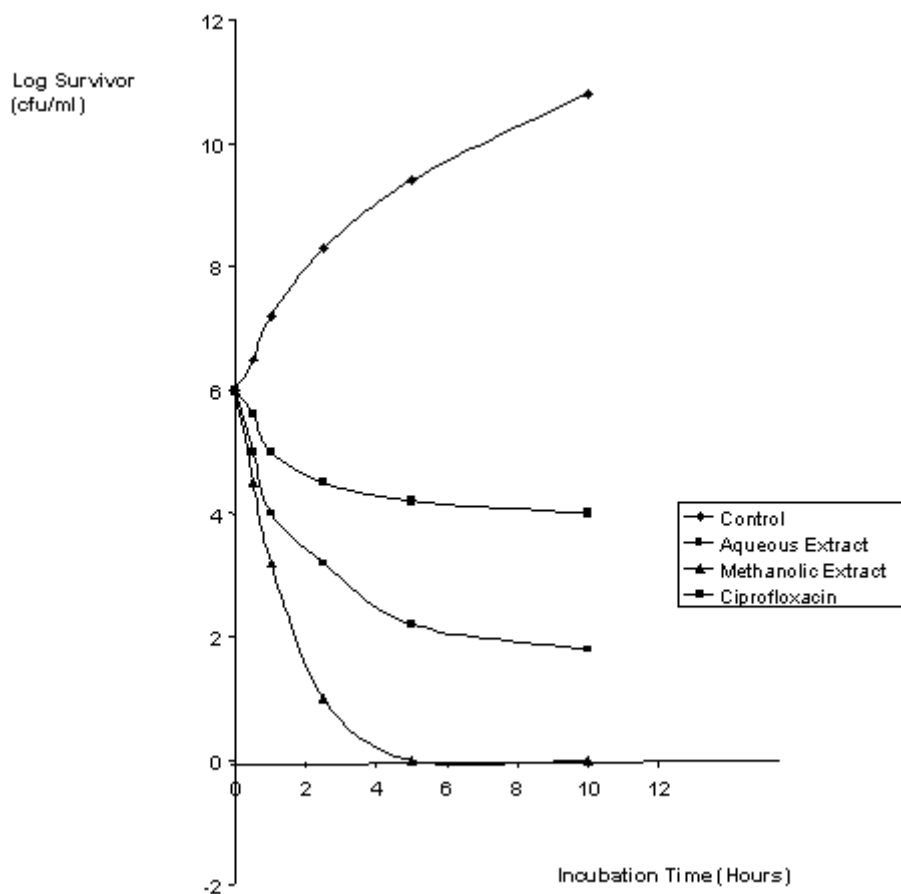
Fig. 1. Comparative Antistaphylococcal activity of *J. curcas* extract at 2 x MIC against *S. haemolyticus*.

extracts is mainly bacteriostatic at lower concentrations as there were no statistically significant differences between the MICs and respective MBCs (P>0.05; n=13). The presence of organic compounds such as tannin and saponin were revealed by qualitative phytochemical screening of the extracts. These phytochemical agents are familiar for their antimicrobial activity (Abioye *et al*., 2004). Tannin, which was detected in the extract, has been shown to form irreversible complexes with proline-rich protein (Hagerman and Butler, 1987) which could result in the inhibition of cell wall protein synthesis. This property may explain the mechanism of action of the *J.*
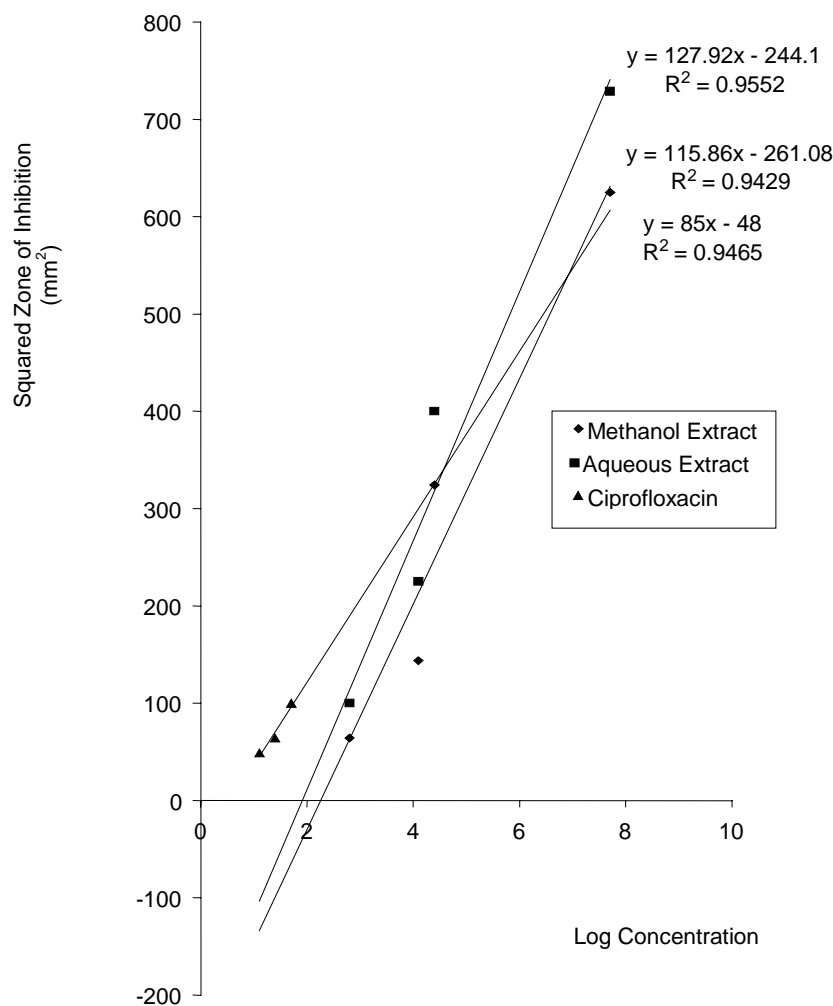
Fig. 2. Graded Concentration effect of *J. curcas* extract on *S. haemolyticus*.

curcas bark extract. Similarly, ciprofloxacin has also been shown to be bactericidal by inhibiting protein synthesis (Sanders *et al*., 1987).

The results of antibacterial susceptibility pattern of *J. curcas* extracts exhibited a concentration – dependent inhibitory activity (bioactivity) on the growth of staphylococcal strains studied. Reactive oxygen species (ROS) has also been implicated in the pathogenesis of staphylococcal infections (Halliwell and Gulteridge, 1990). Elevated synthesis of enzyme methionine sulfoxide reductase (*msr*A) has also contributed significantly to the virulence of *Staphylococcus aureus* (Singh *et al*., 2000). Therefore, the presence of flavonoids in the extract may serve as antioxidant defence mechanisms to ensure removal of reactive oxygen species (ROS) produced by the microorganism, thereby facilitating their rapid death.

The antibiotic resistance profile of the MRSA strain used in this current study indicates resistance to both ciprofloxacin and vancomycin. While ciprofloxacin could be an alternative, vancomycin has been regarded as the "drug of last resort", the most effective in the treatment of MRSA infections. Development of resistance to these antibiotics implies that MRSA infections will soon become untreatable. In a study of 83 MRSA isolates obtained from various sources, ciprofloxacin resistance was detected in 69 isolates (83%) (Raviglione *et al*., 1990). The time-kill analysis of the extracts performed on four strains revealed that the methanol extract exhibited the highest killing rate of 5.79×10^5 cfu/h against *S. aureus* (ATTC 25923). This finding is in fair correlation with the study carried out by Igbinosa *et al*. (2009) who found that the antibacterial activities of the ethanol and methanol extracts of the bark of Jatropha curcas compared favourably with the two standard antibiotics used in their investigation. The low activity (1.78×10^6 cfu/hr) against
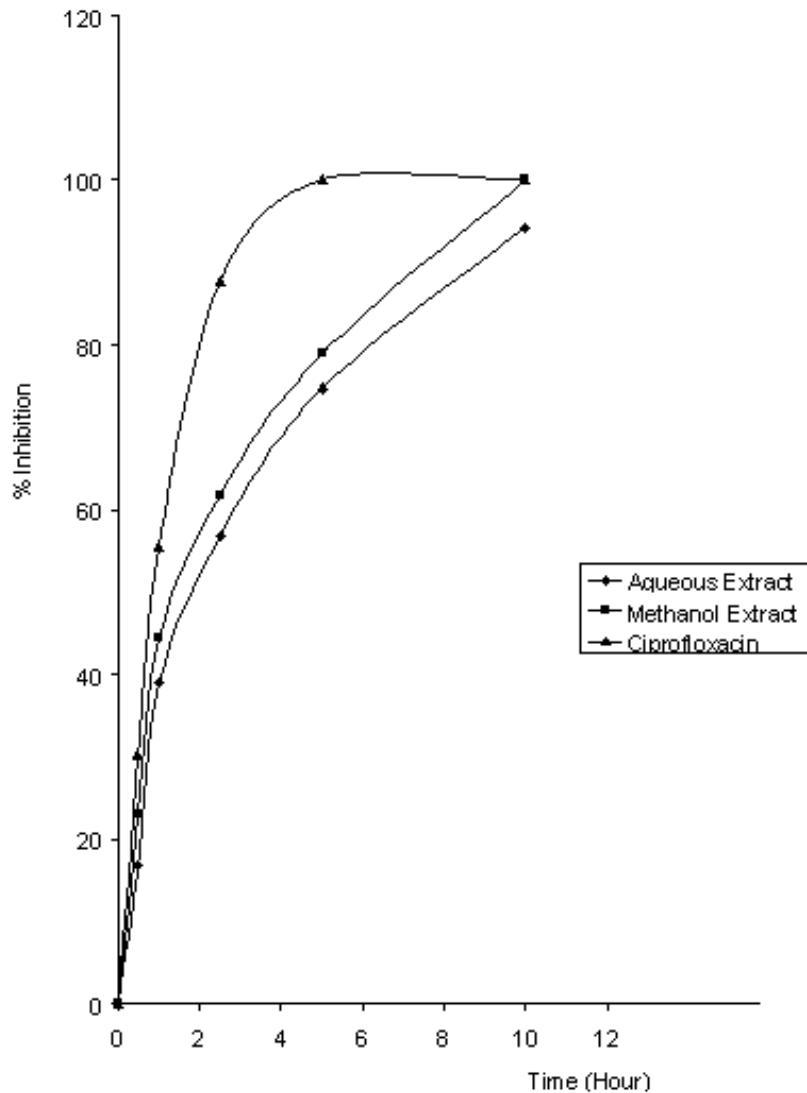
Fig. 3. Effect of *J. curcas* extract on the growth of *S. aureus* (ATCC 25923).

MRSA-G4 could be due to the presence of other compounds, which antagonize the antimicrobial actions of the active principle (Esimone *et al*., 1998). Even so, it is evident that the extract of *J. curcas* has a potential potent bactericidal activity against staphylococcal strains.

The time required to kill 50% population of the microorganism (T_{50}) and the extract concentration that produced 50% (EC_{50}) of the maximal zone of inhibition decreased in the order Aqueous extract > Methanol extract > Ciprofloxacin in most of the strains studied except MRSA-G4 and *S. haemolyticus*. Both extracts and ciprofloxacin did not achieve 100% inhibition of MRSA and *S. aureus* clinical strain (W-388) within 10h of incubation. However, *S. aureus* (ATCC 25923) was completely inhibited (100%) within the first 5hrs and 10hrs by ciprofloxacin and the extracts respectively. We

deduce that MRSA-G4 and *S. haemolyticus* strains were more resistant to ciprofloxacin than the extracts. *Staphylococcus haemolyticus* is one of the main coagulase negative staphylococcal species associated with multidrug resistance, a trend that is also tremendously associated with MRSA (Shittu *et al*., 2005; Akinkunmi and Lamikanra, 2010; Amsterdam *et al*., 2010). Apparently, *J. curcas'* extracts could effectively be employed for the treatments of infections caused by these organisms including MRSA.

CONCLUSION

This study revealed that the aqueous and methanol extracts of the stem bark of *Jatropha curcas* Linn (Euphorbiaceae) are effective antistaphylococcal agents *in vitro*. Further research is consequently required to isolate
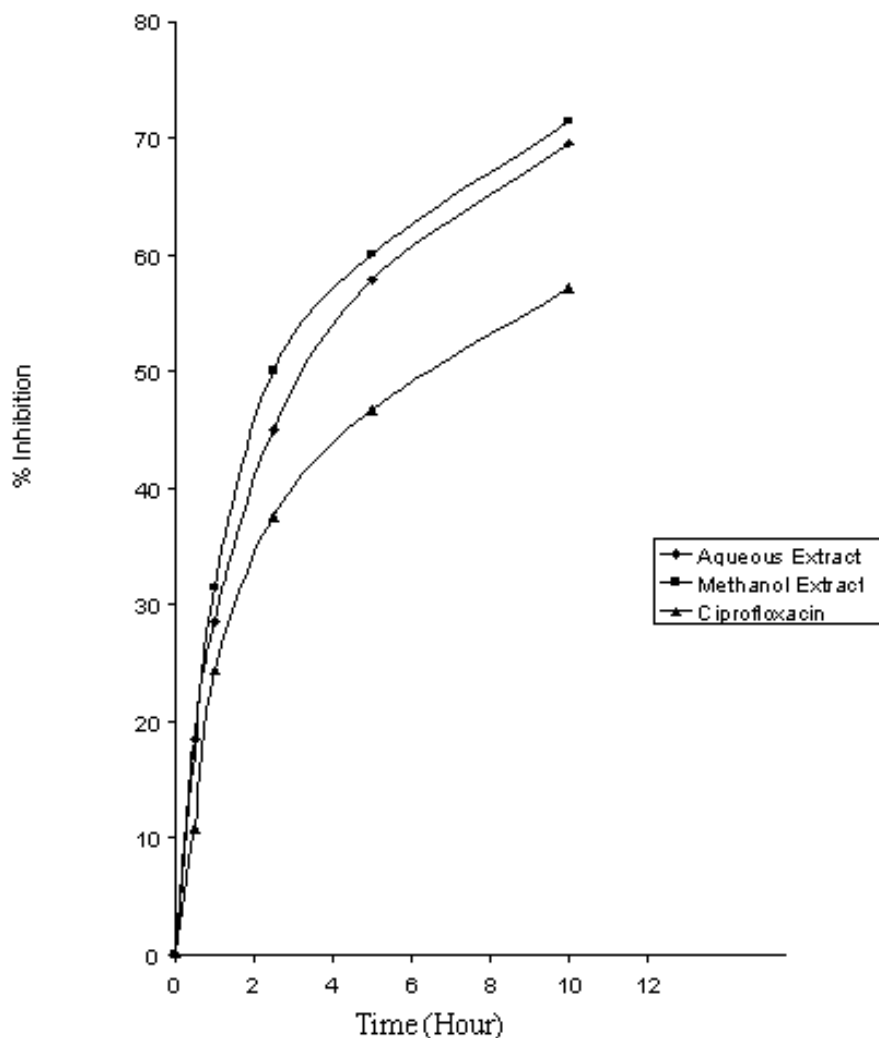
Fig. 4. Effect of *J. curcas* extract on *S. aureus* (MRSA – G4).

the pure active principle responsible for the antimicrobial activity, determine the safety profile and elucidate the molecular basis and mechanism of its activity.

REFERENCES

Abioye, AO., Bamiro, SB., Adesida, SA., Hunpatin, VP. and Adeleke, TI. 2004. Preliminary Phytochemical and antimicrobial Studies of *Phyllantus amarus* Linn (Euphorbiaceae). Nigeria Quarterly Journal of Hospital Medicine. 14:282-287.

Akinkunmi, EO. and Lamikanra, A. 2010. Species Distribution and Antibiotic Resistance in Coagulase-negative Staphylococci Colonizing the Gastrointestinal Tract of Children in Ile-Ife, Nigeria. Tropical Journal of Pharmaceutical Research. 9(1):35-43.

Amsterdam, D., Coombs, G. and Dowzicky, M. 2010. Antimicrobial Susceptibility of Bloodstream Isolates of Staphylococcus aureus: Global Results from the Tigecycline Evaluation and Surveillance Trial, 2004-2008. American Journal Infectious Diseases. 6(1):1-7.

Clinical and Laboratory Standards Institute (CLSI). 2006[a]. Performance standards for antimicrobial disk susceptibility tests; approved standard (9th ed.) Document M2-A9. Wayne, PA, US.

Clinical and Laboratory Standards Institute (CLSI). 2006[b]. Methods for dilution antimicrobial susceptibility tests for bacteria that grow aerobically; approved standard (7th ed.). Document M7-A7. CLSI, Wayne, PA, US.

Eisenberg, DM., Davis, RB. and Ettner, SL. 1998. Trends in alternative medicine use in the United States, 1990-1997. Journal American Medical Association. 280:1569-75.

Elewude, JA. 1986. Jatropha curcas. In: The state of medicinal plant research in Nigeria. Ed. Sofowora, A. Ife University Press, Ife, Nigeria.

Esimone, CO., Adikwu, MU. and Okonta, JM. 1998. Preliminary Antimicrobial Screening of ethanolic extract from the Lichen Usnea subfleridans L. Journal of Pharmaceutical Research and Development. 3:99-102.

Farnsworth, NR., Akerele, O., Bingel, AS., Soejato, DD. and Guo, Z. 1985. Medicinal Plants in Therapy. Bulletin of the World Health Organization. 63:965-981.

Gragg, GM. and Newman, DJ. 2001. Natural product drug discovery in the next millennium. Pharmaceutical Biology. 39:8-17.

Hagerman, AE. and Butler, LG. 1987. The specificity of pro anthocyanidin-protein interactions. Journal of Biological Chemistry. 226:4494-4497.

Halliwell, B. and Gulteridge, JMC. 1990. Role of free radicals and catalytic metal ions in human disease: an overview. Methods in Enzymology. 186:1-85.

Igbinosa, OO., Igbinosa, EO. and Aiyegoro, OA. 2009. Antimicrobial activity and phytochemical screening of stem bark extracts from *Jatropha curcas* (Linn). African Journal of Pharmacy and Pharmacology. 3(2):058-062.

Iwu, M. 1993. Handbook of African medicinal plants. CRC Press, Boca Raton, Florida, US.

Miles, AA., Mistra, SS. and Irwin, JO. 1938. The estimation of the bactericidal power of the blood. Journal of Hygiene. 38:732-749.

Morton, JF. 1980. Carribean and Latin American Folk Medicine and its influence in the United States. Quarterly Journal of Crude Drug Research. 18:57-75.

Nebedum, J., Ajeigbe, K., Nwobodo, E., Uba, C., Adesanya, O., Fadare, O. and Ofusori, D. 2009. Comparative Study of the Ethanolic Extracts of Four Nigerian Plants against Some Pathogenic Microorganisms. Research Journal of Medicinal Plant. 3:23-28.

Odusote, MO., Abioye, AO. and Coker, HAB. 1999. The latex of Jatropha curcas Linn (Euphorbiaceae): A prospective haemostatic agent. Nigeria Quarterly Journal Hospital Medicine. 9: 158-166.

Odusote, MO., Abioye, AO., Coker, HAB. and Muoneke, BC. 1996. Potent bacteriostatic activity of the latex of Jatropha curcas Linn (Euphorbiaceae): A basis for its wound-healing effects. Nigeria Quarterly Journal Hospital Medicine. 6:327-333.

Perez, C., Paul, M. and Bazerque, P. 1990. Antibiotic assay by agar-well diffusion method. ACTA Microbiologica Medica Experimentalis. 15:113-115.

Raviglione, MC., Boyle, JF., Mariuz, P., Pablos-Mendez, A., Cortes, H. and Merlo, A. 1990. Ciprofloxacin-resistant methicillin-resistant Staphylococcus aureus in acute-care hospital. Antimicrobial Agents Chemotherapy. 34(11):2050-2054.

Sanders, CC, Sanders, WE. and Grooving, RV. 1987. Overview of preclinical studies with ciprofloxacin. American Journal Medicine. 82:2-10.

Shittu, AO., Lin, J. and Morrison, D. 2005. The Discovery of a multiresistant *Staphylococcus haemolyticus* clone in the hospital and community environment in Southwestern Nigeria. Ostomy/Wound Management. 51(1):67-70.

Singh, VK., Jayaswal, RK. and Wilkinson, BJ. 2000. Cell wall active antibiotic induced proteins of *Staphylococcus aureus* identified using a proteomic approach. FEMS Microbiology Letters. 199:79-94.

Sofowora, A. 1984. Medicinal Plants and Traditional Medicine in Africa. John Wiley and Sons Limited, London.

Canadian Journal of
pure&applied
sciences

ANTIBIOTICS SUSCEPTIBILITY PATTERNS AND CLONAL RELATEDNESS OF UROPATHOGENIC *ESCHERICHIA COLI* IN ABAKALIKI, EBONYI STATE

*Iroha Ifeanyichukwu Romanus[1] and Ayogu Thomas Eze[2]
[1]Department of Applied Microbiology, Faculty of Biological Sciences
Ebonyi State University, P M B 053, Abakaliki Ebonyi State
[2]Department of Food Technology, Institute of Management and technology
Enugu, P M B 01079, Enugu State, Nigeria

ABSTRACT

Eight months (Feb-Sept. 2009) prospective study was carried out in Ebonyi State University teaching hospital (EBSUTH) Abakaliki to determine the distribution and antibiotic susceptibility pattern of uropathogenic *Escherichia coli* isolated from out-patients with community-acquired urinary tract infections (UTIs) in Abakaliki Ebonyi State, Nigeria. We consecutively collected one hundred and forty (140) non-duplicate isolates of *E. coli* from female out-patient with UTI. Urine samples were analyzed and organisms isolated using standard Microbiology technique, antibiotic susceptibility studies was carried out using Kirby and Bauer method of determining susceptibility. Bla $_{TEM}$ and $_{SHV}$ beta lactamases was determined in resistant isolates by specific PCR and clonal relatedness of strains was determined by randomly amplified polymorphic DNA (RAPD). Antibiotic susceptibility rates for *E. coli* were; aztreonam (86.1%), doxycycline (31%), ampicillin (5%), ceftazidime (99.1%), cefotaxime (95.6%), cefoxitin (91.9%, cefotaxime (96.5%), amoxicillin/clavulanic acid (82.9%), cefepime (89.1%), cefuroxime (89%), imipenem (99%), ciprofloxacin (65.4%), levofloxacin (69.1%), sulphamethoxazole/trimethoprim (6.4%), Nitrofurantoin (96.5%), gentamicin (72%), kanamycin (93.7%) and ticarcillin 39.1%. Bla $_{TEM}$ beta lactamase was polymerase chain reaction positive in all the strains while bla $_{SHV}$ was negative. RAPD analysis grouped our isolates into four clonal groups (A-D) with majority of the isolates belonging to clonal group A (85.7%). Our findings showed high rate of resistance of uropathogenic *E. coli* to ampicillin sulphamethoxazole/trimethoprim, tircarcillin and doxcycline. Uropathogenic *E. coli* resistance to ampicillin and sulphamethoxazole/trimethoprim which is the commonest oral drug of choice in treating UTIs, are worrisome and also the wide distribution of the majority of uropathogenic *E. coli* in one clonal group (A) may have a major public health implications.

Keywords: Uropathgenic *Escherichia coli*, urinary tract infections, susceptibility, random amplified, polymorphic DNA.

INTRODUCTION

The reservoir for urinary tract infections (UTIs) is the human bowel flora and most infections result from uropathogens moving into bladder via the urethra (Kunin, 1997). *E. coli*, a universal bowel inhabitant causes between 80 to 90 percent of out-patients UTIs (Zhang and Foxman, 2003), although only a small fraction of *E. coli* are uropathogenic (Foxman and Riley, 2001). Urinary tract infections are one of the most common bacteria infections in humans both in the community and hospital settings (Tice 1999; Clarridge *et al*., 1998; Sussman, 1998). The incidence of UTI is more frequent in women (17.5% incidence between 18 and 24yrs) (Foxman *et al*., 2000) than in men (0.5% incidence in the same age range) (Krieger *et al*., 1993). The gender difference in the incidence of symptomatic infection is attributed in part to the shorter urethra of women and the proximity of the urethra to the anal opening and vaginal introitus (Hooton *et al*., 1999).

The clinical management of urinary tract infection is complicated by the increasing incidence of infections caused by strains of *E. coli* that are resistant to commonly used antimicrobial agents. Although UTI is not usually thought of as a disease associated with community wide outbreaks, certain multi-drug resistant uropathogenic lineages of *E. coli* have exhibited epidemic behavior (Philips *et al*., 1988). *E. coli* 015:K52:H1 is an endemic cause of urinary tracts infections in Barcelona Spain, (Prats *et al*., 2000). In almost all cases there is a need to start treatment before the final microbiological results are available because antimicrobial susceptibility testing of urinary tract isolates is usually achieved 48 hrs following sampling and therefore in the majority of community acquired UTI, the treatment decision is empirical, being influenced by available data reflecting antibiotic resistance (Blondeau and Tillotson, 1999).

Antibiotics are among the most frequently prescribed drugs in tertiary hospitals and the high consumption of often inappropriate prescribed antibiotics combined with crowding multiple pathology and frequent use of invasive

---

*Corresponding author email: ifynero@yahoo.com

devices is a major factor contributing to high levels of resistance. In the present study, we determined the antibiotic susceptibility patterns and clonal relatedness of uropathogenic *E. coli* in patients attending Ebonyi State University teaching hospital, Abakaliki.

MATERIALS AND METHODS

Sample Collections

Mid-stream urine samples of 140 patients visiting out-patient department of EBSUTH with case of UTI was collected in sterile bottles and innoculated on MacConkey agar plate, incubated at $37^{o}C$ for 24h. Colonies that were positive for lactose and indole were presumptively identified as *E. coli*. One putative *E. coli* colony from each patient's culture was arbitrarily selected for further analysis. A case of *E. coli* UTI was defined as symptoms suggestive of infection and a culture of a clean-catch mid stream urine specimen with more than 10^{2} colony forming units of *E. coli* per milliliter (Manual of Clinical Microbiology, 2002; Gupta *et al*., 1999; Hooton and Stamm, 1997).

Antibiotic Susceptibility Testing

Susceptibility of uropathogenic *E. coli* to 17 different types of antibiotics namely; aztreonam, doxycycline, ampicillin, ceftazidime, cefotaxime, cefepime, cefuroxime, cefoxitin, amoxicillin/clavulanic acid, imipenem, sulpamethoxazole/trimethoprim, Nitrofurantoin, ciprofloxacin, levofloxacin, gentamicin, kanamycin and ticarcillin were determined by Kirby and Bauer method for determining susceptibility. Exactly 0.5 MacFarland equivalent standards of test organisms was inoculated on the surface of sterile Mueller-Hinton agar plate and single antibiotic discs was placed on the surface of the agar plate and incubated for 18-24h at $37^{o}C$. The radial zone of inhibition diameter in mm was taken after the incubation period (Bauer *et al*., 1966). All resistant isolates were further screened for the presence of bla $_{TEM}$ and $_{SHV}$ β- lactamases.

DNA Isolation

Genomic DNA was prepared using the Nucleospin Kit (Macherey & Nagel, Germany) following manufacturer's instructions. Briefly, an overnight culture in a fresh Luria Bertani broth incubated at $37^{o}C$ for 18-24h was prepared of all *E. coli*. 1.5ml of this overnight broth culture was transferred into a reaction tube and centrifuged for 5mins at 8,000rpm and supernatant discarded. Pre-lysis was carried out by re-suspending the pellet in 180µl of T_1 buffer and 25µl of proteinase K, mixed vigorously and incubated at $56^{o}C$ for 30mins with shaking. 200µl of B_3 buffer was added and incubated at $70^{o}C$ for 10mins, 210µl of 96-100% ethanol was added into tube containing 200µl of B_3 buffer and was mixed vigorously until all insoluble particles became soluble. This solution was transferred into a Nucleospin column and centrifuged for

1min at 11,000rpm, flow-through was discarded and the column was placed back into the collection tube. 500µl of BW buffer was added and centrifuged at 11,000rpm for 1min, flow-through was discarded and 600µl of B_5 buffer was added, centrifuged for 1min at 11,000rpm, then flow-through was discarded and the column was centrifuged again for 1min at 11,000. Elution buffer was pre-incubated for 5mins at $70^{o}C$ and 100µl was added into each column and centrifuged for 1 min at 11,000rpm to elute the total DNA. Eluted total DNA was stored at -$20^{o}C$ for further analysis.

PCR Analysis of BLA $_{TEM}$ AND $_{SHV}$ β- Lactamases

Detection of bla $_{TEM}$ and $_{SHV}$ beta-lactamase genes was carried out using specific primers. Appropriate positive and negative controls were used in all cases. The PCR mixture contained 2µl each of buffer, 4.0mM each of dNTP, 2.5µM each of primer, 5µl each of genomic DNA, 1U each of Taq polymerase, and 11µl of water in a total volume of 25µl. The amplification protocol consists of the following steps; initial denaturation at $94^{o}C$ for 5 mins, followed by 34 cycles of denaturation at $94^{o}C$ for 30 sec and a final extension step at $72^{o}C$ for 5 min. Annealing temperatures differed according to the primer pair used and was $42°C$ for TEM and $47°C$ for SHV. Amplified PCR products were separated on 0.8% agarose gels at 100 Volts, stained with ethidium bromide and visualized under UV illumination (Schleslinger *et al*., 2005).

Randomly Amplified Polymorphic DNA (RAPD) analysis of uropathogenic *E. coli* strains

RAPD was performed with all uropathogenic *E. coli* strains using a single primer. The PCR mixture contained 2.5µl each of buffer, 4.0mM each of dNTP, 2.5µM each of primer, 5µl each of genomic DNA, 2U each of Taq polymerase, 1.5µl of $MgCl_2$ and 9.5µl of water in a total of 25µl with the following PCR amplification protocol; initial denaturation at $95^{o}C$ for 5min, followed by 34 cycles of denaturation at $94^{o}C$ for 5min, final extension step of $72^{o}C$ for 5min and $94^{o}C$ for 1 min, final extension step of $72^{o}C$ for 5min and annealing temperature at $37^{o}C$. Amplified PCR products were separated on 1.5% agarose gels at 75Volts, stained with ethidium bromide and visualized under UV illumination (Pacheco *et al*., 1997).

RESULTS

The results of the in-vitro susceptibility testing of uropathogenic *E. coli* are presented in table 1a, 1b. *E. coli* was susceptible to thirteen antibiotics namely; aztreonam (86.1%), ceftazidime (99.1%), cefotaxime (95.6%), amoxicillin/clavulanic acid (82.9%), imipenem (99%), cefepime (89.1%), cefoxitin (91.9%), cefuroxime (89%), gentamicin (72%), kanamycin (93.7%), ciprofloxacin (65.4%), levofloxacin(69.1%) and Nitrofurantoin (96.5%) but resistant to sulphamethoxazole/trimethoprim (94.6%), ampicillin (95%), doxycycline (69%) and tircacillin

(60.9%). PCR analysis for the presence of bla $_{TEM}$ and $_{SHV}$ β- lactamase genes revealed that all uropathogenic *E. coli* (100%) strains were positive for bla $_{TEM}$ and negative for $_{SHV}$. Clonal classification of our isolates by RAPD grouped our isolates into four clonal groups (A-D) with the majority of the strains belonging to clonal group A (85.7%), B(8.3%), C(5.5%) and D(1.5%) (Table 2).

DISCUSSIONS

This paper describes the susceptibility patterns and clonal relatedness of uropathogenic *E. coli* isolated from UTIs out-patients in EBSUTH Abakaliki. We found that over 90% uropathogenic *E. coli* was susceptible to cefoxtin, ceftazidime, cefotaxime, imipenem, nitrofurantoin and kanamycin, while over 65% was susceptible to ciprofloxacin, levofloxacin, amoxicillin/clavulanic acid, cefepime, cefuroxime, aztreonam and gentamicin, while 95% were resistant to ampicillin, (94.6%) to sulpamethoxazole/trimethoprim, 60.9% to ticarcillin and 69% to doxycycline. Resistance of these bacteria to these drugs especially to ampicillin and sulphamethoxazole/ trimethoprim which are the most common oral drugs used in general practice calls for serious concern and therefore empirical treatment of urinary tract infections with these drugs should be avoided. Also regular monitoring is required in order to make reliable information available for optimal empirical therapy for patients with UTIs. Also the wide susceptibility of our *E. coli* to different classes of antibiotics are similar to data's obtained in other countries indicating that *E. coli* is still susceptible to many other antimicrobial agents (Fluit *et al*., 2000; Cunney *et al*., 1992; Jones *et al*., 1999).

Presence of bla $_{TEM}$ beta lactamase in all the strain could be suggested to be responsible to the overwhelming resistance of the uropathogenic *E. coli* to ampicillin and doxcycline, although no further study was done to substantiate this claim. But, it has been established that beta lactamase production is one major mechanism by which Gram- negative organism which *E. coli* is inclusive confers resistance to beta lactam drugs (Medeiros, 1997). Majority of the uropathogenic *E. coli* belong to single clonal group A. This clonal group (A) accounts for 95% of UTI infection caused by *E. coli* strains that were resistant to ampicillin sulpamethoxazole/trimethoprim tircacillin and doxycycline. Although a limited number of isolates were surveyed, this data may suggest that a single *E. coli* clonal group, may cause further increase in antibiotic resistant among *E. coli* isolates from patients with UTI in Abakaliki in the near future. That the *E. coli* isolates with resistance to ampicillin, sulpha-methoxazole/trimethoprim, tircacillin and doxycycline represent a phylogenetically distinct clonal group was suggestive of their similarities to one another. This finding indicates that clonal group A contributes substantially not only to drug-resistant UTIs but also to UTIs in general. Clonal group A appears to represent a new lineage of multi-drug resistant uropathogenic *E. coli* as this is the first reported from this hospital. Although UTIs is usually regarded as a sporadic disease caused by organisms from its hosts own fecal flora, transmission of *E. coli* between sex partners and house hold members had been reported (Foxman *et al*., 1997; Johnson *et al*., 1998). Nosocomial our-break of *E. coli* phylonephrities have also been reported (Tullus *et al*., 1984) and a community wide outbreak of UTI due to single strain have been reported in South London (Philips *et al*., 1988), in California and Minnesota (Manges *et al*., 2001). The presence of these uropathogenic *E. coli* in out-patients revealed prevalence of this infection in the community nevertheless this analysis does not show that this uropathogenic *E. coli* was

Table.1a. Percentage susceptibility of uropathogenic *E. coli* to the cephalosporins.

Amp (%)	Doxy (%)	Ceft (%)	Aztr (%)	Cefo (%)	Cefe (%)	Cefu (%)	Imp (%)	Cefx (%)	Amc (%)
5	31	99.1	86.1	95.6	89.1	89	99	91.9	82.9

Keywords: Amp: ampicillin, Doxy: doxycyxline, Ceft: ceftazidime, Aztr: aztreonam, Cefo: cefotaxime, Cefe: cefepime, Cefu: cefuroxime, Imp: imipenem, Cefx: cefoxitin, Amc: amoxyicillin/clavulanic acid.

Table.1b. Percentage susceptibility of uropathogenic *E. coli* to other antibiotics

Cip (%)	Lev (%)	Gen (%)	Kan (%)	Tic (%)	Nitr (%)	Sxt(%)
65.4	69.1	72	93.7	39.1	96.5	94.6

Keywords: Cip: ciprofloxacin, Lev: levofloxacin, Gen: gentamicin, Kan: Kanamycin, Tic: tircacillin, Nitr: nitrofurantoin, Sxt: sulphamethoxazole/trimethoprim

Table. 2. Percentage distribution of bla $_{TEM}$, bla$_{SHV}$ and Clonal relatedness of uropathogenic *E. coli*.

		Clonal Groups			
Bla TEM (%)	Bla SHV (%)	A (%)	B (%)	C (%)	D (%)
100	0	85.7	8.3	5.5	1.5

circulating in members of the community with cases of UTIs. The presence of majority of the strains in one clonal group could be possible as a consequence of increasing antimicrobial selection pressure or it could be possible that the strains were spread by one or more contaminated products, ingested by community residents which is similar to the way an enteric pathogen such as *E. coli* 015:H7 causes community-wide out break after being disseminated by the consumption of contaminated foods (Bender *et al.*,1997; Dorn, 1993) if a large population of urinary tract infections caused by drug-resistant *E. coli* to commonly used antibiotics in the out-patient settings were due to the ingestion of widely consumed, contaminated foods, this would cause a serious and novel public health problems. In conclusion, we hereby report uropathogenic *E. coli* with high resistance to ampicillin, sulpha-methoxazole/trimethoprim, tircacillin and doxycycline, that majority represent a single clonal group.

ACKNOWLEDGMENT

REFERENCES

Bauer, AW., Kirby, WMM., Sherris, JC. and Turch, M. 1966. Antibiotic testing by standardized single disk method. Am. J. Clin. Path. 45:493-496.

Blondeau, JM. and Tillotson, GS. 1999. Formula to help select rational antimicrobial therapy (FRAT): its application to community and hospital-acquired urinary tract infections. Int. J. Antimicrobio. Agents. 12(2):145-50.

Bender, JB., Hedberg, CW., Besser, JM., Boxrud, DJ., MacDonald, KL. and Osterholm, MT. 1997. Surveillance for *Escherichia coli* 0157:H7 infections in Minnesota by molecular subtyping. N. Engl. J. Med. 33:388-94.

Clarridge, JE., Johnson, JR. and Pezzio, MT. 1998. Cumitech 2B Laboratory Diagnosis of urinary tract infections. Ed. Weissfeld, AS. American Society for Microbiology, Washington, DC, US.

Cunney, R., McNally, J., McNamara, RM., Al-Ansari, EM. and Smyth, EG. 1992. Susceptibility of urinary pathogens in a Dublin teaching hospital. Irish J. Med. Sci. 161:623-5.

Dorn. CR, 1993. Review of food borne outbreak of *Escherichia coli* 0157:H7 infection in the Western United States. J. Am. Vet. Med Assoc. 203:1583-7.

Foxman, B., Zhang, L., Tallman, P., Andree, BC., Geiger, AM., Kospman, JS., Gillespie, BW., Pallin, KA., Sobel, JD., Rode, CK., Bloch, CA. and Marris, CF. 1997. Transmission of uropathogens between sex partners. J. Infect. Dis. 175:989-92.

Foxman, B. and Riley, L. 2001. Molecular epidemiology: Focus on infection. Am. J. Epidemiol. 153: 1135-41.

Foxman, B., Barlow, R. and d' Arcy, H. 2000. Urinary tract infection: estimated incidence and association costs Ann. Epidemiol. 10:509-15.

Fluit, AC., Jonesc, ME., Schnitz, FJ., Acar, J., Gupta, R. and Verhoef, J. 2000. Antimicrobial resistance among urinary tract infection (UTI) isolates in Europe: results from the SENTRY Antimicrobial Surveillance Program 1997. Antonie van Leeuwenhoek. 77:147-52.

Gupta, K., Scholes, D. and Stamm, WE. 1999. Increase prevalence of antimicrobial resistance among uropathogens causing acute uncomplicated cystitis in women JAMA. 281:736-8.

Hooton, T. and Stamm, W. 1997. Diagnosis and treatment of uncomplicated urinary tract infection. Infect. Dis. Clin. North. Am. 11:551-81.

Hooton, TM., Stapleton, AE., Roberts, PL., Winter, C., Scholes, D., Bavendam, T. and Stamm, WE. 1999. Perineal anatomy and urine-voiding characteristics of young women with and without urinary tract infections. Clin. Infect. Dis. 29:1600-1.

Johnson, JR., Brown, JJ., Carlino, UB. and Russo, TA. 1998. Colonization with and acquisition of uropathogenic *Escherichia coli* as revealed by polymerase chain reaction-based detection. J. Infect. Dis. 177:1120-4.

Jones, RN., Kugler, KC., Pfaller, MA., Winokur, PL. and the SENTRY Surveillance Group, North America. 1999. Characteristics of pathogens causing urinary tract infections in hospitals in North America: Results from the SENTRY Antimicrobial Surveillance Program, 1997. Diag. Microbio. Infect. Dis. 35:55-63.

Kunin, CM. 1997. Urinary tract infections. Detection, prevention and management. (5th ed.). Williams & Wilkins. Baltimore, MD, US.

Krieger, JN., Ross, SO. and Simonsen, JM. 1993. Urinary tract infections in healthy university men. J. Urol. 149:1046-8.

Manges, AR., James, MPH., Johnson, RB., Foxman, MD., O' Bryan, TT., Fullerton, KE. and Riley, LW. 2001. Widespread distribution of urinary tract infections by a multi-resistant *Esherichia coli* clonal group. N Engl. J. Med. 345:1007-1013.

Manual of Clinical Micorbiology (7th ed.). 2002. American Society for Microbiology Press, Washington, DC, USA. 442-452.

Medeiros, AA. 1997. Evolution and dissemination of beta- lactamases accelerated by generations of beta-lactam antibiotics. Clin. Infect. Dis. 24 Suppl1:S19-S45.

Pacheco, AB., Guth, BE., Soares, KC., Nishimura, L., de Almeida DF. and Ferreira, LC. 1997. Random amplification of polymorphic DNA reveals serotype-specific clonal clusters among enterotoxigenic *Escherichia coli* from humans J. Clin. Microbiol. 35(6):1521-5.

Philips, I., Eykyn, S., King, A., Gransden, WR., Rowe, B., Frost, JA. and Gross, RJ. 1988. Epidemic multiresistant *Escherichia coli* infection in West Lambert Health District. Lancet. 1038-41.

Prats, G., Navarro, F., Mirelis, B., Dalman, D., Margall, N., Coll, P., Stell, A. and Johnson, JR. 2000. *Escherichia coli* serotype 015:K52:H1 as a uropathogenic clone. J. Clin. Microbiol. 38:201-9.

Schleslinger J., Navon-Venezia, S., Chmelnitsky, I., Hammer-Munz, O., Leavilt, A., Gold, HS., Schwaber, MJ. and Carmeli, Y. 2005. Extended spectrum beta-lactamases among *enterobacter* isolates Obtained in Tel Aviv, Isreal, Antimicrob. Agents Chemother. 49(3):1150-1156.

Sussman, M. 1998. Urinary tract infections. In Topley and Wilsons Microbiology and microbial infections (9th ed.). Eds. Collier, L., Balows. A. and Sussman, M. Arnold, London. 554-636.

Tullus, K., Horlin, K., Svenson, SB. and Kallenius, G. 1984. Epidemic outbreaks of acute pyleonephritis caused by nosocomial spread of P fimbriated *Escherichia coli* in children. J. Infect. Dis. 150:728-36.

Tice, AD. 1999. Short course therapy of acute cystitis: a brief review of therapeutic strategies. J. Antimicrob. Chemother. 43:85-93.

Zhang, L. and Foxman, B. 2003. Molecular epideiomiology o*f Escherichia coli* mediated urinary tract infections. Front Biosci. 8:e235-e244.

Canadian Journal of
pure&applied
sciences

A RESEARCH NOTE

PLANTAIN LEAF BIFURCATION

Godwin Norense Osarumwense Asemota
Department of Electrical and Electronics Engineering
Kigali Institute of Science and Technology, Kigali, Rwanda

ABSTRACT

Bifurcation and phyllotaxy are common and important processes in plants. Plantain leaf bifurcation occurs naturally in Lagos, Nigeria, especially for double-bunching plantains. Plantain leaf bifurcation studies are important because of the perceived special qualities impacted to the plantain pseudostem. Quasi-quantitative techniques were used for this study. As a result, both the physical presentation of the divided leaflets and bunches overhang characteristics were used to predict the most likely positioning of the plantain bunches overhang based on the work done by the plantain pseudostem itself. The results showed that the divergence angle of about 10° between the divided leaflets does not seem to agree with the tenets of the Fibonacci sequence of using the golden mean. The 90° bunches overhang can be used to predict at least two overhang positions. That is, in the same direction and also at 180° out of phase with each other. Similarly, the bifurcated leaflets presentation with four edges to the atmosphere seems to confer some compensatory adaptation to the environment. The thermodynamic implication of the four edges in the bifurcated leaflets ensure increased random mixing and transfer of greater amounts of carbon dioxide, water vapour and energy for improved photosynthate production. Consequently, plantain leaf bifurcation is an efficient self-organising method for coping with more food production under nutrients constraints.

Keywords: Adaptation, divergence angle, double-bunching, fibonacci, pseudostem.

INTRODUCTION

Leaves have been shown to originate from the shoot apical meristem (Puja *et al.,* 2005; Reinhardt *et al.,* 2000), which is a small mound of undifferentiated tissue at the tip of the stem. Reinhardt *et al.* (2000) have further stated that leaf formation begins with the selection of a group of founder cells in the peripheral zone at the flank of the meristem, followed by the initiation of local growth and finally morphogenesis of the resulting bulge into a differentiated leaf. While lateral organ emergence in plant embryos and meristems depends on spatially coordinated auxin transport and auxin response (Ploense *et al.,* 2009) the way some of the tissues of the *Arabidopsis* fruit are moulded indicates how plants may sculpt plant form by modulating the degree of meristematic properties (Girin *et al.,* 2009).

Whereas the mechanisms controlling the switch between meristem propagation and leaf initiation have been identified by genetic and molecular analyses, the radial positioning of leaves, known as phyllotaxis are poorly understood (Reinhardt *et al*., 2000). Phyllotaxy is the arrangement of petals around a flower, leaves around branches, and seeds on seed-heads and pinecones, and are present in many fruits and vegetables (Knott, 2009). Knott has further stated that the appearances which we see in

nature relates to the divergence angle represented by phi. This divergence angle lies in the packing, which gives the best arrangement of objects that minimizes wasted space for optimal resource utilization. Shipman and Newell (2004) demonstrated how phyllotaxis, which is the arrangement of leaves on plants and the deformation configurations seen on plant surfaces, as the energy-minimizing buckling pattern of a compressed shell of the plant's tunica on an elastic deformation. In addition, the strain energy developed is minimized by configurations consisting of special triads of almost periodic deformations. SIAM (2004) has suggested that the origin of external stress in plants is differential growth near the tip of the plant's shoot, which causes an annular region of the plant's tunica (its hardened skin) to undergo compressive stresses. Smith *et al.* (2006) defined phyllotaxis in plants as the regular arrangement of lateral organs around a central axis, where the plant hormone auxin was linked to the molecular mechanisms of morphogenesis and the geometry of phyllotaxis.

Plants are generally made up of branches, leaves, petals, stamens, sepals, florets and trunks (Selvam, 1998), while phyllotaxy or phyllotaxis is the arrangement of leaves on the stem of plants (Korn, 2008; Wikipedia, 2008; Nisoli *et al.,* 2009), which can be arranged in alternate, opposite, whorled or spiral patterns. These leaves branching

_____

Corresponding author email: asemotaegno@yahoo.co.uk

arrangement and architecture are to optimize access to moisture, rainfall, carbon dioxide and sunlight. Seaweed for example, grows with dichotomous branching from an unbranched frond by repeated bifurcations. Naturally, this plant growth is uneven because some branches get out of step with each other and some others cease to divide altogether (Burton, 1998).

Many monocotyledons have leaves of peculiar form. The lamina in a palm arises as a continuous but pleated sheet of tissue, and then, as it expands, it spontaneously tears along the folds so as to form a set of apparent "leaflets". A rather similar result can be achieved when a banana-leaf is torn by the wind, but the palm-leaf is distinctive in tearing automatically to look like compound leaf when mature (Simon *et al.,* 1990). Similarly, the leaves of the banana and other *Musaceae* are split by winds to form what are essentially pinnately compound leaves (Eames and MacDaniels, 2001). The banana (*Musa paradisiaca* subsp. *Sapientum; Musaceae*) is one of the tallest herbaceous plants. Its treelike stem is composed of the sheathing spiral leaf bases, which contain fibres of sufficient strength to make possible the erect habit (Hill and Sharma, 2000; Nelson *et al.,* 2006). Additionally, the plantain, which is a close relative of the banana, is one of the great food plants of the tropics and it is usually eaten cooked or made into powder. Tivy (1998) explained that among the few species of plants which have attained an almost world-wide range in both tropical and temperate latitudes are some of the notorious weeds of domestication and cultivation, such as the plantain (*plantago* spp.). Tivy (1998) further stated that because bananas have been vegetatively propagated for so long, their seed producing capacity has been drastically reduced. This is so because the domestication was the selection of a sterile hybrid able to produce attractive fruit but unable to develop seeds necessary for its perpetuation. Bananas are picked and shipped when green (Nelson *et al.,* 2006). When they are thoroughly ripe, as revealed by their brown blotches on yellow skin; they constitute one of the most healthful and nourishing foods. Bananas have a high content of carbohydrates with some fats and proteins. Indeed, their food value is about three times that of wheat (Hill and Sharma, 2001).

Physiological studies of three plantains in the laboratory, *Plantago major, P. media* and *P. lanceolata* supplied with equal quantities of seeds in three different plots, were given a replicated series of treatments to the soil surface. The different treatments had markedly different selective effects on the emergence of the three species depending upon the type of microenvironment each treatment had created. Quantitative inheritance, being able to measure how much of the phenotypic variation is genetic, as opposed to environments to which different individual plantains are exposed or to random perturbations arising during development, are necessary (Silvertown and

Charlesworth, 2001). However, it is impossible as yet, to tell how much of the phenotypic value of any individual plantain is genetic vs environmental.

Therefore, *Ex post facto* (after the fact) research and hypothesising were the main recourse in this study. These are important research alternatives, which supply the missing links to characteristics and phenomena that occur naturally without the researcher's intervention.

The main objectives of this study include: (i) detailed and systematic examination of plantain leaf midrib division for pattern recognition; (ii) to identify special and specific characteristics of *false horn* plantain leaf division *in situ*. However, only two relevant plantain bunch types are distinguished (Swennen and Vuylsteke, 1987): (1) *False horn* plantain: inflorescence is incomplete at maturity (hands consisting of large fingers followed by few hermaphrodite flowers); (2) *Horn* plantain: inflorescence is incomplete (few hands consisting of few but very large fingers; no hermaphrodite flowers and no male inflorescence; inflorescence axis is terminated by a tail or a deformed glomerule); (iii) to focus on the visual and presentational aspects of plantain leaf bifurcation and its bunches for analyses and possible explanation.

Therefore, *ex post facto* plantain leaf midrib bifurcation was studied from clay soil acidification, ion exchange balance, absorption of available nutrients from soil, effect of calcium deficiency and other ions in the cleavage of middle lamella. Furthermore, enzymatic action on cell wall and separation layers, formation of organometallic complexes, mutations and chromosome abnormalities, and gene-expression, which is correlated with compensatory adaptation to environment have been used for this study.

As a result, literature search, review and soil sample analyses were used to account for the plantain leaf division *in situ*. However, the assumption in the uniform spread of acidity over large neighbouring areas, that ranged from pH 6 to 7 (like neighbouring Oko-Oba and Oke-Aro villages, in Lagos, Nigeria), as reported by Van Wambeke (1992), for south West Africa, was used and this constitutes a major weakness of the research.

MATERIALS AND METHODS

There were two *ex post facto* double-bunching plantain subjects observed to possess bifurcating leaflets in their leaf midribs at Oko-Oba village (August, 2000, Fig. 1) and Oke-Aro village (December, 2001) respectively, near Lagos, Nigeria, which are about 5 Km apart. Photograph of the Oko-Oba village sample (Fig. 1) was taken and a protractor used to measure the angle between the bifurcating (separating) plantain leaflets. The pH of the Oke-Aro soil sample very close to the bifurcating plantain

leaf site was determined later in May 2003 to examine if there were any relationships between plantain leaf bifurcation and pH of soil. Whereas the flaky Oke-Aro soil sample had a pH of 7.5; the clay was mainly composed of Ca^{2+} and Na_2SO_4 (Leached).

But, neither the photograph nor the angle of divergence between the bifurcating plantain leaflets could be obtained for the Oke-Aro plantain pseudostem. This was so because one of the bifurcating leaflets (left hand side) fell over the un-separated leaf portion. And unfortunately, the plantain bunches were harvested soon after this visual observation by the plantains garden owners, before a photograph could be taken.

Because these unpredictable plantain leaf bifurcations occurred naturally, it was thought that *ex post facto* design should be the most appropriate method of study. A weakness of the design was the inability to obtain soil pH soon after the respective visual observations of *false horn* plantain leaf midrib division.

As a result of the peculiar nature of *ex post facto* research, this study was preceded with a review of some factors that could impact on plantain leaf midrib division and analyse the plantain photograph in conjunction with the soil sample, to enable us draw some conclusions about *false horn* plantain leaf bifurcation advantages for enhancing more food production.

Clay soils in tropical regions

Hillel (1998) suggested that the most prevalent minerals in clay fractions of tropical regions are hydrated oxides of iron, and aluminium. The absorbed cations Na^+, K^+, H^+, Mg^{2+}, Ca^{2+} and Al^{3+}, which are not part of the lattice structure could be replaced or exchanged by other cations in the soil solution. This is important in soils as it affects the retention and release of nutrients and other salts as well as for flocculation. Russel (1950) explained that acid soils with displaceable aluminium leach out aluminium compounds when leached with a neutral salt to act as an exchangeable base, which contributes to calcium "exchange acidity". If the pH rises above 5, aluminium hydroxide $(Al(OH)_3)$ are so precipitated that aluminium cations are washed out of acid soils in appreciable quantities (Hillel, 1998). In places with high rainfall and leaching (like Lagos, Nigeria) kaolinite is formed where silica and alkali are removed from soil to form minerals rich in alumina.

Soil leaching and microbial action

Van Wanbeke (1992) related the 11 months (800-1200 mm/year) rainfall of southern parts of West Africa having a pH range of 6 to 7 with a stable and persistent kaolinite soil structure. Leaching of soluble salts, which is formed (Russel, 1950; Van Wanbeke, 1992) during oxidation offers alternative reclamation procedures with technical

and environmental difficulties, caused by soil acidity. This may spread over large neighbouring areas. Allen (1993) explained that some ectomycorrhizal fungi produce calcium oxalate in high concentrations to increase the weathering rates of phosphorous (P) in soils (due to increased cycling rates of cations like Ca, Fe and Al). Because these oxalates preferentially bound Ca, Fe, and Al to phosphates (Russel, 1950), ectomycetes degraded oxalates could enhance soil CO_2 by further weathering P from the clay matrix while maintaining the solution P through binding Ca with secreted oxalates (Allen, 1993). These actions undoubtedly reduce the binding capabilities of Ca and Al and hence (Russel, 1950 and Allen, 1993) increase actively cycling P in the ecosystem. In addition, Russel (1950) explained that leached alkaline soils, with low Ca and high Na, cause accumulation of Sr, which either compromises the vigour of the plant or harm it altogether; these are also important for understanding plantain leaf bifurcation.

Plantain biology

The aerial shoot of bananas and plantains are cylindrical pseudo-stems of overlapping leaf bases, which are tightly rolled around each other to form rigid bundles about 30cm across. New leaves continuously grow up through the centre of the pseudo-stem such that laminas tightly rolled, expand at the top into large, oblong blades with pronounced supporting midrib and well marked, pinnately arranged parallel veins. In addition, each plant carries a crown of ten to fifteen leaves with new ones appearing every 1 or 2 weeks to replace old ones, which have died (Cobley and Steele, 1989). Another study, Norman *et al.* (1996) explained that plantain pseudo-stem commonly have 11 unexpanded leaves within it and carry about 10 expanded leaves for which more than half may have been non-functional, owing to wind damage, senescence and disease. Although both Cobley and Steele (1989) and Norman *et al.* (1996) agreed that when pseudo-stems grown from suckers are about 5.5-10 months old and have produced between 30 and 50 leaves, the apical growing points of the corm becomes reproductive and instead of leaves, it produces an inflorescence which grows up inside the pseudostem on a long un-branched axis.

Because plantain has a free assortment of genes, it cannot remain indefinitely unaffected by mutation of its genes. Simon *et al.* (1990) continued by stating that instances exist where *Plantago coronapus* showed clear evidence that contrasting genes are segregating amongst the population and it is possible to see variations in a whole catalogue of characters such that there is no constant one-to-one relationship between leaf and branch. This is so because a leaf may have no axillary branch or it may have leaves of peculiar form and in some larger ones of warm climates (like that in Lagos, Nigeria), development of the leaf involves an actual separation and destruction of tissue (Fig. 1) like the lamina "leaflets" in palm.

Other literature reviewed, relate symmetry and bifurcation with visual phenotypic patterns and nonlinear mathematical modelling (Golubitsky *et al.,* 2003). Branching with binomial distribution (Mohlenbrock, 2000; Weisstein, 2004), shows a bifurcation as a period doubling, quadrupling, etc, that accompanies the onset of chaos (Khammash and El-Samad, 2004). It could also mean the sudden appearance of a qualitatively different solution as some parameter is varied which in general, is a separation of a structure into two branches or parts.

RESULTS AND DISCUSSION

Two different plantain *false horn* bifurcating leaves were observed at separate time periods in Oko-Oba August 2000 (Fig. 1) and Oke-Aro December, 2001 villages near Lagos, Nigeria that are about 5km apart. The Oko-Oba *false horn* plantain, presented with about 10° angle of divergence between the bifurcating leaflets while the two plantain bunches were pointing approximately in the same direction at about 90° to the horizontal (Fig. 1). Similarly, the Oke-Aro village *false horn* had its bunches approximately at right angles to the horizontal, but about 180° out of phase with each other (pointing in opposite directions).

The angle of divergence between the bifurcating leaflets could not be estimated nor measured because one of the bifurcating leaflets fell over the left hand side of the un-separated region of the bifurcating leaf (probably confirming the a priori assumption of a weak middle lamella of plantain leaf midrib: Allen, 1993; Jones, Jr., 1998; Strafford, 1970). Additionally, before a photograph could be taken soon after the visual observation, these plantain bunches were harvested.
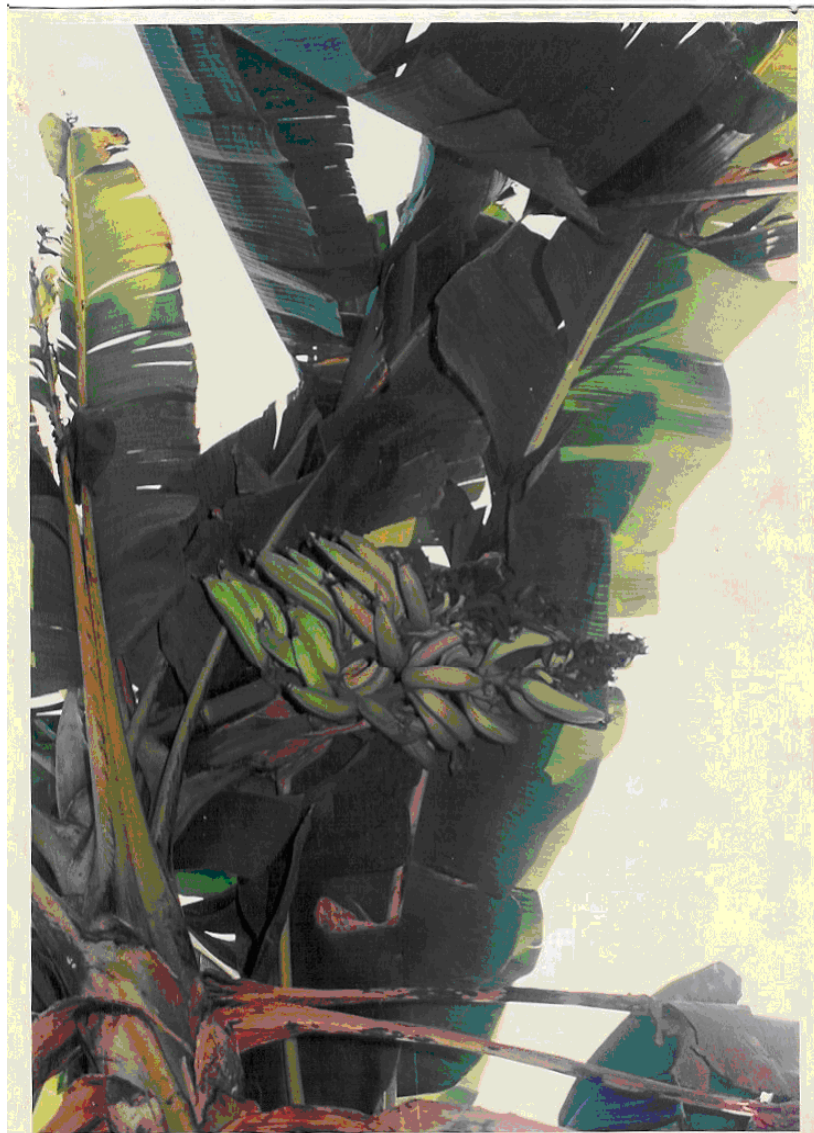
Fig. 1. Plantain Leaf Bifurcation Photograph of Oko-Oba Sample (August 2000).

Although the divergence angle between the bifurcating Oke-Aro plantain leaflets could not be determined, both the cleavage line that seems to derive from the corm and the second right-hand half of bifurcating leaflet were visible, coupled with the 90° bunch overhang. Also, each bifurcating plantain leaf in the two samples was seen to be among the subsisting leaves until bunch harvest. Therefore, we could infer that these subsisting bifurcating leaves until bunch harvest should have positive correlation with fruit formation, maturity as well as genetic compensation for the *false horn* "double bunching" double leafing plantain.

Determinacy of plantain leaf division and bunches overhang

It is, however, not known if there is any regularity or otherwise in determining which leaf sheath would bifurcate or at what angle each bunch would hang, because two samples are not sufficient for generalisation. But, the realisation that such characteristics do exist in plantain pseudo-stems should be instructive for biologists and especially to banana and plantain researchers. This is so because, the bifurcating leaf sheath from the Oko-Oba sample and that from Oke-Aro showed plantains bunches overhang characteristic. Whereas both plantain bunches pointed almost to the same direction for the Oko-Oba sample at about 90° to the horizontal (Fig. 1), those from Oke-Aro lay in the east-west directions and each at about 90° to the horizontal. The 90° bunch overhang observed in these two cases may have been a coincidence, when this overhang phenomenon is placed besides that established fact of plantain bunch direction pointing indeterminacy (Norman *et al.,* 1996). The biophysical, biochemical and/or physiological explanations to confirm or disprove the "double bunching double leafing" 90° bunch overhang is subject to further investigation. It could, also be, a Fibonacci process (Simon *et al*., 1990).

Plant hormones

It has been shown that indole-3-acetic acid (IAA) has been the only receptor with a multiplicity of effects like stimulation of cell division, shoot growth, control of vascular bundle system differentiation, control of apical dominance, senescence delay, promotion of flowering and fruiting which could be explained from knowledge of secondary messengers (Bandurski and Nonhebel, 1989; Jones and MacMillan, 1989; Wilkins, 1989). Thus, the IAA receptor complex could act through a transducer on a Ca^{+2} gate, which in turn affects intracellular calcium and calmodulin-controlled enzymes like the plant NAD kinase. Consequently, the physiological events observed would depend on the most step limiting pathways mediated by calmodulin (Bandurski and Nonhebel, 1989), like media acidification, longer range enzyme changes resulting in the plasticity of cell wall protein matrix, cellulosic matrix, and hemicellulosic matrix. These metabolites act on cell wall, which makes it to divide through newly synthesised wall polymers. These inserted cell wall polymers act as loosening agents that break bonds within or between the cell wall (Jones and MacMillan, 1989).

Wilkins (1989) explained that of the known growth regulators, only IAA initiated growth in the vertical node (Fig. 1). This growth can be initiated in the leaf sheath bases by lowering the pH of the tissue to 3 and terminated by raising the pH to 5 or 7. In addition, the possibility of electrical signal propagation through the tissue during proton transport in apoplasts is known to gravitropically stimulate at least one enzyme system in wheat (possibly plantain) nodes. Horgan, (1989) suggested that growth in a complex multicellular organism like plantain is usually the result of interrelated cell division and cell expansion processes: such that cytokinins respond in the redifferentiation of certain plantain leaf tissue and in combination with auxin, for the regulation of morphogenesis. Furthermore, cytokinins in combination with gibberellins markedly modify the shapes of plantain leaves in intact plantains as to suggest that normal leaf development can be controlled by gibberellins/cytokinins ratio. Milborrow (1989) explained that phytoalexins, which are compounds synthesised in response to attack by a pathogen or damage to plantain tissue, could cause drastic changes in a plantain leaf physiology. Because, IAA can be oxidised by a plantain tissue homogenate, the reaction may be brought about by an unspecific oxidase released from ruptured plantain pseudostem tissues (Allen, 1993; Swanson *et al.,* 1967; Van den Broek, 2002).

Ethylene action

Climateric fruits like banana are characterised by low rates of ethylene production during the pre-climateric or unripe stage, followed by the climacteric stage of sudden increase in ethylene production and respiration, accompanied by other biochemical changes of ripening. Beyer *et al.* (1989) have stated that the purpose of stress ethylene as a "second messenger" is to communicate the effect of stress to the plantain in a way that facilitates a response, such that the synthesis of Acc-synthase results in the accumulation of Acc and onset of stress-ethylene production. Consequently, ethylene-mediated events in the abscission zone of the plantain pseudostem could result in dissolution of the middle lamella of the plantain leaf sheath (Russel, 1950; Strafford, 1970), hydrolysis of the cell walls, and a localised cell enlargement, which facilitates separation by providing shearing action in the plantain leaf. Hilman (1989) related multicellular terrestrial plants and bifurcating plantains with a scissile mode of life and how they have developed strategies to exploit and adapt to their changing environment over time. Because they are continuously developing organisms, their shape is a product of their differential action and activity in regions of their apices; for which,

the cells remain in an embryonic condition called meristems. Mansfield and Snaith (1989) explained that Fusaric acid produced by a fungus causes wilt disease because it impairs the semi-permeability of the plasma membrane by changing the conformational properties of the constituent plantain phospholipids. The theophylin formed, could change the binding of Ca^{2+} and affect plantain membrane function. Sprent (1989) stated that curling and sometimes branching of *plantain leaves* and root hairs are known to precede infection (Allen, 1993), and the way in which such root hair or leaf growth has been modified is not yet, understood.

Enzymatic action and pH-mediated activities
Furthermore, wall-dissolving enzymes such as pectinases, glycosyltransferases, and polygalacturonases act as lectins and are sensitive to Ca^{2+}. Also, wherever bacteria penetrate root hairs (plantain *corm*), Ca^{2+} distribution is altered in the plantain leaf sheath (Bandurski and Nonhebel, 1989; Jones, 1989; Wilkins, 1989). Therefore, the proper amounts of both enzymes and substrate must be present for the curling reaction to occur. But, if there is a problem of ionic balance with more cations (K^+, Ca^{2+}, Mg^{2+}, etc.) being taken up than anions ($H_2PO_4^-$, SO_4^{2-}, Cl^-) as in nitrogen leaving roots for shoots in xylem sap, the plantain must synthesise anions to balance the excess cations in the sap. Consequently, (Clarkson, 1989; Strafford, 1970) the pH balance discrepancies may take biophysical and biochemical pH stats where excess OH^- is neutralised by H^+ from strong organic acids like malate or oxalate made from neutral precursors.

Also, oxalate could be precipitated in plantains as its insoluble Ca^{2+} salt, where malate is transported in the phloem with K^+ to the roots and ultimately to the soil. This process causes soil acidity and reduces the available Molybdenum ($Mo^{-2 \text{ to } +6}$), which is a constituent element of Nitrogenase, Nitrate reductase, and Xanthine dehydrogenase (Clarkson, 1989; Sprent, 1989; Song, 1989; Strafford, 1970). The effects of reduced Mo in soil, which drastically reduces Cd^{2+} availability include poor nitrogen fixation capacity, highly reduced soil fertility and seriously hampered crop production. Hence, the occurrence of plantain leaf bifurcation is to compensate for these adverse effects.

Plant needs and organometallic complexes
Water, reduced carbon, reduced nitrogen, phosphate, potassium, and a diminishing indefinite list of other elements (Canny, 1989) in lesser amounts of magnesium, calcium, sodium, etc. form the general need of all plant cells. Although (Jones, Jr., 1998; Canny, 1989) only reduced carbon and reduced nitrogen are not obtained from the soil, the reduced carbon is made in abundance where the cells are green and remote from the soil. Canny (1989) added, by showing that anions in the sap are principally phosphate and occasionally chloride and

organic anions like malate, which has a sap of pH between 7.5 and 8.5. Clarkson (1989) explained that the packing capacity of plantain phospholipid headgroups when disturbed showed protrusions of intrinsic membrane proteins, which float and displace the headgroups as they do so. Additionally, calcium ions control leakage of plantain solutes through the formation of linkages with negatively charged ions or headgroups. Stronger plantain headgroup linkages result in more rigid headgroup packing when formed with some other divalent (Van den Broek, 2002), like, Cd^{2+} and trivalent, La^{3+} and Al^{3+} cations. These cations inhibit plantain membrane bound enzymes like ATPase and compromise the integrity of plantain cell wall (Russel, 1950; Strafford, 1970).

Bond cleavage and wall weakening
Thomas and Vince-Prue (1989) stressed that plantain leaf perception, transmission and floral evocation are three independent components in a chain; leading to flowering. There is, therefore, a requirement for a number of favourable cycles before the plantain leaves are induced. Sometimes, non-inductive cycles interpolated into a series of inductive cycles do cause flowering. This "fractional induction" has been shown to persist over several weeks of non-inductive cycles as in *Plantago lanceolata*, long day plant (LDP). Jones and MacMillan (1989) stated that transglycosylation in the plantain cell wall results in the cleavage of a glycosyl bond, which causes a weakening of the wall followed by transfer of the polysaccharide terminus to a new position. The formation of a new glycosylic bond in plantain is catalysed by transglycosylases, which serves the dual purpose of plantain glycosylic bond cleavage and synthesis. It has been shown by Beyer *et al.* (1989) that because ethylene participates in all phases of plantain behaviour, like the binding of olefins to metals, it is generally accepted that plantain in vivo ethylene receptor site should contain a metal (Ca, at least), based on the principles of organometallic chemistry.

***False horn* compensatory adaptation to the environment**
Hilman (1989) explained that the plantain apex is a self-determining region, which controls cell differentiation. It also affects those processes that culminate in the non-determinate growth habits of most perennial and vegetative monocarpic plants (*plantain*), reflecting the interplay between gene-expression in cells derived from the plantain meristem and responses to the environment (Fig. 1). Therefore, the successful existence of a plantain leaf bifurcation depends on its sensitivity and responsiveness to environmental changes. This includes adaptive changes that result in compensatory growth effects (plantain leaf bifurcation) as well as, its attendant correlative relationships. Clarkson (1989) explained that physiologically active plantain gibberellins could reduce plantain headgroups reordering, increase ionic

conductance and bilayer fluidity. Therefore, plantain nutrient deficiencies may bring about major changes in the abscisic acid and gibberellins content of plantain shoots and roots, which ultimately affects plantain membrane permeability when interacting with plantain lipid headgroups (Fig. 1).

Chromosome abnormalities
Van den Broek (2002) suggested that many proteins deform plantain DNA when bending, which equally involves, stretching, kinking and/or unwinding of the double helix. The plantain energy cost, if not provided by ATP, is obtained from the contacts between plantain DNA and enzymes. Therefore, whenever the plantain DNA forms a left-handed super helix around the nucleosomes, it must be bent under a constant angle (Fig. 1). During plantain cell division, duplicated chromosomes are pulled apart (Fig. 1) by semi-flexible polymers called microtubules. Overstretching of the plantain DNA structure is only possible when the plantain DNA is not torsionally constrained or when a single strand break is present. Alternatively, the plantain DNA could have its two strands separated as shown in Fig. 1.

Lester and Bohlin (1984) explained plantain leaf bifurcation as chromosomal alterations, regulatory gene mutations and developmental bifurcations caused by an accumulation of minor plantain mutations with reverse patterns of gene expression. This is so because certain plantain gene complexes have been broken and new ones formed with their structural genes changed and expressed phenotypically in plantain leaf bifurcation (Fig. 1).

Simiarti *et al.* (2001) explained near mirror-image plantain leaf bifurcation architecture arising during leaf development from shoot apical meristem (SAM). These results in plantain leaf primary vein bifurcation at the tip to form secondary veins, which elongate basipetally toward the primary vein (Fig. 1). In cases where the cells of the SAM resemble plantain pseudostems that have the capacity for self-regeneration in undifferentiated state, the plantain leaf primordia is generated from its peripheral zone (Fig. 1). Similarly, Tsiantis *et al.* (1999) suggested that disturbed auxin gradient transport both within the plantain leaves and across the plantain vegetative axis could mediate in certain facets of the mutant phenotype. This situation occurs when signals involved in ligular differentiation originate near the plantain leaf midrib during embryogenesis of the plantain leaf sheath (Fig. 1).

Nutrient availability
Hilman (1989) related correlative phenomena with nutrient availability and competition in consonance with compensatory growth effects in apical dominance, coupled with the nutritive state of the plantain. Similarly, Baker (1989) suggested that plantain leaves normally present a very large surface area (Fig. 1) to the surrounding air to facilitate CO_2 assimilation and

transpiration as a consequence of the structural organisation of plantains growing in air (Woodward and Sheehy, 1983). As a result, bifurcated plantain leaves in air further presents a much larger surface area and four leaf edges to the atmosphere to better optimise resources made available to it. Schopfer (1989) related factors such as light interference with the realisation of plantain leaf genetically determined bifurcation patterns by selectively stimulating the expression of defined parts of the genetic information and inhibiting the expression of others. This goes to show that enzyme activities are essential elements in plantain leaf bifurcation due to photo-morphogenetic control (Fig. 1).

Further, Gregory (1978) and Sexton and Woolhouse (1989) explained that the breakdown of chlorophyll and dissolution of the plantain thylakoid membrane may proceed almost to completion with the plantain chlorophyll envelope, mitochondria and plasma membrane remaining intact or showing little signs of plantain leaf midrib disruption (Fig. 1).

Infection and gene modification
Allen (1993) showed mycorrhizal infection to increase the number of vascular bundles, and morphological changes in host plantains and consequently alter the ability of plantains to survive stress and gain access to resources that ultimately improve plantain fitness (Fig. 1). Swanson *et al.* (1967), Simon *et al.* (1990) and Sengbusch (2002) explained plantain leaf diakinesis as the continuation of plantain leaf diplotene where four plantain leaf chromatids are separated into twos, and the bivalent is held together by one or more plantain leaf chiasmata at points in which neighbouring plantain leaf chromatids have broken and rejoined into new arrangements at plantain leaf crossover.

Consequently, particular pairs of plantain leaf-linked genes (Theurer, 1984) (Pl_1 and Pl_2) may be separated (Fig. 1) or combined at different frequencies (Swanson *et al.* 1967), which may be dependent on the physical distance between these plantain leaf genes on their common chromosomes.

Additionally, Swanson *et al.* (1967) suggested plantain leaf fibrils about 40Å in diameter to be the basic longitudinal unit of the plantain leaf chromosome in division, with each plantain leaf chromatid quadripartite and each plantain leaf chromosome, possibly octipartite. Where, of course, plantain leaf ruptured cells are enzymatically relaxed for each plantain leaf chromatid to bifurcate still further (Fig. 1).

Effects of calcium and other cations on plantain leaf division
Strafford (1970), Simon *et al.* (1990) and Russel (1950) explained how Ca^{2+} combines with pectic acid to form

calcium pectate which is a constituent of the middle lamella of the plantain leaf cell wall, such that, a shortage of calcium weakens the plantain leaf cell wall, and causes it to bifurcate (Fig. 1). Similarly, a high number of chromosome abnormalities could be traceable to the roles calcium ions play in plantain leaf chromosome structure in tending to connect protein and plantain leaf DNA components together. Jones, Jr. (1998) suggested four categories of nutrient requirements for banana (and possibly, plantains) whose quantities of supply have implications for plantain leaf bifurcation, and plantain and banana pseudostems survival. So, very high requirements are for $N^{-3\ to\ +5}$, $P^{-3,0,+3,+5}$, K^+; high for: Mg^{+2} and B^{+3}; medium for: $S^{-2,-4,-6}$ and low for: Ca^{+2}, $Cu^{+1,+2}$, $Fe^{+2,+3}$, $Mn^{+4\ to\ +7}$ and Zn^{+2}.

In addition, ammonium toxicity could lead to lesions in plantain pseudostems, cupping of leaves and, decay of conductive tissue at the base of pseudostem (Fig. 1). Magnesium deficiency may also occur while high Phosphorus (P) may interfere with normal Ca nutrition and consequently Ca deficiency in plantain leaf midrib lead to bifurcation (Russel, 1950; Strafford, 1970; Van Wambeke, 1992; Allen, 1993; Kanwal *et al.,* 2008).

Soil analyses
Van Wambeke (1992), Allen (1993) and Russel (1950) explained that calcium deficiency can also occur in alkaline soils low in calcium but high in sodium (Na), especially on highly leached soils that lead to boron (B) deficiency as exemplified by the Oke-Aro soil sample pH. As a consequence, both calcium and boron deficiencies may indirectly interfere with the plantain leaf midrib by allowing other substances like strontium (Sr) to accumulate in the plantain leafsheath tissues so as to either compromise the vigour or actually harm the plantain leaf midrib (Strafford, 1970; Russel, 1950; Smit and Combrink, 2004). In addition, the presence of free calcium carbonate in alkaline calcareous soils can affect the availability of B to plantains. Also, the Ca/B ratio in plantain leaf tissues can be used to assess B deficiency, sufficiency and toxicity in plants. In addition, genotypic variation in crop plants (possibly, plantains) can be related to the quality of B and Ca uptake (Kanwal *et al.,* 2008).

Similarly, Srivastava and Gupta (1996) suggested that boron deficiency affects the activity of the cambium tissue, such that longitudinal plantain leaf midrib cell walls give a serated appearance due to irregular thickening and disorganisation of the middle lamellae with longitudinal lesions appearing along the plantain pseudostem vesicular tissues (as in plantain leaf bifurcation, Fig. 1). Whereas molybdenum (Mo) deficiency results in "whiptail symptom", the appearance of chlorosis in the plantain leaf basal interveinal areas of young leaves progresses toward the leaf margin or midrib

as in Fig. 1, (www.gov.nf.ca/agric/pubfact/Fertility/ nutrition.htm, 2003), to cause plantain leaf midrib bifurcation.

Strafford (1970) related mottling of leaves along the plantain leaf midrib middle lamella with Ca and Mo deficiency. Jones Jr. (1998), Allen (1993) and www.gov.nf.ca/agric/pubfact/Fertility/nutrition.htm, (2003) explained that the middle lamella of the plantain leaf cell wall will not be completely formed with Mo deficiency (Fig. 1). This is so because Mo is strongly absorbed by Fe and Al oxides. This Mo absorption is pH dependent coupled with that fact that, P and Mg enhance Mo uptake while sulphate (SO_4) reduces Mo uptake. The cumulative effects reduce soil fertility, reduce availability of useful cations and anions for good food production, which ultimately leads to dismal harvest.

Heavy metals binding mechanisms
Harborne (1997) explained that heavy metals binding (like Pb, Zn, and Ni) to plantain leafsheath tissues in the plantain root cell wall could result in the accumulation/detoxification of peptide chelates, which show themselves in a divergence (Fig. 1) of biochemical adaptive responses, that are dependent on metals present for both primary and secondary metabolism.

Biochemical factors
Avigad and Dey (1997) suggested plantain frutans to be linear or branched polymers of β-fructofuranosyl-fructose linkages of oligosaccharides where the plantain leaf tetrasaccharides may be cleaved into a linear inulin type structure and a branched (Fig. 1), bifurcose (1 and 6-kestotetraose) levan type structure by invertase enzymes. Lam (1997) explained that plantain leaf genes encode protein kinases with calcium as a signal transduction intermediate, especially with calmodulin as it could change plantain leaf membrane permeability. Consequently, these types of gene regulation appear in naturally occurring plantain leaf tissue differentiation (bifurcating plantain leaflets, Fig. 1), and have their genetic loci controlled by developmental processes. So, plantain leaf midrib mutations at these loci alter the form of plantain leaf organs in both the early and late steps of their phenotypic developments. These occurrences represent the causes and effects between plantain leaf cell linkages and environmental factors for meristematic cells development (Fig. 1).

Whereas other elements like vanadium, tungsten, titanium, nickel, cobalt, copper and chromium (Strafford, 1970 and Hydroponicsbc, 2003) play their parts as participants in enzymatic reactions and DNA synthesis, the genes which differ among themselves and are revealed in phenotypic expression seem to be organised along the length of the chromosome in linear fashion (Swanson *et al*., 1967) which bears resemblance to the longitudinally

length-wise plantain leaf midrib bifurcation observed in the December 2001 and August 2000 plantain leaf (shown in Fig. 1).

Similarly, Lester and Bohlin (1984) explained plantain leaf developmental bifurcation as the small genetic mutations which may accumulate to the point where a new developmental pathway may emerge resulting in drastic morphological changes, where in fact, the difference between evagination (to turn inside plantain leafsheath out or like inverted "vagina") and invagination (to dent or force a plantain leafsheath inwards, or form a hollow in-growth) could be small, but the phenotypic effect is quite noticeable (Fig. 1).

Clay soil acidification, enzymatic dissolution of separation layers, effect of photo-morphogenesis and burden to bear more food, seem responsible for plantain leaf phenotype. Also, the parts ions play in connecting and binding proteins and DNA components together, were equally implicated in plantain leaf bifurcation of two leaflets on a midrib along the cleavage line, which derives from the corm in genetic compensation. Analysis also show that turbulence at leaf-free air interface, results in greater heat, water vapour and carbon dioxide mixing and transfer due to random eddies, for more photosynthate production. These deductions were so because these bifurcated leaflets subsisted until plantain bunch harvest. It was also observed that plantain leaf midrib division seems to give special strength and stability to the plantain pseudostem. This is especially so because the pseudostem was able to carry the plantain bunches as cantilever. The Physics of the work done by the two peduncles carrying the plantain bunches, at right angles to the horizontal is zero. This is so because the value of cosine 90^0 equals zero (Force x distance x cos $90°$ = 0). As a consequence, two directions are possible for the plantain peduncles to overhang at about $90°$ to the horizontal. That is, either in the same direction as in Fig. 1 or diametrically opposite directions at about $180°$ out of phase, to each other. Additionally, the divergent angle between the divided leaflets was about $10°$ ($±0.5°$), while the plantain bunches were hanging at about $90°$ to the horizontal. From literature it was reported that only about 5% of the sunlight is converted by a leaf for photosynthesis (Woodward and Sheehy, 1983). So, the divided leaf of the plantain under study is able to use about 10% of the sunlight available to it. As a result, this plantain midrib leaf division mechanism represents a genetic improvement. It is also able to acquire and convert about twice the quantity of sunlight available for more food production when compared to other undivided plantain leaves. Therefore, bifurcated plantain leaf is about 100% more energy efficient and has higher capacity of resources utilisation, for enhanced food production, compared to the undivided leaf.

CONCLUSION

Despite all the enumerated weaknesses of the *ex post facto* research and hypothesising, the special strengths impacted to the plantain pseudostem and peduncle coupled with the thermodynamic implications of a plantain leaf presenting four edges to the air in the atmosphere, confers some interesting characteristic properties and also nouvelle plantain leaf symmetry. This above plantain leaf symmetry ensures that at least twice the amount of water vapour, carbon dioxide, sunlight energy and other nutrients is transferred into the plantain and converted into photosynthate for more food production, than it would have been without this leaf midrib division. Therefore, plantain leaf midrib bifurcation is both advantageous and important to the plantain form, function, strength and stability. These characteristic phenomena have, thus far, been observed with the "double-bunching" plantain species, which could have arisen principally from Ca^{2+} and Mo deficiencies, thereby leading to genetic improvement. Most importantly, this plantain leaf bifurcation phenotype discussed in this study should be a reliable guide to the genotype, at least, where dominant genes are concerned.

Abbreviations
IAA, indole acetic acid; LDP, long day plant; SAM, shoot apical meristem

REFERENCES

Allen, MF. 1993. The Ecology of Mycorrhizae. Cambridge University Press. London. 1-153.

Avigad, G. and Dey, PM.1997. Carbohydrate Mechanism: Storage Carbohydrates. In: Plant Biochemistry. Eds. Dey, PM. and Harborne, JB. Academic Press. London. 503-515.

Baker, DA. 1989. Water Relations. In: Advanced Plant Physiology. Ed. Wilkins, MB. English Language Book Society/Longman. London. 297-313.

Bandurski, RS. and Nonhebel, HM. 1989. Auxins. In: Advanced Plant Physiology. Ed. Wilkins, MB. English Language Book Society/Longman. London. 1-16.

Beyer, Jr., EM., Morgan, PW. and SF. Yang. 1989. Ethylene. In: Advanced Plant Physiology. Ed. Wilkins, MB. English Language Book Society/Longman. London. 111-124.

Burton, RF. 1998. Biology by Numbers: An Encouragement for Quantitative Thinking. (1st ed.). Cambridge University Press. Cambridge. 97-204.

Canny, MJ. 1989. Translocation of nutrients and hormones. In: Advanced Plant Physiology. Ed. Wilkins, MB. English Language Book Society/Longman. London. 277-294.

Clarkson, DT. 1989. Ionic relations. In: Advanced Plant Physiology. Ed. Wilkins, MB. English Language book Society/Longman. London. 319-343.

Cobley, LS. and Steele, WM. 1989. An Introduction to the Botany of Tropical Crops. (2nd ed.). Longman. London. 1-371.

Eames, AJ. and MacDaniels, LH. 2001. An Introduction to Plant Anatomy. (2nd ed.). Tata McGraw-Hill Publishing Company. New Delhi. 335.

Girin, T., Sorefan, K. and L. Ostergaard. 2009. Meristematic sculpting in fruit development. Journal of Experimental Botany. 60 (5):1493-1502 Doi:10.1093/jxb/erp031.

Golubitsky, M., Langford, WF. and Stewart, I. 2003. Symmetry and bifurcation in biology. Banff International Research Station. Canada. 1-2. Available online:

http://www.pims.math.ca/birs/workshop/2003/03w5075

Gregory, RPF. 1978. Biochemistry of photosynthesis. (2nd ed.). A Wiley Interscience Publication. John Wiley & Sons LTD. Chichester. 132-195.

Harborne, JB. 1997. Biochemical plant ecology. In: Plant Biochemistry. Eds. Dey, PM. and Harborne, JB. Academic Press. London. 503-515.

Hill, AF. and Sharma, OP. 2000. Hill's Economic Botany. (1st ed.). Tata McGraw-Hill Publishing Company. New Delhi. 507-548.

Hillel, D. 1998. Environmental Soil Physics. Academic Press. New York. 75-100.

Hilman, JR. 1989. Apical dominance. In: Advanced Plant Physiology. Ed. Wilkins, MB. English Language Book Society/Longman. London. 127-144.

Horgan, R. 1989. Cytokinins. In: Advanced Plant Physiology. Ed. Wilkins MB. English Language Book Society/Longman. London. 53-70.

Hydroponics-BC. 2003. Available online:
http://www.Hydroponics-BC

Jones, RL. and MacMillan, J. 1989. Gibberellins. In: Advanced Plant Physiology. Ed. Wilkins, MB. English Language book Society/Longman. London. 21-47.

Jones, Jr., BJ. 1998. Plant Nutrition Manual. CRC Press LLC. Florida. 9-138.

Kanwal, S., Aziz, T., Maqsood, MA. and N. Abbas. 2008. Critical ratio of calcium and boron in maize shoot for optimum growth. Journal of Plant Nutrition 31:1-8.

Khammash, M. and El-Samad, H. 2004. Systems biology: From physiology to gene expression. IEEE Control Systems Magazine. 24(4):62-75.

Knott, R. 2009. The Fibonacci Numbers and Nature- Part 2 Available online: http://www.mcs.surrey.ac.uk /Personal/R.Knott/Fibonacci/fibnat2

Korn, RW. 2008. Phyllotaxis: Theories and Evaluation. International Journal of Plant Developmental Biology. 2 (1):1-12.

Lam, E. 1997. Nucleic acids and proteins. In: Plant Biochemistry. Eds. Dey, PM. and Harborne, JB. Academic Press. London.143-195.

Lester, LP. and Bohlin, RG. 1984. The Natural Limits of Biological Change. Zondervan Publishing House: Probe Ministries International. Texas. 126-185.

Mansfield, TA. and Snaith, PJ. 1989. Circadian rhythm. In: Advanced Plant Physiology. Ed. Wilkins, MB. English Language Book Society/Longman. London. 201-214.

Milborrow, BV. 1989. Inhibitors. In: Advanced Plant Physiology. Ed. Wilkins, MB. English Language Book Society/Longman. London. 76-104.

Mohlenbrock, RH. 2000. Leaf reading in Oahu- Brief article. Natural History.

Nelson, SC., Ploetz, RC. and AK. Kepler. 2006. Musa Species (banana and plantain). Species Profiles for Pacific Island Agroforestry. 1-33. Available online: www.traditionaltree.org

Nisoli, C., Gabor, NM., Lammert, PE., Maynard, JD. and VH. Crespi. 2009. Static and Dynamic Phyllotaxis in a Magnetic Cactus. Physical Review Letters. 102 (18):186103.1-186103.4. Available online: ArXiv.Cond-mat/0702335.

Norman, MJT., Pearson, CJ. and GE. Searle. 1996. Tropical Food Crops in their Environment. (2nd ed.). Cambridge Low Price Edition. Cambridge. UK. 319-335.

Plant Nutrition. 2003. Available online:http://www. gov.nf.ca/agric/pubfact/Fertility/nutrition.thm

Ploense, SE., Wu, MF., Nagpal, P. and JW. Reed. 2009. A gain-of-function mutation in IAA18 alters *Arabidopsis* embryonic apical patterning. Development. 136:1509-1517. Doi: 10.1242/10.1242/dev.025932.

Puja., Mishra, SR. and Aroro, D. 2005. Dictionary of Biology. (2nd ed.). AITBS Publishers and Distributors. New Delhi. 269.

Reinhardt, D., Mandel, T. and C. Kuhlemeier. 2000. Auxin Regulates the Initiation and Radial Position of Plant Lateral Organs. Plant Cell. 12:507-518.

Russel, EJ. 1950. Soil Conditions and Plant Growth. (8th ed.). Longman, Green & Co. Ltd. London. 53-94.

Schopfer, P. 1989. Photomorphogenesis. In: Advanced Plant Physiology. Ed. Wilkins, MB. English Language Book Society/Longman. London. 380-405.

Selvam, MA. 1998. Quasicrystalline Pattern Formation in Fluid Substrates and Phyllotaxis. Symmetry in Plants. 1:1-15. Available online: ArXiv:chao-dyn/9806001v1

Semiarti, E., Ueno, Y., Tsukaya, H., Iwakawa, H., Machida, C. and Y. Machida. 2001. The asymmetric leaves2 gene of *arabidopsis thaliana* regulates formation of a symmetric lamina, establishment of venation and repression of meristems-related homeobox genes in leaves. Development .128:1771-1783.

Sengbusch, PV. 2002. Botany online. Cytology, mitosis, meiosis-Meiosis. Available online: http://www.biology.uni-hamburg.de/b-online/eo9/o9h.htm

Sexton, R. and Woolhouse, HW. 1989. Senescence and abscission. In: Advanced Plant Physiology. Ed. Wilkins, MB. English Language Book Society/Longman. London. 409-491.

Shipman, PD. and Newell, AC. 2004. Phyllotactic Patterns on Plants. Physical Review Letters. 92 (16):168102.1-168102.4

SIAM. 2004. Plant Patterns and Phyllotaxis. Available online: http://www.siam.org/news/news.pho?id=263

Silvertown, JW. and Charlesworth, D. 2001. Introduction to Plant Population Biology. (4th ed.). Blackwell Science. London. 22-215.

Simon, EW., Dormer, KJ. and JN. Hartshorne. 1990. Lowson's Textbook of Botany. (15th ed.). Universal Book Stall. New Delhi. 54-312.

Smit, JN. and Combrink, NJJ. 2004. The effect of boron levels in nutrient solutions on fruit production and quality of greenhouse tomatoes. Plant and Soil. South African Journal of Plant and Soil. 21(3):188-191

Smith, RS., Guyomarc'h, S., Mandel, T., Reinhardt, D., Kuhlemeier, C. and P. Prusinkiewicz. 2006. A plausible model of phyllotaxis. Proceedings of the National Academy of Sciences of the United States of America. 103 (5):1301-1306. Doi: 10.1073/pnas.0510457103.

Song, PS. 1989. Phytochrome. In: Advanced Plant Physiology. Ed. Wilkins, MB. English Language Book Society/Longman. London. 354-374.

Sprent, JI. 1989 Nitrogen fixation. In: Advanced Plant Physiology. Ed. Wilkins, MB. English Language Book Society/Longman. London. 249-272.

Srivastava, PC. and Gupta, VC. 1996. Trace Elements in Crop Production. Science Publishers, Inc., USA.

Strafford, GA. 1970. Essentials of Plant Physiology. Heinemann Educational Books Ltd. London. 54-193.

Swanson, CP., Merz, T. and Young, WJ. 1967. Cytogenesis. Foundation of Modern Genetics Series. Prentice-Hall, Inc. NJ. 10-140.

Swennen, R. and Vuylsteke, D. 1987. Morphological Taxonomy of Plantain (*Musa* Cultivars AAB) in West Africa. In: Banana and Plantain Breeding Strategies. Eds. Perseley, GJ. and De Langhe, EA. Proceedings of an International Workshop. ACIAR Proceedings 21:165-171.

Theurer, CJ. 1984. Inheritance of Feather Leaf and Plantain Leaf Characters in Sugarbeet. Crop Science 24:463-464.

Thomas, B. and Vince-Prue, D. 1989. Juvenility, photoperiodism and vernalization. In: Advanced Plant Physiology. Ed. Wilkins, MB. English Language Book Society/Longman. London. 408-435.

Tivy, J. 1998. BioGeography: A Study of Plants in the Ecosphere. (3rd ed.). Longman. Kuala Lumpur. 315-320.

Tsiantis, M., Brown, MIN., Skibinski, G. and JA. Langdale. 1999. Disruption of auxin transport in association with aberrant leaf development in maize. Plant Physiology. 121(4):1163-1168.

Van den Broek, B. 2002. Single-molecule study of DNA tension on restriction enzyme. M. Sc. Thesis, Vrije Universiteit, Amsterdam. 32-70.

Van Wanbeke, A. 1992. Soils of the tropics: Properties and appraisal. McGraw Hill. New York. 239.

Weisstein, E. 2004. Bifurcation. Eric Weisstein's World of Mathematics, Wolfram Research. 1-9. Available online: http://mathworld.wolfram.com

Wikipedia. 2008. Phylotaxis. Available online: http://en.wikipedia.org/wiki/Phyllotaxis

Wilkins, MB. 1989. Gravitropism. In: Advanced Plant Physiology. Ed. Wilkins, MB. English Language Book Society/Longman. London. 163-182.

Woodward, FI. and Sheehy, JE. 1983. Principles and Measurements in Environmental Biology. Butterworths. London. 2-136.

Canadian Journal of
pure&applied
sciences

PROXIMATE AND CHEMICAL COMPOSITIONS OF LEAF SAMPLES OF *BURKEA AFRICANA* FROM MOLE NATIONAL PARK, GHANA

*VC Mbatchou[1], J Sackey[1] and I Sackey[2]
[1]Department of Applied Chemistry and Biochemistry, [2]Department of Applied Biology
University for Development Studies, PO Box 24, Navrongo, Ghana

ABSTRACT

Dry and rainy season leaf samples of *Burkea africana* were analyzed for proximate and mineral compositions, and anti-nutritional contents. Moisture contents of the dry season leaf samples of the plant were relatively low indicating good shelf life characteristics. High ash contents of dry and rainy season leaf samples of plant accounted for high mineral contents. High fibre and protein contents of leaf samples of plant indicate that the leaves could help treat constipation, improve general health and serve in growth and repair of tissues. The study revealed that leaves of the plant are rich in Ca, K, Na and Mg. Concentrations of trace metals in leaves of plant differ, with iron having the highest values of 481.03mg/Kg and 467.85mg/Kg in the rainy and dry season leaf samples respectively. Zinc concentrations range from 10.99mg/Kg in the rainy season leaf sample to 34.02mg/Kg in the dry season leaf sample of the plant. The high proximate and mineral compositions may be the factor to which elephants feed on the leaves of this plant. Also, results indicate that if leaves of *Burkea africana* are properly exploited and processed, they could be a high-quality and cheap source of feed for livestock especially ruminants.

Keywords: Proximate, elemental and anti-nitritional parameters, phytochemicals.

INTRODUCTION

Every mammal needs a daily supply of different types of food materials to enable it to live a healthy life. However, the productive value of any feed depends on the quantity eaten and the extent to which the feed consumed supplies the animals with the required energy, protein, minerals and vitamins.

There are differences among plant species and varieties, but the composition of a plant is also influenced by climate, soil fertility, and stage of maturity and method of feeding (Skerman and Howat, 1990).

However, various food materials are incorporated in plants to boost energy content when eaten by animals. Herbivores feed on different kinds of plants at different times depending on the nutritional content at a particular time or season. Some plants to some herbivores have been found to enhance growth, feed efficiency and improved the physical appearance of leaves which encourages consumption. Also, at any one time what an animal selects to eat is dependent on what is available. Thus, the degree of consumer pressure exerted on a particular plant species will be influenced by both the quality and the quantity of alternative food plants available in the vicinity.

There are many plant species of various classes. Many of these plants have been exploited over the years and from

the basis for important feed. The plants also serve as nursery grounds for traditional herbal medicine. However there are lots of trees which serve as food for man and other lower animals in both humid and semi arid tropics, which have received much less attention from the scientific community (Cannel, 1989).

According to Abudu (2005) to avoid toxic build-up and sustain excellent health, each meal should give the body the following:

- Carbohydrate 90%
- Amino acids.. 4-5%
- Minerals.. 3-4%
- Fatty acids.. 1+%
- Vitamins .... under 1%

Moreover a number of minerals are required by mammals in order to maintain good health. Some of these essential minerals are accumulated in different parts of plants as it accumulates minerals essential for growth from the environment (Oderinde *et al*., 2009). It has been reported that trace metals can be detected in plants and foodstuffs. Recently, plant species have been identified that contain nutrients displaying new beneficial medicinal and therapeutic properties (Almoaruf *et al*., 2000).

The occurrence of toxic or digestibility-reducing compounds could be an important factor restricting the utilization of otherwise nutritious plants by large

---

*Corresponding author email: mcvalentinechi@gmail.com

herbivores. However, little factual information is yet available both on the occurrence of these chemicals in plants, and on their effects on mammalian consumers (Owen-Smith, 1982).

Large herbivores can exert a major impact on vegetation. They remove over 40% of annual grass production (Braun, 1973). This can radically alter the balance between grasses, and woody vegetation and even result in fire and desertification where animals are confined. Elephants in particular can directly change areas of woodland into open grassland (Laws *et al*., 1975).

Elephant dine on a wealth of plant parts; leaves, twigs, bark, shoots, fruits, flowers, roots, tubers and bulbs from as 80 different plant species. The digestive system of elephants is less efficient than those of other herbivores, such as antelope and buffalo. Food passes quickly through the digestive system before nutrients are absorbed, causing elephants to discard about half the plant material they consume. This inefficient digestive system means that elephants must eat large quantities of food to retain and absorb necessary nutrients for good health.

In the wild, elephants devote about three quarters of their day to feeding. An adult elephant eats 200 to 300kg (440 to 630 lb) of food each day. The African elephant species; *Loxodonta africana* and *Loxodonta cyclotis* weigh up to 7,000kg (15,400 lb) and stand up to 4m (13ft) tall (Gordon and Roach, 2009). Elephants do not feed indiscriminately. Some plants only assume importance to them at certain times of the year. For instance, elephants have only been observed to eat *Cordia gharaf* in quantity when the leaves begin to shrivel. Other plants such as the herb, *Digera alternifoli* are eaten at certain growth stage but later dry up and become unpalatable (Bax and Sheldrick, 1963).

Burkea africana is among the few 80 different plant species consumed by elephants. There is little information on the nutritional, anti-nutritional and mineral properties of this plant. The periodic feeding of elephants on *Burkea africana* may be influenced markedly by the extent to which the plant species supply energy, protein, minerals and vitamins. There is therefore the need to identify the various food materials present in the plant as there is no concrete information on it.

The Mole National Park authorities have been concerned over the extent of damages caused by elephants to vegetation for several years. In the dry season, many of the trees are smashed and the herbs and shrubs are eaten down to stumps. There is large scale destruction of *Burkea africana* and ring barking by elephants during this period.

It is considered important to study what elements of the vegetation are eaten as food. This is because an understanding of the reasons for this wide variation in the degree of utilization of the vegetation resources is an essential requirement for enlightened management, whether for secondary production or environmental conservation.

The purpose of this study is to explore salient features such as nutrient contents, toxins and structural attributes of the leaves of *Burkea africana* to which elephants are likely to respond. It is the aim of the work to compare the proximate and elemental components of rainy and dry season leaf samples of plant. The project is geared towards investigating whether there is the possibility of considering the leaves of *Burkea africana* as good source of proteins for mammals, and as mineral supplement to feed. Also, the project is carried out to qualitatively determine some phytochemicals in the dry season root samples of *Burkea africana* which possess anti-typhoidal property. It is known from basic knowledge that nutrients and other components in the soil are absorbed at the roots of plants and transported to other parts of plants.This is an indication that there is a high probability of finding components which are present in the roots of a plant in other parts of the same plant.

MATERIALS AND METHODS

Source of Materials
Leaf and root samples of *Burkea africana* were separately collected at random from Mole national park in the Northern region of Ghana. Parts of plant were identified by Dr. Isaac Sackey and Dr. Walters Kpipki, both from Department of Applied Biology, Faculty of Applied Sciences, University for Development Studies.

Plant Sample Preparation
Dry and rainy season leaf samples of *Burkea africana* were separately air dried for seven days at room temperature and then milled in to fine powder. Each of the prepared samples was later stored in an airtight polythene bag until required for analyses. Fresh dry and rainy season leaf samples were taken for moisture content estimation.

Proximate Analysis of Leaf Samples
Determination of Moisture Content
Moisture content was determined by accurately weighing 2.0g of fresh sample into a previously dried and weighed porcelain crucible. It was then dried in a thermostatically controlled forced convection oven at $105^{o}C$ for six hours to a constant weight. The porcelain crucible was removed and transferred into a dessicator for cooling after which it was weighed. Moisture content was determined by difference and expressed as a percentage (AOAC, 1990).

Determination of AshContent
Ash content was determined by accurately weighing 2.0g of prepared sample into a pre-ignited and previously weighed porcelain crucible, placed in a muffle furnace and ignited for 2 hrs at 600°C. After ashing, the crucible and its content were cooled to about 105°C in a forced convection oven before cooling further to room temperature in a desiccator. The crucible and its contents were weighed and then weight reported as percentage ash content (AOAC, 1990).

Determination of Crude Fat Content
Dried sample (2.0g) from moisture content determination was subjected to fat estimation by refluxing for 16 hours using a soxhlet extractor and 200ml of petroleum ether as the extracting solvent. A round-bottom flask containing a mixture of fat and petroleum ether solvent was detached from the soxhlet extractor and petroleum ether solvent was evaporated on a steam bath. The round-bottom flask and its content were heated to 105°C in an oven for 30 minutes and later cooled in a dessicator. The weight of the extracted fat was determined and expressed as percentage crude fat (AOAC, 1990).

Determination of Crude Fibre Content
The sample (2.0g) from crude fat determination was transferred into a 750ml Erlenmeyer flask and about 0.5g of anti-bombing agent was added. 200ml of boiling1.25% sulphuric acid (H$_2$SO$_4$) was poured in to the flask and immediately transferred onto a hot plate with a cold finger condenser attached to the flask.

The sample was boiled for 30 minutes during which the entire sample was thoroughly wetted while any of it was prevented from remaining on the side of the flask and out of contact with the solvent. After 30 minutes the flask was removed, its content filtered into a conical flask through linen cloth in a funnel and washed with boiling water until the washings were no longer acidic. The content of the linen cloth was washed into another flask with 200ml boiling 1.25% sodium hydroxide (NaOH) solution. The flask was reconnected to the cold finger condenser and boiled for 30minutes. The content was again filtered through linen cloth in a funnel and washed thoroughly with boiling water then with 15ml ethanol. Anti-bombing agents were removed from the residue. The residue was transferred into a previously dried and weighed porcelain crucible dried in an oven at 100°C for 1hour, cooled in a desiccator and weighed. The crucible and its contents were ignited in an electrical furnace at 600°C for 30 minutes; cooled and reweighed. The loss in weight was reported as percentage crude fiber (AOAC, 1990).

Determination of Crude Protein Content
Prepared sample (30.40mg) was weighed into a digestion flask containing 1g catalyst mixture of selenium and potassium sulphate (1: 200), 2ml concentrated sulfuric acid (H$_2$SO$_4$) and 2ml 30% hydrogen peroxide (H$_2$O$_2$).

The prepared sample in the mixture was digested for 30 minutes, cooled and a minimum quantity of distilled water was added to dissolve solids. They were then allowed to cool at room temperature. The digests were transferred to the distillation apparatus, making sure none remain in the flask by rinsing five times with 2ml portions of distilled water.

A 125ml Erlenmeyer flask containing 6ml boric acid solution and 3 drops of indicator solution (methyl orange) was connected to a condenser whose tip extends below the surface of the solution.

8ml of dilute sodium hydroxide solution was added to still and steam distilled until about 50ml distillate collects. The distillate was titrated with 1.0N HCl to violet end point.

Blank determinations were made, using boric acid and indicator. The values obtained were used to calculate the total nitrogen and the percentage crude protein (AOAC, 1990).

Determination of Carbohydrate Content
This was calculated by the difference method.

Elemental Analysis of Leaf Samples
Digestion of Sample
Prepared sample (1.0g) was weighed and transferred into a 100ml volumetric flask. 10ml of acid mixture of nitric (HNO$_3$) and perchloric (HClO$_4$) acids in the ratio 9:4 was added. The contents were mixed and swirled. The flask was placed on a hot plate in a fume hood and heated, starting at 90°C and then the temperature was raised to 180°C. Heating continued until production of red nitrogen (IV) oxide fumes ceased. The contents were further heated until mixture became colorless. The contents were cooled, and the volume was made up with distilled water to the 100ml mark, and filtered using No. 1 Whatman filter paper. The filtrate obtained was used for the elemental estimation.

Estimation of Calcium, Ca
A standard was prepared by weighing 0.2247g of CaCO$_3$ into a beaker and adding 5ml of deionised water to it. This was followed by addition of 10ml of concentrated HCl to ensure complete dissolution of CaCO$_3$. The mixture was poured into a volumetric flask and was made up to 1000ml mark with deionised water to give a concentration of 100μg/ml of calcium solution. Concentrations of 5 μg/ml, 10 μg/ml, 15 μg/ml and 20μg/ml were prepared by measuring 5ml, 10ml, 15ml and 20ml of the stock in to different volumetric flasks and making up the volumes to 100ml mark with deionised water. Deionised water was

used for zero µg/ml concentration of calcium. The atomic absorption spectrophotometer was calibrated with a lamp current of 10mA, a slit width of 0.5nm and at wavelength 422.7nm. After setting the atomic absorption spectrophotometer the standard solution of different concentrations of calcium were atomized and the absorbance recorded for the respective concentrations of calcium. A graph of concentration of calcium against their corresponding absorbance was plotted. 5ml of the digested sample solution was poured into a 100ml volumetric flask and made up to the 100ml mark. It was atomized and the absorbance was recorded. The corresponding concentration for the absorbance was recorded which represents the content of Calcium in the sample solution.

Estimation of Magnesium, Mg
$MgSO_4$ (10.14g) was weighed into 250ml of deionized water in a 1000ml volumetric flask. The volume was made up to 1000ml mark. This gave a concentration of 1000µg/ml of magnesium solution. Under this procedure the preparation of standard curve the estimation and the calculation procedure are the same as described for calcium estimation. The atomic absorption spectrophometer was calibrated with a lamp current of 3mA, slit width of 0.7nm and a wavelength of 285.2nm.

Estimation of Zinc, Zn
Pure zinc (1.0g) was dissolved in 20ml of HCl (1:1), and later diluted to 100ml mark with deionized water in a volumetric flask. This gave 1mg/ml Zn stock solution. The working solution was obtained by diluting the stock solution from 100 to 1000 times to obtain 10µg/ml to 1µg/ml concentrations. The preparation of the standard curve, the estimation and the calculation procedure are the same as described for calcium estimation. The atomic absorption spectrophotometer was calibrated to a wavelength of 218nm and slit width of 0.7nm.

Estimation of Iron, Fe
Pure iron wire (1.0g) was dissolved in 30ml of HCl (1:1), and later diluted to1000ml mark with deionized water to obtain 1mg/ml of standard Fe. Working solutions of different concentrations were obtained by further dilution. The atomic absorption spectrophotometer was calibrated to a wavelength of 248.3nm and a slit width of 0.2nm. The preparation of the standard curve, the estimation and the calculation procedure are the same as described for calcium estimation.

Estimation of Copper, Cu
Pure copper metal (1.0g) was dissolved in 30ml of HCl (1:1), and later diluted to 1000ml mark with deionized water. This gave 1mg/ml copper solution. Further dilutions were done to obtain the working solutions.The atomic absorption spectrophotometer was calibrated to a wavelength of 324.7nm and a slit width of 0.7nm. The

preparation of the standard curve, the estimation and the calculation procedure are the same as describe for calcium estimation.

Estimation of Manganese, Mn
Pure manganese metal (1.0g) was dissolved in 30ml of HCl (1:1), and later diluted to 1000ml mark with deionized water. This gave 1mg/ml Mn solution. Further dilutions were done to obtain the working solutions. The atomic absorption spectrophotometer was calibrated to a wavelength of 279.5nm and a slit width of 0.7nm. The preparation of the standard curve the estimation and the calculation procedure are the same as described for calcium estimation.

Estimation of Sodium, Na
Pure NaCl (1.806g) was dissolved in deionized water and made up to 1000ml mark. This gave 1mg/ml Na solution.100ml of this solution was diluted to 1,000ml, and this gave 100µg/ml Na solution. 5, 10, 15 and 20ml of the stock solution were poured into 100ml volumetric flasks top up to the 100ml mark. This gave 5, 10, 15 and 20µg/ml concentrations of Na respectively.The atomic absorption spectrophometer was calibrated to a wavelength of 589.0nm and a slit width of 0.2nm.The preparation of the standard curve, the estimation and the calculation procedure are the same as described for calcium estimation

Estimation of Potassium, K
Pure KCl (1.908g) was dissolved in deionized water and made up to 1000ml mark. This gave 1mg/ml concentration of K solution. 100ml of this solution was further diluted to 1,000ml to give 100µg/ml concentration of K. 5, 10, 15 and 20ml of the stock solution was diluted to 100ml to give 5, 10, 15 and 20µg/ml concentrations of K respectively. The atomic absorption spectrophometer was calibrated to a wavelength of 766.5nm, a lamp current of 6mA and a slit width of 0.5nm. The standard curve was prepared using 0, 5, 10, 15 and 20µg K/ml. A blank was prepared the same way without adding plant digested material. 5ml of the sample was further diluted to 100ml. It was atomize on the calibrated atomic absorption spectrophotometer on which the standard curve has also been prepared. The absorbance was recorded against each sample and the concentration of K for the particular absorbance observed for the sample was calculated.

Estimation of Lead, Pb
Pure lead (1.0g) was dissolved in 30ml of HCl (1:1) and later diluted to 1000ml mark with deionized water in a volumetric flask to give 1mg/ml concentration of lead solution. The working solution was obtained by diluting the stock from 100 to 1000 times to obtain 10µg/ml to 1µg/ml. The atomic absorption spectrophotometer was calibrated to a wavelength of 283.3nm and a slit width of 0.7nm. The preparation of the standard curve, the

estimation and the calculation procedure are the same as described for calcium estimation.

Estimation of Cadmium, Cd

Pure cadmium (1.0g) was dissolved in 30ml of HCl (1:1) and later diluted to 1000ml mark with deionized water in a volumetric flask to obtain 1mg/ml concentration of cadmium solution. Working solutions of different concentrations were obtained by further dilution. The atomic absorption spectrophotometer was calibrated to a wavelength of 228.9nm and a slit width of 0.7 nm. The preparation of the standard curve the estimation and the calculation procedure are the same as described for calcium estimation.

Anti-Nutritional Analysis
Determination of Hydrogen Cyanide (HCN)

Prepared sample (10g) was soaked in a mixture of 200cm^3 of distilled water and 10cm^3 of orthophosphoric acid. The mixture was left for 12 hours to release all bound hydrocyanic acid. Anti-bumping agents were added and the solution distilled until 150cm^3 of the distillate was collected. 20cm^3 of the distillate was taken into a conical flask and diluted with 40cm^3 of water; 8.0cm^3 of 6.0 mol/dm^3 ammonium hydroxide and 2.0cm^{3}of 5% (w/v) potassium iodide solutions were added. The mixture was titrated with 0.02 mol/dm^3 silver nitrate using a micro burette until a faint but permanent turbidity was obtained (1cm^3 0.02 mol/dm^3 AgNO$_3$ = 1.08mg HCN) (Anhwange *et al.*, 2009).

Determination of Phytate

Prepared sample (4.0g) was soaked in 100cm^3 of 2% hydrochloric acid for five hours and was filtered. 25.0cm^3 of the filtrate was taken into a conical flask and 5.0cm^3 of 0.3%ammonium thiocyanate solution was added. The mixture was titrated with a standard solution of iron (III) chloride until a brownish-yellow colour persisted for five minutes (Anhwange *et al.*, 2009).

Determination of Saponins

Prepared sample (10g) was taken into 100ml of 20% aqueous ethanol in water and mixture agitated with a mechanical shaker for twelve hours. The solution was filtered using Whatman No. 1 filter paper and residue was re-extracted with 200ml of 20% aqueous ethanol. The extracts were combined and reduced to about 40 ml vacuums using rotary evaporator. The extract and 20ml diethyl ether were transferred into a 250ml separatory funnel and was shaken vigorously. The aqueous layer was discarded. The purification process was continued until a colourless aqueous extract was obtained. The pH of the aqueous solution was adjusted to about 4.5 by adding sodium chloride, and the solution was shaken with butanol. The butanoic extract was washed twice with 10ml of 5% sodium chloride and was evaporated to dryness in a fume cupboard, to give the saponin, which

was weighed and expressed in percentage (Anhwange *et al.*, 2009).

RESULTS AND DISCUSSION

Results in table1 represent the proximate composition of dry and rainy season leaf samples of *Burkea africana*. The moisture contents of dry and rainy season leaf samples of this plant were obtained as 3.44% and 7.46% respectively, which are relatively low indicating good shelf life characteristics. The ash content recorded for the dry season leaf samples of the plant was 4.08%, whereas for the rainy season leaf samples the ash content was 4.31%.The ash content of rainy season leaf samples of the plant was higher than that of dry season leaf samples. The higher ash content of rainy season leaf samples can be due to the transportation of minerals by rain water from areas of high concentrations to where the plant is for absorption. In general, the ash contents of both the rainy and dry season leaf samples of *Burkea africana* determine their mineral compositions.

The crude fat content ranges from 2.99% to 3.5% with the rainy season leaf samples recording the least, and the dry season leaf samples recording the highest. The fibre content ranges from 11.30% to 15.85% with the rainy season leaf samples recording the least, and the dry season leaf samples recording the highest. These values were high for the leaf samples. Rainy season leaf samples of the plant recorded higher percentage values of protein than the dry season leaf samples. The dry and rainy season leaf samples of *Burkea africana* recorded percentage values of carbohydrate of 15.41% and 7.77% respectively. The sum of moisture and carbohydrate contents for the dry season leaf samples of *Burkea africana* was higher than that for the rainy season leaf samples of the same plant. The dry season leaf samples recorded 18.85% while the rainy season leaf samples recorded15.23%. The organic matter contents range from 95.69% to 95.92% for the rainy and dry season leaf samples repectively.

Table 2 shows the mean elemental contents of dry and rainy season leaf samples of *Burkea africana*. A total of ten elements (Ca, K, Na, Mg, Mn, Pb, Cd, Zn, Cu and Fe) were determined in the dry and rainy season leaf samples of the plant by Atomic Absorption Spectrophotometry (AAS). On the whole, the average elemental concentrations of dry season leaf samples were relatively higher than those of rainy season leaf samples. The lower concentrations of rainy season leaf samples can be attributed to elemental dilution by rain. The exceptional elements with lower average concentrations of the dry season leaf samples were K, Pb, Cd and Fe. This study shows that the leaves of *Burkea africana* are rich in Ca, K, Na, Mg, Cu and Fe.

Cadmium concentrations range from 1.91 mg/Kg to 2.51 mg/Kg with the dry season leaf samples having the least and the rainy season the highest. Cd and Pb are considered as heavy metals, while Cu, Fe, Zn and Mn are considered micronutrients. The WHO limits for these metals have not yet been established (Motsara *et al.*, 2008). Allaway reported the ranges of Cu and Zn in agricultural products to be between 4 and 155ppm and 15 to 200ppm respectively. Comparably, the concentration of Cu in this study was found to be within this range for the rainy season leaf samples and not for the dry season leaf samples. This can be attributed to dilution by rain water. Zinc concentrations were within the stipulated range for both the dry and rainy season leaf samples (Allaway, 1968).

The results obtained indicated that both the dry and rainy season leaf samples of *Burkea africana* contain large amount of nutrients, rich in Ca, K, Na and Mg.   The abundance of Ca, K and Mg in the result of this analysis is in agreement with previous findings that these three elements represent the most abundant element constituents of many plants (Canel and Saura, 1982). Lead concentrations range from 3.69 mg/Kg to 4.80 mg/Kg for the dry and rainy season leaf samples respectively. The permissible limit for plants, based on ADI (Acceptable Daily Intake) for lead is 10mg/Kg (Oderinde *et al.*, 2009). *Burkea africana* accumulates this metal at a level appreciably below the permissible level.

Though much is known about the functional role of a number of elements, the mineral nutrition lies in obtaining the correct amount of supplementation in the right form at the right time. Mg and Zn have important role in the metabolism of cholesterol as well as heart diseases (Oderinde *et al.*, 2009). The presence of Mn may be correlated with therapeutic properties against diabetic and cardiovascular diseases (Schwart, 1975). Mn is also known to aid formation of skeleton and cartilage. The appreciable high content of potassium signifies that if the leaves are taken, it will help in the regulation of body fluid and maintained normal blood pressure. It will also help in controlling kidney failure, heart oddities and respiratory flaw. Iron which carries oxygen to the cells and is necessary for the production of energy, synthesis of collagen and the proper functioning of the immune system, were found to be high in both samples of plant. Deficiency or excess of Cu, Mn, Zn, Ca, Mg and K may cause a number of disorders; they also take part in neurochemical transmission and function as cofactors for various enzymes in different metabolic processes (Oderinde and Ajayi, 1998).

Table 3 results represent the average anti-nutritional constituent of the dry season leaf sample of *Burkea africana*. The average concentration of hydrogen cyanide recorded was 1.49mg/g for the plant sample. This value

falls within the threshold value (0.5-3.5 mg/g) reported as safety limit (Anhwange *et al.*, 2009; Kumar, 1991).

Hydrogen cyanide is an extremely poisonous substance formed by the action of acids on metal cyanides. Cyanide is a fast-acting potentially deadly chemical that prevents the cells of the body from using oxygen properly. Gettle and Baine (1938) reported that intake of large dose of hydrogen cyanide can cause death within few minutes. Smaller dose intake may result to stiffness of the throat, chest, palpitation and muscle weakness. Phytate content was found to be 0.19mg/g for *Burkea africana*. This average value is lower when compared to 0.28mg/g concentration value reported for Musa sapientum (banana) peels by Anhwange *et al.* (2009). Phytic acid is a strong chelator of important minerals such as calcium and zinc despite its therapeutic effects as a protective against osteoporosis which makes it a beneficial phytochemical.

Saponin content for *Burkea africana* was 1.067×10^{-4} mg/g. This average value is relatively lower when compared to the 3×10^{-4} mg/g concentration value reported by Kumar (1991) as the minimum safe value for animals especially cattle. Eric (1978) observed that saponin consumption can result to paralysis of the sensory system. It is found to inhibit growth in swine and poultry; though it increases the excretion of cholesterol in the body (Anhwange *et al.*, 2006).

Table 1. Percentage proximate composition of dry and rainy season leaf samples of *Burkea africana* (% by mass).

Parameter	Dry Season Sample	Rainy Season Sample
Moisture	3.44	7.46
Ash	4.08	4.31
Fat	3.50	2.99
Fibre	15.85	11.30
Protein	57.72	66.17
Carbohydrate	15.41	7.77

Table 2. Average mineral contents of dry and rainy season leaf samples of *Burkea Africana* (mg/Kg).

Element	Dry Season Sample	Rainy Season Sample
Ca	6108.92	5889.81
K	2772.02	3125.95
Na	230.93	221.36
Mg	2340.01	1944.02
Mn	33.00	32.00
Pb	3.69	4.80
Cd	1.91	2.51
Zn	17.02	10.99
Cu	239.84	138.27
Fe	467.85	481.03

Table 3. Average anti-nutritional constituents of dry season leaf samples of *Burkea africana* (mg/g).

Parameter	*Burkea Africana*
Hydrogen cyanide	1.49
Phytate	0.19
Saponin	1.067×10^{-4}

CONCLUSION

The present study shows that, the leaves of *Burkea africana* are good sources of organic matter and minerals. The low moisture content of the dry season leaf samples is an indication of good shelf life characteristics. The high protein content of the dry and rainy season leaf samples is an indication that leaves of the plant can serve as a good source of protein to mammals since protein is used for growth and repairs of warn out tissues. The high fibre content of the plant also indicates that the leaves could help prevent constipation, improve general health and well being. The ash content of leaves of plant is analogous to other staples measured as good sources of minerals. The macronutrient concentrations are high, while the toxic trace metal concentrations are relatively low for both leaf samples. The total elemental concentration of dry season leaf samples (12,21519mg/kg) is greater than that of rainy season leaf samples (11,850.74mg/kg). Concentrations of elements fall within ranges and standards. Thus, the leaves of *Burkea africana* plant are a good source of minerals. The high nutritional (especially the protein) and mineral contents may be the factor to which elephants feed on leaves of the plant. The anti-nutritional contents of the dry season leaf samples fall within acceptable threshold values. Thus, they have no influence on the nutritional and mineral compositions of the plant's leaves as sources of feed. These natural toxicants in foods inhibit the absorption and utilization of minerals and proteins, and also inhibit oxidative phosphorylation (Sinclair and Howat, 1980; Ross and Bacin, 1997). This means that with the low natural toxicant levels, the leaves of the plant can serve as a good source of feed for livestock if properly processed.

RECOMMENDATION

On the whole, it is recommended that the leaves of *Burkea africana* should be used as a source of both protein and *as* a source of minerals for livestock.

ACKNOWLEDGEMENT

REFERENCES

Abudu, AO. 2005. Eat for Health and Long Life. International Millennium Ventures (GH) Ltd. 214-215.

Allaway, WH. 1968. Agronomic controls over environmental cycling of trace elements. Advance Agronomy. 20:235-274.

Almoaruf, OA., Muibat, OB., Isiaka, AO. and Nureni, OA. 2000. Heavy trace metals and macronutrients status in herbal plants of Nigeria. Food Chemistry. 85:67-71.

Anhwange, BA., Ajibola, VO. and Okibe, FG. 2006. Nutritive values and anti nutritional factors in *Hibibiscus sabdariffa*. J. of Fisheries International. 1(2-4):73-76.

Anhwange, BA., Ugye TJ. and Nyiaatagher, TD. 2009. Chemical composition of *Musa sapientum* peels. Electronic Journal of Environmental, Agriculture and Food Chemistry. 8 (6):437-442.

Association of Official Analytical Chemists (AOAC). 1990. Official Methods of Analysis (15th edi.). Philip Harris (Holdings) Ltd. Washington, DC. 836-79.

Bax, PN. and Sheldrick, DLW. 1963. Some Preliminary Observations on the Food of Elephants in the Tsavo Royal National Park (east) of Kenya. East African Wildlife Journal. 1:40-53.

Braun, HM. 1973. Primary production in the Serengeti: Purpose, methods and some results of research. Annales de l'Universite d'Abidjan, Serie E (Ecologie). 6 (2):171-188.

Canellas, J. and Saura-Calixto. 1982. Mineral composition of almond varieties (*Prunus amygdalus).* Zeitschrift fr lebensmittel-Untersuchung undforschung. 174:129-131.

Cannel, MGR. 1989. Food crop potential tree. Experimental Agriculture. 25:313-326.

Eric, A. 1978. The study of phytochemical and comparative analysis of saponins. Longman press, London. pp. 22-28.

Gettle, AO. and Baine, JO. 1938. The toxicology of cyanide. Am. J. Med. Sci. 195:182-198.

Gordon, DG. and Roach, R. 2009. ''Elephant". Microsoft® Student 2009 [DVD]. Redmond, WA: Microsoft Corperation.

Kumar, R. 1991. Anti nutritional factors, the potential risk of toxicity and methods to alleviate them. Proceedings of FAO Experts consultation held at the Malaysia Agricultural Research & Development Institution Kuala Lumpur, Malaysia. 14-18.

Laws, RM., Parker, ISC. and Johnstone, RCB. 1975. *Elephants and their habitats.* The ecology of elephants in North Bunyoro, Uganda. Clarendon Press, Oxford.

Motsara, MR. and Roy, RN. 2008. Guide to Laboratory Establishment for Plant Nutrient Analysis. FAO Fertilizeer and Plant Nutrient Bulletin. 19:235-242.

Oderinde, RA. and Ajayi, IA. 1998. Metal and oil characteristics of *Terminali acatappa.* La Rivista Italiana Delle Sostanze Grasse. 75:361-362.

Oderinde, RA., Ajayi, IA. and Adewuyi, A. 2009. Evaluation of the mineral nutrients, characterization and some possible uses of *Blighia unijugata bak* seed and seed oil. Electronic Journal of Environmental, Agriculture and Food Chemistry. 8(2):120-129.

Owen-Smith, N. 1982. Factors influencing the consumption of plant products by large herbivores. In: The Ecology of Tropical Savanna. Eds. Huntley, BJ. and Walker, BH. Berlin Springer Verlag. 359-404.

Ross, K. and Bacin, W. 1997. Cardiac stimulant activity of the saponins of *Achyranthes aspera L.* Indian. Journal of Medical Research. 80:132-8.

Schwart, MK. 1975. Role of trace elements in Cancer, Cancer Research. 35:3481-3484.

Sinclair, JT. and Howat, MF. 1980. Alkaloids in rural nutrition. Journal of the American College of Nutrition. 13:98-100.

Skerman, PT. and Howat, MF. 1990. Tropical Grasses: FAO of the UN, Rome. 231-235.

TOTAL ANTIOXIDANT CAPACITY, NUTRIENT COMPOSITION, MICROBIAL LOAD AND PERCENTAGE INHIBITORY ACTIVITY OF UNRIPE PLANTAIN FLOUR

*Eleazu Chinedum O, Amajor, JU and Ikpeama A
Department of Biochemistry, National Root Crops Research Institute
Umudike Umuahia, Abia State, Nigeria

ABSTRACT

In the present study, an evaluation of the total antioxidant capacity, nutrient composition, microbial load and percentage inhibitory activity of methanolic extract of unripe plantain flour on DPPH radical was carried out. The total antioxidant capacity of the extract as determined by the quantities of quercetin and peroxidase present was 0.532ug/ml and 52% ± 0.00 while the percentage inhibition on DPPH radical was 78.57%. Analysis of the proximate and phytochemical compositions of the flour using the AOAC methods showed that it contained 3.16 ± 0.04% protein, 0.21 ± 0.003% lipid, 5.2 ± 2.82% moisture, 5.5 ± 0.42% ash, 1.58 ± 0.04% tannin,1.82 ± 0.05% saponin, 1.37 ± 0.05% alkaloid and 0.98 ± 0.00% flavonoid. Further microbial analysis carried out revealed that the flour had good viable and fungal counts in addition as indicated by the low concentrations of *S. Aureus* and *R. Stolonifer* observed in the processed flour though the fungal counts was higher than the bacterial counts. These findings suggest that unripe plantain flour could serve as a natural source of antioxidants with free radical scavenging activity and its shelf life could be extended if packaged well and stored.

INTRODUCTION

Food processing is probably the most important source of income and employment in Africa, Asia and Latin America. The Food and Agriculture Organization of the United Nations has stated that value added through marketing and processing of raw materials can be much greater than the value of primary production (Anonmous, 1995). Some micro-organisms produce chemicals that color, flavor and stabilize foods, thereby increasing their storage lives (Ogunjobi *et al.*, 2005). These types of foods are important because of their increased nutritional values as well as improved flavor and aroma characteristics.

For a long period of time, plants have been a reliable source of natural products for maintaining human health, especially in the last decade, with more intensive studies devoted to natural therapies (Kumar *et al.*, 2005; Pourmorad *et al.,* 2006). The World Health Organization has recommended that this should be encouraged especially in areas where access to conventional treatment is not adequate (WHO, 1980).

Fruits and vegetables are good sources of proximates and phytochemicals such as carotenoids, flavonoids and other phenolic compounds. Studies have indicated that these phytochemicals especially polyphenols have high free radical scavenging activity, which helps to reduce the risk of chronic diseases such as cardiovascular disease, cancer, etc (Ames *et al.*, 1993). In addition, phytochemicals also act as potent antioxidants in both fat soluble and water soluble body fluids and cellular components (Mathur and Mathur, 2001) and also posses biological characteristics like anti-carcinogenicity, anti-mutagenecity, anti-aging activity and anti-cholesterol activity.

Unripe plantain is a plant that is well known to the traditional medical practioners in Nigeria. It's used in the treatment of diabetic conditions and other related ailments in addition to its nutritive components.

Since free radicals have been associated with some of these disorders and being that the phytochemicals present in plants are known to possess anti-oxidative or free radical scavenging activity, the antioxidant and nutrient composition of this plant ought to be investigated.

This thus leads to the basis of this research which is designed to understudy the total antioxidant capacity, nutrient composition, microbial load and percentage inhibitory activity of unripe plantain flour.

MATERIALS AND METHODS

Chemicals
Quercetin and DPPH (2, 2 – diphenyl - 1- picrylhydrazyl) used were products of Sigma Chemical Company (UK). Peroxidase used was purchased from Horseradish. All

---

*Corresponding author email: eleazon@yahoo.com

other chemicals used were purchased from Associated Laboratories, Aba, Abia State, Nigeria.

Plant Materials
Unripe plantain used was bought locally from the market in Umuahia, Abia State, Nigeria. It was thoroughly washed, peeled, sliced and oven dried for 24hours at a temperature of 50°C.

Preparation of Plant Materials for Analysis
The peeled portion of the unripe plantain was processed into flour using a food processor and the flour was then used for analysis.

Proximate Composition of Unripe Plantain Flour
Moisture, crude protein, crude fat and total carbohydrates were analyzed according to the AOAC (1990) methods. The values reported are means of triplicate samples with their standard deviations.

Phytochemical Composition of Unripe Plantain Flour
The gravimetric method of Harbone (1967) was used in the determination of the total alkaloid content while the AOAC (1984) method was used in the determination of other phytochemical constituents of the sample.

Assay of DPPH Radical Scavenging Activity
The free radical scavenging activity of the plantain extract was determined using the modified method of Blois (1985). 1ml of different concentrations (500, 250, 125, 62.5, 31.25ug/ml) of extracts and standard quercetin was added to 1ml of 0.3mm DPPH in methanol to bring the final concentration of 250, 125, 31.25, and 15.62ug/ml. The mixture was vortexed and incubated in a dark chamber for 30minutes and the absorbance read at 517nm against a DPPH control which contained 1ml of methanol.

The Percentage Inhibition was calculated as:

$$\% \text{ Inhibition} = \frac{\text{Absorbance of Control - Absorbance of Sample}}{\text{Absorbance of Control}} \times \frac{100}{1}$$

Assay of Total Antioxidant Activity
The total antioxidant activity was measured according to the method described by Hsu *et al*. (2003). 0.2ml of peroxidase + 0.2ml of H_2O_2 (50um) + 0.2ml ABTS (100um) + 1ml distilled water were mixed together and left in the dark to form a bluish green complex.

After adding 1ml of methanolic plantain flour extract, the absorbance was measured at 734nm to represent the total antioxidant activity.

Microbial Analysis
The total viable counts and fungal counts of the flour were determined using the Pour plate technique (Ezeama, 2007). 5g of the flour was blended in 45ml of 0.1% peptone water (PH 7.2 ± 0.2) to obtain a dilution 1:10,

from which subsequent dilutions were made and appropriate aliquot used to determine the total viable counts (TVC) on Trypton Soya Agar and Potato Dextrose Agar for total fungal count (TFC). After aerobic incubation at 35 – 37°C for 18-24hours for TVC and room temperature for 2-5days for TFC, the colonies were observed and counted and results expressed as Colony forming unit per gram (Cfug $^{-1}$). Colonies were purified by sub-culturing on fresh Tryptophon Soya Agar and grams stained for morphological examination. Further biochemical tests were done for characterization and identification of the isolates. The colonies of the fungi emerging within 2 - 5days of inoculation were identified under the light microscope (x 40) and recorded. Each experiment was performed in triplicates.

Statistical Analysis
Statistical analysis was conducted using the means ± std of 3 experiments. Results were considered significant at P < 0.05.

RESULTS AND DISCUSSION

In the study carried out, the proximate composition of the locally consumed unripe plantain flour showed that it contained low quantities of ash which reflected the mineral contents of the plantain (Table1). Plantains have been reported to contain low quantities of minerals (Ketiku, 1973).

The low fat contents obtained in the unripe plantain flours were in accordance with previous reports (Agunbiade *et al.,* 2006). The low crude protein content obtained in the plantain flours were also in accordance with previous studies (Brakohiapa *et al.*, 2001). Since a healthy adult needs about 0.75g of protein per kg per day, plantains alone cannot meet adult protein diet.

The low total carbohydrate obtained in the unripe plantain flour would be expected since unripe plantain contains large amount of starch and low sugar in its green stage (Table 1). Similar results have been reported (Ahenkora *et al.*, 1998). The moisture content was also found to be in agreement with earlier reports Ketiku (1973).

Table 1. Proximate Composition of Unripe Plantain Flour.

Proximate Analyzed	Percentage Composition
Ash	5.50 ± 0.420
Carbohydrate	39.14 ± 0.212
Protein	3.15 ± 0.042
Lipid	0.21 ± 0.028
Moisture	5.2 ± 2.800

Values in the table were obtained by calculating the mean ± std of 3 experiments.

Phytochemical Composition of Unripe Plantain Flour

The phytochemical composition of unripe plantain flour showed that it contained some quantities of flavonoids, saponins and alkaloids (Table 2). Saponins are known to possess both beneficial (cholesterol lowering) and deleterious (cytotoxic permeabilization of the intestine) properties (Price *et al.*, 1987). However, the levels of saponin in the flour are quite too low to cause any deleterious effects.

Flavonoids, alkaloids and tannins are polyphenolic compounds with antioxidant properties. Phenolics have been associated with antioxidant properties of food (Robbins, 2003). It has also been reported that phenolic compounds in plants possess antioxidant activity and may help protect cells against the oxidative damage caused by free radicals (Kirakosyan *et al.*, 2003).

The present study results show that unripe plantain flour contains considerable amount of phenolics and this implies that it may be useful in relation to diseases involving free radical reactions.

Table 2. Phytochemical Composition of Unripe Plantain Flour.

Phytochemical	Percentage Composition
Tannin	1.577 ± 0.004
Alkaloid	1.37 ± 0.048
Saponin	1.827 ± 0.0042
Flavonoid	0.981 ± 0.0014

Each value in the table is the average of triplicate experiments ± standard deviation.

Inhibitory Activity of Unripe Plantain Flour

The high scavenging activity of the unripe plantain flour extract as observed is a major significant finding in this study (Table 3). This is attributable to the phenolic content and presence of other phytochemicals in the unripe plantain. However, we could not prove if the free radical scavenging activity came solely from the phenols present or other phytochemicals or a combination of both.

Antioxidant Activity of Unripe Plantain Flour

The high antioxidant activity of the methanolic extract of unripe plantain flour as obtained in table 3 is another significant finding in this study. This is thought to arise from the presence of phenolics and phytochemicals in the unripe plantain flour which are high potency antioxidants with free radical scavenging activities. These results obtained indicate the potentials in unripe plantain flour as a natural source of antioxidants and could be of medicinal purposes in treatment of ailments implicating free radicals.

Table 3. Total Antioxidant Activity of Unripe Plantain Flour/Percentage Inhibition on DPPH Radical.

Antioxidant/DPPH	Activity/Inhibition
Peroxidase	52%
DPPH Radical	78%

Each value in the table was derived by calculating the average of 3 experiments ± standard deviation.

Microbial Analysis

The Total Fungal Counts and Viable Counts of the processed unripe plantain flour as observed in table 4 were 1.6×10^2 and 3.6×10^3 colony forming units per gram ($cfug^{-1}$) respectively. The flour had higher bacterial counts than fungal counts. The processing techniques minimized contamination and oven drying helped to inhibit microbial proliferation. The micro-organisms isolated from the flour include *Staphylococc aureus* and *Rhizopus stolonifer*. Although the organisms are potential pathogenic organisms, the counts recorded are quite low to cause any health hazards. Our results obtained are consistent with FAO (2003) and this implies that the flour analyzed are quite safe for consumption and their shelf life could be extended if packaged well and stored.

Table 4. Total Viable Counts and Total Fungal Counts of Unripe Plantain Flour.

Sample	Total Viable Counts ($cfug^{-1}$)	Total Fungal Counts ($cfug^{-1}$)
Unripe Plantain Flour	3.6×10^3	1.6×10^2

Results under the table are the means of triplicate experiments and are in coliform units per gram ($cfug^{-1}$). Values are significant at $P < 0.05$.

In conclusion, that unripe plantain flour is a good source of antioxidants with free radical scavenging activity has been demonstrated in this study. Although it was found to contain *S. aureus* and *R. stolonifer* which are potential pathogenic organisms, however their concentrations are quite too small to cause any health hazards indicating good microbial load for the flour and this implies that its shelf life could be extended if packaged well and stored.

ACKNOWLEDGEMENT

REFERENCES

Agunbiade, SO., Olanlokun, JO. and Olaofe, OA. 2006. Quality of chips produced from rehydrated dehydrated plantain and banana. J. Nutrition. 5(5):471-473.

Ahenkora, K., Kyei, MA., Marfo, EK. and Banful, B. 1998. Nutritional composition of false horn Apantuba plantain during ripening and processing. J Food Chem. 455-458.

Ames, BM., Shigena, MK. and Hagen, TM. 1993. Oxidants, antioxidants and the degenerative diseases of ageing. Proceedings of the National Academy of Science. 90:7915-7922.

Anonmous. 1995. Food for Consumers. Food and Agriculture Organization, Rome, Italy.

Association of Official Analytical Chemists. 1990. Official Methods of Analysis. Ed. Horwitz, W. (13th ed.). 233-234.

Association of Official Analytical Chemists. 1984. Official Methods of Analysis. (14th ed.). 242 - 245.

Brakohiapa, LA., Quaya, IK., Amoah, AG., Harrison, EK., Kennedy, DO., Kido, Y. and Ofei, E. 2001. Noguchi Memorial Institute for Medical Research. University of Ghana Region, Accra. 220-221.

Blois, MS. 1985. Antioxidant determination by use of stable free radicals. Nature. 29:1199-1200.

Ezeama, CF. 2007. Food Microbiology, Fundamentals and Applications. Natural Prints Limited, Lagos, Nigeria. 64-68.

FAO. 2003. The State of Food Security in the World. Food and Agricultural Organization, Rome, Italy.

Kirkosyan, A., Seymour, E., Kaufman, OB., Warber, SE. and Chang, SC. 2003. Antioxidant capacity of polyphenolic extracts from leaves of *Crataegus laevigata* and *Crataegus monogyna* (Hawthorn) subjected to drought and cold stress. J. Agricultural and Food Chemistry.51:3973-3976.

Kumar, RS., Sivakuma, T., Sunderem, RS., Gupta, M., Murujesh, K., Rajeshwa, Y., Kumar, MS. and Kumar, KA. 2005. Antioxidant and antimicrobial activities of *Bauhima Recemosa* L Stem Bark. J. Med. Biol. Res. 38:1015-1024.

Marthur, NK. and Marthur,V. 2001. Antioxidants: Natural ingredients and additives for food. Beverage Food World. 5:13-15.

Ogunjobi, AA., Adebayo-Tayo, BC. and Ogunshe, AA. 2005. Microbiological, proximate analysis and sensory evaluation of processed Irish potato fermented in brine solution. Afr, J. Biotechnol. 14:1409-1412.

Pourmorad, F., Hosseinimehr, SJ. and Shanabi, MN. 2006. Antioxidant activity, phenolic and flavonoid content of some selected Iranian medicinal plants. Afr. J. Biotechnol. 5(11):1142-1145.

Price, KR., Johnson, IT. and Fenwic, CR. 1987. The chemical and biological significance of saponins in food and feeding stuff. Unpublished Critical Reviews in Food science and Nutrition. 26:27-135.

Robbins, RJ. 2003. Phenolic acids in foods. An overview of analytical methodology. J Agricultural and Food Chemistry. 51:2886-2887.

WHO. 1980. Expert committee on diabetes mellitus. Second Report. Technical Report Series 646. World Health Organization, Geneva. 12-15.

STUDY OF *IN VITRO* ANTHELMINTIC ACTIVITY
OF *CAESALPINIA BONDUC* LEAVES

Geeta Kaura[1] , *Ashish Suttee[1], Disha Arora[2] and Anupum Sharma[2]
[1]Department of Pharmaceutical Sciences, Lovely Professional University, Phagwara, Punjab
[2]University Institute of Pharmaceutical Sciences, Panjab University, Chandigarh-160014, India

ABSTRACT

The *in vitro* anthelmintic activity of *Caesalpinia bonduc* leaves was evalauated. Four extracts viz. Petroleum ether, Dichloromethane (DCM), Ethyl acetate and Ethanol extracts of *Caesalpinia Bonduc* leaves were investigated for the anthelmintic activity against Earthworms (*Eisenia foetida*). Three concentrations (20, 40, 60mg/ml) of each extract were studied which included the determination of time of paralysis and time of death of earthworms. Piperazine citrate (10mg/ml) was used as standard drug and distilled water containing 2% Tween 80 was used as control. All the extracts exhibited dose dependent anthelmintic activity. The decreasing order of activity of extracts was ethyl acetate, ethanol, DCM and petroleum ether extracts. An Ethyl acetate extract of plant leaf exhibited in vitro anthelmintic activity in a concentration range of (20-60mg/ml). Conclusively, ethyl acetate extract of *Caesalpinia bonduc* leaves possesses vermicidal activity and found to be effective as an anthelmintic.

Keywords: *Caesalpinia bonduc, Eisenia foetida,* anthelmintic, piperazine citrate.

INTRODUCTION

There are about 60 Species in the genus *Caesalpinia* which are tropical and subtropical and widely used for medicinal purposes. This genus contains mostly trees or climbing shrubs. In this study, anthelmintic activity of one species of this genus viz. *Caesalpinia bonduc* has been evaluated. *Caesalpinia bonduc* is a large, thorny, straggling, shrub which behaves like a strong woody climber, taking support of trees. The branches are armed with hooks and straight hard yellow prickles. Leaves are large, double compound, with 7 pairs of pinnae, and each with 3-8 pairs of leaflets with 1-2 small recurved prickles between them on the underside. Flowers are yellow, in dense long-stalked racemes at the top. Fruits are inflated pods, covered with prickles. Seeds are 1-2 per pod, oblong or globular, hard, grey with a smooth shiny surface. The hard and shiny seeds are green, turning grey (Kirtikar and Basu, 1999).

Leaves and seeds after roasting with castor oil are applied externally to inflammatory swellings especially to inflamed piles (Kirtikar and Basu, 1999).

Common names include fever nut, bonduc nut (Kirtikar and Basu, 1999). The chemical constituents present in it are flavonoids, terpenoids, alkaloids, glycosides, phenols, tannins and phytosterols.

MATERIALS AND METHODS

Collection of plant material and its identification
The leaves of *Caesalpinia bonduc* were collected from

*Corresponding author email: ashish7sattee@gmail.com

Dindigul, Tamil Nadu, India, during the month of August 2009. The botanical identity of the plant was confirmed by Regional Research Institute, Bangalore, India. A voucher specimen (RRI/BNG/SMP/Drug Authentication/ 2009-10/552) has been deposited at the Museum of the Department of Pharmacognosy, Lovely School of Pharmaceutical Sciences, Phagwara, Punjab, India.

Traditional uses: The leaves are used traditionally as emmenagogue, abortifacient, laxative, purgative and cathartic. The flowers are used as anthelmintic and in the treatment of cough and catarrh (Khare, 2007).

Extracts used: Four extracts were used viz. petroleum ether, DCM, ethyl acetate and ethanol extracts which were prepared by adopting the successive solvent extraction method using the Soxhlet apparatus.

Organism used: Adult same age Earthworms (*Eisenia foetida*) were used and were procured and authenticated from Ujjwal Ujala Vermi Group, Amritsar.

Anthelmintic activity: Test samples of all the four extracts were prepared in the concentrations, 20, 40 and 60 mg/ml in 25ml of distilled water containing 2% Tween 80. Six earthworms of approximately same size were placed in petridish (diameter 9cm) containing above solution of extracts. Piperazine citrate (10mg/ml) was used as standard drug and distilled water containing 2% Tween 80 was used as control. Anthelmintic activity of Piperazine citrate mediates through hyper polarization that leads to muscle relaxation and flaccid paralysis (Martin, 1985). Time for paralysis was noted when no movement of any sort could be observed except when the

worms were shaken vigorously. Time of death for worms was noted when the earthworms neither moved when shaken vigorously nor when dipped in warm water 50˚C (Kosalge, 2009). Indian earth worms resemble intestinal round worm parasite of human beings (Vidyarthi, 1967; Chatterjee, 1967). Tannins produce anthelmintic activity by binding to free protein in the gastrointestinal tract of the host animal (Athnasiaduo, 2001) or glycoprotein on the cuticle of the parasite (Thompson, 19950 and phenolic compounds by uncoupling oxidative phosphorylation hinder the energy production in helminth parasites (Martin, 1997). Phytochemical analysis of leaves of *C. Bonduc*revealed the presence of tannins as one of the constituent.

RESULTS AND DISCUSSION

As reported in the tables 1 and 2. All the extracts exhibited dose dependent anthelmintic activity against earthworms. *C. bonduc* leaf extracts showed significant effects (P<0.001) at the tested concentrations (20-60mg/ml) as determined by the paralysis and death time (Table 1and 2). Ethyl acetate extract was most effective in causing death of earthworms at all concentrations. The decreasing order of anthelmintic activity of different extracts taken comes out to be - ethyl acetate > ethanol > DCM > petroleum ether extracts. Ethyl acetate extract exhibits better anthelmintic activity than the standard. In the case of petroleum ether extract, paralysis was caused earlier howver death time was longer. In the case of DCM extract, the paralysis time was longer at lower dose (20mg/ml) but shorter at higher doses (40-60 mg/ml). The death time was long but shorter than that of petroleum ether extract. In case of ethyl acetate and ethanol extracts, paralysis and death times were nearly similar to all doses. Further study is to be done to determine the mechanism involved and constituent responsible for anthelmintic property.

Table 1. Effects of control and standard drug on earthworms (Gbolade, 2008).

Conc. (mg/ml)	Control		Standard	
	Paralysis time (min.)	Death time (min.)	Paralysis time (min.)	Death time (min.)
10	-	-	30.3±0.88	80.67±0.67

Table 2. Effects of *C. bonduc* leaf extracts on earthworms (Gbolade, 2008).

Conc. (mg/ml)	Petroleum extract		DCM extract		Ethyl acetate extract		Ethanol extract	
	Paralysis time (min.)	Death time (min.)	Paralysis time (min.)	Death time (min.)	Paralysis time (min.)	Death time (min.)	Paralysis time (min.)	Death time (min.)
20	21 ± 0.58**	481.67 ± 0.88**	122.3 ± 1.45**	210.67 ± 0.67**	8.33 ± 0.88**	13.67 ± 0.88**	62.7 ± 1.45**	76 ± 1.0**
40	18 ± 0.58**	361 ± 1.0**	32.3 ± 1.45	165 ± 0.58**	5 ± 0.58**	9.33 ± 0.67**	16.8 ± 1.64**	22 ± 0.58**
60	15.67 ± 0.67**	301.67 ± 0.88**	20.3 ± 0.88**	119.67 ± 0.33**	3.5 ± 0.29**	5.5 ± 0.29**	13.5 ± 0.29**	21.67 ± 0.88**

Significant at *P<0.05, **P<0.01 (One way ANOVA followed by Dunnet test: compare all vs. standard applied) Standard vs. low, medium and high doses of CP. Values are mean ± SEM, n = 3. CP- *Caesalpinia bonduc*
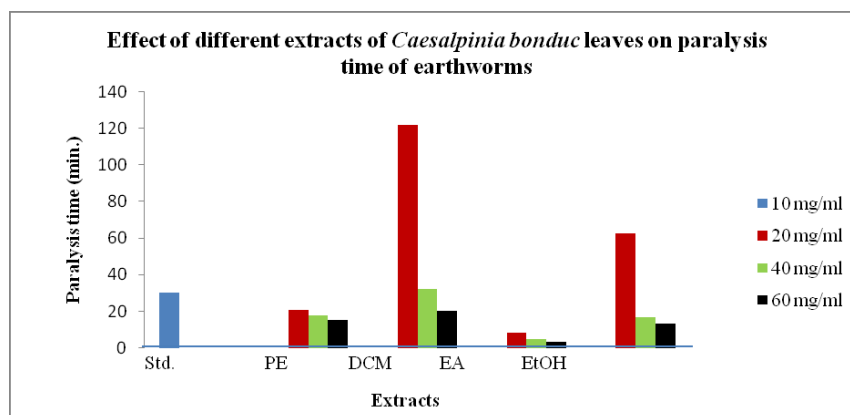

Fig. 1. Graph showing effect of different extracts of *Caesalpinia bonduc* leaves on paralysis time of earthworms. PE- Petroleum ether, DCM- Dichloromethane, EA- Ethyl acetate, EtOH- Ethanol, Std.- Standard (Piperazine citrate).
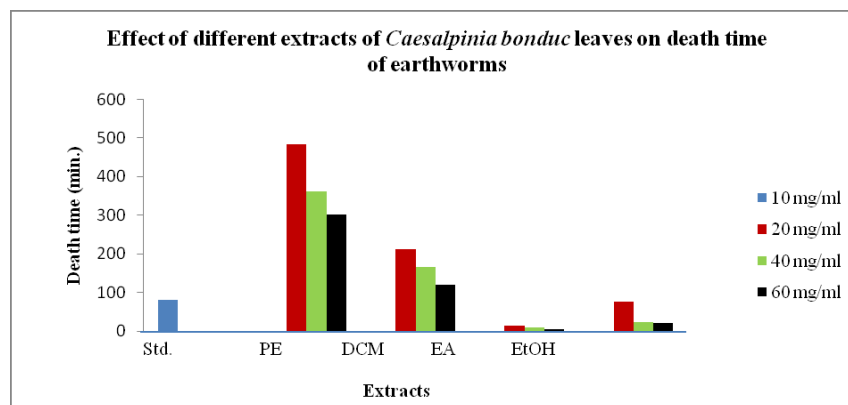
Fig. 2. Graph showing effect of different extracts of *Caesalpinia bonduc* leaves on death time of earthworms.
PE- Petroleum ether, DCM- Dichloromethane, EA- Ethyl acetate, EtOH- Ethanol, Std.- Standard (Piperazine citrate)

REFERENCES

Athnasiaduo, S., Kyriazakis, I., Jackson, F. and Coop, RL. 2001. Direct anthelmintic effect of condensed tannins towards different gastrointestinal nematodes of sheep, *in vitro* and *in vivo* studies, Vet parasitol. 99:205-219.

Chatterjee, KD. 1967. Parasitology, Protozoology and Helminthology. (6th ed.). Guha Ray Sree Saraswathy Press Ltd, Calcutta, India.

Gbolade, AA. and Adeyemi, AA. 2008. Anthelmintic activities of three medicinal plants from Nigeria, Fitoterapia. 7:223-225.

Gbolade, AA. and Adeyemi, AA. 2008. Investigation of *in vitro* anthelmintic activities of *Pycnanthus angolensis* and *Sphenocentrum jollyanum*, Fitoterapia. 79:220-222.

Khare, CP. 2007. Indian Medicinal Plants. An Illustrated Dictionary, Springer Science & Business Media, LLC., Spring Street, New York, USA.

Kirtikar, KR., Basu, BD., Singh, B. and Singh, MP. 1999. Indian Medicinal Plants. Dehradun, India.

Kirtikar, KR. and Basu, BD. 1999. Quality Standards of Indian Medicinal Plants. Indian Council of Medical Research, New Delhi.

Martin, RJ. 1985. γ – Amino butric acid and Piperazine activated single channel current from *Ascaris suum* body muscle. Br. J. Pharmacol. 84:445-461.

Martin, RJ. 1997. Mode of action of Anthelmintic Drugs. Vet. J. 154:11-34.

Vidyarthi, RD. 1967. A Text Book of Zoology (14th ed.). S. Chand and Co, New Delhi, India.

Kosalge, SB. and Fursule, RA. 2009. Investigation of anthelmintic potential of some plants claimed by Tribals of Satpuda Hills. Int. J. Pharm. Tech Res. 1:68-72.

Thompson, DP. and Geary, TG. 1995. The structure and function of helminthes surfaces: In: Biochemistry and Molecular Biology of Parasites. Ed. Marr, JJ. (1st ed.). Academic Press, New York, USA. 203-232.

SHORT COMMUNICATION

ANTIMICROBIAL ACTIVITY OF SOME MEDICINAL PLANTS USED IN SAUDI ARABIA

Amal Abdulaziz Al-Juraifani
Department of Biology, Faculty of Science
Dammam University, P O Box 838, Dammam-31113, Saudi Arabia

ABSTRACT

The antimicrobial activity of four plants' extracts (Thyme leaves (*Thymus vulgaris*), Sage leaves (*Salvia officinalis*), Myrrh exudates (*Boswelia carterii*) and Oliban (*Boswelia carterii*)), used in traditional medicine in Saudi Arabia and other Middle East countries, were evaluated against the following seven bacterial species, *Streptococcus* sp., *Staphylococcus aureus, Vibrio tubiashii, Micrococcus luteus* ATCC 9341, *Cellulosimicrobium cellulans, Bacillus cereus* and *Legionella pneumophila* and two fungi species, *Aspergillus flavus* and *Fusarium oxysporum* f. sp. *Lycopersicii.* Our results showed that the highest antimicrobial activity was observed for the extracts of Thyme, Myrrah and Sage, and the Oliban extracts did not present any antimicrobial activity at any concentration. The minimum inhibitory concentration ranged from 2.0-4.0 % (v/v) for Thyme and Myrrh. The fungal species tested differed significantly in their susceptibility to plant extracts, with complete inhibition by Thyme to all tested microorganisms.

Keywords: Antimicrobial activity, medicinal plants, plant extract.

INTRODUCTION

Even though pharmacological industries have produced a number of new antibiotics in the last three decades, resistance to these drugs by microorganisms has increased. In general, bacteria has the genetic ability to transmit and acquire resistance to drugs, which are utilized as therapeutic agents (Cohen, 1992). This is a cause for concern as the numbers of patients in hospitals have suppressed immunity, due to new bacterial strains, which are multi resistant. Consequently, new infections can occur in hospitals resulting in high mortality. Herbal medicines are widely used for the treatment and prevention of various illnesses (Taha Al-Sayed, 2000), and it is adapted to local environment and conditions, compared with any introduced species (Mahasneh and El-Oqlah, 1996, 1999; Jaouhari *et al*., 2000). Several kinds of extracts and metabolites from various Gulf region plants have been isolated and their chemical structure has been elucidated (Al-Easa *et al.,* 1990; Mahasneh, 2000; Saadabi, 2006; Abou-zeid *et al.*, 2008; Fardos, 2009; Nehal and Rokayah, 2009). However, the biological activity of such extracts and compounds against certain bacteria and fungi are poorly investigated. The literature search has indicated a total absence of information about the antimicrobial activity of Saudi medicinal plants. In this study an attempt was made to investigate the four commonly used plants in traditional medicine for their possible antimicrobial and antifungal activities.

Corresponding author email: land8080@gmail.com

MATERIALS AND METHODS

Medicinal plant materials
Samples of four medicinal plants i.e. Thyme leaves (*Thymus vulgaris*), Sage leaves (*Salvia officinalis*), Myrrh exudates (*Boswelia carterii*) and Oliban (*Boswelia carterii)* were collected during summer 2010 from different stores in Dammam, Saudi Arabia and identified by Pharmacology Department, in King Saud University, Riyadh. The plants were brought to the laboratory and thoroughly washed in running tap water to remove debris and dust particles and dried in shade then stored until use.

Plant Extract Preparation:
The plants were finely grinded to powder form and homogenized in 200 ml of ethanol (96%) and distilled water (20:80 V: V) for 10 min., then left in dark glass bottles for 72hours for tissue maceration. The extracts were filtered through thin cheesecloth sheets. The final extracts were collected separately in other dark glass bottles and exposed to 60°C in water bath for 3 min. for ethanol evaporation. The collected extracts were then stored in refrigerator at 5°C until needed (Table 1).

Microbial Culture and Growth Conditions:
Tested microorganisms included seven bacterial species: *Vibrio tubiashii, Staphylococcus aureus, Streptococcus* sp., *Micrococcus Luteus* ATCC9341, *Cellulosimicrobium cellulans, Bacillus cereus, Legionella pheumophila* and two fungal species. *Aspergillus flavus* and *Fusarium oxysporum* f sp. *Lycoperscii.* Cultures of bacteria were

grown for 12hours in 50ml nutrient broth (NA) (Difco, USA) at 37°C and were maintained on nutrient agar (Difco, USA) at 4°C. Cultures of fungi were grown in malt broth (Oxoid, UK) at 28°C and were maintained on Potato dextrose agar (PDA) (Difco, USA) plates. All the test organisms were obtained from Biological Sciences Department of the University of Dammam.

Antimicrobial Activity Assay:
The plant extracts were added to conical flasks containing sterilized PDA (Potato dextrose agar) for fungi culture and NA (Nutrient agar) for bacterial culture before its solidifying to obtain the proposed concentrations of 2,4,6,8,10 % (v/v). Twenty ml of amended media were poured into 9cm diameter, Petri dishes, and another set of untreated PDA, and NA plates were used as control (Nehal and Rokayah, 2009). All plates were inoculated individually with 0.5cm diameter of the tested organisms' culture. Plates with fungal species were incubated in the dark at 25 ± 2°C till the organism reached full growth whereas the bacterial cultured plates were incubated at

30-32°C for 24hours. Antimicrobial activity was recorded as the width (in millimeters) of the growth in the agar. The results were reported as positive (+) if there was inhibition of growth and negative (-) if there was no inhibition of growth. Triplicate sets of plates were prepared and the mean of three readings was calculated and used in the analysis for Minimum Inhibitory Concentration (MICs) which were determined after 24hours for the bacteria and after 48hours for fungi. The MICs were determined as the lowest concentration of plant extract inhibiting the visible growth of each organism on the agar plate. The presence of one or two colonies was regarded as no growth (Mitscher *et al.*, 1987; Kawther, 2007).

RESULTS AND DISCUSSION

The results (Table 2) showed that the inhibitory activity increases with increased concentrations of plants' extracts. The extracts from Thyme, Sage, Myrrah and Oliban presented antimicrobial activity to the most of the

Table 1. Botanical classification and active principles of the plants.

Common Name	Scientific Name	Plant Parts Used	Descriptions
Thyme	*Thymus vulgaris L.*	Stripped and dried and flowers	Chemical oils (thymol and carvacrol), flavonoids, tannins and triterpenes
Sage	*Salvia officinalis L.*	Leaves	rosmarinic, caffeic, chlorogenic acids, carnosol, flavonoids, essential oil (thuyone and cineole)
Oliban	*Boswelia carterii*	Stem exudates	Resin, gum, essential oil (filandrin, painen) and oliben compound
Myrrh	*Commiphora molmol*	Stem exudates	Resin, gum and essential oil (Determine B-eudesmol and α –copaene)

Table 2. Antimicrobial activity caused by plant extracts through agar Diffusion method.

Micro-organisms	Thyme					Extract Sage					Myrrh					Oliban				
	2	4	6	8	10	2	4	6	8	10	2	4	6	8	10	2	4	6	8	10
Fusarium oxysporum	+	++	+++	+++	+++	-	-	-	-	+	-	-	+	++	++	-	-	-	-	+
Aspergillus flavus	+++	+++	+++	+++	+++	++	++	+++	+++	+++	+++	+++	+++	+++	+++	-	-	-	-	-
taphylococcus aureus	++	++	+++	+++	+++	-	+	++	+++	+++	-	+	++	++	++	-	+	+	++	++
Vibrio tubiashii	++	++	+++	+++	+++	-	+	++	+++	+++	++	+++	+++	+++	+++	-	+	++	+++	+++
Streptococcus sp.	++	++	+++	+++	+++	-	+	++	+++	+++	++	++	++	+++	+++	-	+	+	++	++
Cellulosimicrobium cellulans	++	+++	+++	+++	+++	-	+	++	+++	+++	+	+	++	++	++	-	+	+	++	++
Micrococcos luteus	++	+++	+++	+++	+++	+	++	+++	+++	+++	-	+	+	+	++	+	++	++	+++	+++
Legionella pneumophila	++	+++	+++	+++	+++	-	+	++	+++	+++	++	++	+++	+++	+++	-	++	+++	+++	+++
Bacillus cereus	+	++	++	++	++	-	+	++	+++	+++	+	++	++	+++	+++	-	+	++	++	++

Data are presented as follows, - = No inhibition of fungal growth, + = Slight inhibition, ++ =Moderate inhibition, +++= Strong inhibition.

tested microorganisms. The extracts from Thyme and Myrrah presented the highest activities followed by Sage and then Oliban. However the tested bacteria showed high significant susceptibility to these extracts more than the tested fungi. The Oliban had no activity against *Aspergillus flavus* and slightly inhibitory action at concentration of 10% (v/v) against *Fusarium oxysporum* f. sp. *Lycopersici.* The minimum inhibitory concentration ranged from 4 – 6 %(v/v) for Thyme and Myrrh, 6 -8 %(v/v) of Sage, and from 8 -10 %(v/v) of Oliban.

This present study, showed high inhibitory action of plants extract to tested microorganisms (Table 2). There was high positive correlation between the increased concentration and an antimicrobial activity until a certain limit (Cimanga *et al.,* 2002; Marcelo *et al.*, 2006; Nehal and Rokayah, 2009). Thyme extract showed the highest activity against the two fungal species and seven bacterial species (Dorman and Deans, 1999; Gislene *et al.,* 2000; Marcelo *et al.,* 2006). Moreover Essawi and Srour (2000) and Al-Turki (2002) added that the activity was attributed to the presence of several compounds working together such as, thymol, carvacrol, flavonoids and tannins. Our results showed that Thyme and Myrrh demonstrated higher anti microbial activity compared with Sage, this data is in agreement with Hammer *et al.* (2001), Al-Turki (2002) and Mahasneh (2002). The fungal strains tested differed significantly in their susceptibility to plants extract. On the contrary, Oliban extract showed no inhibitory action on two fungal strains and lowest inhibitory action on bacterial strains compared with another plants extract that can be traced back to the Resin, Gum, essential oil, filandrin and painen.

Antimicrobial phytochemicals are rosmarinic, caffeic, chlorogenic acids carnosol, flavonoids, rein, gum and essential oils plus other compounds. The mechanisms thought to be responsible for these phytochemicals against microorganisms vary and depends on these compounds (Mossa *et al.*, 2001; Rios and Recio, 2005; Aly and Bafiel, 2008). Their mechanism of action may include enzyme inhibition by the oxidized compounds, and act as a source of stable free radical often leading to inactivation of the protein and loss of function. They have the ability to intercolate with DNA, formation of ion channels in the microbial membrane (Ali, 1999), competitive inhabitation of adhesion of microbial proteins to host polysaccharide receptors (Cowan, 1999). Therefore, it is important that the plant species which have demonstrated growth inhibiting activity in this assay be further investigated to evaluate the significance of these extracts, clinical role and the medical system of indigenous people. Additional research is also necessary to isolate and characterize their active compounds for pharmacological testing.

REFERENCES

Abou Zeid, AM., Altalhi, AD. and El-Fattah, RI. 2008. Fungal control of pathogenic fungi isolated from some wild plants in Taif Governorate, Saudi Arabia. Mal. J. Microbial. 4 (1):30-39.

Al-Easa, HS., Mann, J. and Rizk, A. 1990. Guainolides from *Centaurea sinaica*. Phytochemistry. 29:1324-1325.

Ali, AA. 1999. Studies on some medicinal plants as a source of antifungal substances in North Africa. M.Sc. Thesis, Inst. of African Res. and Studies, Cairo University.

Al-Turki, AI. 2002. Antibacterial effect of thyme, peppermint, sage, blackpepper and garlic hydrosols against *Bacillus Subtilis* and *Salmonella enteritidis.* J. food, Agriculture & Environment. 5(2):92-94.

Aly MM. and Bafiel, S. 2008. Screening for antimicrobial activity of some medicinal plants in Saudi Arabia. World Conference on Medical and Aromatic. 5(3):211-220.

Cimanga, K., Kambu, K., Tona, L., Apers, S., Debruyne, N., Hermans, J.,Totte, J. ,Pieters, L. and Vlietinck, AJ. 2002. Correlation between chemical composition and antibacterial activity of essential oils of some aromatic medicinal plants growing in the Democratic Republic of Congo. J. Ethnopharmacology. 79(2):213-220.

Cohen, ML. 1992. Epidemiology of drug resistance: implications for a post-antimicrobial era. Science 257:1050-1055.

Cowan, MM. 1999. Plant products as antimicrobial agents. Clin. Microbial. Rev. 12:564-582.

Dorman, HJD. and Deans, SG. 1999. Antimicrobial agent from plants: antimicrobial activity of plant volatile oils. J of Applied Microbiology. 88(2):308-316.

Essawi, T. and Srour, M. 2000 .Screening of some palastinian medicinal plants for antibacterial activity. J. of Ethnopharmacology. 70(2):343-349.

Fardos, MB. 2009. Antifungal activity of some medicinal plants used in Jeddah, Saudi Arabia. Mycophath. 7(1):51-57.

Gislene, GF., Juliana, L., Paulo, CF. and Giuliana, LS. 2000. Antibacterial activity of plant extracts and phytochemicals on antibiotic- resistant bacteria. Brazilian J. of Microbiology. 31(4): 247-256.

Hammer, KA., Carson, CF. and Rily, TV. 2001. Antimicrobial activity of essential oils and other plant extracts. J. Applied Micro. 86(6):985-990.

Jaouhari, JT., Lazrek, HB. and Jana, M. 2000 . the hypoglycemic activity of *Zygophyllum gaetulum* extracts in alloxan induced hyperglycemic rats. J. Ethnopharm. 69:17-20.

Kawther, FA. 2007. Antibacterial and anticandidal activity of essential oils of some medicinal plants in Saudi Arabia. Saudi J. of Biological sciences. 14(2):245-250.

Mahasneh, AM. 2002. Screening of some indigenous Qatari medicinal plants fro antimicrobial activity. Phytother Res. 16:751-753.

Mahasneh, AM. and El-Oqlah, AA. 1996 . Antimicrobial activity of extracts of herbal plants used in the traditional medicine of Bahrain. Phytother Res. 10:251-253.

Mahasneh, AM. and El-Oqlah, AA. 1999. Antimicrobial activity of extracts of herbal plants used in the traditional medicine of Jordan. J. Ethnopharm. 64:271- 276.

Marcelo, CP., Chalfoun, SM., Carlos, JP., Carolina, LA. and William, PM. 2006. Species fungi mycelial development and ochratoxin A production. Scientific Research and Essay. 1(2):038-042.

Mitscher, LA., Drake, S., Gollapudi, SR. and Okwute, SK. 1987. A modern look at folkloric use of anti-infective agents. J. Nat. Prod. 50:1025-40.

Mossa, JS,. Hammer, KA., Carson, CF. and Riley, TV. 2001. Antimicrobial activity of essential oils and other plant extracts. J. Applied Microbiology. K. 86(6):985-990.

Nehal, SE. and Rokayah, SA. 2009. Inhibitory effects of powdered caraway and peppermint extracts on pea root rot under greenhouse conditions. S. J. of Plant Protection Research. 49(1):93-96.

Rios, JL. and Recio, MC. 2005. Medicinal plants and antimicrobial activity. J. Ethnopharmacol.100(1-2):80-84.

Saadabi, AMA. 2006 . Antifungal activity of some Saudi plants used in traditional medicine. Asian J. Plant Sci. 5:907-909.

Taha Al-Sayed, H. 2000. Brine shrimp bioassay of ethanol extracts of *Sesuvium verrucosum, Salsola baryosma* and *Zygophyllum quatarense* medicinal plants from Bahrain. Phytother. Res.14:48-50.

COMMON FIXED POINT THEOREMS FOR OCCASIONALLY WEAKLY COMPATIBL MAPS IN FUZZY METRIC SPACES

*M Alamgir Khan and Sumitra
[1]Department of Mathematics, Eritrea Institute of Technology, Asmara, Eritrea, NE Africa

ABSTRACT

The intent of this paper is to introduce the notion of occasionally weakly compatible (owc) maps and prove common fixed point theorems for single and set valued maps without considering the completeness of the space and continuity of maps in fuzzy metric space. Our results extend, generalize and unify several results existing in the literature.

AMS Mathematics subject classification. 2000. 47H10, 54H25.

Keywords: Weak compatible maps, occasionally weakly compatible maps, fixed points and fuzzy metric space.

INTRODUCTION

It was a turning point in the development of mathematics when Zadeh (1965) introduced the concept of fuzzy set. This laid the foundation of fuzzy mathematics. Consequently, the last three decades were very productive for fuzzy mathematics. Several authors like Deng (1982), Erceg (1979), Kaleva and Seikkala (1984) and Kramosil and Michalek (1975) have introduced the concept of fuzzy metric space in different ways. The concepts of weak commutatively, compatibility, non-compatibility and weak compatibility were frequently used to prove fixed point theorems for single and set valued maps satisfying certain conditions in different spaces.

Al-Thagafi and Shazad (2008) weakened the notion of weakly compatible maps by introducing a new concept of occasionally weakly compatible (owc) maps. This concept is more general among all the commutativity concepts and has opened a new venue for many mathematicians. This newly defined concept has also fascinated many authors like Alamgir and Sumitra (2010), Bouhadjera and Thobie (2008, 2009), Abbas and Rhoades (2007), Gairala and Rawat (2009), and Chandra and Bhatt (2009).

The main purpose of the present paper is to introduce the concept of occasionally weakly compatible (owc) maps in fuzzy metric space and to prove common fixed point theorems for single and set valued maps under strict contractive condition.

Our improvements in this paper are five-fold as:

(i)   Relaxed the continuity of maps completely
(ii) Completeness of the space removed
(iii) Minimal type contractive condition used

*Corresponding author email: alam3333@gmail.com

(iv) The condition $\lim_{t \to \infty} M(x, y, t) = 1$ not used
(v)   Weakened the concept of compatibility by a more general concept of occasionally weak compatible (owc) maps .

We first give some preliminaries and definitions.

1. Preliminaries

Definition 1.1. A binary operation $* : [0,1] \times [0,1] \to [0,1]$ is continuous $t - norm$ if $*$ is satisfying the following conditions:

(i) $*$ is commutative and associative
(ii) $*$ is continuous
(iii) $a * 1 = a \ for \ all \ a \in [0,1]$
(iv) $a * b \le c * d \ whenever \ a \le c \ and \ b \le d$, $a, b, c, d \in [0,1]$.

Definition 1.2. A triplet $(X, M, *)$ is said to be a fuzzy metric space if X is an arbitrary set, $*$ is a continuous $t - norm$ and M is a fuzzy set on $X^2 \times (0, \infty)$ satisfying the following;

(FM-1) $M(x, y, t) > 0$

(FM-2) $M(x, y, t) = 1 \ if \ and \ only \ if \ x = y.$

(FM-3) $M(x, y, t) = M(y, x, t)$

(FM-4) $M(x, y, t) * M(y, z, s) \le M(x, z, t + s)$

(FM-5) $M(x, y, \bullet) : (0, \infty) \to (0,1] \ is \ continuous.$

Note that $M(x, y, t)$ can be thought of as the degree of nearness between x and y with respect to t .

Example 1. (Induced fuzzy metric space) Let (X, d) be a metric space, denote $a * b = ab$ for all $a, b \in [0,1]$ and let M_d be fuzzy set on $X^2 \times (0, \infty)$ defined as follows;

$$M_d(x, y, t) = \frac{t}{t + d(x, y)}.$$

Then $(X, M_d, *)$ is a fuzzy metric space. We call this fuzzy metric induced by a metric d.

Example 2 Let $X = N$. Define $a * b = \max\{0, a + b - 1\}$ for all $a, b \in [0,1]$ and let M be a fuzzy set on $X^2 \times (0, \infty)$ as follows;

$$M(x, y, t) = \begin{cases} \dfrac{x}{y} \text{ if } x \le y \\ \dfrac{y}{x} \text{ if } y \le x \end{cases} \text{ for all } x, y \in X. \text{ Then } (X, M, *)$$

is a fuzzy metric space.
Note that in the above example, there exists no metric d on X, satisfying

$$M(x, y, t) = \frac{t}{t + d(x, y)}, \quad where (X, M, *) \text{ is}$$

defined in above example. Also note that the above function M is not a fuzzy metric with the $t - norm$ defined as $a * b = \min\{a, b\}$.

Through out the paper X will represent the fuzzy metric space $(X, M, *)$ and $CB(X)$, the set of all non-empty closed and bounded sub-sets of X. For $A, B \in CB(X)$ and for every $t > 0$, denote

$$H(A, B, t) = \sup\{M(a, b, t; a \in A, b \in B)\}$$
and
$$\delta_M(A, B, t) = Inf\{M(a, b, t); a \in A, b \in B\}.$$

If A consists of a single point a, we write $\delta_M(A, B, t) = \delta_M(a, B, t)$. If B also consists of a single point b, we write $\delta_M(A, B, t) = M(a, b, t)$.

It follows immediately from definition that

$$\delta_M(A, B, t) = \delta_M(B, A, t) \ge 0$$
$$\delta_M(A, B, t) = 1 \Leftrightarrow A = B = \{a\} \text{ for all } A, B \in CB(X)$$

Definition 1.3. A point $x \in X$ is called a coincidence point (respective fixed point) of $A : X \to X$, $B : X \to CB(X)$ if $Ax \in Bx$ (respective $x = Ax \in Bx$)

Definition 1.4. Maps $A : X \to X$ and $B : X \to CB(X)$ are said to be compatible if $ABx \in CB(X)$ for all $x \in X$ and $lin_{n \to \infty} H(ABx_n, BAx_n, t) = 1$ whenever $\{x_n\}$ is a sequence in X such that $Bx_n \to M \in CB(x)$ and $Ax_n \to x \in M$.

Definition 1.5. Maps $A : X \to X$ and $B : X \to CB(X)$ are said to be weakly compatible if they commute at coincidence points. i.e., if $ABx = BAx$, whenever $Ax \in Bx$.

Definition 1.6. Maps $A : X \to X$ and $B : X \to CB(X)$ are said to be occasionally weakly compatible (owc) if there exists some point $x \in X$ such that $Ax \in Bx$ and $ABx \subseteq BAx$.
Clearly weakly compatible maps are occasionally weakly compatible (owc). However, the converse is not true in general as shown in the following example.

Example 3. Let $X = [0, \infty)$ with $a * b = \min\{a, b\}$ for all $a, b \in [0,1]$ and

$$M(x, y, t) = \frac{t}{t + d(x, y)} \text{ for all } t > 0.$$

Define the maps $A : X \to X$ and $B : X \to CB(X)$ by setting

$$Ax = \begin{cases} 0, & 0 \le x < 1 \\ x + 1, & 1 \le x < \infty \end{cases},$$

$$Bx = \begin{cases} \{0\}, & 0 \le x < 1 \\ [1, x + 2], & 1 \le x < \infty \end{cases}$$

Here '1' is a coincidence point of A and B but A and B are not weakly compatible as

$$BA(1) = [1, 4] \ne AB(1) = [2, 4].$$

Hence A and B are not compatible.

But A and B are occasionally weakly compatible (owc) as A and B are weakly compatible at $x = 0$ as $A(0) \in B(0)$ and $AB(0) \subseteq BA(0)$. i.e., $A\{0\} = 0 \subseteq B(0) = \{0\}$

2. RESULTS AND DISCUSSION

Now, we prove the following result.

Theorem 1. Let $(X, M, *)$ be a fuzzy metric space with $t * t = t$. Let $A, B : X \to X$ and $S, T : X \to CB(X)$ be single and set valued mappings respectively such that the maps (A,S) and (B,T) are (owc) and satisfy the inequality

(1.1)
$$\delta_M(Sx, Ty, t) \geq \phi\left[\min\left\{\begin{matrix} M(Ax, By, t), H(Ax, Sx, t), \\ H(By, Ty, t), H(Ax, Ty, \alpha t) * H(By, Sx, (2-\alpha)t) \end{matrix}\right\}\right]$$

for every $x, y \in X$, $t > 0$, $\alpha \in (0,2)$, where $\phi : [0,1] \to [0,1]$ is continuous function such that $\phi(s) > s$ for each $0 < s < 1$. Then A, B, S and T have unique common fixed point in X.

Proof. Since the pairs (A,S) and (B,T) are occasionally weakly compatible (owc) maps, therefore, there exist two elements u, v in X such that $Au \in Su$, $ASu \subseteq SAu$ and $Bv \in Tv$, $BTv \subseteq TBv$.

First we prove that $Au = Bv$. As $Au \in Su$, $Bv \in Tv$, so, $M(Au, Bv, t) \geq \delta_M(Su, Tv, t)$ and $M(Bv, Su, t) \geq \delta_M(Tv, Su, t)$

Suppose that $Au \neq Bv$, then $\delta_M(Su, Tv) < 1$. Using (1.1) for $x = u, y = v$

$$\delta_M(Su, Tv, t) \geq \phi\left[\min\left\{\begin{matrix} M(Au, Bv, t), H(Au, Su, t), \\ H(Bv, Tv, t), H(Au, Tv, \alpha t) * H(Bv, Su, (2-\alpha)t) \end{matrix}\right\}\right]$$

Since $*$ is continuous, letting $\alpha \to 1$, we get

$$\delta_M(Su, Tv, t) \geq \phi\left[\min\left\{\begin{matrix} M(Au, Bv, t), H(Au, Su, t), \\ H(Bv, Tv, t), H(Au, Tv, t) * H(Bv, Su, t) \end{matrix}\right\}\right]$$

$$\geq \phi\left[\min\{M(Au, Bv, t), 1, 1, M(Au, Tv, t) * M(Bv, Su, t)\}\right]$$

$$\geq \phi\left[\min\{M(Au, Bv, t), 1, 1, \delta_M(Su, Tv, t) * \delta_M(Su, Tv, t)\}\right]$$

$$= \phi\left[\min\{M(Au, Bv, t), 1, 1, \delta_M(Su, Tv, t)\}\right]$$

$$= \phi\left[\delta_M(Su, Tv, t)\right] > \delta_M(Su, Tv, t), \text{ a contradiction.}$$

Therefore, $\delta_M(Su, Tv, t) = 1$ and hence $Au = Bv$

Now, we prove that $A^2u = Au$.
Also,
$$M(AAu, Au, t) = M(AAu, Bv, t) \geq \delta_M(SAu, Tv, t)$$

Suppose $A^2u \neq Au$, then $\delta_M(SAu, Tv, t) < 1$

Using (1.1) for $x = Au, y = v$ with $\alpha = 1$

$$\delta_M(SAu, Tv, t) \geq \phi\left[\min\left\{\begin{matrix} M(AAu, Bv, t), H(AAu, SAu, t), \\ H(Bv, Tv, t), H(AAu, Tv, t) * H(Bv, SAu, t) \end{matrix}\right\}\right]$$

$$\geq \phi\left[\min\left\{\begin{matrix} M(AAu, Bv, t), 1, 1, \\ M(AAu, Tv, t) * M(Bv, SAu, t) \end{matrix}\right\}\right]$$

$$\geq \phi\left[\min\left\{\begin{matrix} M(AAu, Bv, t), \delta_M(SAu, Tv, t), 1, \\ \delta_M(SAu, Tv, t) * \delta_M(Tv, SAu, t) \end{matrix}\right\}\right]$$

$$= \phi\left[\delta_M(SAu, Tv, t)\right] > \delta_M(SAu, Tv, t), \text{ again a}$$

contradiction and hence $\delta_M(SAu, Tv, t) = 1$, which yields $AAu = Au = Bv$.

Similarly, we can prove that $B^2v = Bv$

Putting $Au = Bv = z$, then $Az = z = Bz$, $z \in Sz$ and $z \in Tz$.

Therefore, z is a common fixed point of A, B, S and T.

For uniqueness, let $z' \neq z$ be another fixed point of A, B, S and T. Then (1.1) with $\alpha = 1$, gives

$$\delta_M(Sz, Tz', t) \geq \phi\left[\min\left\{\begin{matrix} M(Az, Bz', t), H(Az, Sz, t), \\ H(Bz', Tz', t), H(Az, Tz', t) * H(Bz', Sz, t) \end{matrix}\right\}\right]$$

$$\geq \phi\left[\min\left\{\begin{matrix} M(Az, Bz', t), M(Az, Sz, t), \\ M(Bz', Tz', t), M(Az, Tz', t) * M(Bz', Sz, t) \end{matrix}\right\}\right]$$

$$= \phi\left[\min\left\{\begin{matrix} M(z, z', t), M(z, z, t), \\ M(z', z', t), M(z, z', t) * M(z', z, t) \end{matrix}\right\}\right]$$

i.e.,
$$\delta_M(z, z', t) = \delta_M(Sz, Tz', t) > \phi\left[M(z, z', t)\right] > M(z, z', t) > \delta_M(z, z', t)$$

, again a contradiction and hence $z = z'$.

Example 4. Let $(X, M, *)$ be a fuzzy metric space in which $X = [0, \infty)$, $a * b = \min\{a, b\}$ for all $a, b \in [0,1]$ and $M(x, y, t) = \dfrac{t}{t + d(x, y)}$ $\forall t > 0$

Define the maps $A, B : X \to X$ and $S, T : X \to CB(X)$ by setting

$$A(x) = \begin{cases} x, & 0 \le x \le 1 \\ 2, & 1 < x < \infty \end{cases},$$

$$B(x) = \begin{cases} 1, & 0 \le x \le 1 \\ x+1, & 1 < x < \infty \end{cases}$$

$$S(x) = \begin{cases} \{1\}, & 0 \le x \le 1 \\ \{0\}, & 1 < x < \infty \end{cases},$$

$$A(x) = \begin{cases} \{x\}, & 0 \le x \le 1 \\ [1, x+2], & 1 < x < \infty \end{cases}$$

Define $\phi:[0,1] \to [0,1]$ as $\phi(0) = 0$, $\phi(1) = 1$ and $\phi(s) = \sqrt{s}$ for $0 < s < 1$, then $\phi(s) > s$.

The pair (A,S) and (B,T) are occasionally weakly compatible (owc) as

$A(1) = 1 \in S(1) = \{1\}$ and $AS(1) \subseteq SA(1)$. ie.,

$A\{1\} = 1 \subseteq S(1) = \{1\}$ and

$B(1) = 1 \in T(1) = [1,3]$ and $BT(1) \subseteq TB(1)$.

Also the contractive condition (1.1) of our theorem is satisfied.

Thus all the conditions of our theorem are satisfied and '1' is the unique common fixed point of A, B, S and T.

Corollary 1. Let $(X, M, *)$ be a fuzzy metric space with $t * t = t$. Let $A, B : X \to X$ and $S, T : X \to CB(X)$ be single and set valued mappings satisfying

(1.2) The pairs (A,S) and (B,T) are owc
(1.3)

$$\delta_M(Sx, Ty, t) \ge \phi \left[\min \left\{ \begin{array}{l} M(Ax, By, t), H(Ax, Sx, t), \\ H(By, Ty, t), H(Ax, Ty, \alpha t) * H(By, Sx, (2-\alpha)t) \end{array} \right\} \right]^h$$

for every $x, y \in X, t > 0, \alpha \in (0,2), 0 < h < 1$, where $\phi:[0,1] \to [0,1]$ is continuous function such that $\phi(s) > s$ for each $0 < s < 1$. Then A, B, S and T have unique common fixed point in X.

Corollary 2. Let $(X, M, *)$ be a fuzzy metric space with $t * t = t$. Let $A, B : X \to X$ and $S, T : X \to CB(X)$ be single and set valued mappings satisfying (1.2) and

(1.4) $\delta_M(Sx, Ty, t) \ge \left[\phi\{ H(Ax, By, t) \} \right]^h$

for every $x, y \in X, t > 0, 0 < h < 1$, where $\phi:[0,1] \to [0,1]$ is continuous function such that $\phi(s) > s$ for each $0 < s < 1$. Then A, B, S and T have unique common fixed point in X.

If we put A=B and S=T in theorem 1, we obtain the following result.

Corollary 3. Let $(X, M, *)$ be a fuzzy metric space with $t * t = t$. Let $A : X \to X$ and $S : X \to CB(X)$ be single and set valued mappings respectively such that (A,S) is (owc) and satisfy the inequality

(1.5)

$$\delta_M(Sx, Sy, t) \ge \phi \left[\min \left\{ \begin{array}{l} M(Ax, Ay, t), H(Ax, Sx, t), \\ H(Ay, Sy, t), H(Ax, Sy, \alpha t) * H(Ay, Sx, (2-\alpha)t) \end{array} \right\} \right]$$

for every $x, y \in X, t > 0, \alpha \in (0,2)$, where $\phi:[0,1] \to [0,1]$ is continuous function such that $\phi(s) > s$ for each $0 < s < 1$. Then A and S have unique common fixed point in X.
If we put A=B, we get another corollary.

Corollary 4. Let $(X, M, *)$ be a fuzzy metric space with $t * t = t$. Let $A : X \to X$ and $S, T : X \to CB(X)$ be single and set valued mappings respectively such that the maps (A,S) and (A,T) are (owc) and satisfy the inequality

(1.6)

$$\delta_M(Sx, Ty, t) \ge \phi \left[\min \left\{ \begin{array}{l} M(Ax, Ay, t), H(Ax, Sx, t), \\ H(Ay, Ty, t), H(Tx, Ty, \alpha t) * H(Ay, Sx, (2-\alpha)t) \end{array} \right\} \right]$$

for every $x, y \in X, t > 0, \alpha \in (0,2)$, where $\phi:[0,1] \to [0,1]$ is continuous function such that $\phi(s) > s$ for each $0 < s < 1$. Then A, S and T have unique common fixed point in X.

Now, we prove the projection of theorem 1, from fuzzy metric space to metric space.

Theorem 2. Let (X, d) be a metric space. Let $A, B : X \to X$ and $S, T : X \to CB(X)$ be single

and set valued mappings respectively such that the maps (A,S) and (B,T) are (owc) and satisfy the inequality

$$(1) \quad d\left(Sx,Ty\right)\le\phi\left[\max\left\{\begin{array}{l}d\left(Ax,By\right),d\left(Ax,Sx\right),\\ d\left(By,Ty\right),\dfrac{1}{2}\{d\left(Ax,Ty\right)+d\left(Ty,Sx\right)\}\end{array}\right\}\right]$$

for every x, $y \in X$, where $\phi:R^+ \to R^+$ be a non-decreasing and $\phi(t) < t$ for every $t > 0$. Then A, B, S and T have unique common fixed point in X.

Proof. The proof follows from theorem 1. Considering the induced fuzzy metric space $\left(X,M,*\right)$ where

$$a*b = \min\left\{a,b\right\} \text{ and } M\left(x,y,t\right)=\frac{t}{t+d\left(x,y\right)}$$

Remark 1. In view of theorem 2, it is clear that some results of Abbas and Rhoades (2007); Al-Thagafi and Shahzad (2008, 2009); Bouhadjera *et al.* (2008); Bouhadjera and Djoudi (2008); Bouhadjera and Thobie (2008); Bouhadjera and Thobie (2009); Chandra and Bhatt (2009) are special cases of our main results in fuzzy metric space.

REFERENCES

Abbas, M. and Rhoades, BE. 2007. Common fixed point theorems for hybrid pairs of occasionally weakly compatible mappings satisfying generalized condition of integral type. Fixed point theory appl. Article ID 54101.

Al-Thagafi, MA. and Shahzad, N. 2009. A note on occasionally weakly compatible maps. Int. J. Math. Anal. 3(2):55-58.

Al-Thagafi, MA. and Shahzad, N. 2008. Generalized I-non expansive self maps and invariant approximation. Acta Mathematica Sinica. 24:867-876.

Alamgir, KH. and Sumitra, D. 2010. Common fixed point theorems for occasionally weakly compatible maps in fuzzy metric spaces. Far East Journal of Mathematical Sciences. 41(2):285-293.

Bouhadjera, H., Djoudi, A. and Fisher, B. 2008. A unique common fixed point theorem for occasionally weakly compatible maps. Surveys in Mathematics and its Appli. 3:177-182

Bouhadjera, H. and Djoudi, A. 2008. Common fixed point theorems for single and set valued maps without continuity. An. St. Univ. Ovidius Constanta. 16(1):49-58.

Bouhadjera, H. and Thobie, CG. 2008. Common fixed point theorems for occasionally weakly compatible single and set valued maps. Hal-00273238.1:12-19.

Bouhadjera, H. and Thobie, CG. 2009. Common fixed point theorems for occasionally weakly compatible maps. ArXiv. 0812.373 [math. FA]. 2:123:131

Chandra, H. and Bhatt, A. 2009. Fixed point theorem for occasionally weakly compatible maps in probabilistic semi-metric space. Int. J. Math. Anal. 3(12):563-570.

Deng, Z. 1982. Fuzzy pseudo-metric space. J. Math. Anal. Appl. 86:74-95.

Erceg, MA. 1979. Metric spaces in fuzzy set theory. J. Math. Anal. Appl. 69:205-230.

Gairola, UC. and Rawat, AS. 2009. A fixed point theorem for two pairs of maps satisfying a contractive condition of integral type. Int. Mathematical Forum. 4(4): 177-183.

Kramosil, I. and Michalek, J. 1975. Fuzzy metric and statistical metric spaces. Kybernetica. 11:326-334.

Kaleva, O. and Seikkala, S. 1984. On fuzzy metric spaces. Fuzzy Sets Systems. 12 : 215-229.

Zadeh, LA. 1965. Fuzzy Set. Information and Control. 8:338-353.

Canadian Journal of
pure&applied
sciences

STUDY OF THE STRUCTURES AND PROPERTIES OF THE MOLECULES PYRIMETHAMINE AND SULFADOXINE USING AB INITIO AND DFT METHODS

*Geh Wilson Ejuh[1,2], Ndjaka Jean Marie[2] and Amar Nath Singh[3]
[1]Department of Physics, Gombe State University PMB 127, Gombe
[2]Université de Yaoundé I, Faculté des Sciences, Département de Physique, B P 812 Yaoundé, Cameroun
[3]Department of Physics, Banaras Hindu University Varanasi, India

ABSTRACT

Density functional theory (DFT) and ab- initio Quantum Mechanical calculations have been used to study the structures and properties of the Molecules Pyrimethamine and Sulfadoxine. Their molecular stabilities, structures, dipole moments, charges transfer, polarizability tensors, average polarizability anisotropy, energies, IR and Raman vibrational frequencies have been predicted. Tentative assignments for their intense IR active frequencies have been carried out and represented. We have used the Restricted Hartree-Fock (RHF) and density functional Becke3LYP (B3LYP) theories by employing 6-311++G** basis set for inclusion of electron correlation. From our results we observe that the molecules are more stable at the RHF level of theory than at the B3LYP level of theory. The frequency calculations obtained at the B3LYP level are closer to some experimental values than those obtained at the RHF level due the effect of electron correlation. The magnitude of the dipole moment is higher in the RHF level and the polarizability tensor components, the average polarizability and the anisotropy are greater at the B3LYP level. This implies that the inclusion of electron correlation decreases the dipole moment and increases the polarizability tensors, the average polarizability and the anisotropy. The IR and Raman spectra of the molecules have also been presented and the IR spectrum of Pyrimethamine lies in the same range as that given by some experimental results.

Keywords: DFT, RHF, pyrimethamine, sulfadoxine, ab-initio quantum mechanical calculations.

INTRODUCTION

Daraprim, also called Pyrimethamine, was first developed in 1952 by Crud, Davy and Rose from the synthesis of the antifolate drug Paludrine or Proguanil (chlorguamide Hydrochloride) (Kakkilaya, 2008). It is an antiparasitic compound and a hydrofolate reductase inhibitor essential for the synthesis of Folic acid (Winstanley, 2006; Alexis, 2006). It is essential for the synthesis of folic acid. Pyrimethamine possesses blood schizonticidal and some tissue schizonticidal activity against malaria parasite in human (Marina *et al*., 2005). Its inhibition activity leads to either killing a pathogenic organism (malaria parasite) or to modify some aspects of metabolism of the body that are functioning dormally. Daraprim interferes with the biosynthesis of the parasite by inhibiting the enzyme dihydrofolate reductase of plasmodia thereby blocking the biosynthesis of purine and pyrimidine which are essential for DNA synthesis and cell multiplication (http://www.Drug bank showing Pyrimethamine (DB002050).mht). This leads to failure of nuclear division at the time of schizont formation in the erythrocytes and liver. Daraprim is a weak basic drug and sparingly soluble in water. It has a half life of 4.2days (Alexis, 2006). The resistance of Pyrimethamine is due to its long half life. Pyrimethamine is the most widely used

anti malarial antifolate drug. For almost three quarters of a century, Daraprim is used as one of the anti malaria resistance drug in some countries or places where Quinine and its derivatives failed to treat malaria. It is recommended to patients infected in areas where susceptible plasmodia exist (Michelle and Qin Cheng, 2006). Although the drug has antimalarial activity when used alone, parasitological resistance can develop rapidly (Winstanley *et al*., 2004). When used in combination, it produces a synergistic effect on the parasite and can be effective even in the presence of resistance to individual component. Pyrimethamine is usually used in combination with Sulfadoxine [4-amino-N-(5, 6-dimethoxy-Pyrimidin-4-yl) benzenesulfoamide] and Sulfalene (Alexis, 2006).

The structure of Pyrimethamine and its derivatives have been studied by Clare E. Samsom et al using modeling techniques (Clare *et al*., 1989). Molecular dynamics calculations have been carried out in order to understand the resistance of Pyrimethamine (Giulio *et al*., 2005 and Reinaldo *et al*., 2002). X-ray analysis of Pyrimethamine and its hydrochloride salt was carried out by Rumiko Tanaka *et al*. (2004). Onyeji *et al*. (2009) studied the powder X-ray diffraction analysis and Fourier transformation infrared spectroscopy of Pyrimethamine

---

*Corresponding author email: gehwilsonejuh@yahoo.fr

Onyeji *et al*. (2009) and Maitarad *et al*. (2009) carried out comparative field analysis (CoMFA) while Phornphimon *et al*. (2009) carried out some ab intio quantum chemical calculations on some derivative of Pyrimethamine.

Sulfadoxine [4-amino-N-(5, 6-dimethoxy-Pyrimidin-4-yl) benzenesulfoamide or 4,5 dimethoxy-6-Sulfanilamidopyrimidine] was first synthesized by the standard scheme from 4-acetylaminobenzenesulfonyl chloride and 4-amino-5,6-dimethoxypyrimidine. Sulfadoxine is similar to other Sulfanilamides however, but it possesses very prolonged action. It has a half life of 120 to 200hours (Ruben and Victor, 2006). It is an antiparasitic agent, anti protozoan agent, anti-infective agent and an anti malaria agent. It is also a hydrofolate reductase inhibitor. Sulfadoxine also inhibits the production of an enzyme involved in the synthesis of folic acid within the parasite. Although this drug has antimalaria activity when used alone, parasitological resistance can also develop (Winstanley *et al*., 2004). It is more effective when used in combination with other drugs for example Pyrimethamine.

Sulfadoxine and Pyrimethamine are both antifolate drugs. They both inhibit the production of enzymes involved in the synthesis of folic acid within the parasites. Sulfadoxine-Pyrimethamine combination act synergistically to inhibit two enzymes important in the parasite's folate biosynthetic pathway; dihydrofolate reductase (DHFR) and dihydropteroate synthetase (DHPS). Michelle and Qin Cheng (Michelle and Qin Cheng, 2006) have shown that the DHFR gene confer resistance to Pyrimethamine while the DHPS gene confer resistance to Sulfadoxine. Although some works have been done on these molecules, yet detail works are required to improve the understanding of their electronic structures and physico-chemical properties.In this work, ab initio calculations have been performed in order to predict the molecular stabilities, structures, dipole moments, atomic charges, polarizability tensors, average polarizability, anisotropy, energies, IR and Raman vibrational frequencies of Daraprim and Sulfadoxine. The computational methodology and the results of our calculations are reported in this article.

MATERIALS AND METHODS

Computational Method
Theoretical frame work
This section gives a brief outline of the theoretical methods that are performed in this work.

The Hartree-Fock (FH) Method
The HF method is used to solve the time independent Schrödinger equation for a multi-electron atom or molecule as described in the Born-Oppenheimer approximation (Colin, 1992). In the HF theory, each electron is assigned to a molecular orbital, and the wave function is expressed as a single Slater determinant (Slater, 1974) in terms of the molecular orbitals. For a system with n electrons, the wave function ψ is given as:

$$\psi(\chi_1, \chi_2, ..., \chi_n) = \frac{1}{\sqrt{n!}} \begin{vmatrix} \phi_1(\chi_1) & \phi_2(\chi_2) & \cdots & \phi_n(\chi_1) \\ \phi_1(\chi_2) & \phi_2(\chi_2) & \cdots & \phi_n(\chi_2) \\ \cdots & \cdots & \cdots & \cdots \\ \phi_1(\chi_n) & \phi_2(\chi_n) & \cdots & \phi_n(\chi_n) \end{vmatrix} \quad (1)$$

ϕ_i represent a molecular orbital and χ_i designates the spatial and the spin coordinates of the electron i. If we define two spin functions α and β as follows $\begin{matrix} \alpha(\uparrow)=1 & \alpha(\downarrow)=0 \\ \beta(\uparrow)=1 & \beta(\downarrow)=0 \end{matrix}$, we can build a closed shell wave function by defining n/2 molecular orbital for a system with n-electrons and then assigning electrons to these orbitals in pairs of opposite spin as follows:

$$\psi(\vec{r}) = \frac{1}{\sqrt{n!}} \begin{vmatrix} \phi_1(\vec{r_1})\alpha(1) & \phi_1(\vec{r_1})\beta(1) & \cdots & \phi_{\frac{n}{2}}(\vec{r_1})\alpha(1) & \phi_{\frac{n}{2}}(\vec{r_1})\beta(1) \\ \phi_1(\vec{r_2})\alpha(2) & \phi_1(\vec{r_2})\beta(2) & \cdots & \phi_{\frac{n}{2}}(\vec{r_2})\alpha(2) & \phi_{\frac{n}{2}}(\vec{r_2})\beta(2) \\ \cdots & \cdots & \cdots & \cdots & \cdots \\ \phi_1(\vec{r_n})\alpha(n) & \phi_1(\vec{r_n})\beta(n) & \cdots & \phi_{\frac{n}{2}}(\vec{r_n})\alpha(n) & \phi_{\frac{n}{2}}(\vec{r_n})\beta(n) \end{vmatrix}$$

(2)

From the case of the closed-shell, the spin coordinates can be eliminated so that we can formulate the equations in terms of spatial orbitals.

The molecular orbitals are expressed as a linear combination of atomic orbtals φ_μ

$$\phi_i(r) = \sum_{\mu}^{n} C_{\mu i} \varphi_\mu(r)$$

(3)

Expressing the nonrelativistic time-independent Schrödinger's equation using a wave function of this form yields a generalized eigenvalue problem, the (Roothaan, 1951) equations.

$$\sum_{v=1}^{N} \left(F_{\mu v} - \varepsilon_i S_{\mu v} \right) C_{vi} = 0 , \qquad \mu = 1, 2, ...N \quad (4)$$

This equation can be rewritten in matrix form as:

$$FC = SC\varepsilon \quad (5)$$

In which F represent the Fock matrix, S is the overlap matrix, C is the molecular orbital coefficients matrix with elements C_{vi} and ε is diagonal matrix of orbital

energies. The Fock matrix can be expressed as a sum of one-electron part H^{core} (the core Hamiltonian) and a two-electron part G, and its elements are given as follows in the atomic orbital basis (Janssen and Neilsen, 2008).

$$F_{\mu\nu} = H_{\mu\nu}^{core} + G_{\mu\nu} \qquad (6)$$

$$F_{\mu\nu} = H_{\mu\nu}^{core} + \sum_{\rho\lambda} P_{\rho\lambda} \left[(\mu\nu/\rho\lambda) - \frac{1}{2}(\mu\lambda/\rho\nu) \right] \qquad (7)$$

The elements $P_{\rho\lambda}$ of the density matrix p are computed from the molecular orbital coefficients (assumed to be real).

$$P_{\rho\lambda} = 2\sum_{i}^{n/2} C_{\rho i} C_{\lambda i} \qquad (8)$$

where the sum runs over all occupied molecular orbitals i. The electronic contribution of the Hartree-Fock energy can be computed as follows:

$$E_{el} = \frac{1}{2} \sum_{\mu\nu} P_{\mu\nu} \left(H_{\mu\nu}^{core} + F_{\mu\nu} \right) \qquad (9)$$

And the total Hartree-Fock energy is the sum of the electronic energy and the nuclear repulsion energy $E_{HF} = E_{el} + E_{nuc}$.

$$H^{core}(1) = -\frac{1}{2}\nabla_1^2 - \sum_{\alpha} \frac{Z_{\alpha}}{r_1\alpha} \qquad (10)$$

is the one-electron core Hamiltonian.

The term $(\mu\nu/\rho\lambda)$ in equation (7) signifies the two-electron repulsion integrals. Under the Hartree-Fock treatment, each electron sees all of the other electrons as an average distrubtion, there is no instantaneous electron – electron included in the Schrödinger's equation.

Density Functional Theory (DFT)

It is a quantum mechanical theory used in physics and chemistry to investigate the electronic structure (principally the ground state) of many body systems, in particular atoms, molecules, and the condensed phases. DFT is among the most popular and versatile methods available in condensed-matter physics, computational physics and computational chemistry. DFT has its conceptual roots from the Thomas – Fermi model and Slater's fundamental work in quantum chemistry in 1950. DFT approach is based upon a strategy of modeling electrons via general functional (functions of functions) of the electron density. DFT was put on a firm theoretical footing by the Hohenberg – Kohn theorem (Hohenberg and Kohn, 1964) which shows the existence of a unique functional which determines the ground state energy and density of a system exactly. The theorem does not provide the form of the functional.

Following on the work of Kohn and Sham (Kohn and Sham, 1965), the approximate functional employed by the current DFT method partition the electronic energy into several terms.

$$E = E^T + E^v + E^j + E^{xc} \qquad 11$$

E^T = kinetic energy (arising from motion of electrons)
E^v = potential energy of the nuclear–electron attraction and of the repulsion between pairs of nuclei.
E^{xc} = exchange – correlation term and includes the remaining part of the electron–electron interaction. The exchange correlation functional used is the Becke-style three – parameter functional generally known as Becke3LYP (B3LYP) which in build in the Gaussian computer code. The exchange correction potential which is the functional derivative of the exchange correction energy functional with respect to the density is approximated. The approximations used are the local density approximation and the generalized gradient approximations (Leeuwen and Baerends, 1995). The exchange correction potential determines the Kohn-Sham orbitals ϕ$_i$ and their one-electron energies. It also determine the density, which is obtained from the squares of occupied Kohn-Sham orbitals times their occupation number f_i;

$$\rho(r) = \sum_{i}^{N_{occ}} f_i \left| \phi_i(r) \right|^2 \qquad (12)$$

The exact exchange correction potential which is unique yields the exact density of the system. After having iteratively found the exchange correction potential which generates the accurate target density, we immediately obtain Kohn-sham orbitals and the one electron energies to very good accuracy.

COMPUTATIONAL METHODOLOGY

The molecular structures and geometries of Daraprim and Sulfadoxine were completely optimized by using ab-initio quantum mechanical calculations at the Restricted Hartree-Fock (RHF) level of theory without using any symmetry constraints. Initial geometry optimizations were performed using the ab-initio RHF method with 3-21G basis set. Subsequently, its results were utilized to the 6-31G basis set and final calculation were carried out with 6-311++G** basis set. The structures were refined further using Density Functional Theory which is a cost effective method for inclusion of electron correlations with the three-parameter density functional generally known as Becke3LYP (B3LYP), which includes Becke's gradient exchange corrections (Becke, 1988) the Lee *et al.* (1988) correlation functional and Vosko *et al.* (1980) with a 6-311++G** basis set. At the first step, geometry optimizations were carried out then, the IR and Raman frequencies were calculated using the Hessian which is

the matrix of second derivatives of the energy with respect to geometry.

The optimized molecular structures were tested by computing the second derivatives and checking that all the harmonic vibrational frequencies are found to be real at all level of calculations. All calculations in the present work were performed using Windows version of Gaussian 03 (Gaussian 03, 2004) suit of ab initio quantum chemical program.

RESULTS AND DISCUSSION

Molecular structures and Geometries
The geometry of a molecules or system gives more information on its physical and chemical properties. The geometric optimization of any system gives the ground state geometry of that system. The total ground state energy of a system is as a function of the coordinates of the nuclei from Born-Oppenheimer (BO) approximation. The ground state geometry corresponds to the minimum total ground state energy whereas a first order saddle point on the BO surface gives the transition state geometry.

The geometric parameters of Daraprim molecule are listed in table 1, while the molecular structure is shown by figure 1. The calculated bond lengths at RHF/6-311++G** level are slightly (0.01Å to 0.04Å) smaller than the corresponding values obtained at the DFT/B3LYP/6-311++G** level. The bond angles vary from 0.1 to 2 degree in both RHF and DFT levels of theories with the 6-311++G** basis set except for the angle A_{21}. Its RHF value is greater than its corresponding B3LYP value by approximately 4 degree. The six member carbon ring (Phenyl) and the other ring with two of the carbon atom replaced by Nitrogen atoms (pyrimidine) possibly gives added stability to the molecule. The Nitrogen atoms (N11, N12, N14 and N17) play a major role in the electron density configuration. Appreciable changes in bond angles are noted both at RHF/6-311++G** and B3LYP/6-311++G** levels, but no significant change in the bond length is noticed.

Table 1. Optimized geometrical parameters of Daraprim molecule obtained at RHF and B3LYP methods by employing 6 311++G** basis sets. Bond Lengths are given in Armstrong (Å) and Bond Angles are in degrees (°).

Geomet. Parameters	RHF/ 6311++G**	B3LYP/ 6311++G**	Experiment (a,b,c)
R(C1C2)	1.4676	1.4419	1.399
R(C1C6)	1.5191	1.5084	
R(C1C7)	1.3529	1.3909	
R(C2C3)	1.3312	1.3592	1.386
R(C3C4)	1.4600	1.4411	1.402
R(C4C5)	1.3161	1.3397	
R(C5C6)	1.4999	1.4900	
R(C7C8)	1.4836	1.4645	
R(C7C10)	1.4947	1.4891	
R(C20C21)	1.5302	1.5348	
R(C4Cl13)	1.7454	1.7604	1.725
R(C5H30)	1.0749	1.0834	
R(C2H28)	1.0683	1.0794	
R(C3H27)	1.0742	1.0832	
R(C6H29)	1.0848	1.1032	1.082
R(C20H22)	1.0873	1.0969	
R(C20H23)	1.0814	1.0902	
R(C21H24)	1.0858	1.0931	
R(C21H25)	1.0813	1.0895	
R(C21H26)	1.0855	1.0931	
R(C8N11)	1.2712	1.3002	
R(C8N20)	1.5198	1.5226	1.40
R(C9N11)	1.3892	1.3865	1.360
R(C9N12)	1.2761	1.3006	
R(C9N17)	1.3479	1.3611	
R(C10N12)	1.3866	1.3870	1.391
R(C10N14)	1.2599	1.2937	
R(N14H16)	1.0046	1.0221	1.036
R(N17H18)	0.9919	1.0065	
R(N17H19)	0.9928	1.0071	
A(C4C5H30)	120.989	121.0876	119.60
A(C1C2H28)	119.4443	119.4605	
A(C3C2H28)	117.7976	117.5702	
A(C2C3H27)	120.1191	120.0862	
A(C4C3H27)	118.1486	118.5468	
A(C6C5H30)	116.9048	117.6603	
A(C8C20H22)	108.2771	108.5762	109.46
A(C1C6H15)	108.0402	108.2218	
A(C1C6H29)	109.9126	109.6664	
A(C5C6H15)	108.4750	109.1419	
A(C5C6H29)	109.4080	111.3224	
A(C8C20H23)	109.7684	109.9217	
A(C21C20H22)	109.0559	108.7757	
A(C21C20H23)	109.4436	109.5586	
A(C20C21H24)	109.4153	109.8469	
A(C20C21H25)	111.3222	111.1172	
A(C20C21H26)	110.9702	110.9170	
A(C3C4Cl13)	116.9139	117.4104	119.80
A(C2C1C6)	116.0590	116.2501	
A(C2C1C7)	122.3605	122.0668	
A(C6C1C7)	121.5044	121.5384	
A(C1C2C3)	122.6049	122.7434	
A(C3C4C5)	120.888	120.8603	
A(C5C4Cl13)	122.1929	121.7226	
A(C4C5C6)	122.0977	121.2497	
A(C1C6C5)	116.5419	117.4778	
A(C1C7C8)	125.528 0	124.5085	
A(C1C7C10)	123.0658	122.1469	
A(C8C7C10)	111.2219	113.2535	
A(C7C8C20)	122.8700	122.7951	
A(C8C20C21)	112.6834	112.8448	
A(C2C3C4)	121.7085	121.3239	
A(C7C8N11)	120.5857	121.5168	
A(N11C8C20)	116.2653	115.3545	

Geomet. Parameters	RHF/ 6311++G**	B3LYP/ 6311++G**	Experiment (a,b,c)
A(N11C9N12)	126.3676	126.3414	
A(N11C9N17)	113.0728	113.7140	113.9
A(N12C9,17)	120.5194	119.9025	
A(C7C10N12)	115.6151	117.2364	
A(C7C10N14)	121.8607	121.4397	
A(N12C10N14)	122.4825	121.2770	122.3
A(C8N11C9)	117.5250	117.1495	114.4
A(C9N12C10)	117.4445	117.8609	
A(C10N14H16)	109.0621	107.7203	
A(C9N17H18)	117.9875	117.8709	113.90
A(C9N17H19)	117.7085	117.8803	
A(H18N17H19)	118.9561	119.0952	
A(H22C20H23)	107.4679	106.9812	109.01
A(H24C21H25)	108.7557	108.7960	
A(H24C21H26)	108.0855	108.0803	
A(H25C21H26)	108.2063	107.9960	
A(H15C6H29)	103.6641	99.4445	

a= (Hellwege *et al.,* 1976) b=(Roussy *et al.,* 1986)
c=(Herzberg, 1966).

The geometric parameters of Sulfadoxine molecule are listed in table 2, while its molecular structure is shown by figure 2. The calculated bond lengths at RHF/6-311++G** level are slightly (0.01Å to 0.04Å) smaller than the corresponding values obtained at the B3LYP/6-311++G** level. The bond angles vary from 0.1 to 2 degrees at both levels of theories except for the angles A_6 and A_9. For the angle A_6, its RHF value is greater than its corresponding B3LYP value by approximately 9 degrees while for the angle A_9, its RHF value is less than its corresponding B3LYP value by approximately 10 degrees. The Phenyl group and the pyrimidine possibly give added stability to the molecule. The Nitrogen atoms (N4, N17, N18 and N32) and the oxygen atoms (O6, O7, O20 and O21) play a major role in the electron density configuration. Appreciable changes in bond angles are noted both at RHF/6-311++G** and B3LYP/6-311++G** levels of theory, but no significant change in the bond length is noticed.

In both molecules, the RHF/6-311++G** and B3LYP/6-311++G** bond lengths and bond angles are approximately equal to the experimental values determined by Hellwege *et al.* (1976), Roussy *et al.* (1986) and Herzberg (1966). The B3LYP/6-311++G** theoretical calculated values are in better accord to the experimental values than their corresponding RHF/6-311++G** theoretical calculated values.

Table 2. Optimized geometrical parameters of Sulfadoxine molecule obtained at RHF and B3LYP methods by employing 6- 311++G** basis sets. Bond Lengths are given in Armstrong (Å) and Bond Angles are in degrees (°).

Geomet. Parameters	RHF/ 6311++G**	B3LYP/ 6311++G**	Experiment (a,b,c)
R(C1-C2)	1.3906	1.4012	1.392
R(C2-C8)	1.3827	1.4015	
R(C22-C23)	1.3881	1.3956	
R(C22-C24)	1.3862	1.3947	
R(C23-C25)	1.3765	1.3855	
R(C24-C27)	1.3778	1.3855	
R(C25-C29)	1.3975	1.4069	
R(C27-C29)	1.3958	1.4065	
R(C3-H5)	1.0755	1.0857	1.084
R(C9-H10)	1.0814	1.0907	
R(C9-H11)	1.0795	1.0882	
R(C9-H12)	1.0813	1.0906	
R(C13-H14)	1.0858	1.0942	
R(C13-H15)	1.0807	1.0889	
R(C13-H16)	1.0823	1.0902	
R(C24-H28)	1.0723	1.0814	
R(C25-H30)	1.0755	1.0848	
R(C27-H31)	1.0755	1.0848	
R(C23-H26)	1.0740	1.0827	
R(C1-O6)	1.3173	1.3445	1.364
R(C2-O7)	1.3543	1.3687	
R(O6-C9)	1.4166	1.4385	
R(O7-C13)	1.4151	1.4407	1.364
R(C1-N4)	1.3163	1.3312	
R(C3-N4)	1.3175	1.3337	1.431
R(C3-N18)	1.3073	1.3257	
R(C8-N17)	1.3781	1.3848	1.391
R(C8-N18)	1.3251	1.3396	
R(N32-H33)	0.9943	1.0079	1.036
R(N32-H34)	0.9943	1.0079	
R(N17-H35)	0.9970	1.0139	
R(N17-S19)	1.6583	1.7155	1.764
R(S19-O20)	1.4262	1.4622	1.485
R(S19-O21)	1.4192	1.4554	
R(S19-C22)	1.7516	1.7771	1.799
A(C2-C1-N4)	122.0420	122.1251	
A(C2-C8-N17)	118.6527	118.3754	
A(C2-C8-N18)	122.4360	122.3286	
A(C25-C29-N32)	120.3621	120.5146	
A(C27-C29-N32)	120.4731	120.5838	
A(N4-C1-O6)	120.0894	119.9435	
A(C2-C1-O6)	117.8659	117.9303	
A(C1-C2-O7)	123.8872	125.3592	124.5
A(O7-C2-C8)	120.3521	118.6734	
A(C1-C2-C8)	115.6604	115.8060	
A(C23-C22-C24)	120.2114	120.7773	120.64
A(C22-C23-C25)	120.0296	119.5987	
A(C23-C25-C29)	120.294	120.5735	
A(C24-C27-C29)	120.4646	120.7318	
A(C25-C29-C27)	119.1143	118.8467	
A(C22-C23-H26)	119.9901	119.9711	119.88
A(C1-C2-H14)	117.7478	108.6403	
A(C8-C2-H14)	104.2631	114.1031	
A(C25-C23-H26)	119.9746	120.4233	
A(C22-C24-H27)	119.8824	119.4706	119.88
A(C22-C24-H28)	119.6725	119.6918	
A(H27-C24-H28)	120.4451	120.8367	
A(C23-C25-H30)	119.8702	119.7538	
A(C29-C25-H30)	119.8271	119.6671	
A(C24-C27-H31)	119.7763	119.6580	
A(C29-C27-H31)	119.7575	119.6094	

Geomet. Parameters	RHF/ 6311++G**	B3LYP/ 6311++G**	Experiment (a,b,c)
A(O7-C2-H14)	50.7482	50.8964	
A(O6-C9-H10)	110.7581	110.7862	
A(O6-C9-H11)	105.2635	104.9192	
A(O6-C9-H12)	110.6851	110.6751	
A(O7-C13-H14)	110.5706	110.3087	
A(O7-C13-H15)	106.4787	105.6954	
A(O7-C13-H16)	110.7179	110.7691	
A(N4-C3-H5)	116.2226	116.2719	
A(N4-C3-N18)	127.2166	127.1283	
A(N17-C8-N18)	118.8764	119.2504	
A(H5-C3-N18)	116.5587	116.5974	
A(C1-N4-C3)	116.5062	116.4994	114.4
A(C1-O6-C9)	119.2710	117.6077	
A(C2-O7-C13)	116.3092	116.8824	
A(H10-C9-H11)	110.4156	110.6829	
A(H10-C9-H12)	109.3575	109.1557	
A(H11-C9-H12)	110.3109	110.5784	
A(H14-C13-H15)	109.5910	109.7055	
A(H14-C13-H16)	109.8328	110.1695	
A(H15-C13-H16)	109.5887	110.1021	
A(C2-H14-C13)	63.1271	63.9766	
A(C8-N17-S19)	127.3534	126.2279	
A(S19-N17-H35)	112.7488	111.5772	
A(C3-N18-C8)	116.1111	116.0613	
A(N17-S19-O20)	101.7478	101.4478	
A(N17-S19-O21)	109.3153	109.4086	
A(N17-S19-C22)	106.7402	105.4150	
A(O20-S19-O21)	120.6094	121.4704	121.25
A(O20-S19-C22)	108.7478	108.8046	106.5
A(O21-S19-C22)	108.7671	109.0257	
A(S19-C22-C23)	119.57	00	119.2582
A(S19-C22-C24)	120.2075	119.9573	
A(C8-N17-H35)	116.8378	115.8576	
A(C29-N32-H33)	116.4304	117.4914	114.92
A(C29-N32-H34)	116.4674	117.4960	114.92
A(H33-N32-H34)	113.1870	114.0313	113.90

a=(Hellwege *et al*., 1976) b=(Roussy *et al*., 1986)
c= (Herzberg, 1966)

Energies and Dipole moments

The dipole moments (in Debye) and total electronic energies (a.u) without zero point correction (E_1), with zero point correction (E_2), with thermal energy correction (E_3) and with enthalpy correction (E_4) for the molecule are listed in table 3. The scaling factor for the zero-point vibrational energy is 0.9877 for the 6-311++G** basis set (Andersson and Uvdal, 2005). The zero point energy is a correction of electronic energy to account for the effects of molecular vibrations which persist at 0K. It is the minimum energy due uncertainty principle. Dipole moment is the first derivative of the energy with respect to the applied electric field. It is a measure of symmetry in molecular charge distribution. The dipole moment of a molecule gives the strength of the polarity of the molecule. The magnitude of the dipole moments obtained at B3LYP/6-311++G** level of theory is smaller as compared to the corresponding values of the dipole moment at RHF/6-311++G** level of theory for both

Daraprim and Sulfadoxine molecules. This is due to the effect of electron correlation at the B3LYP/6-311++G** level of theory. The difference in the dipole moments between the two methods is 23.25 percent for Pyrimethamine and 4.47 Percent for Sulfadoxine. Nitrogen atoms draw more electrons from their neighboring carbon atoms, become highly electronegative in these molecules and attract electrons more strongly than the other atoms.

Table 3. Dipole moments and Total electronic energies without and with zero point energy corrections, with thermal energy correction and with enthalpy correction of Daraprim and Sulfadoxine molecules obtained using RHF and B3LYP methods by employing 6-311++G** basis set. All energies are given in Kilocalories/Mol.

	Methods/Basis Set			
	Daraprim		Sulfadoxine	
	RHF/ 6-311++G**	B3LYP/ 6-311++G**	RHF/ 6-311++G**	B3LYP/ 6-311++G**
μ	3.1524	2.4189	6.0206	5.7513
E_1	-714990.50	-718172.66	-864401.87	-868487.65
E_2	-714891.82	-718078.38	-864222.55	-868321.18
E_3	-714882.40	-718068.33	-864210.72	-868308.44
E_4	-714881.81	-718067.74	-864210.13	-868307.85

μ =Dipole moment
E_1=Total Electronic Energy without Zero point correction,
E_2=Total Electronic Energy with Zero point correction,
E_3=Total Electronic Energy with Thermal energies, E_4=Total Electronic Energy with enthalpies

Atomic Charges and Polarizability

The electrostatic potential derived charges using the CHelpG scheme of Breneman on at different atomic positions of Daraprim and Sulfadoxine molecules at RHF/6-311++G** and B3LYP/6-311++G** levels of theories are given in Table 4 and 5 respectively. The Mulliken population analysis partitions the charges among the atoms of the molecule by dividing orbital overlap evenly between two atoms. Whereas the electrostatic potential derived charges assign point charges to fit the computed electrostatic potential at a number of points on or near the Van der Waal surface. Hence, it is appropriate to consider the charges calculated by CHelpG scheme of Breneman instead of Mulliken population analysis. Within a molecular system, atoms can be treated as a quantum mechanical system. On the basis of the topology of the electron density, the atomic charges in the molecule can be explained.

From table 4 it is clear that the amount of charges on C2,C3, C7, C12, H15, H23, H29, N11 N12, N14 N17 and C13 atoms is negative while C1, C4, C6, C8, C9, H16, H18, H19,C20, H22,H24,H25H26, H27,H28, H30 atoms are positive at RHF/6-311++G** level of theory and at B3LYP/6-311++G** level of theory for the Daraprim

Table 4. Electrostatic Potential Derived Charges on different atomic positions of Daraprim.

S. No. Atom	RHF/ 6-311++G**	B3LYP/ 6-311++G**	S. No. Atom	RHF/ 6-311++G**	B3LYP/ 6-311++G**
1 C	0.192053	0.134847	16 H	0.395010	0.345307
2 C	-0.245038	-0.180216	17 N	-1.086988	-0.969737
3 C	-0.057188	-0.025741	18 H	0.436246	0.399691
4 C	0.159353	0.082126	19 H	0.437308	0.406305
5 C	-0.358067	-0.232976	20 C	0.051870	0.026295
6 C	0.422854	0.302053	21 C	-0.154424	-0.088515
7 C	-0.605130	-0.468105	22 H	0.033451	0.038177
8 C	0.700480	0.538939	23 H	-0.008479	-0.010396
9 C	1.268641	1.096434	24 H	0.044388	0.027084
10 C	1.002893	0.872279	25 H	0.047563	0.025608
11 N	-0.891348	-0.767659	26 H	0.034966	0.021404
12 N	-1.046270	-0.921292	27 H	0.121116	0.102252
13 Cl	-0.170415	-0.141227	28 H	0.099245	0.082839
14 N	-0.953443	-0.837950	29 H	-0.017111	-0.011049
15 H	-0.021981	-0.004421	30 H	0.168444	0.135547

Table 5. Electrostatic Potential Derived Charges on different atomic positions of Sulfadoxine.

S. No. Atom	RHF/ 6-311++G**	B3LYP/ 6-311++G**	S. No. Atom	RHF/ 6-311++G**	B3LYP/ 6-311++G**
1 C	0.829167	0.664160	19 S	1.358718	1.109000
2 C	-0.346762	-0.223034	20 O	-0.656988	-0.560633
3 C	0.654243	0.519349	21 O	-0.617873	-0.524356
4 N	-0.815720	-0.688231	22 C	-0.220339	-0.092523
5 H	0.043688	0.035156	23 C	0.013868	-0.055445
6 O	-0.321893	-0.270138	24 C	0.071994	-0.033149
7 O	-0.398941	-0.377867	25 C	-0.363883	-0.257738
8 C	0.879255	0.754729	26 H	0.118861	0.116012
9 C	-0.000386	-0.037434	27 C	-0.406594	-0.277854
10 H	0.075553	0.074989	28 H	0.132097	0.129016
11 H	0.076619	0.085538	29 C	0.574641	0.449034
12 H	0.062655	0.065823	30 H	0.166902	0.138133
13 C	0.221497	0.229324	31 H	0.171939	0.143852
14 H	0.019746	0.010558	32 N	-0.902917	-0.832951
15 H	0.034284	0.030178	33 H	0.368124	0.351824
16 H	-0.006662	-0.018385	34 H	0.360857	0.350497
17 N	-0.791444	-0.739795	35 H	0.423783	0.402920
18 N	-0.808861	-0.670559			

molecule. From table 5, the amount of charges on C2, N4, O6, O7, H16, N17, N18, O20, O21, C22, C25, C27 and N32 atom are negative while on the C1, C3, H5, C8, C9, H10, H11, H12, C13, H14, H15, S19, C23, C24, H26, C28, C29, H30, H31, H33, H34, H35 atoms is positive in the case of Sulfadoxine molecule.

Polarizability is a property which depends on the second derivative of the energy with respect to the applied electric field. It gives information about the distribution of electrons in the molecule. The rotational excitation of a polyatomic molecule by electron collision is considered as caused by the polarization interaction as well as by the electrostatic interaction (Yukikazu, 1971). The polarizability tensor components, the average polarizability and the anisotropy of Daraprim and Sulfadoxine obtained at RHF/6-311++G** and B3LYP/6-311++G** level of theories are listed in table 6. All the six polarizability tensor components of Daraprim and Sulfadoxine molecules α_{xx}, α_{xy}, α_{yy}, α_{xz} α_{yz} and α_{zz} components changes significantly at both level of theory considered here. But they do not follow any regular pattern. For Pyrimethamine, only the α_{yz} component is negative while for Sulfadoxine α_{xy}, α_{xz}, and α_{yz}

Table 6. Polarizability tensors, average polarizability and anisotropy of Daraprim and Sulfadoxine using RHF and
B3LYP methods by employing 6-311++G** basis set.

| | Methods/Basis set | | | |
| | Daraprim | | Sulfadoxine | |
Tensor component	RHF/ 6-311++G**	B3LYP/ 6-311++G**	RHF/ 6-311++G**	B3LYP/ 6-311++G**
α_{xx}	266.054	334.059	228.290	277.071
α_{XY}	7.639	9.782	-14.833	-15.615
α_{YY}	165.501	188.045	182.697	209.664
α_{XZ}	5.719	9.684	-6.978	-10.415
α_{YZ}	-15.555	-17.344	-14.318	-15.950
α_{ZZ}	121.812	126.994	145.186	156.648
$<\alpha>$	184.456	216.033	205.391	214.461
$\Delta\alpha$	115.883	184.287	72.114	104.373

Table 7. IR intense vibrational frequencies and their approximate description of Daraprim molecule obtained using
B3LYP methods by employing 6-311++G** basis set.

No.	Freq theory	expt (a)	Approximate description
1	219.81		Symmetrical bending of Pyrimidine and phenyl rings
2	223.00		Rings distortion+stretching of N17-H10, 18+C21-H24,25,26 (CH$_3$) vibration
3	349.60		N-H Waging of NH2 (N17-H18, H19)+ pyrimidine ring breathing
4	367.52		Rings distortion
6	608.65		Rings distortion +Breathing of CH$_3$
7	634.85		Do as above
8	652.99		Rings distortion + waging of C-H bond of phenyl group (C6- H15,H29)
9	677.18		Rings breathing
10	723.25		Do as above
11	895.92		C-H bond rotations
12	958.15		N-H bond Rotation of NH$_2$ (N14-H16) group
13	968.35		Do as above
14	1169.12		Distortion of CH$_2$-CH$_3$ group
15	1466.27	1280	C-N stretching vibrations
16	1483.03		C-H bond symmetrical stretching of the CH$_3$ group
17	1485.55		C-H bond symmetrical bending of the Phenyl group (C5-H15,29)
18	1513.71		C=C-H bond waging of the phenyl group (H28C2=C3H27)
19	1555.56		C-H bond bending of the CH$_2$ group (C28-H22,23)
20	1558.42		C-H bond asymmetrical stretching of the CH$_3$ group
21	1571.47	1394	C-H bond symmetrical bending of CH$_3$
22	1674.26		N-H bond symmetrical bending of NH$_2$ group
23	1680.24	1400	C=C bond symmetrical stretching of the Carbons binding the two rings
24	1728.12		N-H bond symmetrical bending of NH$_2$ group +C=C stretching of benzene ring
25	1775.29		C=N bond symmetrical stretching of Pyrimidine ring
26	1788.79	1649	C=N-H bond stretching +C=C-H bond stretching of benzene ring
27	1802.45		Benzene ring distortion + C=N stretching of the NH group
28	3070.44	2931	C-H bond symmetrical stretching of CH$_3$ and CH$_2$ group
29	3073.95		Do as above
30	3099.34		C-H bond symmetrical stretching of benzene ring
31	3118.62		C-H bond asymmetrical stretching of benzene ring
32	3125.89		C-H bond asymmetrical stretching of the CH$_3$ group
33	3146.13		C-H bond asymmetrical stretching of CH$_3$ and CH$_2$ group
34	3170.79		Do as above
35	3238.38	3149	C-H bond stretching of benzene ring (C5-H30)
36	3246.57		C-H bond stretching of benzene ring (C3-H27)
37	3300.72		C-H bond stretching of benzene ring (C2-H28)
38	3606.60		N-H bond stretching of NH group
39	3707.02	3467	N-H bond symmetrical stretching of NH$_2$ group
40	3836.31		N-H bond asymmetrical stretching of NH$_2$ group

a = Onyeji *et al.* 2009

components are negative. From the table, we can see that the tensor α_{xx} is responsible for the greatest contribution both in the average polarizability and the anisotropy for the two molecules at all levels of theory. We can also see

Table 8. IR intense vibrational frequencies and their approximate description of Sulfadoxine molecule obtained using B3LYP methods by employing 6-311++G** basis set.

No.	Freq	Approximate description
1	347.742	N-H waging of the NH_2 group (N32-H33,34) + breathing of phenyl ring.
2	438.036	D0 as in above.
3	484.362	N-H bond rotation of NH group + breathing of phenyl ring + twisting of the pyrimidine ring.
4	553.061	N-H bond rotation of NH group.
5	563.264	Twisting of the pyrimidine ring.
6	601.55	C-O-H bond angle bending.
7	647.33	Twisting of the phenyl ring.
8	1012.44	C-O bond stretching of the mehoxyl group (C13-O7).
9	1020.54	C=C bond symmetrical and asymmetrical stretching of phenyl ring.
10	1072.97	S=O bond symmetrical stretching of SO_2 (S19=O20,21).
11	1127.25	S-C bond stretching (S19-C22) and O=S=O bond angle bending.
12	1206.4	C-H bond symmetrical bending of phenyl ring.
13	1293.89	N-H bond rotation of NH group + twisting of the pyrimidine ring.
14	1346.6	C-H bond rotation of the pyrimidine ring (C3-H5).
15	1443.04	C-H bond bending of methoxyl group (C9-H10,11,12) + C-H bond rotation of pyrimidine.
16	1481.11	C-H bond rotation of methoxyl group (C9-H10,11,12).
17	1498.74	H-C-H bond angle bending methoxyl group (C-H10,12).
18	1601.23	C-N bond symmetrical stretching of pyrimidine group (C1,8-N4,18).
19	3049.51	C-H bond symmetrical stretching of methoxyl group (C9-H10,11,12).
20	3109.66	C-H bond symmetrical and asymmetrical stretching of methoxyl group (C13-H14,15,16).
21	3123.12	C-H bond asymmetrical stretching of methoxyl group (C9-H10,12).
22	3143.06	C-H bond symmetrical stretching of methoxyl group (C13-H15,16).
23	3151.41	C-H bond symmetrical and asymmetrical stretching of methoxyl group (C9-H10,11,12).
24	3165.9	C-H bond asymmetrical stretching of the phenyl ring (C25,27-H30,31).
25	3166.51	C-H bond asymmetrical stretching of the phenyl ring (C25,27-H30,31) and C-H bond rotation (C3-H5).
26	3203.12	C-H bond stretching of phenyl ring (C23-H26).
27	3587.29	N-H bond symmetrical stretching of NH_2 group.
28	3691.5	N-H bond symmetrical stretching of NH_2 group.
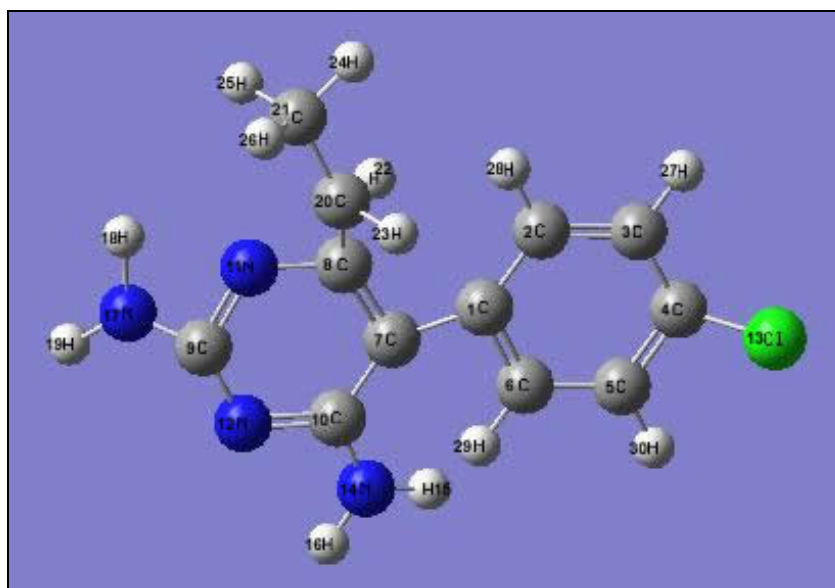
Fig. 1. DAraprim.

that the inclusion of electron correlation affect the average polarizability $<\alpha>$ and the anisotropy $\Delta\alpha$. We equally observe that the effect of inclusion of electron correlation increases $<\alpha>$ by 17.1 percent and $\Delta\alpha$ by 59 percent for Pyrimethamine and increases α by 4.4 percent and $\Delta\alpha$ by 44.7 percent for Sulfadoxine molecule.

Vibrational Frequencies and Assignments

The vibrational frequencies, IR intensities and Raman activities for pyrimethamine and Sulfadoxine molecules at RHF and B3LYP levels with 6-311++G** basis set have been calculated. This was done by calculating the matrix of second derivative of energy (the Hessian or Force constant matrix) which upon diagonalization yields the
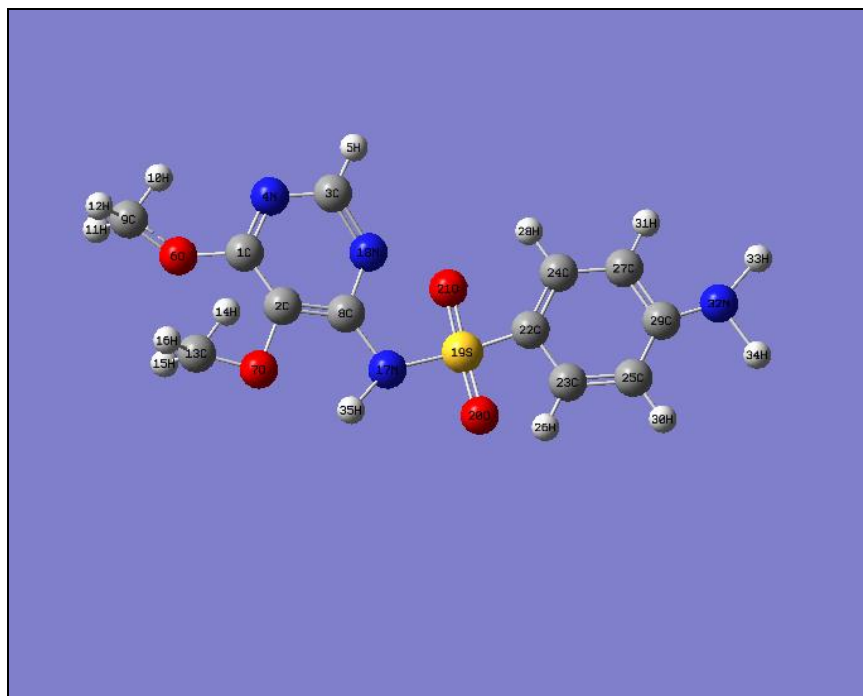
Fig. 2. Sulfadoxine.
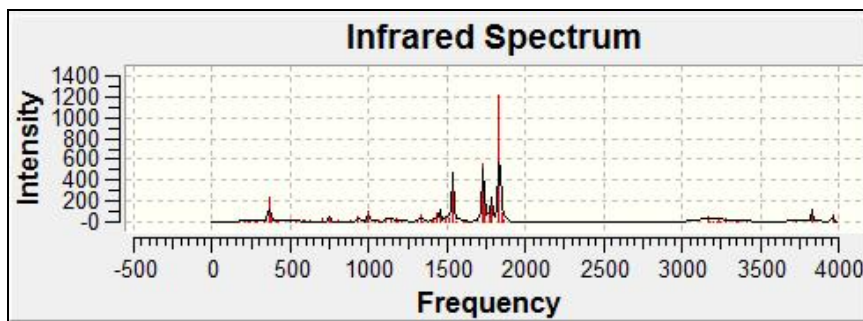
Fig. 3. Infra Red spectrum of Daraprim at RHF/6-311++G**
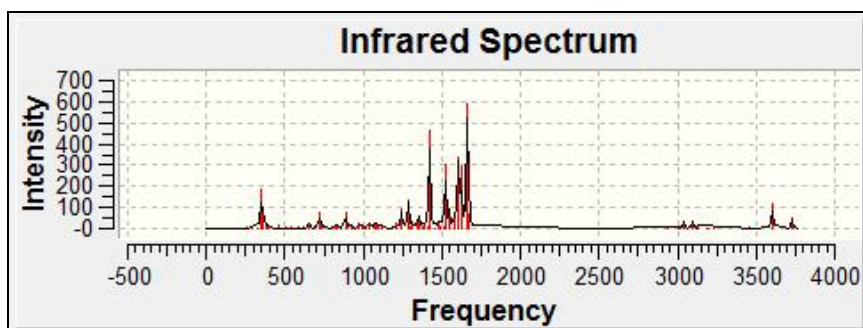
Fig. 4. Infra Red spectrum of Daraprim at B3LYP/6-311++G**

harmonics vibrational frequencies. The frequencies reported were scaled so as compare them with other results. The scaling factor for the vibrational frequencies is 0.9679 and 1.0100 for low-frequency vibrations (Andersson and Uvdal, 2005) for the 6-311++G** basis set. The B3LYP results show significant lowering in magnitude of the calculated frequencies bringing them in

better accord with other theoretical and experimental results (Barbara *et al*., 2010; Onyeji *et al*., 2009). No experimental values were obtained for Sulfadoxine. The B3LYP results for Sulfadoxine showed significant lowering in magnitude of the calculated vibrational frequencies bringing them in better accord with results obtained from Barbara *et al*. (2010).
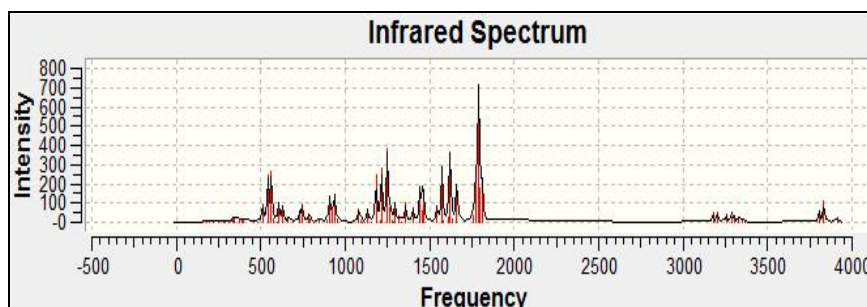
Fig. 5. Infra Red spectrum of Sulfadoxine at RHF/6-311++G**
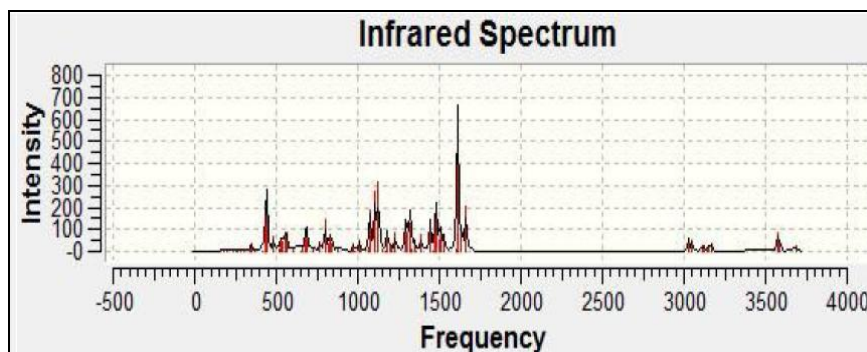
Fig. 6. Infra Red spectrum of Sulfadoxine at B3LYP/6-311++G**
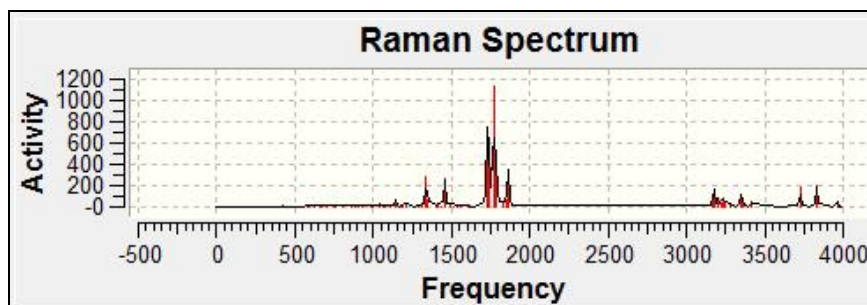
Fig. 7. Raman spectrum of Daraprim at RHF/6-311++G**
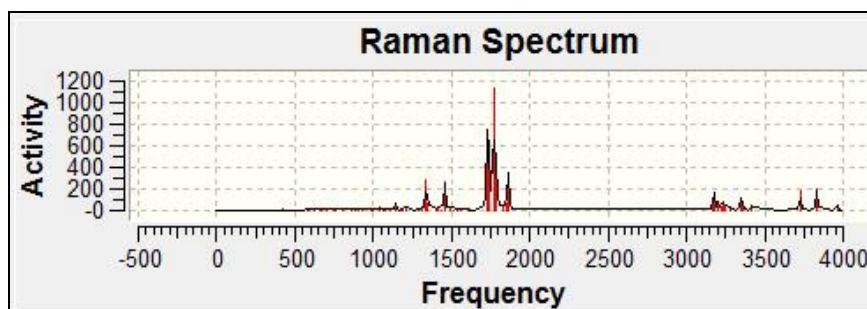
Fig. 8. Raman spectrum of Daraprim at B3LYP/6-311++G**

Table 7 and 8 gives the more prominent vibrational frequencies values and their tentative assignment for Pyrimethamine and Sulfadoxine molecules respectively which have been made on the basis of the relative displacements of the atom associated with different calculated frequencies. Onyeji *et al.* (2009) have carried out a spectroscopic study of Daraprim and presented some assignments for the observed spectra in the region 1400-3500 cm^{-1}. Some of more prominent vibrational frequencies values given by Onyeji are reported in table 7. From table 7, it is clear that our theoretical values are closed to the experimental values of Onyeji *et al.* (2009).
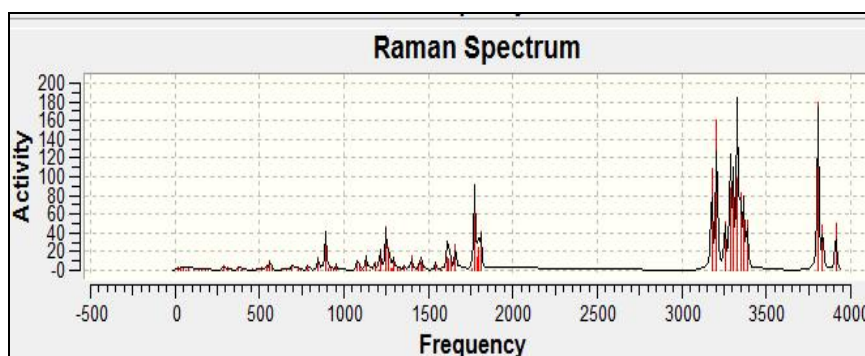
Fig. 9. Raman spectrum of Sulfadoxine at RHF/6-311++G**
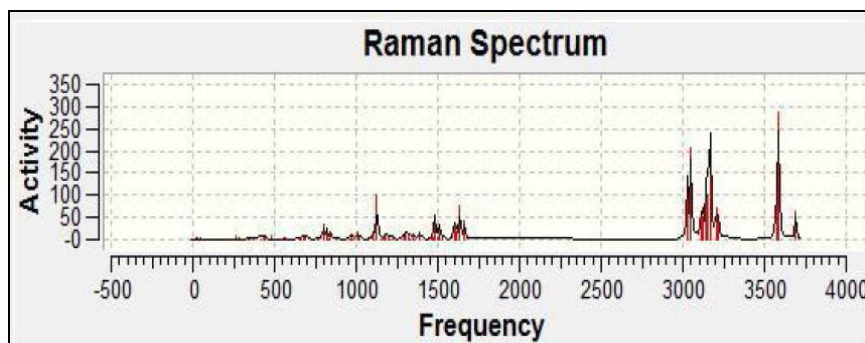
Fig. 10. Raman spectrum of Sulfadoxine at B3LYP/6-311++G**

The agreement between our theoretical and experimental values is within 10-15 percent. This may be due anharmocity effects. The theoretical obtained vibrational spectra for RHF/6-311++G** level of thoery are shown in figure 3, 5, 7, 9 and at B3LYP/6-311++G** level of thoery are shown in figure 4, 6, 8, 10 for Pyrimethamine and Sulfadoxine. The infrared spectra at both levels of theory are with the range 400-4000cm^{-1} which lies within the same range as that of the FT-IR spectrum obtained by Oneyeji *et al*. (2009), and generated using KBr dish method for Pyrimethamine molecule. The B3LYP results of the calculated vibrational frequencies were in better accord with experimental values as given by Colin (1992) and Onyeji *et al*. (2009) for Daraprim molecule.

CONCLUSIONS

In this paper we have studied the structure, energy, charges and vibrational frequencies of Pyrimethamine and Sulfadoxine molecules. We have seen that the charges on the same label atoms have same sign both in RHF and B3LYP levels of theories. The molecules are more stable at the B3LYP level of theory than at the RHF level of theory due to the low electronic energies obtained at the B3LYP level of theory. The frequency calculations obtained at the B3LYP level are closer to the experimental value than those obtained at the RHF level due the effect of electron correlation. The magnitude of the dipole moment is higher in the RHF level and the polarizability tensor components are greater at the B3LYP

level. This implies that the inclusion of electron correlation decreases the dipole moment and increases the polarizability tensors, the average polarizability and the anisotropy. The IR and Raman spectra of the molecules have also been presented and the IR spectrum of Pyrimethamine lies in the same range as that given by experiment.

ACKNOWLEDGEMENT

REFERENCES

Alexis, N. 2006. The past, present and fuure of antifolates in the treatment of plasmodium falciparum infection. Journal of Antimicrobial Chemotherapy. 57(6):1043-1054.

Andersson, MP. and Uvdal, P. 2005. New Scale Factors for Harmonic vibrational Frequencies using the B3LYP Density Functional Method with triple-Zeta Basis set 6-311++G**. Journal Phys. Chem. A. 109(12): 2937-2941.

Barbara, S., Bill, G. and Peter, M. acol. 2010. Modern Infrared Spectroscopy. John Wiley & Sons. New York, USA.

Becke, BD. 1988. Density-functional exchange-energy approximation with correct asymptotic behavior. Phys. Rev. B. 38:3098-3100.

Clare, E., Sansom, CH., Schwalbe, Peter, AL., Roger, JG. and Malcolm, FGS.1989. Structure studies on bio-active compounds. Part xv. Structure-activity relationships for Pyrimethamine and a series of diaminopyrimidine analogues versus bacterial dihydrofolate reductase. Biochemical et biophysical Acta (BBA)-Protein structure and molecular Enzymology. 995:21-27.

Colin, NB. 1992. Fundamentals of Molecular Spectroscopy. Tata McGraw-Hill Publishing Company Limited.

Gaussian 03, Revision C.02, Frisch MJ., Trucks GW., Schlegel HB., Scuseria GE., Robb MA., Cheeseman JR., Montgomery JA., Vreven JrT., Kudin KN., Burant JC., Millam JM., Iyengar SS., Tomasi J., Barone V., Mennucci B., Cossi M., Scalmani G., Rega N., Petersson GA., Nakatsuji H., Hada M., Ehara M., Toyota K., Fukuda R., Hasegawa J., Ishida M., Nakajima T., Honda Y., Kitao O., Nakai H., Klene M., Li X., Knox JE., Hratchian HP., Cross JB., Adamo C., Jaramillo J, Gomperts R., Stratmann RE., Yazyev O., Austin AJ., Cammi R., Pomelli C., Ochterski JW., Ayala PY., Morokuma K., Voth GA., Salvador P., Dannenberg JJ., Zakrzewski VG., Dapprich S., Danniels AD., Strain MC., Farkas O., Malick DK., Rabuck AD., Raghavachari K., Foresman JB., Ortiz JV., Cui Q., Baboul AG., Clifford S., Cioslowski J., Stefanov BB., Liu G., Liashenko A., Piskorz P., Komaromi I., Martin RL., Fox DJ., Keith T., Al-Laham MA., Peng CY., Nanayakkara A., Challacombe M., Gill PMW., Johnson B., Chen W., Wong MW., Gonzalez C., and Pople JA., Gaussian, Inc., Wallingford CT, (2004).

Giulio, R., Worachart, S., Porthep, ST., Tirayut, V., Sumalee, KP., Rachel, Q., Gordon, L., Yodhathai, T. and Yongyuth, Y. 2005. Interaction of Pyrimethamine Cycloguanil, WR99210 and their analogues with Plasmodium falciparum hydrofolate reductase: Structural basis of antifolate resistance. Journal of Bio organic and medicinal Chemistry. 8:1117-1128.

Hellwege, KH., Hellwege, AM. and Landolt-Bornstein. 1976. Atomic and Molecular Physics 7: Structure Data of Free Polyatomic Molecules. Springer-Verlag. Berlin.

Herzberg, G.1966. Electronic spectra and electronic structure of polyatomic molecules. Van Nostrand, New York, USA.

Hohenberg, P. and Kohn, W. 1964. Inhomogeneous Election Gas. Physical Review B. 136:864.

http://www. Drug bank showing Pyrimethamine (DB002050).mht.

Janssen, CL. and Neilsen, IMB. 2008. Parallel Computing in Quantum Chemistry. CRC Press, Taylor & Francis Group, New York, USA.

Kakkilaya, BS. 2008. History, Aetiology, Pathophysiology, Clinical features, diagnosis, treatment of complications and control of Malaria. www.malariasite.com.

Kohn, W. and Sham, LJ. 1965. Self-consistent equations including exchange and correlation effects. Phys. Rev. A.140 (4):1133-1138.

Lee, C., Yang, W. and Parr, RG. 1988. Development of the Colle-Salvetti correlation-energy formula into a functional of the electron density. Phys. Rev. B. 37:785-789.

Leeuwen, RV. and Baerends, EJ. 1995. Energy expressions in density functional theory using lin integrals. Physical Review. A .51(1):170-178.

Marina, P., Anna, MG., Lucrezia, G., Marco, DF., Isabella, Q., Metello, L., Manrizio, C., Walter, M. and Antonello, G. 2005. Pyrimethamine (2,4-Diamino-5-*p*-Chlorophenyl-6-ethylpyrimidine) Induces Apoptosis of Freshly Isolated Human T Lymphocytes, by passing CD95/Fas Molecule but Involving Its Intrinsic Pathway. Journal of Pharmacology and Experimental Therapeutics. 315(3):1046-1057.

Michelle, LG. and Qin, C. 2006. *Plasmodium falciparum* infection dynamics and transmission potential following treatment with sulfadoxine-pyrimethamine. Journal of Anti-microbial Chemotherapy. 58:47-48.

Onyeji, CO., Sharon, IO., Francis, AO. and Julius, OS. 2009. Physiochemical characterization and dissolution properties of Pyrimethamine and 2- hydroxypropyl-β-Cyclodextrin. African Journal of Biotechnology. 8:1651-1659.

Reinaldo, TD., Osvaldo, AS. and Jose, DF. 2002. Molecular Modeling of wild-type and antifolate resistant mutant plasmodium falciparum DHFR. Biophysical Chemistry. 98(3):287-300.

Roothaan, CJ. 1951. New Developments in molecular Orbital Theory. Rev. Mod. Physics. 23(2):69-89.

Roussy, G. 1986. A Nonat "Determination of the Equilibrium Molecular Structure of Inverting Molecules by Microwave Spectroscopy: Application to Aniline. J. Mol. Spec. 118:180-188.

Ruben, V. and Victor, JH. 2006. Synthesis of essential Drug, Amsterdam: Elsevier ISBN 0444521666.

Rumiko, T., Tomoko, A. and Noriaki, H. 2004. Structure of Pyrimethamine Hydrochloride. Analytical Sciences. 20 175-76

Phornphimon, M., Patchreenart, S., Supa, HS., Kamchonwongpaisan, Bongkoch, T. and Yongyuth, Y. 2009. Particular interaction between pyrimethamine derivatives and quadruple mutant type dihydrofolatereductase of Plasmodium falciparum: CoMFA and quantum chemical Calculations studies. Journal of Enzyme Inhibition and Medical Chemistry. 24(2):471-497.

Slater, JC. 1974. Quantum Theory of Molecular and Solids 4: The Self Consistent Field for Molecular and Solids. McGraw-Hill, New York, USA.

Van Gisbergen, SJA., Kootstra, F., Schipper, PRT., Gritsenko, OV., Snijders, JG. and Baerends, EJ. 1998. Density functional theory response-property calculations with accurate exchange- correlation potentials. Physical Review. A. 57(4):2556-2571.

Vosko, SH., Wilk, L. and Nusair, M. 1980. Accurate spin-dependent electron liquid correlation energies for local spin density calculations: A critical analysis. Can. J. Phys. 58(8):1200-1211.

Winstanley, P. 2006. Modern chemotherapeutic options for Malaria. Lancet infect. Dis.1:242-250.

Winstanley, P., Ward, S., Snow, R. and Breckenridge, 2004. A Therapy of Falciparum Malaria in sub-Saharan Africa from Molecule to policy. Clinical Micro-biology. Reviews. 17:612-637.

Yukikazu, I. 1971. Effects of Polarization Force on the Rotational Transition in Polyatomic Molecules by Electron Collision. Journal of Physical Society of Japan. 31:1532-1535.

STRANGE BEHAVIOR IN SEMICONDUCTOR LASER SUBJECTED TO OPTICAL FEEDBACK AT DIFFERENT TEMPERATURES

Firas Sabeeh Mohammed and *Aurangzeb Khurram Hafiz
Department of Physics, Jamia Millia Islamia (Central University), New Delhi-110025, India

ABSTRACT

In this paper we present significant study on the effect of temperature on the characteristics of a diode laser system subjected to external optical feedback. The presence of the feedback is seen to reduce the threshold current and slope efficiency which are important parameters for the solitary diode laser. In this sense the threshold reduction is a good indicator of the feedback level. At certain temperatures, the effect of optical feedback was actually seen to cause slight increase on the threshold current value. The results presented in this paper with regard to the temperature dependence and single optical feedback effect on the threshold and optical power output of diode laser systems will help in understanding the dynamical behavior of such systems.

Keywords: Diode Lasers, optical feedback, external cavity, temperature effect, light-current characteristics.

INTRODUCTION

Unlike light from standard sources such as light bulbs, laser light is highly coherent. The coherent light of a laser is achieved by coupling the active medium with a laser cavity. The cavity selects some of the photons emitted spontaneously to re-propagate through the medium. These photons 'stimulate' other photons to propagate in the same direction with the same phase or constant phase difference. In order to obtain laser output one of the reflective ends of the cavity is made semi-reflective, thus allowing some of the coherent light to escape. Since some of the laser's output will be reflected back into the cavity. It is important to choose a laser diode with highly reflective coating on the back face and a reduced reflectivity coating on the output face. While many low power diode lasers do not have such coatings, diode lasers that produce 30mW or more output power generally have these extra coatings (Al-Dwayyan *et al*., 2007). In this work a laser diode with an output power rating of < 5mW was used. The phenomena of optical feedback in semiconductor lasers is considered undesirable (Servagent *et al*., 1998) as it significantly affects the operating behavior of the laser. Conversely, optical feedback has also been found to be useful in purposes such as mode selectivity and line width reduction (Lang and Kobayashi, 1980; MacAdam *et al*., 1992). The use of feedback can be extended into many other applications including target displacements, range finding and velocity measurement (Bosch *et al.*, 1998a; Bosch *et al.* 1998b; Amann *et al.*, 2001), optical microscopy (Katagirl and Hara, 1998) and various medical applications (Mito *et al*., 1993). In addition, optical feedback of appropriate level has been found to increase the side mode suppression, narrow the

line width, and provide enhanced tunability and frequency stability, relative to that of the solitary diode laser (Goldberg *et al*., 1982; Osmudsen *et al*., 1983). A source for coherent optical communication systems and spectroscopic applications is required to be single frequency, narrow linewidth, and continuously tunable over a wide range of wavelengths (Helms *et al*., 1992; Olsson and van der Ziel, 1987). There are many spectroscopic techniques for which diode lasers with feedback are ideal sources (Yabuzaki *et al*., 1991; Boshier *et al.*, 1991). The reflection of the light emitted by the laser, due to the presence of an external mirror, is capable of inducing chaotic dynamics at the output intensity (Takiguchi *et al.*, 1998; Liu *et al.*, 2001; Fujita and Ohtsubo, 2005; Buldu, 2003). The output power is one of the most important parameter to characterize a diode laser. Figure 1 shows the typical light-current (L-I) characteristics, which depicts output power of a typical continuous wave (cw) semiconductor diode laser as a function of injection current (L-I curve) (Derry *et al.*, 1995).

When the forward bias current is below threshold, the laser diode operates like a light-emitting diode (LED) where the carrier density in the active layer is not high enough for population inversion, spontaneous emission dominates producing a small amount of incoherent light (see Fig. 1). As the bias increases, population inversion occurs, stimulated emission becomes dominant and cavity losses are compensated at a certain bias current, the current at this point is called *threshold current*. The injection current above the threshold induces the abrupt onset of lasing action and coherent light is emitted from the diode laser. The laser threshold current is evaluated by extrapolating the linear part of the characteristic to zero output power (Ye, 2004).

---

*Corresponding author email: akhafiz@gmail.com

A semiconductor laser is subjected to both internal and external losses. For lasing to begin, i.e. to reach threshold, the gain must be equal to these optical losses. The threshold gain per unit length is given by:

$$g_{th} = \alpha_i + \frac{1}{2L} ln \left(\frac{1}{R_F R_R} \right) \qquad (1)$$
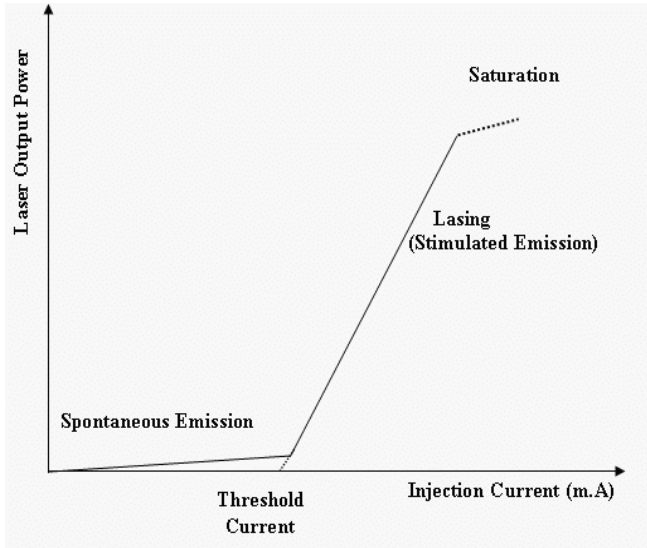

Fig.1. Schematic light output versus current curve.

Where α_i is the internal loss per unit length, L is the laser cavity length, and R_F and R_R are the front and rear facet reflectivity. The internal loss is a material parameter determined by the quality of the semiconductor layers (Ye, 2004). On the operation side, typical threshold current is few milliamperes and varies from device to device (Osmudsen et al., 1983). Incident spontaneous emission light propagating to the reflection mirror is amplified by stimulated emission and comes back to initial position after a round trip inside the laser cavity as well as external cavity (Ye, 2004). Thus, the percentage of the light re-injected into the laser diode is complicated for estimation. In direct estimation is possible by studying the characteristics of the diode laser subjected to external optical feedback.

The aim of this paper is to study experimentally the characteristics of semiconductor lasers with optical feedback under the influence of certain range of temperatures (10 – 30°C). This range of temperature is of particular interest as maximum diode laser applications are performed on this range. Even in telecommunication applications, the range of temperature is often centered between 25 and 30°C (Alter, 2003). The study is of special interest not only from the point of view of nonlinear dynamics, but also for its application to optical communication. The motivation for the current work is therefore to understand the dynamics of how increasing the temperature of the semiconductor laser affects its

output (stability and power) for this kind of systems. The output can, hence, be adjusted for a given application that can be achieved with a specific temperature range. In the following sections we describe the experimental setup and the results obtained followed by the conclusion.

MATERIALS AND METHODS

The system mainly consists of two controlling units (for temperature and current) and the laser diode which is made up of AlGaInP with the operating wavelength around 660nm. There was no particular choice for the laser diode chip as the effects discussed in this paper will not differ much for other types of diode lasers. As shown in figure 2, the external cavity consists of the uncoated facet of the laser diode (LD), an external high reflecting mirror (R _ 90%). A cubic beam splitter (25mm) is used to divide the light intensity equally (50%) between the cavity arm with the external mirror and the detector connected to the power meter. The length of the cavity arm is L=1.5m corresponding to round trip frequency of (f =c/2L = 100 MHz) and an external round trip time of (τ=1/f =10 ns).

For diode lasers, the peak wavelength of emitted light is dependent on the temperature of the laser diode chip. Increase in temperature not only increases the lattice vibrations in the semiconducting material thereby changing the length of the internal cavity but also suppresses the radiative recombination of the charge carriers by increasing the scattering losses. The peak wavelength drifts typically by about 0.1nm per degree change in temperature with the drift being towards the red-shift for rise in temperature. Thus with the change in temperature, phenomena of mode hopping is also observed. A Precise control of the temperature of the laser mount is, therefore, essential for the long term reliable operation of the laser at a particular wavelength. The temperature of laser mount is controlled within an accuracy of ± 0.05°C, using a thermistor, thermoelectric cooler and thermocouple (the remaining circuitry is contained in an external unit). This mount is designed to allow both for effective stabilization as well as good thermal contact with an Aluminum plate (base) situated below the mount. Figure 3 illustrates the basic construction of the mount and the schematic diagram of the whole system. There are two parts of the laser mount structure: 1) the aluminum base holder fixed on the anti-vibration optical table, and 2) the base that contained the major components. The laser holder is a small piece of Aluminum plate into which the laser diode (LD) and the thermistor are inserted. It rests on the thermoelectric cooler (TEC), making good thermal contact using a thermally conductive compound. This block is held to the heatsink by nylon screws to minimize direct heat transfer. The heat sink rests on a small fan for effective dissipation of heat to the surrounding. The laser diode is inserted into
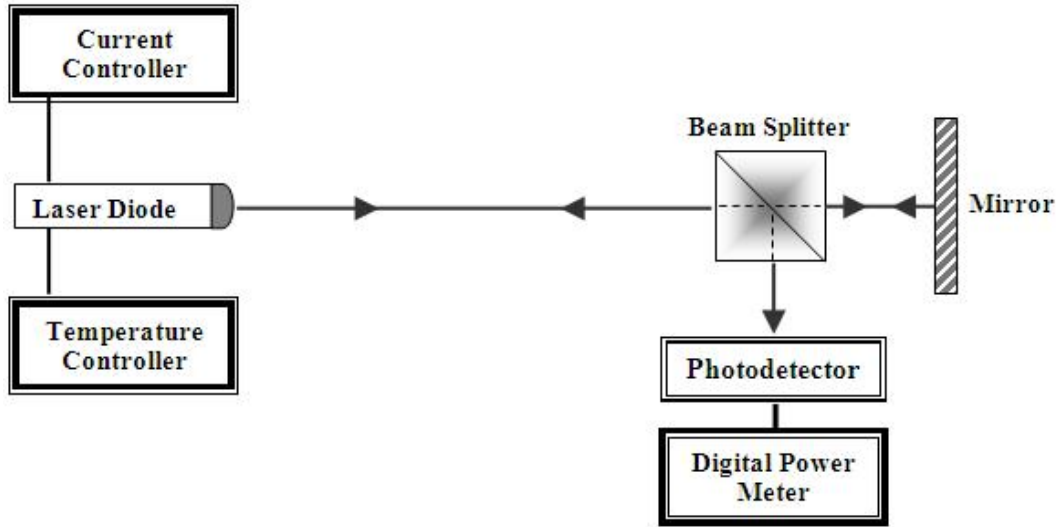
Fig. 2. Experimental Setup of Semiconductor Laser with External Cavity.
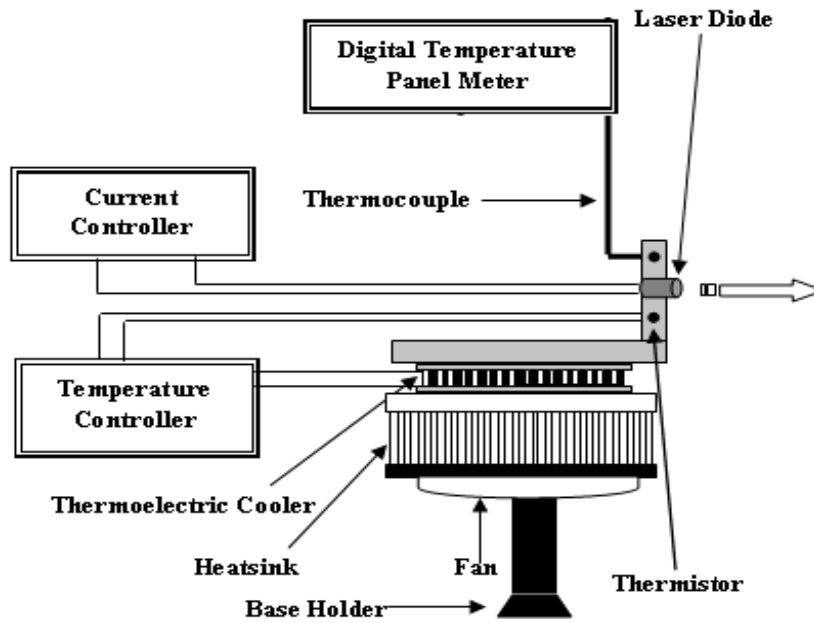
Fig.3. Schematic diagram of the Laser Mount connected to Current and Temperature Controllers.

the hole at the middle of the mount and very close to the thermistor, thermoelectric cooler and thermocouple.

The output of the diode laser strongly depends on the injection current. With the increase in the injection current above the threshold value, not only the optical power increases but the operating wavelength is blue-shifted. The current controller with an accuracy of ± 0.01 mA is therefore used for effective stabilization of the output. The optical power emitted by the laser without feedback is measured using an optical power meter placed

in front of the laser diode. The injection current is scanned from zero to about 40mA in steps of 0.1mA and the corresponding optical power is measured each time. This process is repeated for different temperature values. The whole experiment is repeated by constructing an external optical cavity as shown in figure 2. The differential slope efficiency (dL/dI) is the slope of the L-I characteristic at a particular current value. Slope efficiency for a laser should be constant above and below the threshold region. Any variation in slope efficiency above the threshold along with the so called kinks in the

laser characteristics may point to internal defects in the laser. Hence the slope efficiency is an important factor in determining the quality of a laser beyond threshold

RESULTS AND DISCUSSION

Figures 4 through 6 describe the behavior of the output characteristics of the diode laser with changes in temperature and optical feedback. The plots in figure 4 describe the variation of the threshold current with temperature in the absence [curve (a)] and presence [curve (b)] of optical feedback. The detail values are given in table 1. Clearly, it can be seen that the value for the threshold current increases in general with the increase in temperature. This results from the fact that, as the temperature increases, the lattice vibrations in the active region increases, thereby, increasing the losses as well as suppressing carrier recombination. The process of optical feedback is seen to reduce the threshold value up to a certain temperature (21˚C in our experiment). This is along the expected lines that optical re-injection 'stimulates' recombination process in the active region which results in the decrease of the threshold value. It is interesting to note that above that temperature (21˚C for our setup), there is an actual increase in the threshold current value due to optical feedback. Interestingly this temperature was also the temperature of the surroundings i.e. room temperature. Though the observed change in the

threshold value as a result of optical feedback was small, the effect was regular.

Figure 5A shows the output optical power versus input current for the solitary laser diode, in the absence of optical feedback. The L-I curve was measured at different temperatures. The input current is varied from 0mA to 37mA. The L-I characteristics of the laser was then measured with optical feedback as shown in figure 5B. Small variations in the slope of the L-I characteristics (small kinks, or nonlinearity), can be observed around the threshold current, but these were most likely due to the onset of fluctuations in the output power due to the optical feedback, that influences the output power versus current characteristics (through the threshold injection current and slope efficiency dL/dI). The effect of optical feedback on the threshold and output power of the laser diode system has been explicitly shown in figure 6. For temperatures, below a certain temperature (which is 21˚C for our setup), optical feedback causes reduction in the value of the threshold current which can act as a good indicator of the feedback level. For higher temperatures optical feedback has the effect of increasing the threshold value and decreasing slightly the slope efficiency compared to that of the solitary diode laser.
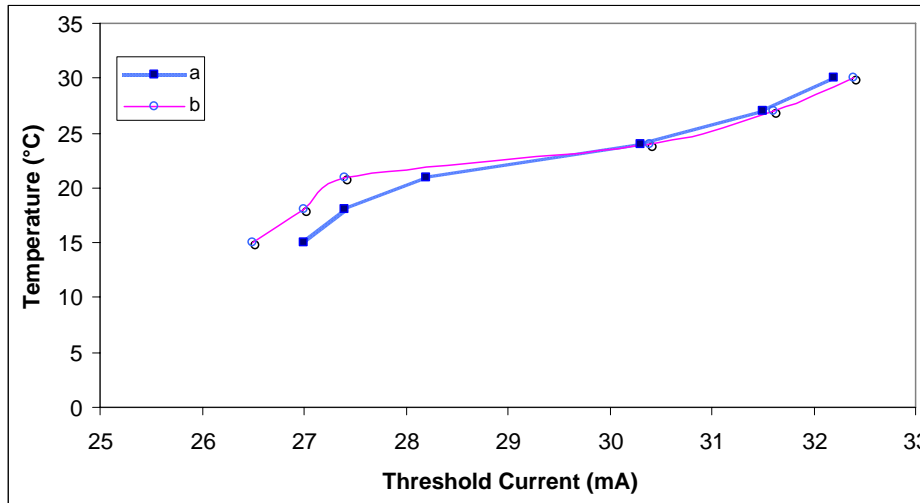

Fig. 4. Variation of threshold current of laser diode with temperature (a) without and (b) with optical feedback.

Table 1. Threshold Current for different temperature.

| Temperature	15 ˚C	18 ˚C	21˚C	24 ˚C	27 ˚C	30 ˚C
Threshold Current of Solitary Laser Diode (mA)	27	27.4	28.2	30.3	31.5	32.2
Threshold Current with Optical Feedback (mA)	26.5	27	27.4	30.4	31.6	32.4
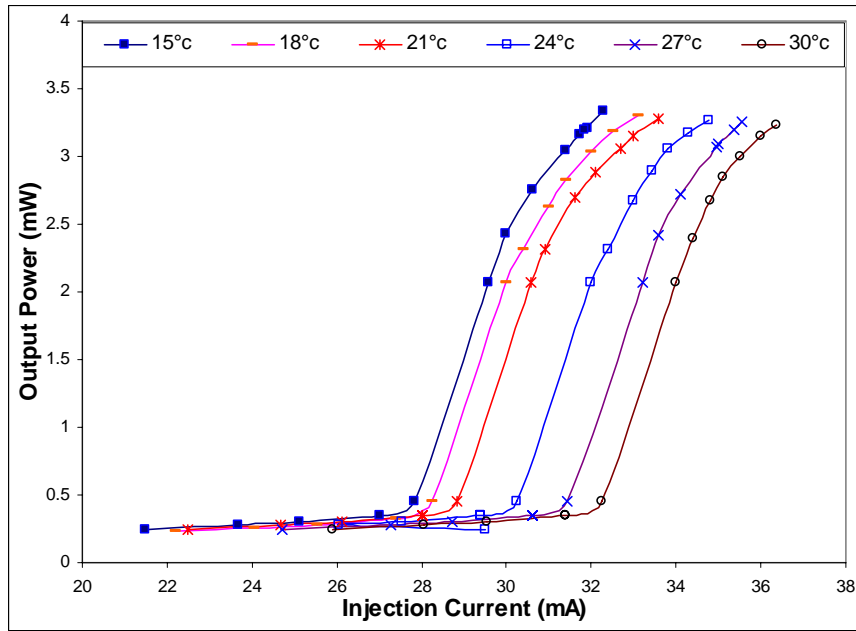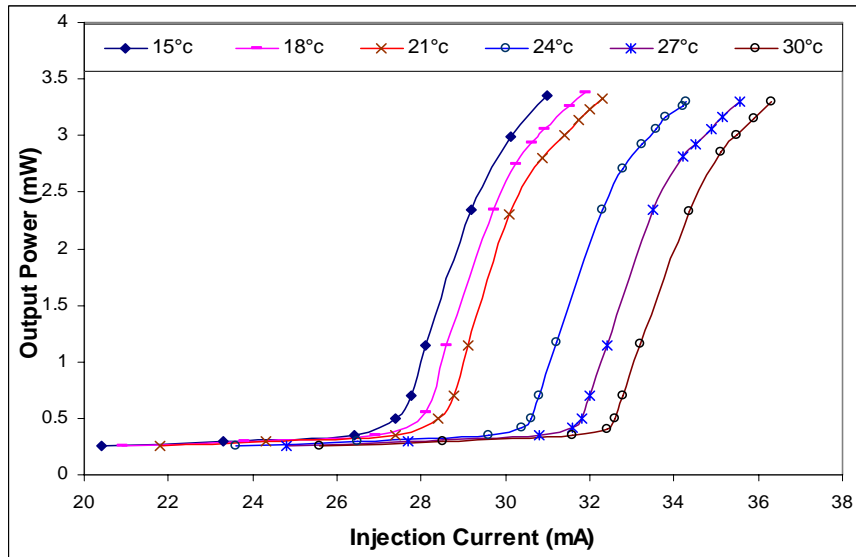
Fig. 5. Plots for injection current versus output power for diode laser (A) without and (B) with optical feedback at different temperatures.

The experiments were performed up to a maximum temperature of 30˚C keeping in mind the operating temperatures of optical communication systems. However, it will be interesting to carry out the experiments at much higher temperatures and with different types of semiconducting materials.

The observed increase in the threshold value and slope efficiency of the diode laser with the increase in temperature is well known resulting from the increase in optical losses. The effect of optical feeedback normally reduces the threshold value of the applied injection current to the diode laser due to the increase in optical density. Contrary to this we observed an actual increase in the value of the threshold at certain temperatures as a result of optical feedback. This 'strange' or anomalous behavior can be possibly explained as a combined effect of temperature and optical feedback. Increase in temperature results in red-shift of the oscillating frequency of the diode laser and hence mode-hopping. Not all modes respond in the same manner to optical feedback. Certain modes may destructively interact with the re-injected optical fields thereby suppressing the output optical power (amplitude decay). This will result in an increase in the threshold value.
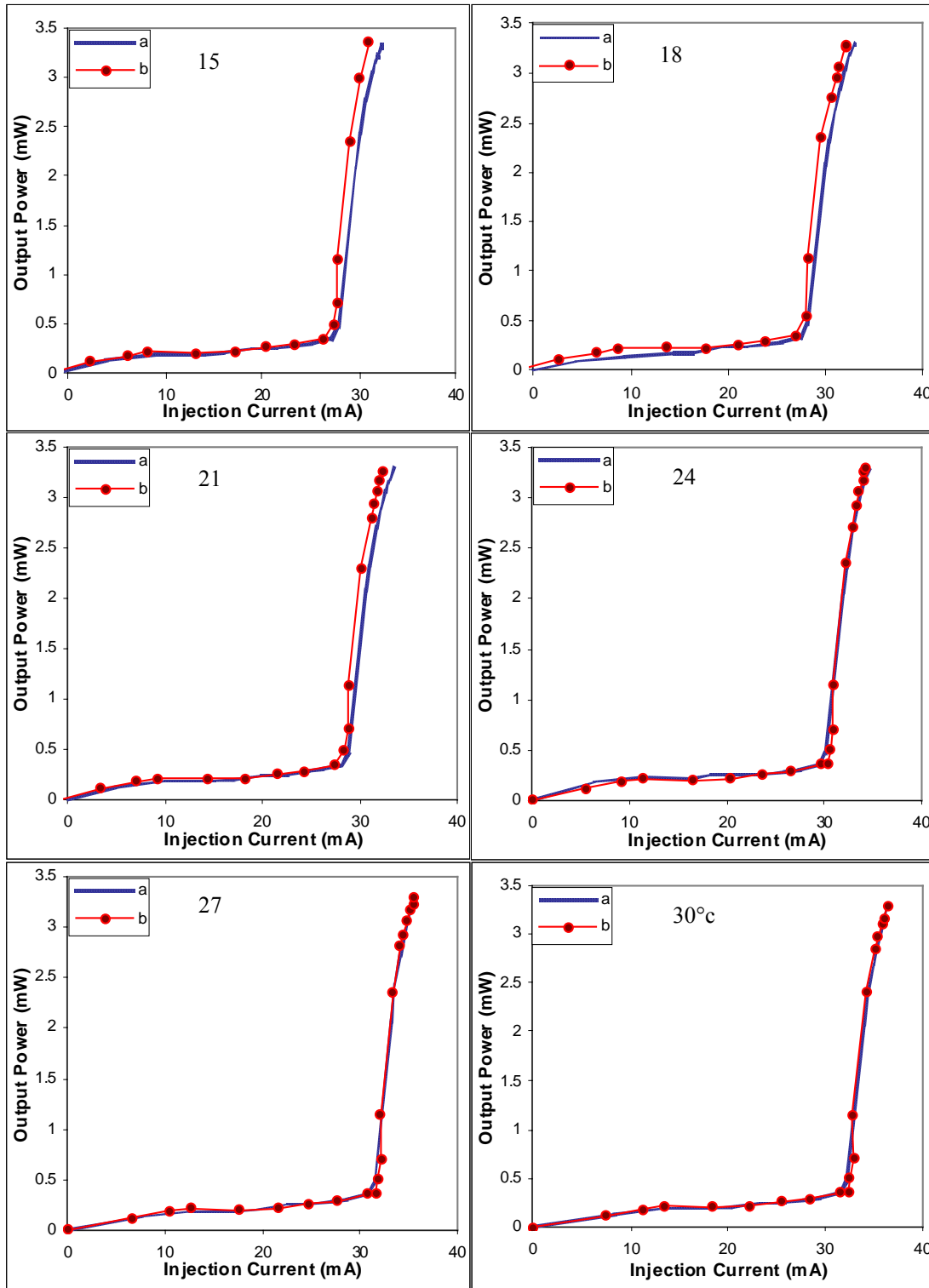
Fig. 6. Laser L-I characteristics (a) without and (b) with optical feedback at different temperatures.

CONCLUSION

In conclusion, we have experimentally analyzed the characteristics of the solitary diode laser and in presence

of single optical feedback under the effect of temperature. The results obtained show dependence of the threshold current value on the temperature. With the increase in temperature the threshold is seen to increase while the

output optical power gets reduced due to increase in the cavity losses. Below certain temperature (21˚C for our set up) the presence of the optical feedback is shown to reduce the threshold current and increase the slope efficiency relative to the solitary diode laser in this sense the threshold reduction is a good indicator of the feedback level. At higher temperatures, interestingly strange behavior is observed where the threshold current is seen to increase while the slope efficiency was only slightly affected by the optical feedback. This 'anomalous' behavior can be attributed to the combined effect of temperature and optical feedback on the oscillating mode resulting in its suppression due to destructive interference with the re-injection beam. With regard to temperature effect in this kind of systems these results are very helpful.

ACKNOWLEDGMENTS

REFERENCES

Alter, DM. 2003. Thermoelectric Cooler Control Using a TMS320F2812 DSP and a DRV592 Power Amplifier. Application Report SPRA873.

Al-Dwayyan, AS., Al-Dukhayel, AM., Azzeer, AM. and Kamal, AM. 2007. Polarization Instability of Vertical Cavity Surface Emitting Lasers. Available: http://ipac.kacst.edu.sa/eDoc/2007/165161_1.pdf.

Amann, MC., Bosch, T., Lescure, M., Myllyla, R. and Rioux, M. 2001. Laser ranging: a critical review of usual techniques for distance measurement. Optical Engineering. 40:10-19.

Bosch, T., Servagent, N., Chellali, R. and Lescure, M. 1998[a]. Three-dimensional object construction using a self-mixing type scanning laser range finder. IEEE Transactions on Instrumentation and Measurement. 47:1326-1329.

Bosch, T., Servagent, N., Gouaux, F. and Mourat, G. 1998[b]. The self-mixing interference inside a laser diode: application for displacement, velocity and distance measurement. Proceedings of the SPIE, International Society for Optical Engineering. 3478: 98-108.

Boshier, MG., Berkeland, D., Hinds, EA. and Sandoghdar, V. 1991. External-cavity frequency-stabilisation of visible and infrared semiconductor lasers for high resolution spectroscopy. Opt. Comm. 85:355-359.

Buldu, JM. 2003. Entrainment of SL: Noise, Modulation and Synchronization. PhD Thesis, Terrassa Departament de Fı´sica i Enginyeria Nuclear, Universitat Polite`cnica de Catalunya, Colom 11, E-08222 Terrassa, Spain.

Derry, PL., Figueroa, L. and Hong, C. 1995. Semiconductor Lasers. In: Handbook of Optics (vol. 1). Optical Society of America. 13:6.

Fujita, Y. and Ohtsubo, J. 2005. Optical-feedback-induced stability and instability in broad-area semiconductor lasers. Applied Phys. Lett. 87:031112-14.

Goldberg, L., Taylor, HF., Dandridge, A., Weller, JF. and Miles, RO. 1982. Spectral characteristics of semiconductor lasers with optical feedback. IEEE J. Quantum Electron. QE-18:555-564.

Helms, J., Kurtzke, C. and Petermann, K. 1992. External feedback requirements for coherent optical communication systems. J. Lightwave Technol. LT-10:1137-1141.

Katagirl, Y. and Hara, S. 1998. Scanning-probe microscope using an ultrasmall coupled-cavity laser. Measurement Science & Technology. 9:1441-1445.

Lang, R. and Kobayashi, K. 1980. External optical feedback effects on semiconductor injection laser properties. IEEE Journal of Quantum Electronics. QE-16:347-55.

Liu, Y., Chen, HF., Liu, JM., Davis, P. and Aida, T. 2001. Synchronization of optical-feedback-induced chaos in semiconductor lasers by optical injection. Phys. Rev. A. 63:031802(R).

MacAdam, KB., Steinbach, A. and Wieman, C. 1992. A narrow-band tunable diode laser system with grating feedback, and a saturated absorption spectrometer for Cs and Rb. American Journal of Physics. 60:1098-1111.

Mito, K., Ikeda, H., Sumi, M. and Shinohara, S. 1993. Self-mixing effect of the semiconductor laser Doppler method for blood flow measurement. Medical and Biological Engineering and Computing. 31:308-310.

Olsson, NA. and van der Ziel, JP. 1987. Performance characteristics of 1.5 μm external cavity semiconductor lasers for coherent communication. J. Lightwave Technol. LT-5:510-515.

Osmudsen, JH. and Gade, N. 1983. Influence of optical feedback on laser frequency spectrum and threshold conditions. IEEE J. Quantum Electron. QE-19:465-469.

Servagent, N., Mourat, G., Gouaux, F. and Bosch, T. 1998. Analysis of some intrinsic limitations of a laser range finder using self-mixing interference. Proceedings of the SPIE, International Society for Optical Engineering. 3479:76-83.

Takiguchi, Y., Liu, Y. and Ohtsubo, J. 1998. Low-frequency fluctuation induced by injection-current modulation in semiconductor lasers with optical feedback. Optics Letters. 23:1369-1371.

Yabuzaki, T., Mitsui, T. and Tanaka, U. 1991. New type of high-resolution spectroscopy with a diode laser. Phys. Rev. Lett. 67:2453-2456.

Ye, C. 2004. Tunable External Cavity Diode Lasers. World Scientific Publishing Co. Texas A&M University, USA.

Canadian Journal of
pure&applied
sciences

SOLIDIFICATION BEHAVIOR AND FORGEABILITY OF STIR-CAST ALUMINUM ALLOY METAL MATRIX COMPOSITES

Rabindra Behera[1], S Kayal[1], D Chatterjee[2] and *G Sutradhar[3]
[1]Department of Mechanical Engineering, Jadavpur University, Kolkata, West Bengal
[2]Department of Mechanical Engineering, Bengal Engineering College, Kolkata, West Bengal
[3*]Department of Mechanical Engineering, Jadavpur University, Kolkata, West Bengal, India

ABSTRACT

The present paper aims to investigate the solidification behavior and the forgeability of Aluminum alloy (LM6)-SiCp composites at different section of three-stepped composite castings. LM6 metal matrix composites (MMCs) containing SiC particles (5 and 10 wt %) of 400mesh (average size) were prepared by using stir casting route. The temperature of the cast composites during solidification was measured by putting K-type thermocouples at the centre of the each step, from which the solidification curves were constructed. The forgeability of the as cast MMCs were also measured at different step of the casting. The results show that the forgeability of cast metal matrix composites at the middle section i.e. step-II of the casting is minimum compared to both end section of a three-step casting. The solidification curves of Aluminum alloy (LM6)-SiCp composites compared with the unreinforced alloy (LM6) and the results reveal that significant increase in solidification time with the addition of SiC particles. The curves also show that the rate cooling and the solidification time are different at different section of the castings. This practical research analysis and test results on solidification behavior and the forgeability of Al/SiCp-MMC will provide useful guidelines to the present day manufacturing engineers.

Keywords: Metal matrix composites (MMCs), casting, solidification, cooling rate, forgeability.

INTRODUCTION

The developments in materials technology have resulted in several new materials like metal–matrix composites (MMCs). Composites have developed with great success by the use of fiber reinforcement in metallic materials (ASM Metal Hand Book, 1998). Metal–matrix composites (MMCs) have been one of the key research subjects in materials science during the past two decades (Lindroos *et al*., 1995). MMCs have emerged as potential material alternatives to conventional alloys and widely used in aircraft and automobile industries because of its excellent physical, mechanical and development properties. But, the difficulties in production and the manufacturing cost is the key factor, which comes as an obstacle for their wider application in modern industry, although potential benefits in weight saving, improved mechanical properties and increased component life. Now a day, even in those terms, MMCs are still significantly more expensive than their competitors. Only simpler production methods, higher production volumes, and cheaper reinforcements can achieve the cost reductions (Charles, 1990; Klimowicz, 1994). The search for cheaper, easily available reinforcement has led to the wider use of SiC and Al_2O_3 particles (Klimowicz, 1994). Therefore, the particle reinforced MMCs are now dominating the MMC market. There are several methods are used for the manufacturing of MMCs, of which, stir

casting method is quite popular due to its unique advantages. In this casting method, the reinforcing particles has introduced into the melt and stirred thoroughly to ensure their proper mixing with the matrix alloy. The properties of particle-reinforced metal matrix composites produced by stir cast method has influenced by various parameters such as type, size & weight fraction of reinforcement particles and its distribution in cast matrix metal. It also depends on their solidification behavior during casting. The rate of solidification has a significant effect on the microstructure of cast composites, which in turn affects their mechanical properties. Nath *et al*. (1987) studied on the distribution of mica particle in Al-Cu-Mg melt solidified in a variety of moulds under different heat flow configurations and concluded that thin castings of 12.5mm could easily be produced with a homogeneous distribution of mica particles. Dutta and Surappa (1998) studied macro- and micro-structure of Al–Cu–SiCp composites under multidirectional solidification conditions and concluded that an increase in particle volume fraction and cooling rate reduced the extent of macro-segregation of reinforcements in the composites. Rajan *et al*. (2007) studied on solidification and casting / mould interfacial heat transfer characteristics of aluminum matrix composite. They have shown that, addition of ceramic reinforcement particles with the aluminum alloy reduces the total solidification time in all the moulds (i.e. sand, graphite and metal mould) studied at lower volume fractions and increases at higher volume fractions. They

---

*Corresponding author email: cast_1963@rediffmail.com

have also concluded that the total solidification time is very less in case of graphite comparison to steel and sand mould, because of high thermal conductivity of graphite.

Particulate metal matrix composites have produced economically by conventional casting techniques. However, the stiffness, hardness and strength to weight ratio of cast MMCs are increased, but a substantial decrease in ductility has obtained. It has observed that some improvements in strength and ductility has found with the application of plastic forming processes i.e. forging to the cast composites. The forged MMCs having better mechanical properties compared to cast MMCs, such as it improves density, hardness and tensile strength etc. the forging process also avoids the use of secondary operation like machining. The forgeability is one of the important parameter, which gives information regarding the limitation of forging.

Ismail *et al*. (2000) studied on the effect of forging on the properties of particulate-SiC reinforced aluminium-alloy composites. They have shown that the forged samples had strength values superior to those of the as-cast counterparts. After forging, the yield strength and tensile strength increased and there has improvement in ductility of the composite material. Ceschini *et al*. (2009) studied on forging of the AA6061/23 vol. % Al_2O_3p and AA2618/20 vol. % Al_2O_3p composite: Effects on microstructure and tensile properties. They have shown that forging process induced a slight increase in hardness, tensile strength, elastic modulus and an evident increase in tensile elongation. SEM analyses of the fracture surfaces of the tensile specimens showed substantially similar morphologies for the as-cast and forged composites, both at room and high temperature. He *et al*. (1996) studied on the microstructure and mechanical properties of an Al/SiC composite cold die forged gear. They have observed that cold forging of SiC reinforced Aluminium based metal matrix composites reduce the grain size, defects, and the fracturing of the secondary phase and SiC particulates. Because of a cold plastic deformation, a large crystal distortion occurred resulting in the increase in the dislocation density that enhanced mechanical properties. The minimum isostatic pressure to prevent fracturing during cold die forging has found to be 650 MPa.

The objective of the present investigation is to study the effect of varying weight percentage of SiCp on the solidification curves of aluminum-silicon alloy (LM6) matrix composites during solidification at different step of the casting in sand mould and the forgeability of as cast MMCs at different step. The rate of solidification at section of the casting and the metallographic properties has studied at different weight percentage of silicon carbide particles. The results are compared with the solidification behavior of aluminum alloy i.e.LM6.

## MATERIALS AND METHODS

Experimental procedure

The aluminum–silicon alloy i.e.LM6, which is a well-known alloy of aluminum, is used as the base/matrix metal in the experiments for the fabrication of the composites that has been reinforced with 5 and 10 wt% of SiCp of average 400 mesh size. The chemical composition of the matrix material (LM6) and the thermo physical properties of aluminum alloy, SiCp & sand have given in the tables 1 and 2. The composites have fabricated by the liquid metal stir casting technique. The aluminum alloy i.e. LM6 is melted in clay graphite crucible using an electric resistance furnace and 3wt% Mg has been added with the liquid metal, in order to achieve a strong bonding by decreasing the surface energy (wetting angle) between the matrix alloy and the reinforcement particles. The addition of pure magnesium has also enhanced the fluidity of the molten metal. The melt has mechanically stirred by using an impeller after addition of the pre-heated silicon carbide particle (about 850-900^{0}C). The processing of the composite has carried out at a temperature of 750^{0}C with a stirring speed of 400-500rpm. The melt has poured at a temperature of 745^{0}C into a stepped silica sand mould. Three (i.e.T_1, T_2 & T_3) K-type thermocouples of 0.3mm size has used at the centre of the different section of the mould to measure the temperature variation with respect to time in seconds in the casting during solidification has shown in figure1. One more K-type thermocouple has inserted into the sand mould to measure the temperature variation of the molding sand after pouring of molten metal and during solidification of the castings. The solidification curves of the castings and the variation of temperatures at different sections in the mould are recorded with the help of a computer aided data acquisition system, the schematic sketch of the computer aided temperature data acquisition set up has shown in figure 2. The figure of composite casting with thermocouples has shown below in figure 3. Finally, the solidification curves of LM6-SiCp composites have compared with the unreinforced LM6 matrix alloy at different section of the casting. The micro structural characteristics of the alloys and composites at different section of the castings have also evaluated.

Table 1. Chemical Composition (LM6).

Elements	Si	Cu	Mg	Fe	Mn	Ni	Zn	Pb	Sb	Ti	Al
Percentage (%)	10-13.0	0.1	0.1	0.6	0.5	0.1	0.1	0.1	0.05	0.2	Remaining

Table 2. Thermo physical properties of the matrix, reinforcement particle and sand.

Properties	LM6	SiC particulates	Sand
Density (gm/cm^3)	2.66	3.2	1.6
Average particle size (mesh)	--------	400	-----
Thermal conductivity (W/m-K)	155	100	0.52
Specific heat (J/Kg-K)	960	1300	1170
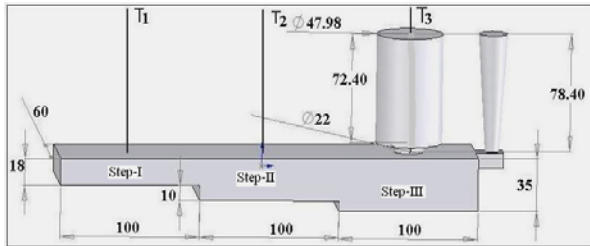
Fig. 1. The geometry of mould cavity with K type-thermocouples (T_1, T_2 & T_3). (All dimensions are in mm).
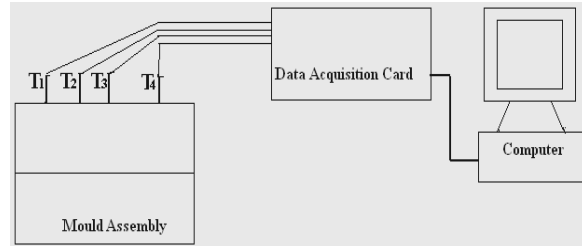
Fig. 2. Schematic sketch of the computer aided temperature data acquisition set up. (T_1, T_2 & T_3 Thermocouples attached different section of casting and T_4 inserted into the sand).
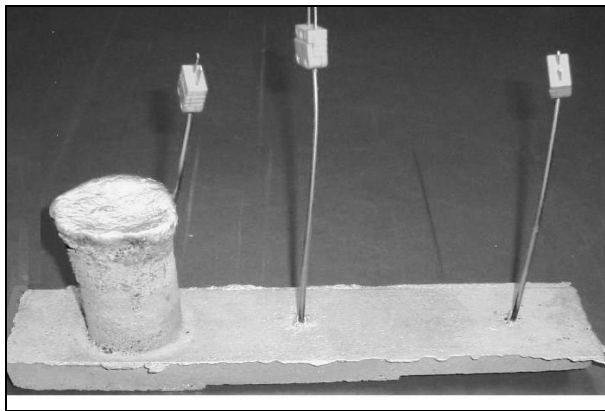
Fig. 3. Composite casting with thermocouples.

RESULTS AND DISCUSSION

Microstructural Analysis

Samples of as cast MMCs for metallographic examination were prepared by grinding through 320, 400, 600, 800, 1200 and 1500 grit papers followed by polishing with 6μm diamond paste. Then the samples were etched with the etchant i.e. Keller's reagent. The etched samples were dried by using electric drier and then the microstructure observed by using optical microscope (Olympus, CK40M) at different magnification. The microstructure of the as cast LM6 MMCs are shown in figures 4 and 5 at different modulus of the casting. The micrograph of MMC castings at different step shows that the distributions of SiC particles are not uniform throughout the casting and segregation of particles are more in the eutectic region. This tendency may be attributed to the fact that the rate of cooling is not uniform throughout the casting due to change in thickness of the casting and lower rate of cooling in the sand mold.
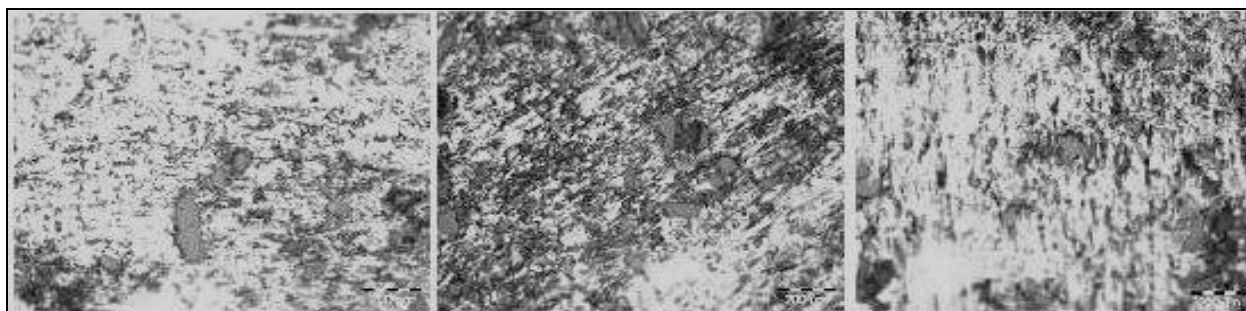
a. Modulus 6.97 (step-I)   b. Modulus 8.69(step-II)   c. Modulus 8.95(step-III)

Fig. 4. Microstructure of LM6/5wt% SiCp as cast MMC at different modulus of the casting.

a. Modulus 6.97   b. Modulus 8.69   c. Modulus 8.95
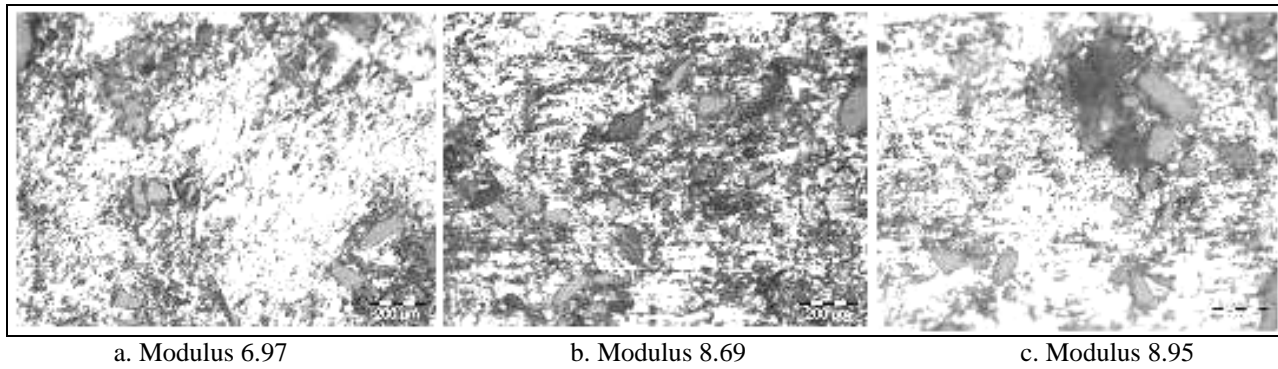
Fig. 5.   Microstructure of LM6/10wt% SiCp as cast MMC at different modulus of the casting.

Analysis of Cooling curves and Solidification Behavior of cast MMCs

When any alloying element or second phase particles added with the matrix alloy then the various time and temperature parameters of its solidification curve has affected. The variation in the nature of the cooling curve always has a significant impact on the microstructure and mechanical behavior of the material. Figures 6-8 shows the cooling curve of the Al alloy (LM6) and LM6 reinforced with 5 and 10wt% of SiCp metal matrix composites. The cooling curves for different step of castings at different weight fraction of SiCp indicates that the rate of cooling decreasing on increasing the weight percentage of SiCp in the cast MMCs. The cooling curves also show that the eutectic solidification time (i.e. the time interval between the start and the end of the eutectic phase solidification) increases on increasing the weight percentage of SiC particles in the aluminum alloy matrix. It has also observed that the introduction of SiC particles in the matrix metal lowers the liquidus temperature when compared with the unreinforced alloy. This can be attributed to the unfavorable primary aluminum nucleation condition prevailing at the reinforcement surface and the depression in the freezing point due to the presence of reinforcement, which is considered as an impurity. Studies by Gowri and Samuel (1992) have also shown that addition of particles lowers the liquidus temperature by about 10^oC. The similar trend has also observed by Rajan *et al*. (2007). It is observed that the eutectic solidification of the matrix alloy (LM6) starts at a temperature of 574^oC and ends at 572^oC. After addition of reinforcement particles i.e. SiCp in matrix alloy, the start and end temperature of eutectic solidification changes.

The reinforcement of SiCp with matrix metal increases the eutectic solidification time as compared with the cooling curve of unreinforced aluminum alloy (LM6). The eutectic solidification time also changed with the modulus of the casting, the cooling curve indicates that on decreasing the section modulus of the MMC castings the eutectic solidification time decreases at different weight fraction of SiC particles i.e. in case of lowest modulus the eutectic solidification time is less compared to highest modulus. This validates that the Chvorinov's rule still applies to the solidification process, irrespective of what additives are added to the molten metal (Stefanescu, 2000; Cambell, 1991). The cooling curve shows that the eutectic solidification time enhanced on increasing the weight fraction of reinforcement particles compared to unreinforced matrix alloy. That means the total solidification time (i.e. the time interval between the start of primary aluminum phase nucleation and the end of the eutectic phase solidification) increases on increasing wt% of SiCp. This trend may be attributed to the fact that the amount of heat extraction reduced on increasing the weight percentage of SiC particles in the liquid matrix metal as the presence of SiC particles in the matrix metal reduced the thermal conductivity and thermal diffusivity (Rajan *et al*., 2007).
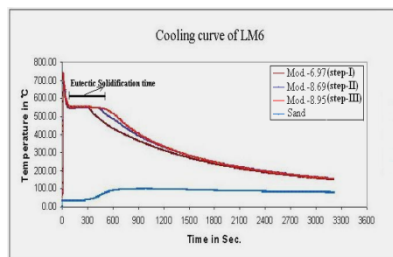

Fig.6.Cooling curves of Al (LM6) composites at different modulus of the casting.
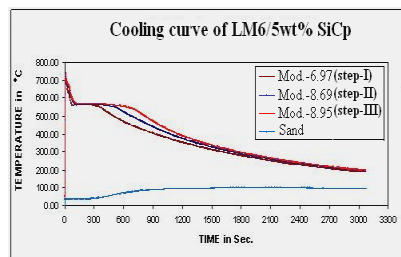
Fig.7.Cooling curves of Al (LM6) - 10wt%SiC composites at different modulus of casting.
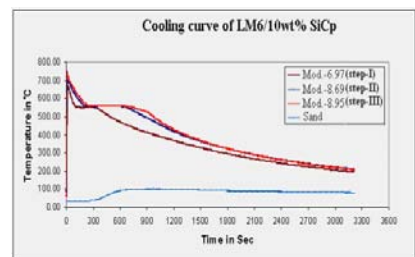
Fig.8. Cooling curves of Al (LM6) - 10wt%SiC composites at different modulus of casting.

Analysis of Forgeability

The forgeability of as cast composites at different step of castings have evaluated by means of upset method. Cylindrical specimens were prepared from each step of the castings by turning operation. The L/D ratio of the prepared specimens (L= height of the cylindrical specimen and D= diameter of the specimen) was 1.5, for forgeability test.

The limit of forgeability is expressed as the critical reduction in height by the following equation:

$$\text{\% of Critical reduction in height} = \frac{100 \, (\text{Initial height} - \text{Final height})}{\text{Initial height}}$$

Where, the initial height and the final height of the sample in mm. Critical reductions under unlubricated conditions only have compared to assess the forgeability of the experimental materials. The load was applied at room temperature on samples of different section of as cast MMCs reinforced with 5 and 10 wt% of SiCp. At different load, the percentage of deformation investigated. These results have presented in figure 9. The figure shown the percentage of deformation due to acting load is different at different step of the casting i.e. the percentage of deformation is lowest in step–II (middle section) comparison to step-III & I. The percentage of deformation is highest in step-I in comparison to step -III. This indicates that the higher percentages of SiC particles have accumulated at the middle section of the casting i.e. at step-II, in comparison to the step -III & I. The above result indicates that the distributions of silicon carbide particles are not uniform throughout the casting, which is same as micro structural result. This has occurred because of non-uniform rate of solidification of liquid metal at different step of the casting. It has also observed that on increasing the weight percentage of silicon carbide particles in cast composites the percentage of deformation decreases that means the forgeability of cast composites decreases on increasing the reinforcement ratios, as the presence of very hard SiCp in the cast MMCs decreases its ductility and enhances its hardness & brittleness.

CONCLUSIONS

The cooling curves have recorded experimentally for Al alloy (LM6) reinforced with 5 wt% & 10 wt% of SiC particles and compared with cooling curves of the unreinforced matrix alloy.i.e.LM6. The forgeability of cast MMCs have measured at the different step of the castings by upsetting method. The following conclusions are obtained:

a) The cooling rate decreases with the introduction of SiCp with increasing SiCp content due to lower heat transfer rates within the solidifying melt owing to the reduction of thermal conductivity and effective thermal diffusivity of the composite system. That indicates the cooling rate is faster in case of unreinforced matrix alloy or containing low fraction of SiCp in the matrix.

b) The addition of ceramic reinforcement to alloy enhances the eutectic solidification time, as the presence of insulating dispersoids i.e. SiCp plays a dominant role in reducing the cooling rates. The solidification time is also varied with the change in thickness of castings. The solidification time is less in case of thinner section in comparison with thicker section, due to rapid cooling of thinner section. This trend is similar to the monolithic metal and its alloys.

c) The forgeability i.e. percentage of deformation decreases on increasing the percentage of SiCp and the middle part of the casting (i.e. step–II) shows low forgeability comparison to the both end steps in the three-step casting component, due to accumulation of higher percentage of SiCp in this step. That indicates the distribution of SiCp is not uniform through out the casting.

ACKNOWLEDGEMENT
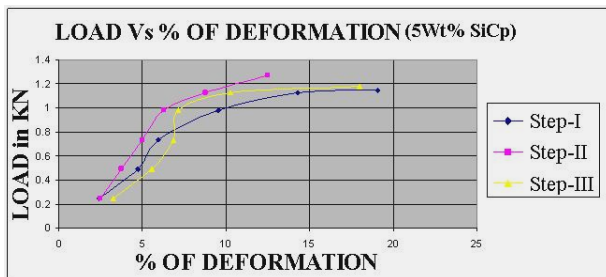
(a)
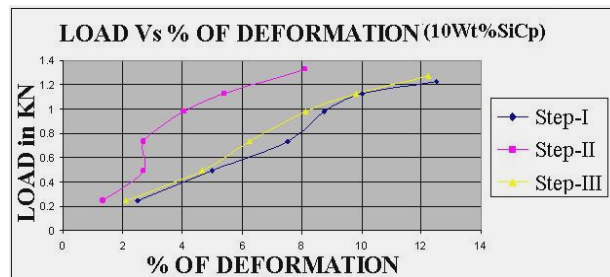
(b)

Fig. 9. Load Vs % of Deformation curve of as cast MMCs at different step of MMCs casting reinforced with (a) 5wt%SiCp and (b) 10wt%SiC.

REFERENCES

ASM Metals Hand Book. 1998. Casting. 15(9):323-327.

Charles, D. 1990. Metal matrix composites-ready for take-off? Methods Mater. 6:78-82.

Campbell, J. 1991. Castings, Butterworth Heinemann. 130-131.

Ceschini, L., Minak, G., Morria, A. and Tarterini, F. 2009. Forging of the AA6061/23 vol.%Al_2O_3p composite: Effects on microstructure and tensile properties. Materials Science and Engineering A. 513-514.

Ceschini , L., Minak, G. and Morri, A. 2009. Forging of the AA2618/20 vol.% Al_2O_3p composite: Effects on microstructure and tensile properties. Composites Science and Technology. 69:1783-1789.

Dutta, B., Surappa, MK. 1998. Microstructure evolution during multidirectional solidification of Al–Cu–SiC composites. Composites. 29A:565-573.

Gowri, S. and Samuel, FH. 1992. Effect of cooling rate on the solidification behaviour of Al-7Pct Si- SiCp metal matrix composites. Metall Trans A. 23:3369-76.

He, W., Zhang, YF., Lee, KS., Lu, L Xie, SS. and Jin, QJ. 1996. Microstructure and mechanicalproperties of an Al/SiCp, composite cold die forged gear. Materials & Design. 17(2): 97-102.

Ismail, OÈ zdemir, UÈ mit CoÈ cen. and Kazim OÈ nel. 2000. The effect of forging on the properties of particulate-SiC- reinforced aluminium-alloy composites, Composites Science and Technology. 60:411-419.

Klimowicz, TF. 1994. The large scale commercialization of aluminum-matrix composites. Journal of Materials. 46:49-53.

Lindroos, VK. and Talvite, MJ. 1995. Recent advances in metal matrix composites. Journal of Material Processing Technology. 53:273-284.

Nath, D., Asthana, R. and Rohatgi, PK. 1987. Particle distribution control in cast aluminium alloy–mica composites. Journal of Material Science. 22:170-176.

Rajan, TPD., Narayana, PK., Pillai, RM. and Pai, BC. 2007. Solidification and casting/mould interfacial heat transfer characteristics of aluminium matrix composites. Composite Science Technology. 67:70-78.

Stefanescu, DM. 2002. Science and Engineering of Casting Solidification, Kluwer Academic/Plenum Publishers,NewYork.311-319.

Canadian Journal of
pure&applied
sciences

A DOMESTIC SOLAR POWER TOWER USING STIRLING ENGINE TECHNOLOGY

*Irfan Younas, Muhammad Zahoor and Saad Ul Haq
HITEC University Taxila Cantt., Pakistan

ABSTRACT

The world is undergoing significant changes both technologically and socially. Societies have witnessed growth unparallel in history over the past century. This growth world-over has been at the expense of ever increasing demand on energy; this demand is not showing any sign of abating. However the world's energy resources are depleting at a very fast rate, particularly fossil fuels. Solar energy is a renewable energy source that can be used to generate energy using heat engines. In this work we outline an innovative approach to generate electricity using a combination of existing technologies such as the solar tower, Fresnel reflectors and Stirling engines. It is proposed to erect a domestic solar tower that has embedded Stirling engines for power production. The UAE has vast amount of solar irradiation which on yearly average is about 400 - 500 Watts/m^2. Used intelligently, with carefully deployed Linear Fresnel reflectors, this technology can deliver electricity to far flung off-grid locations as well as feed into domestic electricity grid.

Keywords: Concentrated solar power, solar tower, linear fresnel reflectors, stirling engine technology.

INTRODUCTION

The world's energy demand is ever increasing. This is partly due to a growing population and technological advancements, but our very way of life is heavily dependent on the continuous and steady availability of energy. The developing countries are catching up with the developed world in terms of living standard and this very desire would inherently require increased access to, and consumption of energy. It is no secret that wealth and economic growth in society is fundamentally intertwined with continuous and uninterrupted power supply. As availability of fossil fuels are in sharp decline and can no longer be solely relied upon to cater for our growing energy demand, the quest for reliable and renewable energy resources has never been so important.

The world energy consumption has exceeded 508 quadrillion Btu (10^{15} Btu) in 2010 and is expected to increase by a rate of 8-10 quadrillion Btu per year (IEA, 2009). One major reason for this increase is the phenomenal growth of the Indian and Chinese economies which are expected to be the biggest contributor to the annual rise in energy consumption. Therefore most countries have, and wisely so, begun investing in renewable energy technologies in order to gradually shift the emphasis from conventional power production to that using renewable energy resources.

Energy production using thermal solar power is one important source of power production. This is due to the fact that the sun is abundantly available particularly in the

_____
*Corresponding author email: iyounas101@gmail.com

Middle East region, which is classified as dry tropical region of the earth. The Gulf Corporation Countries (GCC) and the UAE in particular have shown enormous interest in developing expertise, and realise solar powered energy technologies for the nation (Kerney, 2008).

DISCUSSION

CSP Overview
Solar thermal electricity may be explained as the result of a process by which directly collected solar energy is converted to electricity through the use of some sort of heat to electricity conversion device (Mills, 2004). Essentially energy of a system is measured as the maximum useful work that can be extracted during a process which brings the system into equilibrium with a heat reservoir (Perrot, 1998). Although solar radiation has a high radiosity (rough estimate indicates that it is larger than 60 MW/m^2 at the surface of the sun) the significant dilution of solar flux due to Earth's geometric position and reflection of solar rays caused by Earth's atmosphere, leaves solar energy to be less suitable for terrestrial use. Broadly speaking, solar flux available is slightly higher than 1 kW/m^2; therefore an essential requisite for solar thermal power plants and high-temperature solar applications is to deploy optical concentration devices which enable the thermal conversion to be carried out at high intensity and with relatively little heat loss.

The CSP system design combines a relatively large, efficient optical surface, for example a field of highly reflective mirrors where the incoming solar radiation is concentrated and reflected onto a solar receiver with a small aperture area. This solar receiver should be a highly

absorbent and transmittance material with low reflectance. Its heat exchanger should as much as possible emulate a black body having negligible convection and conduction losses. In the case of a solar thermal power plant, the task is to transfer concentrated solar flux onto a thermal fluid which then attains a temperature high enough to feed a heat engine or a steam turbine that can be used as a power generator. The solar thermal element can be a parabolic trough, a Fresnel reflector or a parabolic dish, all with a common purpose of concentrating the terrestrial solar radiation to a high degree such that electromechanical work can be extracted with high efficiency.

Parabolic trough
Parabolic trough is a curved, mirrored trough (receiver) which reflects the direct solar radiation onto a glass tube containing a fluid. The trough is parabolic along one axis and linear in the orthogonal axis (Mills, 2004).

The absorber tube positioned above the reflector along the axis of the trough contains the Heat Conducting Fluid (HCF) that is usually enclosed in a glass vacuum chamber. The vacuum significantly reduces convective heat losses. As the HCF passes through the tube it becomes increasingly hot. The heated fluid is directed towards a heat engine where approximately one third of the heat is converted to electrical power.

As the sun changes its position during the course of a day an electronic tracking system tilts the trough from east to west so that the direct radiation remains focused on the receiver. It should be noted that during seasonal changes, or where the troughs are globally positioned away from equator, the sun is rising at an angle, but that does not require adjustment of the mirrors, since the light is simply concentrated elsewhere on the receiver. Thus the parabolic trough design does not require tracking on a second axis.

Current operational parabolic trough power plants are installed in the USA and Spain, others are under construction elsewhere in the world. The USA boasts a 354 MW plant in the Mojave Desert in California. This plant comprises a collection of 9 separate power units. Another is placed in the Nevada desert generating 64 MW power. Many power installations using this technology are also visible at various locations in Spain where a range of parabolic power systems having capacity from 20-100 MW are operational (Martin *et al*., 2010; The free Library, 2010).

Solar power tower
The solar tower is utilising the solar energy projected by a group of sun-tracking mirrors known as Heliostats. These heliostats are collectively capable of concentrating solar heat at the top of the tower, where heat can reach in excess of 1000 degree Celsius. Hence the name solar tower (Spiros and Bernhard, 2010).

A receiver located at the top of the tower acts as an energy exchanger. Typical receivers are made from ceramic or other metal structures capable of withstanding high energy density and exhibiting little thermal stress.

The attained heat is thereafter transported via ambient air to a thermo hydraulic circuit that feeds into a dedicated heat recovery steam generator.

World first solar power tower in Seville, Spain generates 11 MW, also known as the PS10. Subsequently the PS20 commercial Solar power tower was constructed (also in Seville) which produces 20MW of electricity (Garcia-Sobrinos and Gonzalo, 2007).

Yet another Solar tower installation known as the Sierra Sun tower by eSolar in California produces 5MW (Biello, 2009). Other relative small solar towers in Germany and France generate about 1.5 MW (Mark Schmitz, 2009).

Solar Stirling Dish
The Stirling engine was invented by Robert Stirling in 1816 also known as an externally operated heat engine. It operates by cyclic compression and expansion of air or other gas at different temperature levels such that there is a net conversion of heat energy into mechanical work. Since the Stirling engine is simple in design and construction it can be operated easily (Walker, 1980). There are various types of Stirling engine also known as the alpha, beta and gamma types. These types differ only in design and their basic principle remains the same.

The Stirling engine has been attracting more interest lately as a good foundation to an electro-mechanical renewable energy system using a concentrating solar dish. Although many concentrating solar dish systems have been designed using Stirling technology, but this technology is yet to gain widespread acceptance; currently only one commercially operational system exists in the USA with a power output of 1.5 MW (Patty, 2004).

Linear Fresnel Technology
The linear Fresnel Technology system consists of long mirrors which are flat or have a slightly curved optical surface. These mirrors are positioned in long parallel lines such as to reflect the direct sunlight onto a long target or receiver. This receiver could be a long absorber tube with a re-concentrator made from linear Fresnel lens technology as depicted in figure 1.

The linear Fresnel technology is relative new and currently deployed in the USA, Spain and Australia. A demonstration plant is placed at Bakersfield in California (Morrison, 2008) producing 5 MW. Another plant has

been built at New South Wales (Mills, 2004) generating about 2 MW, while a third plant in Murcia, Spain (Ishan and Pallav, 2010) produces 1.4 MW. This CSP technology is new but relative mature and if deployed correctly on barren land or in a desert could potentially produce 10's of Megawatts.
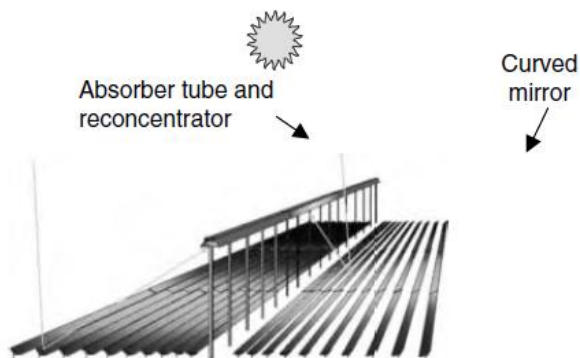

Fig. 1. Power generation using Linear Fresnel Lenses.

Solar flux and the UAE
It is an established fact that regions on or near the Earth's equator are subjected to more sunlight that other areas of the globe. Particularly the region between latitudes 40°N and 40°S, also referred to as the "solar belt" that witnesses abundant solar radiation.

The United Arab Emirates in general and Abu Dhabi in particular which lie in the solar belt region will be the subject of this study. Abu Dhabi has *latitude and longitude* denominations given as 24°28N and 54°22E respectively. An earlier study has shown that approximately 4500hours of sunlight per year can be expected for this region (Aksakal and Rehman, 1999). Solar radiation is usually divided into direct and diffuse radiation. We will however not make this distinction and simply use the total radiation that can be measured using a pyroheliometer.

(Islam *et al.*, 2009, 2010) have made extensive temperature and solar flux measurement for Abu Dhabi over the period of one year and their results are summarised in table 1. It can be seen from table 1 that the monthly average solar irradiance varies from approximately 300 W/m^2 to almost 500 W/m^2 during the course of a year. It is also noted that the yearly visibility index is around sixty percent which is adequate for a CSP power plant.

Therefore Solar Thermal Power is realisable power source that can be adapted and deployed throughout the United Arab Emirates and beyond. In the next section we present our take on how it could be deployed in the UAE.

Table 1. Solar Characteristics for Abu Dhabi (Islam *et al.*, 2009, 2010).

Month	Solar irradiance [Watts/m^2]	Temp. [°C]	Clearness index [0-1]
Jan	430.0	20	0.55
Feb	412.5	22	0.59
Mar	463.33	25.5	0.59
Apr	490.83	31.1	0.59
May	493.33	35	0.6
Jun	397.5	36.1	0.59
Jul	354.17	36.2	0.59
Aug	302.5	35.5	0.6
Sep	478.33	34.8	0.61
Oct	474.17	32	0.62
Nov	442.5	27.5	0.57
Dec	339.17	21.1	0.46
Average	423.19	29.7	0.58

The idea of the Solar Thermal Tower is not new and it has already been successfully deployed at various locations around the world. Spain has taken the lead with a plant producing around 20 MW of power. However there is an immense cost associated with this scale of power production which may not be viable for certain developing countries. Hence, we introduce the idea of a solar tower that has imbedded Stirling engines and powered by an array of Linear Fresnel Reflectors in the configuration shown in figure 2. This figure shows a schematic view of the total solar plant configuration. Linear Fresnel Reflectors (LFRs) are mounted on a rooftop and they are facing east. On the East side of the building a solar tower a positioned such that it is exposed to the high intensity concentrated solar radiation from the LFRs. This concentrated heat is then channelled through conduction to an array of Stirling Engines positioned at the lower parts of the Solar Tower. The acquired heat is used by the heat exchanger of each Stirling engine. A good choice for the conductive material would be pure copper encapsulated by glass shielded vacuum tubes.

For the Stirling engine the β-type engine was preferred because it has the displacer - and power piston arranged within the same cylinder and mounted on the same shaft (see Fig. 3). The displacer piston is used only to shuttle the working gas between the hot and cold ends of the cylinder. This configuration avoids the problem of hot moving seals, and both pistons are connected on a flywheel through connecting rods (Halit *et al.*, 2009).

Mechanical power extracted from each engine is converted into electricity using a synchronous electric generator. This generator can subsequently feed into the domestic electricity grid or charge powerful batteries for

electric storage and later usage. The β-type type Stirling Engine was chosen as it operates efficiently at constant Revolutions per Minute (RPM).
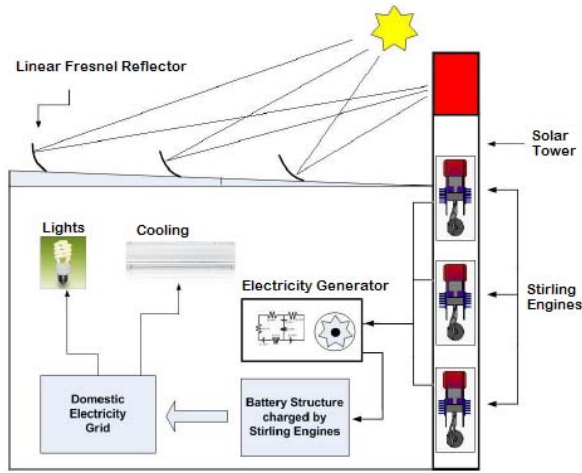

Fig. 2. Solar Tower with embedded Stirling Engines powered by Linear Fresnel Reflectors.
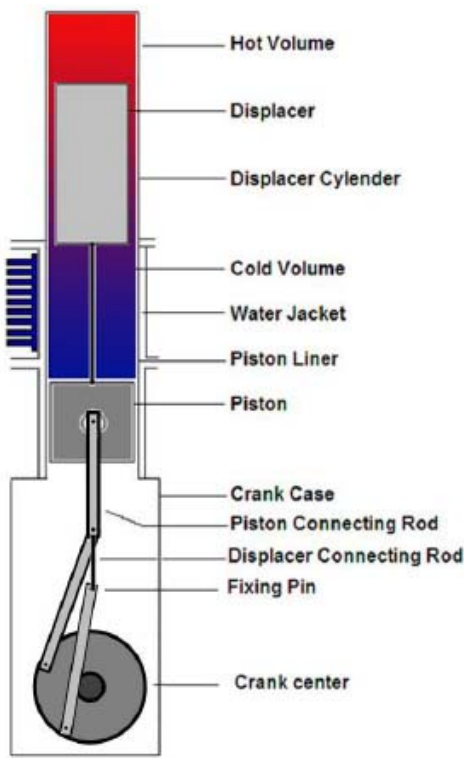
Fig. 3. A high level overview of a β-style Stirling engine.

For the chosen values for temperature difference between hot and cold side of the cylinder, area of swept volume, the working gas and operating pressure a power exceeding 100 Watts can be achieved (see Fig. 4). For the given configuration it can be seen that RPM of 450 would produce a power in excess of 125 Watts.

CONCLUSION

It is now generally accepted that CSP technologies are viable alternatives in generating power ranging from a few hundred watts to ten's of Megawatts. Spain has taken the lead, only followed by the USA and Australia.

A new approach to generate electricity using a combination of the solar tower, linear Fresnel reflectors and Stirling engine technologies has been presented in this research.

This approach is particularly useful for residential purposes where a huge amount of power is not required. It is envisaged that approximately 10 KW can be generated using the right configurations for Linear Fresnel Reflectors, Stirling engines, and battery backup.

This method for generating electricity is exceptionally valuable for the UAE where abundant amount of solar radiation is available, and technology deployment in far-flung areas will not be a problem. The solar power system can also be built as part of the design for a residential building where the Fresnel reflectors placed on roof top will generally not be visible.
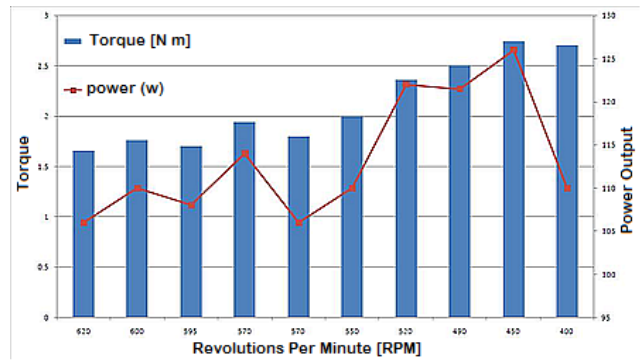

Fig. 4. Power and Torque output for given values of RPM of the Stirling engine.

REFERENCES

Aksakal, A. and Rehman, S. 1999. Global solar radiation in northeastern Saudi Arabia. Renewable Energy. 461-72.

Biello, D. 2009. First US "Power Tower" Lights up California. Scientific American Inc.

Garcia-Sobrinos. and Gonzalo. 2007. Tower of Power. Civil Engineering. 42-49.

Halit, K, Hüseyin, S Yücesu., Can, Ç. and Fatih, A. 2009. An experimental study on the development of a β-type Stirling engine for low and moderate temperature heat sources. Applied Energy. 86:68-73.

Iberdrola Renovables. 2009. Sustainability Report 2009 <http://www.iberdrolarenovables.es/wcren/corporativa/iberdrola?IDPAG=ENRENINFANUALINFSOSTE09>

International Energy Agency (IEA). 2009. World Energy Outlook. 75739 Paris Cedex 15, France.

Ishan, P. and Pallav, P. 2010. Techno-economic evaluation of concentrating solar power generation in India Energy Policy. 38(6):3015-3029.

Islam, MD., Kubo, I., Ohadi, M. and Alili, AA. 2009. Measurement of solar energy radiation in Abu Dhabi, UAE. Applied Energy. 86:511-515.

Islam, MD., Alili, AA. and Kubo, I. 2010. Measurement of solar energy (direct beam radiation) in Abu Dhabi, UAE. Renewable Energy. 35:515-519.

Kerney, AT. 2008. Tapping the sun: Solar energy in Middle East. ATKERNEY, Inc., Chicago, IL, USA.

Mills, D. 2004. Advances in solar thermal electricity technology. Solar Energy. 76(3):19-31.

Mark, S. 2009. Solar Institut Julich. Salt-Free Solar: CSP Tower Using Air. Renewable energy world.

Martin, R. and Hans, MS. 2010. Concentrating on Solar Electricity and Fuels, Science. 329(5993):773-774.

Mills, D. 2004. Advances in solar thermal electricity technology. Solar Energy Congress. 19-31.

Morrison, C. and Venture, B. 2008. Ausra's first solar thermal plant starts up. (New York Times, Oct 23, 2008).

Patty Garcia-Likens, P. and Coates, J. 2004. SRP and Tessera Solar Announce 1.5 MW Maricopa Solar Plant with Stirling Energy Systems SunCatcherTM Technology in Peoria. Stirling Energy Systems.

Perrot, P. 1998. A to Z of Thermodynamics. Oxford University Press. United Kingdom.

Spiros, A. and Bernhard, H. 2010. Solar tower power plant in Germany and future perspectives of the development of the technology in Greece and Cyprus. Renewable Energy 35:1352-1356.

The Free Library. 2010. Clean Energy Technologies: Wind Power, Solar Power, Biofuels, and Fuel Cells - Global Strategic Business Report.

www.thefreelibrary.com/Research and Markets: Clean Energy Technologies: Wind Power, Solar...-a0226581641>.

Walker, G. 1980. Stirling Engines. Oxford: Clarendon Press.

Canadian Journal of
pure&applied
sciences

HORIZONTAL GLOBAL SOLAR RADIATION
BASED ON SUNSHINE HOURS OVER ENUGU, NIGERIA

*Udosen E Akpan and Mfon David Umoh
Department of Physics, University of Uyo, PO Box 3718, Uyo, Akwa Ibom State, Nigeria

ABSTRACT

In this study statistical model of estimating global solar radiation over Enugu, Nigeria is presented. The study employed multiple regression analysis to estimate the monthly sunshine hours using four meteorological parameters for a period of eleven years (1997 to 2007). The parameters used included relative humility, temperature, rainfall and wind speed. The results showed the correlation coefficient of 0.849. Statistical test RMSE, MBE and MPE were employed to test accuracy the models used. The values of sunshine hours obtained were used to fit the Armstrong-Prescott equation to obtain the global solar radiation for Enugu.

Keywords: Global solar radiation, sunshine hours, Enugu, Nigeria.

INTRODUCTION

Knowledge of global solar radiation at any sight is essential requirement in most of the solar energy applications such as simulation of crop growth in agriculture, solar energy system design solar collector performances and other applications. In developing countries such as Nigeria, it has been very difficult measuring global solar radiation due to unavailability of equipment or non functioning of these equipments. Duration of sunshine has thus becomes immediate alternative for estimating global solar radiation in the country. Sunshine duration is one of the most widely measured and applied meteorological parameters in the determination of global solar radiation data. This is because it highly correlated with global solar radiation, air temperature, relative humidity and other climatic factors.

Sunshine duration is not only easy to use at networks of stations, it is relatively reliable. It enables spatial interpolation thus filling in gaps left by missing or unavailable data. One of the earliest correlations was proposed by Angstrom (1924) and relates global solar radiation to hours of bright sunshine. Several empirical models have since been developed to calculate global solar radiation using various parameters (Andretta *et al*., 1982; Nguyen and Pryor, 1997; Gautan and Kaushika, 2002; Udo, 2002; Almorox and Hontoria, 2004; Skeiker, 2006; Chiemeka, 2008; Safanri and Gasore, 2009; Huashana *et al*., 2010; Ali *et al*., 2010). The parameter used as input in the calculations include, sunshine duration, mean temperature, soil temperature, relative humidity, number of rainy days, altitude, latitude, total precipitable water, albedo, atmospheric pressure, cloudiness and evaporation. The most commonly used

*Corresponding author email: udosenakpan@yahoo.com

parameter for estimating global solar radiation is sunshine hours which can be easily and reliably measured, and data are widely available. In this work, we developed equations that correlate monthly average daily sunshine hours with certain meteorological parameters for Enugu in Eastern Nigeria. The applicability of the models is also examined.

MATERIALS AND METHODS

Methodology
The following meteorological data were obtained from the Nigerian meteorological Agency (NIMET) in Oshodi, Lagos. They include monthly average Sunshine Hours (S), Relative Humidity (RH), Maximum and Minimum Temperature (Tmax,Tmin), Rainfall (RF) data and Wind Speed (W). The data covered a period of eleven years (1997 to 2007). Enugu is located at a Latitude 6°40'55.3''N. Monthly averages (over the eleven year period) of the data are presented in table1.

Multiple linear regression equation for estimating S with four parameters is as follows
$$Y = a + bx_1 + cx_2 + dx_3 + ex_4$$
Where a …e, are the regression coefficients and x_i is the correlated parameter. The estimated values were compared to measured values in each regression equation through correlation coefficient R and standard error of estimate σ

CORRELATIONS
The Various meteorological parameters shown in Table1 are all related to sunshine hours in varying degrees. In order not to overlook any particular parameter or group of parameters multiple linear regression of four parameters (RH, T, RF, W) were employed to estimate the sunshine hours. Here S is the monthly average daily sunshine hour,

RH is the monthly average relative humidity in percentage, RF is the monthly average daily rainfall in meters, W is the monthly average daily wind speed in m/s.

The various linear regression analyses are as follows.

One variable correlation:
This correlation gives the highest value of R as 0.797 for T and lowest value of R as 0.048 for W.

$$S = 1.827 + 0.374T \quad (R = 0.797, \sigma = 0.72658) \qquad 1$$
$$S = 6.006 - 0.086W \quad (R = 0.048, \sigma = 1.2014) \qquad 2$$

Two variable correlation
The highest value of R is 0.837 for T and W and lowest value of R is 0.682 for RF and W.
$$S = 4.180 + 0.406T - 0.451W \quad (R = 0.837, \sigma = 0.69314) \quad 3$$
$$S = 9.049 - 7.109RF - 0.441W \quad (R = 0.729, \sigma = 0.86788) \qquad 4$$

Three variable correlation
The highest value of R is 0.847 for RF, RH and W and lowest value of R is 0.808 for RH, T and RF.

$$S = 15.384 + 6.790RF - 0.65W - 0.128RH$$
$$(R = 0.847, \sigma = 0.71504) \qquad 5$$
$$S = -3.304 + 0.037RH + 0.657T + 1.599RF$$
$$(R = 0.808, \sigma = 0.79222) \qquad 6$$

Four Variable Correlation
$$S = 10.279 + 5.519RF - 0.586W - 0.079RH + 0.217T$$
$$(R = 0.849, \sigma = 0.75881) \qquad 7$$

RESULTS AND DISCUSSION

Models 1, 3, 5, 7 have the highest value of correlation coefficient while models 2, 4, 6 have the lowest values of R. however, the applicability of the proposed correlations is tested by estimating the sunshine duration values for Enugu location used in the analysis. Estimated values of sunshine duration for Enugu along with the measured data are shown in table2. Inspection of the table shows that the models estimate sunshine hours fairly accurately.

The following observations can be made from a study of table 2 and table 3. Based on the RMSE, model 7 produces the best correlation while model 2 gives the worst with larger value of RMSE. For MBE, the result shows that model 1 and model 3 are the best while model 6 is the worst. With respect to MPE, model 5 offers the best correlation while model 2 gives the worst.

The MPE is an overall measure of the forecast bias computed from the actual difference between a series of forecasts and actual data points observed; each different being expressed as a percentage of each observed data point the summed and the average. The values of the

Table1. Sunshine hours and relevant meteorological data for Enugu.

Month	S (hrs)	RH%	$T_{max}{}^oC$	$T_{min}{}^oC$	T^oC	RF (mm)	W (m/s)
Jan.	6.13	37.00	33.94	21.10	12.84	8.00	6.13
Feb.	6.32	38.00	35.68	22.71	12.97	14.00	5.92
Mar.	5.58	48.55	35.01	24.18	10.83	56.00	6.57
Apr.	6.05	58.36	33.42	24.13	9.29	180.00	6.24
May	6.32	66.27	32.29	23.41	8.88	265.00	5.31
Jun.	5.03	68.36	30.81	22.87	7.94	284.00	5.27
Jul.	3.67	71.18	29.93	22.63	7.30	274.00	5.88
Aug.	3.64	72.00	29.48	22.45	7.03	211.00	5.36
Sep.	4.28	71.36	30.14	22.63	7.51	288.00	5.23
Oct.	5.54	63.64	31.18	22.36	8.82	222.00	4.54
Nov.	6.98	48.09	33.04	21.91	11.13	17.00	4.54
Dec.	6.98	37.55	33.91	19.77	14.14	2.00	5.51

Table 2. Derived empirical correlations describing relation between S and meteorological variables fro Enugu for the period (1997-2007).

Model No.	Regression Equation	Regression Coeff. (R)	MBE	RMSE	MPE
1	S = 1.827 + 0.374T	0.797	-0.0342	0.6487	1.2825
2	S = 6.006 - 0.086W	0.048	0.0017	1.0971	3.1758
3	S = 4.180 + 0.406T - 0.451W	0.837	0.0008	0.6001	2.120
4	S = 9.049 - 7.109RF - 0.441W	0.729	-0.0017	0.7530	2.1683
5	S = 15.387 + 6.790RF - 0.650W - 0.128RH	0.847	-0.1330	0.5840	1.0925
6	S = -3.304 + 0.037RH + 0.657T + 1.599RF	0.808	0.0058	0.6467	5.6583
7	S = 10.279 + 5.519RF - 0.586W – 0.079RH + 0.217T	0.849	0.0025	0.5796	1.9175

MBE represent systematic error or bias. A positive value of MBE shows an error estimate by the model. The MBE and MPE offer information regarding overestimation of the estimated data; low values of these mean errors are desirable. The RME provides information on the short term performance of the correlations by allowing term-by-term comparison of the deviation between the calculated and the measured values. The smaller the value, the better the model (Almorox *et al.*, 2008).

R^2 denotes the multiple coefficient of determination, which is a measure of how well the multiple regression equation fits the sample data. A perfect fit would result in $R^2 = 1$. A very good fit results in a value near 1 while a very poor fit results in a value of R^2 close to 0. The R^2 has serious flaws however; this is because, as more variables are included R^2 increases. This is not supposed to be so. Consequently, it is better to use the adjusted R^2 when comparing different multiple regression equations because it adjusts the R^2 value based on the number of

variables and the sample size (Triola, 1998). From model 7,

$$S = 10.279 + 5.519RF - 0.586W - 0.079RH + 0.217T$$

the value of $R^2 = 0.721$ indicates that 72.1% of the variation in sunshine hours is related to the effect of relative humidity, temperature, rainfall and wind speed. Hence the adjusted R^2 value is 0.562. This shows that 56.2% of the variation in sunshine hours is related to the effect of relative humidity, temperature, rainfall and wind speed.

Figure 1 shows plots of model 7 with the least value of RMSE together with the monthly average daily sunshine hours measured for eleven years. This gives almost exact fit to the sunshine hours data.

Based on model 7 the values of global solar radiation (H), were computed and presented in table 2.

Table 3. Values of the measured and the estimated sunshine hours for Enugu.

Month	S	Model 1	Model 2	Model 3	Model 4	Model 5	Model 6	Model 7
Jan.	6.13	6.23	5.48	6.44	6.29	6.67	6.51	6.59
Feb.	6.32	6.68	5.50	6.60	6.34	6.73	6.65	6.70
Mar.	5.58	5.88	5.44	5.42	5.75	5.23	5.70	5.25
Apr.	6.05	5.30	5.47	4.95	5.02	5.04	5.25	5.02
May	6.32	5.15	5.55	5.23	4.82	5.21	5.41	5.32
Jun.	5.03	4.80	5.55	4.87	4.17	5.10	4.90	5.06
Jul.	3.67	4.56	5.50	4.32	4.51	4.27	4.56	4.31
Aug.	3.64	4.46	5.55	4.46	5.19	4.08	4.32	4.24
Sep.	4.28	4.64	5.56	4.70	4.70	4.77	4.73	4.67
Oct.	5.54	5.13	5.62	5.58	5.47	5.76	5.20	5.73
Nov.	6.98	5.99	5.62	6.52	6.93	6.36	5.81	6.33
Dec.	6.81	7.12	5.53	7.27	6.60	6.97	7.38	7.16
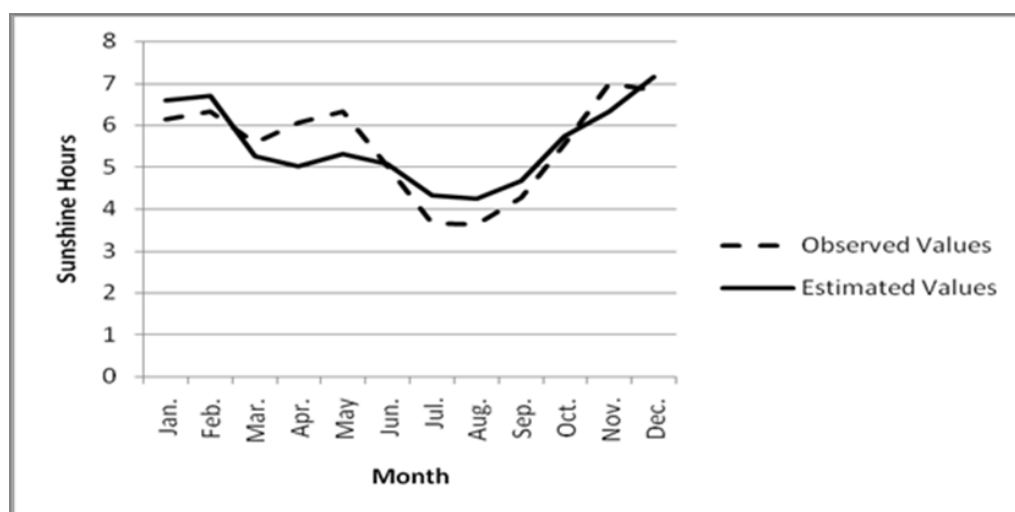
Fig. 1. Comparison of measured and estimated data of monthly average daily sunshine hours for Enugu.

Table 4. Values of Global solar radiation for Enugu.

Month	H (MJ/m^2)	Ho (MJ/m^2)	S (hrs)	So (hrs)	S/So	H/Ho
Jan.	16.64	33.91	6.59	11.66	0.57	0.49
Feb.	17.66	35.98	6.70	11.80	0.57	0.49
Mar.	16.01	37.90	5.25	11.96	0.44	0.42
Apr.	15.95	38.82	5.02	12.15	0.44	0.41
May	16.31	38.63	5.32	12.30	0.43	0.42
Jun.	15.73	38.29	5.06	12.38	0.41	0.41
Jul.	14.68	38.40	4.31	12.35	0.35	0.38
Aug.	14.62	38.82	4.24	12.21	0.35	0.38
Sep.	15.34	38.40	4.67	12.03	0.39	0.40
Oct.	16.20	36.71	5.73	11.85	0.48	0.44
Nov.	16.33	34.49	6.33	11.69	0.54	0.47
Dec.	17.11	33.33	7.16	11.62	0.62	0.51

Computation of Global solar radiation

The linear regression model used in computing Global solar radiation data is given after Angstrom (1924) and later modified by Prescott (1940);

$$H = H_o \{ a + b[S/S_o] \}$$

Where,

H is the monthly mean horizontal daily total terrestrial solar radiation.

H_o is the monthly mean horizontal daily total extraterrestrial solar radiation

$$H_o = 24/\pi * I_{sc} [1 + 0.033 Cos (360/365)*dn]*[(\omega Sin\Phi Sin\delta) + (Cos\Phi Cos\delta Sin\omega)]$$

I_{sc} = solar constant
δ = declination angle
Φ = latitude of the location of study
ω = sunset hour angle
and
$\omega = Cos^{-1}(-tan\delta tan\Phi)$
dn = mean day of month
S = the monthly mean of daily hours of sunshine
S_o = number of hours of insolation
$S_o = (2/15)\omega$

CONCLUSIONS

Multiple regressions analysis has been used in this study to develop several correlation models used to describe the dependence of sunshine hours on other meteorological data for Enugu. The result shows that the four variables correlation which is the model with the highest R gives the best result when considering the error term (RMSE). Hence the multiple regression equation that could be employed for the purpose estimating sunshine hours of locations that have the same climate and latitude as Enugu, Nigeria is correlation equation with the least value of RMSE, that is:

$$S = 10.279 + 5.519RF – 0.586W – 0.079RH + 0.217T$$

Based on table 4, the greatest amount of global solar radiation was received in February (17.66MJ/m^2) and the least amount of Global solar radiation was received in August (14.62MJ/m^2).

REFERENCES

Ali, MA., Maylaa MK. and Ali, JM. 2010. Estimation of solar radiation on horizontal surface using routine meteorological measurements for difference cities in Iraq. Asian Journal of Scientific Research. 3(4):240-248.

Almorox, J., Benito, M. and Hontoria, C. 2008. Estimation of global solar radiation in Venezuela. Comunicaciones Report. 33(4):280-283.

Almorox, J. and Hontoria, C. 2004. Global solar radiation estimation using sunshine duration in Spain. Energy conservation and management. 45(9-10):1529-1535.

Andretta, A., Bartoli, B., Coluzzi, B., Coumo, V., Francisca M. and Serio C. 1982. Global solar radiation estimation from relative sunshine hours in Italy. Journal of Applied Meteorology. 121:1377-1384.

Angstrom, AS. 1924. Solar and terrestrial radiation. Meteorological Society 50:121-126.

Chiemeka, IU. 2008. Estimation of solar radiation at Uturu, Nigeria. Intl. Journal of Physical Sciences. 3(5):126-130.

Gautan, NK. and Kaushika, ND. 2002. A model for the estimation of global solar radiation using Fuzzy random variables. Journal of Applied Meteorology. 41:1267-1276.

Huashan, L., Weibin, M., Yongwang, L. and Xianlong, W. 2010. Estimating daily global solar radiation by day of year in China. Applied Energy. 87:3011- 3017.

Nguyen, BT. and Pryor, TL. 1997. The Relationship between global solar radiation and sunshine duration in Vietnam. Renewable Energy. 1(11):47-60.

Skeiker, K. 2006. Correlation of global solar radiation with common geographical and meteorological parameters for Damascus Province, Syria. Energy Conversion and Management. 47:331-345.

Prescott, JA. 1940. Evaporation from water surface in relation to solar radiation. Trans. R. Soc. Sci. Austr. 64:114-118.

Safari, B. and Gasore, J. 2009. Estimation of global solar radiation in Rwanda using empirical models. Asian Journal of Scientific Research. 2(2):68-75.

Triola, MF. 1998. Elementary Statistics; Adison Wesley Longman Inc, USA.

Udo, SO. 2002. Contribution to the relationship between solar radiation and sunshine duration in the tropics. A case study of experimental data at Ilorin, Nigeria. Turkish Journal of Physics. 26:229-236.

Canadian Journal of
pure&applied
sciences

MAGNITO-EXCITON IN NARROW-GAP *InSb* CYLINDRICAL LAYER QUANTUM DOT

Marwan Zuhair
Department of physics, College of Sciences, Mosul University, Iraq

ABSTRACT

In frameworks of Kane model we explored the effects of Coulomb electron-hole correlations and magnetic confinement for several cylindrical size combinations in a narrow-gap *InSb* cylindrical layer quantum dot for the heavy hole-electron and light hole-electron. The influence of excitonic effects on the behavior of the energetic spectrum of said system was discussed using a perturbation theory framework. Dependences of the electron-hole energetic spectrum versus the internal radius, external radius, and magnetic field are presented. It was shown that the exciton energy for both type of electrons strongly influenced by changing the geometrical parameters and the value of applied magnetic field. In addition to that it was found that the heavy hole-electron is less sensitive to those parameters comparing with the light hole-electron.

Keywords: Quantum layer, magneto-excitons, narrow-gap, III-V semiconductors.

INTRODUCTION

The Coulomb interaction near the absorption edge leads to considerable changes in the optical properties of matter. The Coulomb interaction leads to the formation of electron-hole pairs which are called excitons. The excitons are to some extent similar to positronium atom in which an electron is bound to a positron through the Coulomb attraction. The electron in an exciton is bound to the hole and the resulted quasi-particle is electrically neutral. An exciton can move like a free atom through the crystal. The existence of excitons yields in intense absorption lines below the energy gap region. As a result of the Coulomb attraction, the photo, due to the exciton transition, has less energy in comparison with the energy gap. Therefore, the phenomenon of photon absorption in a crystal corresponds to direct formation of excitons in the media. The photoluminescence method is one of the interesting methods in studying optical properties of semiconductors. Also, one can use the magneto luminescence to study the optical phenomena in the presence of strong magnetic fields (Knox, 1963; Shields *et al*., 2001). In addition, Wójs and Quinn (2007) and Wójs *et al*. (2000) have studied the spectrum of excitons formed in quantum wells in both singlet and triplet states through considering the Coulomb interaction among the electrons and the holes for Al_xGa_{1-x} $As/GaAs$ samples. Riva *et al*. (2000) have studied the binding energy of trion by considering it as a function of the applied magnetic field. Senger and Bajaj (2003) determined the binding energy of excitons as a function of quantum well width by introducing a function including three variational parameters. The so-called stochastic variational method developed by Shi and Gan (2003) and Wan *et al*. (2001)

was used to study the properties of excitons and determine their correlation energy as a function of the quantum well width. Excitons in a quantum wire have also been studied at the absence of magnetic fields (Slachmuylders *et al*., 2007; Sidor *et al*., 2005; Sidor *et al*., 2007). In addition, Charge confinement in InAs/InP self-assembled quantum wires have been investigated theoretically using the adiabatic approach within the effective-mass approximation (Maes *et al*., 2004). On the other hand, concerning the use of the zero-dimensional structures (the quantum dots (QDs)) as an element base for the lasers in the infrared regions of spectrum the necessity of the realization of the narrowband zero-dimensional semiconductor structures arises (Asryan and Suris, 2003, 1996). Recently, Moiseev *et al*. (2007) reported the first results on the growth of *InSb* QDs by liquid-phase epitaxy on *InAs* substrates. They obtained QD arrays with an average height of L = $(3.471)10^{-7}$cm and an average radius of R = $(27.277.5)10^{-7}$ cm.

As is well known, *InSb* is a narrow-gap semiconductor that offers a promising basis for the creation of QD lasers operating in the IR spectral range. In the frames of Kane's model Kazaryan *et al*. (2007) have calculated the interband absorption coefficient in a system of cylindrical QD *InSb* and showed that the absorption threshold is indeed in the infrared region. Note, that geometrical form of the QD defines the symmetry of the one-particle Hamiltonian, which describes the particle behavior in the system under discussion. In terms of simplicity of description for one-particle states in QD's, the most suitable of objects are QD's with a spherical shape (Leonard, 1993; Ferreyra and Proetto, 1999; Phillips *et al*., 1998; Sigrist *et al*., 2004; Vartanian *et al*., 2008). However, such systems have only one geometrical

Corresponding author email: marwanzt@yahoo.com

parameter – the radius of the QD – which can be used to adjust its energetic spectrum. In this consideration, systems with Cylindrical symmetry is preferred, since for these elements one may manipulate two parameters: the height of the cylinder, and its radius.

One of the first articles, where one and many-electron states in a quantum ring QR were studied, is the work of Chakraborty's and Pietilainen's (Chakraborty and Pietiläinen, 1994). Here, the authors studied the effect of electron-electron interaction on the magnetic moment of electrons in a QR. They have introduced a model, where the electron makes a circular motion in a parabolic confinement simulating a quantum ring, which is subjected to a perpendicular magnetic field (Chakraborty's - Pietilainen's model). Here the electron states in such a ring with and without the Coulomb interaction have been investigated. In addition Barticevic *et al.* (2000) studied the effects of an external electric field on the excitonic and optical spectra of a semiconductor quantum ring threaded by a magnetic flux, a detailed analysis of the ground-state properties of radially polarized excitons and its dependence with magnetic fields applied perpendicular to the ring plane and electric fields parallel to the ring plane were made. The authors found that the electric field breaks the azimuthal symmetry and mixes the eigenfunctions with different angular momentum. Also they found that the low-lying energy levels are almost independent of the magnetic field up to a region in energy where periodic Aharonov-Bohm-type oscillations appear. The effect of magnetic field and geometric confinement on excitons confined to a quantum ring was also studied in Song and Ulloa (2001) they use analytical matrix elements of the Coulomb interaction and diagonalize numerically the effective-mass Hamiltonian of the problem. Also they explored the Coulomb electron-hole correlation and magnetic confinement for several ring width and size combinations.

The Aharanov-Bohm oscillations of exciton Characteristics predicted for one-dimensional rings are found to not be present in these finite-width systems. Subsequently, the properties of excitons in a quantum ring with parabolic confinement in magnetic fields were discussed in Song and Ulloa (1996). The binding energy and electron-hole separation of the exciton are calculated versus the strength of external magnetic fields. They also explored the effects of Coulomb electron-hole correlations and magnetic confinement for several ring width and size combinations in the quantum ring. The linear optical susceptibilities as a function of magnetic fields are also discussed.

It is important to mention, that the realization of layered and ring shape nanostructures, in which radial motion of charge carriers is limited both on inner and on outer borders, has brought a new class of theoretical problems about the physical processes in such systems (Andreev and O'Reilly, 2000).The important feature of theoretical description of layered and ring shape structures is the opportunity of realization of limiting transitions to quantum wells, wires and also to QDs of various geometry. Really, if we fix the thickness of cylindrical nano-layer and increase internal and external radii the system becomes similar to quantum well. On the other hand, if we set the height of cylindrical quantum layer to infinity, and vanishes the internal radius we will get a quantum wire with circular cross section. If we fix the height and vanishes only internal radius we will get a cylindrical QD. Thus, the results received for layered and ring shape systems have general character and for this reason cause essential interest .The authors of Marwan *et al.* (2009), Zoheir *et al.* (2008), Marwan (2010) and Marwan *et al.* (2008) performed a theoretical investigation of electronic states and interband transition in a narrow-gap *InSb* spherical and cylindrical layer quantum dot under the influence of both magnetic and electric field. The authors discussed the transition from the light hole and heavy hole states to the electron state of conduction band in addition to that the interband absorption coefficient, threshold frequencies and the selection rules for different electric field orientation in the presence and absence of magnetic field were calculated.

In the present work, and within the frames of the two-bands of Kane model and parabolic dispersion law, it is interesting to investigate the specifications of the exciton energy spectrum of the heavy hole- electron and light hole-electron pairs in the cylindrical layer quantum dots from *InSb* in the presence of a magnetic field. By writing the Hamiltonian of the exciton in cylindrical coordinates and using an approximate analytical method we obtained the exciton wave function and the corresponding energy as functions of radii and applied magnetic field.

MATERIALS AND METHODS

Electronic states in magnetic field
Consider one-particle states in a cylindrical layer QD with the inner radius R_1, outer radius R_2 and with height L (Fig. 1). Let us determine the energy spectrum and the wave function assuming the existence of the homogeneous magnetic field, directed along OZ-axis, taking into account that the radial motion of an electron is bounded by both the outer and inner radii. The confining potential of the layer is approximated with the infinitely high rectangular walls

$$V_{con}(\rho,z) = \begin{cases} 0, R_1 \le \rho \le R_2, +\dfrac{L}{2} \le Z \le \dfrac{L}{2} \\ \infty, \rho < R_1, \rho > R_2, |Z| > \dfrac{L}{2} \end{cases} \qquad (1)$$
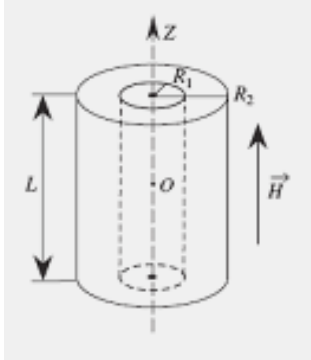
Fig.1. Cylindrical layer quantum dot.

The corresponding Schrödinger equation according to the parabolic dispersion law can be presented in the following form:

$$\frac{1}{2\mu_{lh,hh}}(\vec{p} - \frac{e^{lh,hh}}{c}\vec{A})^2 \psi(\rho,\varphi,z) = E_{lh,hh}\psi(\rho,\varphi,z) \quad (2)$$

where $\mu_{lh,hh}$ are the effective mass of both the *lh* and *hh* respectively. The wave function must obey the following boundary condition $\psi(\pm L/2) = \psi(R_1) = \psi(R_2) = 0$. We will search the solution of Eq. (2) in the form.

$$\psi(\rho,\varphi,z) = \frac{1}{\sqrt{2\pi}}e^{im\varphi}\sqrt{\frac{2}{L}}\begin{Bmatrix}\sin\dfrac{\pi n}{L}Z\\\cos\dfrac{\pi n}{L}Z\end{Bmatrix}f(\rho) \quad (3)$$

Substituting Eq. (3) in Eq. (2) we get a new equation for function $f(\rho)$.

$$\frac{\eta^2}{2\mu}(f'' + \frac{1}{\rho}f' - \frac{m^2}{\rho^2}f) + [E_{lh,hh} - E_{n_{lh,hh}} - \frac{\mu\omega_H^2\rho^2}{8} - \frac{\eta\omega_{H_{lh,hh}}m}{2}]f = 0 \quad (4)$$

Where $\omega_{H_{lh,hh}} = eH/\mu_{lh,hh}c$ is the cyclotron frequency and $E_{n_{lh,hh}} = n^2\pi^2\eta^2/2\mu_{lh,hh}L^2$. The solution of Eq. (4) can be expressed in terms of confluent hypergeometric functions

$$f_{lh,hh}(\rho) = \left\{c_1F\left(-\left(\beta_{lh,hh} - \frac{|m|+1}{2}\right),|m|+1,\frac{\rho^2}{2a_{H_{lh,hh}}^2}\right) + c_2U\left(-\left(\beta_{lh,hh} - \frac{|m|+1}{2}\right),|m|+1,\frac{\rho^2}{2a_{H_{lh,hh}}^2}\right)\right\}e^{\frac{\rho^2}{4a_{H_{lh,hh}}^2}}\rho^{|m|} \quad (5)$$

Here. $\beta_{lh,hh} = 1/\eta\omega_{H_{lh,hh}}(E_{lh,hh} - E_{n_{lh,hh}}) - m/2$ and $a_{H_{lh,hh}} = \sqrt{\eta/\omega_{H_{lh,hh}}}$ is the magnetic length taking into account that the wave function (5) should vanish at the boundaries (f(R$_1$) = f(R$_2$) = 0). For the determination of the energy spectrum of the system we must have the zero determinant condition

$$\begin{vmatrix}F\left(-\left(\beta_{lh,hh} - \frac{|m|+1}{2}\right),|m|+1,\frac{R_1^2}{2a_{H_{lh,hh}}^2}\right) & U\left(-\left(\beta_{lh,hh} - \frac{|m|+1}{2}\right),|m|+1,\frac{R_1^2}{2a_{H_{lh,hh}}^2}\right)\\ F\left(-\left(\beta_{lh,hh} - \frac{|m|+1}{2}\right),|m|+1,\frac{R_2^2}{2a_{H_{lh,hh}}^2}\right) & U\left(-\left(\beta_{lh,hh} - \frac{|m|+1}{2}\right),|m|+1,\frac{R_2^2}{2a_{H_{lh,hh}}^2}\right)\end{vmatrix} = 0 \quad (6)$$

Solving transcendent Eq. (6) numerically we can find our energy spectrum $E_{lh,hh}$.

Excitonic effects

Let us consider the contribution of hole-electron interactions (excitonic effects)on the electronic states using perturbation theory. The authors of (Wang *et al.*, 1996) conducted a theoretical examination of the influence of an external magnetic field on the properties of excitons in a potential of finite height. Their theoretical results for the diamagnetic shift are in very good agreement with experimental results. Halonen *et al.* (1992) presented a theoretical investigation of the quantum disk, taking into account the Coulomb interaction between the electron and the hole. They calculated the ground-state energy (as well as the energy of the excited states), the binding energy, and the diamagnetic shift of an exciton in a quantum disk for a hard wall confinement properties of a two-dimensional exciton in a parabolic QD in a magnetic field. Liu *et al.* (2003) studied the optical spectra and exciton states in vertically stacked, self-assembled quantum disks in a vertically applied electric field.

Furthermore, in this work, we assume that the quantization in the direction of the disk axis (OZ) is very strong. Therefore, in this case we will consider motion in OZ direction using the framework of the single-particle model. In other words, we will consider a two-dimensional exciton. In the limit of infinitely high walls, the Hamiltonian of a magneto-exciton takes the following form

$$\hat{H}_{ex} = \hat{H}_e + \hat{H}_h - \frac{e^2}{\varepsilon|\vec{\rho}_e - \vec{\rho}_h|}, \quad (7)$$

where

$$\hat{H}_i = \frac{1}{2\mu^i}(\hat{p}_i - \frac{e^i}{c}A_i) + V(r_i)$$

and

$$\hat{H}_i\psi_i = E_i\psi_i, i = e,h$$

We consider the third term of equation (7) as a small perturbation for the Hamiltonian $\hat{H}_e + \hat{H}_h$. Therefore, the wave function of the magneto-exciton, in a first order approximation, may be presented in the following form

$$\psi_{ex}^0(r_e,r_h) = \psi_e(\rho_e,\varphi_e,z_e)\psi_h(\rho_h,\varphi_h,z_h), \quad (8)$$

The correction for the energy is given by the following expression

$$\Delta E_0 = \int \psi_{ex}^{0*}(r_e,r_h)(-\frac{e^2}{\varepsilon\sqrt{\rho_e^2 - \rho_h^2 - 2\rho_e\rho_h\cos(\varphi_e - \varphi_h)}})\psi_{ex}^0 dV_e dV_h,$$
(9)

which can be reduced according to Janssens (2001) to the following form

$$\Delta E_0 = -\frac{8\pi e^2}{\varepsilon}\int_{R_1}^{R_2}\rho_2 d\rho_2\int_{R_1}^{R_2}\frac{g(\rho_1,\rho_2)}{\rho_1 + \rho_2}\times K\left(\frac{4\rho_1\rho_2}{(\rho_1 + \rho_2)^2}\right)\rho_1 d\rho_2,$$
(10)

Here

$$g(\rho_1,\rho_2) = \psi_{ex}^{0*}(r_e,r_h)\psi_{ex}^0(r_e,r_h),\text{ and}$$

$$K(m) = \int_0^{\pi/2}\frac{d\varphi}{\sqrt{1 - m\sin^2\varphi}}\text{ is a complete elliptic}$$

integral of the first kind. Thus, for the energy we have:

$$E = E_e + E_h + \Delta E_0,$$
(11)

DISCUSSION

For the qualitative analysis of the obtained result let us consider *InSb* cylindrical layer for which $E_{g=}0.18$ eV, $\mu_e= 0.015m_e$, $\mu_{lh}= 0.015m_e$ and $\mu_{hh}= 0.51m_e$ (m_e is the mass of free electron). In (Fig. 2A) the dependence of the energy spectrum of the lh-electron transition (solid curve) on the inner radius R1 for fixed value of outer radius

$R_2 = 300*10^{-8}/a_{B_{lh}}$ and different values of magnetic field (B, 1, 5, 10 T) are presented. As it follows from the figure, the energy levels increase monotonically with increasing R_1. This is connected to the increase of the role of size quantization (layer thicknesses L =R_2-R_1 decrease). This can be explained by the fact that in the parabolic dispersion, the energy depends on the momentum square, as well as on the inverse square of the thickness. In addition, we note that the energy levels depend on the value of the applied magnetic field which can be explained as a result of the dispersion laws.

Also as can be seen in (Fig. 2A) (the dot curve), due to the increase in the energy with increasing R_1 at fixed value of R_2 different behavior takes place for the exciton energy which increase with increasing R_1.This last fact is explained by the more considerable decrease of the absolute value of the Coulomb integral compared with the increase in the energy of the single-particle state (Tadic and Peeters, 2004). In addition, we note that with increasing the magnitude of the magnetic field strength, the energy increase which can be attributed to the well-known fact that the interaction energy for a Coulombic system increases with magnetic field strength (Landau and Lifshitz, 1989).

An opposite picture appears in (Fig. 2B) when we fix the inner radius R_1 ($R_1 = 100*10^{-8}/a_{B_{lh}}$) and increase R_2. In this case the layer thickness increases and, correspondingly, the size quantization weakens. This explains the lowering of the energy levels with the increase of R_2. Also we note that the exciton energy
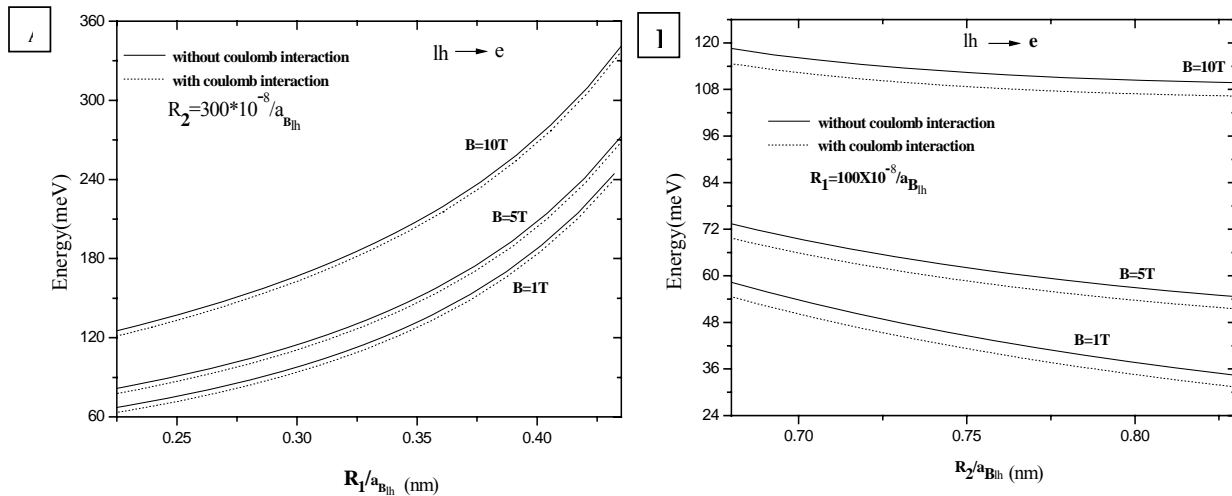

Fig. 2. Dependencies of the energy spectrum for *lh- e* on (A) inner radius R_1 for a fixed value of the outer radius R_2 (B) Outer radius R_2 for a fixed value of R_1 without considering the coulomb interaction (solid curve) and with considering the coulomb interaction (dot curve) for $m = 0$, $n = 1$, and different value of magnetic field B.

decrease with increasing R_2 which can be explained as a result of the increase in the absolute value of the Coulomb interaction.

In figure 3 A and B, the dependencies of the energy spectrum for the *hh*-electron on the inner R_1 (fixed R_2) and outer R_2 (fixed R_1) radii and different values of magnetic field (B, 1, 5, 10 T) with coulomb interaction (solid curve) and without coulomb interaction (dot curve) are presented. We see the same behavior as that appears in figure 1(A and B) the only difference is that the coulomb interaction for the *hh*- electron appears to be less

sensitive to the change of the geometrical parameters than that in the case of *lh*- electron which can be explained as a result of the difference in masses between the light and heavy holes. Hence, upon the change of layer parameters, the energy level of the heavy hole has less energy shift than once of the light hole. But the electron levels possess the same energy shift, as the light hole.

As can be seen in figure 4 the dependencies of the energy for (A) *lh*- electron (B) *hh*- electron pairs on the value of the applied magnetic field at fixed value of both the inner and outer radii (R_1 and R_2) without considering the
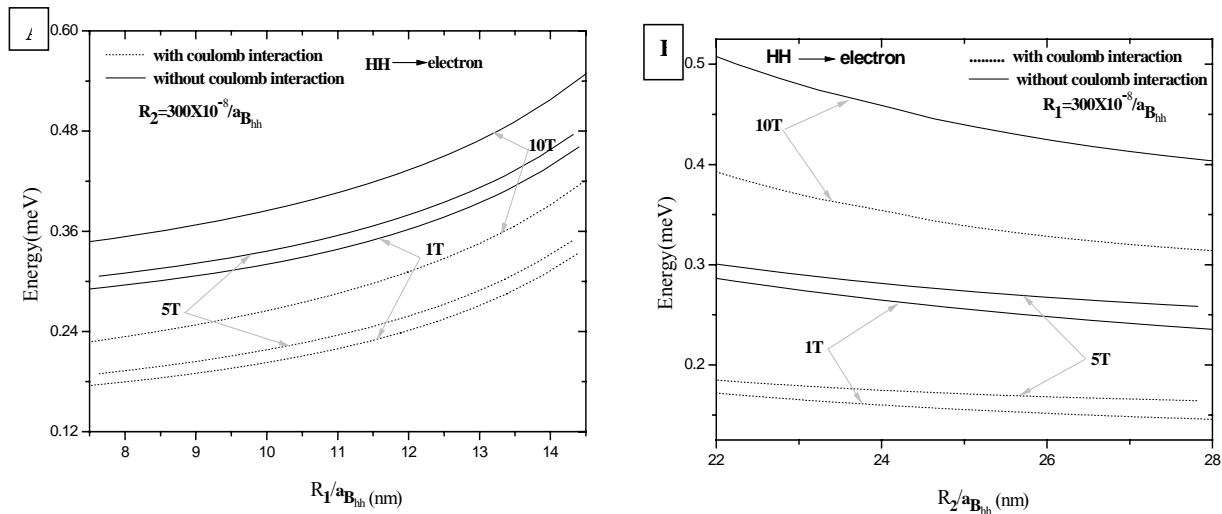
Fig. 3. Dependencies of the energy spectrum for *hh*- *e* on (A) inner radius R_1 for a fixed value of the outer radius R_2 (B) Outer radius R_2 for a fixed value of R_1 without considering the coulomb interaction (solid curve) and with considering the coulomb interaction (dot curve) for $m = 0$, $n = 1$, and different value of magnetic field B.
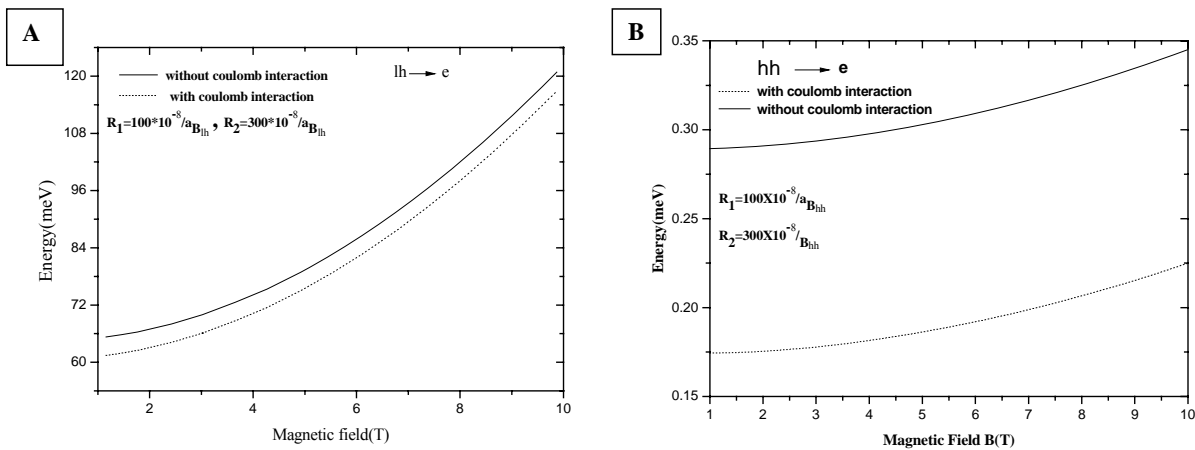
Fig. 4. Dependencies of the energy for (A) *lh*- *e* (B) *hh*-*e* pairs on the value of the applied magnetic field at fixed value of both the inner and outer radii (R_1 and R_2) without considering the coulomb interaction (Solid curve) and with considering the coulomb interaction (dot curve) for $m = 0$, $n = 1$

coulomb interaction (solid curve) and with considering the coulomb interaction (dot curve) .The energy level increase with increasing the applied magnetic field for both cases which attributes to the dispersion law. In addition to that we note that the *hh*- electron is less sensitive to the change of the applied magnetic field than that of the *lh*- electron which can be explained by the fact that the expression for the potential energies in two cases is the same in Hamiltonian, meanwhile the changes in the region of localization of the electron in the case of *hh*- electron are strong and it is clear that with the increase of the magnetic field the region of localization will decrease considering the expression for the energies of the electron in the presence of the magnetic field (Marwan *et al.*, 2009).

$$E_{lh,hh}(H) = \frac{1}{2\mu_{lh,hh}}(\vec{p} - \frac{e^{lh,hh}}{c}\vec{A})^2$$

Due to the electron-hole interaction, the total energy increases with increasing the magnetic field (Atayan *et al.*, 2008). This can be attributed to the well-known fact that the interaction energy for a Coulombic system increases with magnetic field strength. With an increase in the magnitude of the magnetic field, the system tends to become a one-dimensional one. Therefore, the Coulomb energy increases (Landau and Lifshitz, 1989).

CONCLUSION

In the present work we investigated the effect of changing the geometrical parameters and the magnetic field strength on the exciton energy of the narrow band *InSb* cylindrical quantum layer for the *lh*- electron and *hh*- electron. It is shown that the exciton energy for both type of electron strongly influenced by change those parameters. It should be underlined that the *hh*-electron is less sensitive to the change of geometrical parameters and the magnetic field than those of the *lh*-electron.

ACKNOWLEDGEMENTS

REFERENCES

Asryan, LV. and Suris, RA.1996.Inhomogeneous line broadening and the threshold current density of a semiconductor quantum dot laser. Semicond. Sci. Techno. 11:554-567.

Asryan, LV. and Suris, RA. 2003. Two lasing thresholds in semiconductor lasers with a quantum-confined active region. Appl. Phys. Lett. 83(26): 5368-5370. id. 073107.

Atayan, AK., Kazaryan, EM., Meliksetyan. AV. and Sarkisyan, HA. 2008. Magneto-absorption in cylindrical quantum dots. Eur. Phys. J. B. 63:485-492.

Andreev, AD. and O'Reilly, EP. 2000. Theoretical study of the electronic structure of self-organized GaN/AlN QD's". Nanotechnology. 11:256-262.

Barticevic, Z., Pacheco, M. and Latge, A. 2000. Quantum rings under magnetic fields: electronic and optical properties. Phys. Rev. B 62:6963-6966.

Chakraborty, T. and Pietiläinen, P. 1994. Electron-electron interaction and the persistent current in a quantum ring. Phys. Rev. B 50:8460-8465.

Ferreyra, JM. and Proetto, CR. 1999. Quantum size effects on excitonic Coulomb and exchange energies in finite-barrier semiconductor quantum dots. Phys. Rev. B 60(15):10672-10675.

Garcia, JM. and Moshchalkov, VV. 2004. Electron wave-function spillover in self-assembled InAs/InP quantum wires. Phys. Rev. B 70 .155311:7338-7344.

Halonen, V., Chakraborty, T. and Pietilainen, P. 1992.Excitons in a Parabolic Dot in Magnetic Fields. Phys. Rev. B 45. 5980(11):5980-5985.

Janssens, KL, Partoens, B. and Peeters, FM. 2001. Magneto-exciton in single and coupled type II quantum dots. Phys. Rev. B64:15324-153231.

Knox, RS. 1963. Theory of Excitons. Academic Press, New York, USA.

Kazaryan, EM, Meliksetyan, AV. and Sarkisyan, HA. 2007. The interband transitions in cylindrical InSb quantum dots .Tech. Phys. Lett. 33(22):48-55.

Landau, LD. And Lifshitz, EM. 1989. Quantum mechanics, Nauka, Moscow.

Leonard, D. 1993. Direct formation of quantum sized dots from uniform coherent island of *InGaAs* on *GaAs* surfaces. Appl. Phys. lett. 63:3202-3209.

Liu, Jin-Long., Li, Shu-Shen., Niu, Zhi-Chuan., Yang, Fu-Hua. and Feng, Song-Lin. 2003. Optical Spectra and Exciton State in Vertically Stacked Self-Assembled Quantum Discs. Chinese Physics Letters. 20:1120-1127.

Maes, J., Hayne, M., Sidor, Y., Partoens, B., Peeters, FM., Gonzalez, Y., Gonzalez, L. and Fuster. 2004. Confinement in self-assembled *InAs/InP* quantum wires studied by magneto-photoluminescence. Physica E. 21(2-4):261-264.

Marwan, Z., Manaselyan, AKH. and Sarkisyan, HA. 2009. Magneto- and electroabsorption in narrow-gap *InSb* cylindrical layer quantum dot. Physica. E. 41:1583-1590.

Marwan, Z. 2010. The electroabsorption in narrow gap *InSb* quantum ring –rotator model. Armenian Journal of Physics. 3(1):61-68.

Marwan, Z., Aram, M. and Hayk, S. 2009. Magnito and electroabsorption in narrow –gap InSb cylindrical layer quantum dot. Physica. E. 41:1583-1590.

Marwan, Z., Aram, M. and Hayk, S. 2008. Interband transition in narrow gap InSb spherical layer quantum dot in the presence of electric field. Journal of Physics: Conference Series 129. doi. 10.1088/1742-6596/129/1/012017.

Moiseev, KD., Parkhomenko, Ya.A., Ankudinov, AV. and Mikhailova, MP.2007. The growth of InSb quantum dots by liquid phase epitaxy on InAs substrates Tech. Phys. Lett. 33(4):295-298.

Phillips, J., Kamath, K. and Bhattachary, P.1998. Far-infrared photoconductivity in self-organized *InAs* quantum dots, Appl. Phys. lett. 72:2020-2027.

Riva, C., Peeters, FM. and Verga, K. 2000. Theory of trions in quantum wells. Physica E 12:543-545.

Senger, RT. and Bajaj, KK. 2003. Polaronic exciton in a parabolic quantum dot. Phys. Stat. Sol. B:82-89.

Shields, PA., Nicholas, RJ., Grandjean, N. and Massies, J. 2001. Magneto photoluminescence of GaN/AlxGa1-xN quantum wells: valence band reordering and excitonic binding energies. Phys. Rev. B 63:1930-1922.

Shi, JJ. and Gan, ZZ. 2003. Effects of piezoelectricity and spontaneous polarization on localized excitons in self-formed *InGaN* quantum dots. J. Appl. Phys. 94:407-412.

Sidor, Y., Partoens, B. and Peeters, FM. 2005. Exciton in a quantum wire in the presence of parallel and perpendicular magnetic fields. Phys. Rev. B 71(7):812-820. id. 075405.

Sidor, Y., Partoens, B., Peeters, FM., Ben, T., Ponce, A., Sales, DL., Molina, SI., Fuster, D., Gonzalez, L. and Gonzalez, Y. 2007. Excitons in coupled *InAs/InP* self-assembled quantum wires. Phys. Rev. B. 75(12). 125120:2444-2450.

Sigrist, M., Fuhrer, A. Ihn, Ensslin, T. and Ulloa, SE. 2004. Magnetic-field-dependent transmission phase of a double-dot system in a quantum ring. Physical Review Letters. 93(6):1579-1585. Id. 066802.

Slachmuylders, AF., Partons, B. and Peeters, FM. 2007. Trions in cylindrical nano wires with a dielectric mismatch. Phys. Rev. B.76:2416-2419.

Song, J. and Ulloa, SE. 2001. Magnetic field effects on quantum ring excitons. Physical Review. B. 63(12):3054-3057. id. 125302.

Song, J. and Ulloa, SE. 1996. Geometrical-confinement effects on excitons in quantum disks. American Physical Society, Ohio Section Spring Meeting.

Tadic, M. and Peeters, FM. 2004. Binding of electrons, holes, and excitons in symmetric strained InP/In0.49Ga0.51P double quantum-dot molecules, J. Phys. Condens. Matter. 16:8633-8652.

Vartanian, AL., Vardanyan, LA., Kazaryan. and Eduard, M. 2008. Effect of electric and magnetic fields on the binding energy of the coulomb impurity bound polaron in a quantum dot. Physica. E. 40(5):1513-1516.

Wan, SP., Xia, JB. and Chang, K. 2001. Effects of piezoelectricity and spontaneous polarization on electronic and optical properties of wurtzite III–V nitride quantum wells. J. Appl. Phys. 90:621-628.

Wójs, A. and Quinn, JJ. 2007. Exact-diagonalization studies of trion energy spectra in high magnetic fields. Phys. Rev. B. 75. 085318:636-649.

Wójs, A., Quinn, JJ. and Hawrylak, P. 2000.Charged excitons in a dilute two-dimensional electron gas in a high magnetic field. Phys. Rev. B. 62:4630-4637.

Wang, PD., Merz, JL., Fafard, S., Leon, R., Leonard, D., Medeiros-Ribeiro, G., Oestreich, M., Petroff, PM., Uchida, K., Miura, N., Akiyama, H. and Sakaki, H. 1996. State filling and time-resolved photoluminescence of excited states in *InₓGa₁₋ₓAs/GaAs* self-assembled quantum dots Phys. Rev. B. 54 (16):11548-11554.

Zoheir, M., Manaselyan, AKH. and Sarkisyan, HA. 2008. Electronic states and the stark shift in narrow band InSb quantum spherical layer. Physica. E. 40:2945-2949.

THE SOLUTION OF MATHEMATICAL MODEL FOR TRANSPORT OF OXYGEN IN PERIPHERAL NERVE WITH THE FIRST-ORDER CHEMICAL KINETICS USING FINITE-DIFFERENCE TECHNIQUE DURING PRANAYAMA

*Sarita Singh[1], V K Katiyar[2] and P Pradhan[1]
[1]Gurukul Kangri Univerisity, Haridwar, Uttrakhand
[2]Department of Mathematics, Indian Institute of Technology Roorkee, India

ABSTRACT

We modeled time dependent transport of oxygen in peripheral nerve by the simulation of steady-state oxygen tension, diffusion, chemical reactions and consumption of oxygen in capillaries using Krogh cylinder symmetry. These parameters were assumed to change rapidly to new. To characterize the approach of the oxygen tension to a new value, a monoexponential function is defined. Diffusion of oxygen is radial from capillary to a surrounding cylinder tissue and from arterial distance to veins, diffusion is axial. The time-dependent transport of oxygen is peripheral nerve with forward and backward reactions including first-order chemical kinetics has been considered, which makes this model different from the earlier studied models. We used Finite difference technique for the solution of this model.

Keywords: Nerve oxygen consumption, peripheral nerve, oxygen transport, tissue, forward and backward reaction, first order chemical kinetics.

INTRODUCTION

Through a physical solution in water oxygen is transported by the blood partly with hemoglobin. This transport is affected by forward and backward reactions. Kreutzer (1982) shows a comparison of oxygen consumption following zero-order, first -order or Michaclies-Menten kinetics in a plot of the peripheral tissue oxygen pressure against capillary length shows that kinetics of zero-order provides the lowest values but Michaclies-Menten and first-order kinetics having higher value of oxygen pressure both in capillary as well as in tissue. Krogh (1919) and Reneau *et al*. (1967) formulated mathematical models of the release of oxygen from hemoglobin and diffusion from capillaries into surrounding tissue in various cases. After this Reneau *et al*. (1969) considered time-dependent aspects of transport of oxygen.

Low *et al*. (1986) established that peripheral nerve tissue could resist moderate degrees of ischemia or hypoxemia and continue to conduct impulses for minutes to hours. This is not true for brain nerve. The mechanisms of the relative resistance of a peripheral nerve to ischemia are not completely known. The role of hemoglobin and myoglobin is facilitating oxygen transport to tissue. A totally different approach to the mathematical study of oxygen transport to tissue intended to describe on large scale, convection and diffusion of oxygen occurs over a very large distance within the tissue. Diffusion is the process whereby particles of liquids, gases, and solids blend together as the result of their spontaneous movement caused by thermal campaigning and dissolved substance moves from higher to lower concentration. Similarly, in the human body, transport of oxygen occurs. Lagerlund and Low (1993) studied transport of oxygen and diffusion process in peripheral nerve is steady-state. A non steady state condition which effects a sudden change in arterial oxygen tension blood flow velocity or nerve oxygen consumption rate on the distribution of oxygen tension in endoneurial tissue around a capillary. Sharan *et al*. (1997) examined the transport of oxygen in the blood flowing through the systemic capillaries, the blood has been considered as a homogenous model for transport of oxygen in the capillary and surrounding tissue.

Sharma *et al*. (2004) investigated endoneurial oxygen transport in capillary and a surrounding Krogh cylinder of tissue with forward and reverse chemical reaction. A sudden change in arterial oxygen tension affects blood flow velocity and nerve oxygen consumption rate with forward and backward reactions.

The objective of the present study was to investigate endoneurial transport of oxygen in capillary and a surrounding cylinder of tissue with generation or degeneration in oxygen due to forward and backward chemical reaction in capillary, but a first-order chemical kinetics for tissue.

MATHEMATICAL MODEL

We used a modified version of the mathematical model of Reneau *et al*. (1969) for the calculation of endoneurial

*Corresponding author email: saritamath@gmail.com

oxygen profiles as a function of time by numerical solution of differential equations which describe the oxygen transport in a capillary and a surrounding cylinder of tissue(the Krogh cylinder). In the capillary region, transport of oxygen takes place both by convection and by diffusion, and oxygen is generated due to its dissociation in the hemoglobin inside the red blood cell and its transport to the blood plasma across the cell membrane, there is only diffusion of oxygen in tissue region by the tissue cells. We assume that P(r, x, t) be the partial pressure of oxygen. r is the radius of capillary v(r, t) the velocity of blood in the fully developed flow in the capillary. To calculate the partial pressure P in the capillary the differential equation is:

$$\frac{\partial P}{\partial t} = D_b\left(\frac{\partial^2 P}{\partial r^2} + \frac{1}{r}\frac{\partial P}{\partial r} + \frac{\partial^2 P}{\partial x^2}\right) - vE\left(\frac{\partial P}{\partial x}\right) - k_f P + k_r P \tag{1}$$

Where $\quad E = 1 + \left(\frac{C_b \eta}{S_b P_{50}}\right)\frac{(P/P_{50})^{\eta-1}}{\left[1+(P/P_{50})^\eta\right]^2} \tag{2}$

Where k_f and k_r are the rate of forward and backward reaction due to erythrocyte boundaries. x is the distance along the capillary from the arterial end i.e. axial coordinate, r is the distance from the capillary centre i.e. radial distance, t is time, D_b is the oxygen diffusivity in blood, v is the velocity of flowing blood, S_b is the solubility of oxygen in blood, C_b is the oxygen content of blood, η is the Hill's coefficient for the hemoglobin dissociation curve, P_{50} is the oxygen tension for 50% hemoglobin saturation.

The model for the partial pressure P' (r, x, t) in the tissue, are given by partial differential equation:

$$\frac{\partial P'}{\partial t} = D_t\left(\frac{\partial^2 P'}{\partial r^2} + \frac{1}{r}\frac{\partial P'}{\partial r} + \frac{\partial^2 P'}{\partial x^2}\right) - K\left(\frac{C}{S_t}\right) \tag{3}$$

The terms including second partial derivative with respect to x and with respect to r, are the axial & radial diffusion of oxygen from capillary into surrounding tissue. D_t the diffusivity of oxygen in tissue [Michael's-Menten], S_t Oxygen solubility in tissue, and C is the consumption rate of tissue oxygen and given as:

$$C = C_{max}\frac{P}{P + C_{50}} \tag{4}$$

C_{max} is the value of consumption rate at very high tension; C_{50} is a constant representing the oxygen tension at which consumption decreases to 50% of its maximal value. Equation (1) and (3) are solved simultaneously following by the boundary conditions:

$$\frac{\partial P}{\partial x} = 0 \qquad r_c \le r \le r_t \quad , \quad x = 0 \tag{5}$$

$$\frac{\partial P}{\partial x} = S(r) \quad 0 \le r \le r_c \qquad x = l \tag{6}$$

$$\frac{\partial P}{\partial r} = 0 \qquad \text{for } r = 0 \quad \text{and all } x \tag{7}$$

$$P = P' \qquad \text{for } r = r_c \quad \text{and all } x \tag{8}$$

$$\frac{\partial P'}{\partial x} = S(r) \quad \text{for} \quad r_c \le r \le r_t \quad , \quad x = l \tag{9}$$

$$\left(D_b S_b \frac{\partial P}{\partial r}\right)_{capillary} = \left(D_t S_t \frac{\partial P'}{\partial r}\right)_{tissue} \qquad \text{for } r = r_c$$

and all x $\tag{10}$

$$\frac{\partial P'}{\partial r} = 0 \qquad \text{for } r = r_t \quad \text{and all } x, \tag{11}$$

$$P = P_0(r,x) \qquad \text{for } t = 0 \quad \text{and } \forall r, x \tag{12}$$

$$P = P_a - \left(\frac{C_{max}}{4D_b S_b}\right)\left(\frac{r_t^2}{r_c^2}-1\right)\left(r^2 - \frac{r_c^2}{2}\right) \quad 0 \le r \le r_c \quad x = 0 \tag{13}$$

Here P_a is the arterial oxygen tension, r_c capillary radius, r_t radius of Krogh tissue cylinder (one-half of intercapillary distance), l is the capillary length. Equation (5) states that there is no axial diffusion into tissue cylinder at the arterial end, Equation (6) specifies the rate at which oxygen diffuse axially out of the venous end of the capillary as a function S_r. Equation (7) states that there is no radial diffusion at $r = 0$ (from the capillary centre). Equation (8) is the continuity of tensions at the capillary wall. Equation (9) uses a non- zero value for axial diffusion of oxygen out of the venous end of the tissue cylinder because this seems to represent better the actual situation than would a value of zero. Here the axial derivative of P' in tissue is arbitrary taken to be equal to its value at the capillary wall by Reneau et al. (1967). Equation (10) guarantees that the rate of diffusion out of the capillary equal to the rate of diffusion into the tissue at the capillary wall. Equation (11) is for the fact that there is no radial diffusion of oxygen out of tissue cylinder. Equation (12) specifies the initial oxygen tension P (at time t=0at each point is equal to the steady-state oxygen tension $P_0(r,x)$, calculated as a solution of equation (1) and (3) at the initial values of parameters ($P_a = P_i, v = v_i$ and $C_{max} = C_v$) with time derivative set at zero i.e. totally steady-state condition. After time t=0 these parameters are as follows:

$$P_a = P_f + (P_i - P_f)e^{-t/\tau_p}$$

$$v = v_f + (v_i - v_f)e^{-t/\tau_v}$$

$$C_{max} = C_f + (C_i - C_t)e^{-t/\tau_c}$$

Where P_i, v_i, C_i are initial values; P_f, v_f, C_f are final values; τ_p, τ_v, τ_c are time constant that determine the rate of change of P_a, v and C_{max}. Equation (13) is for the

radial dependence of capillary oxygen tension at the arterial end. Here the radial diffusion outward from the capillary centre. In this study we solve equation (1) and (3) analytically as well as numerically, only numerical solution we considered for the first-order chemical kinetics to calculate the oxygen tension in tissue. There is a good agreement between previous results and ours. For the numerical solution of equation (1) and (3) we use finite difference technique.

RESULTS AND DISCUSSION

Figure 1 shows oxygen tension time profiles at point near the arterial end of the capillary when the arterial oxygen tension changes from normal to 50% of normal with time interval 0.1 second.

Similarly figure 2 shows oxygen tension time profiles at maximum distance from the arterial end, it is clear from the figure 2 that oxygen tension changes sharply at points
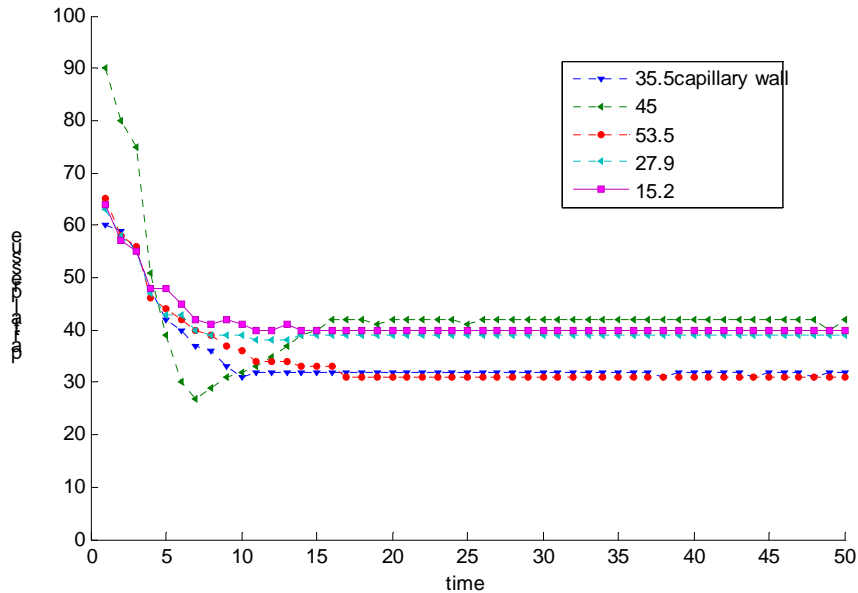
Fig. 1. Time profiles of tissue oxygen tension at arterial end of capillary for various radial distances from capillary centre for 50% of oxygen tension with time constant 0.1 second.
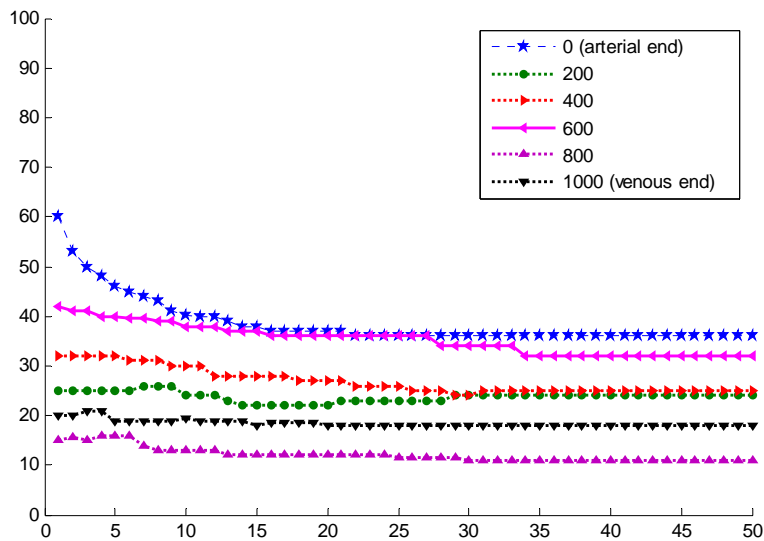
Fig. 2. Time profile at the maximum distance from capillary for various axial distances for 50% of oxygen tension with time constant 0.1 second.
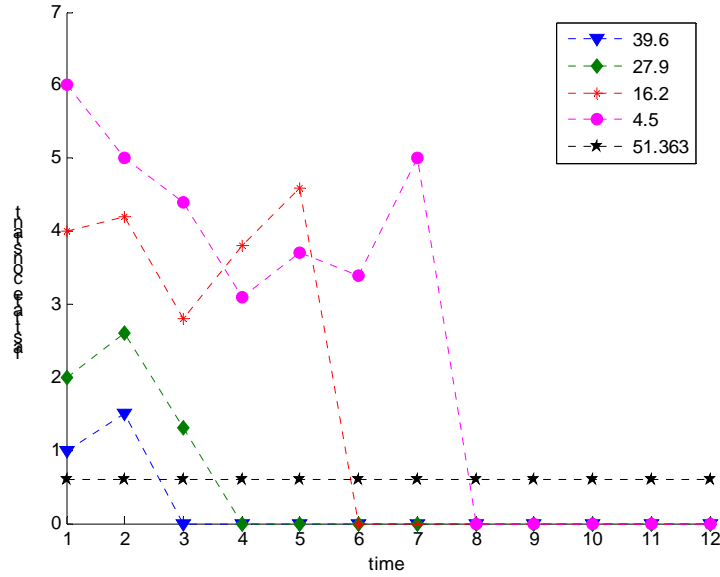
Fig. 3. Axial profiles of fast rate constant for various capillary centre when arterial oxygen tension changes from normal to 50% with time constant 0.1 second.
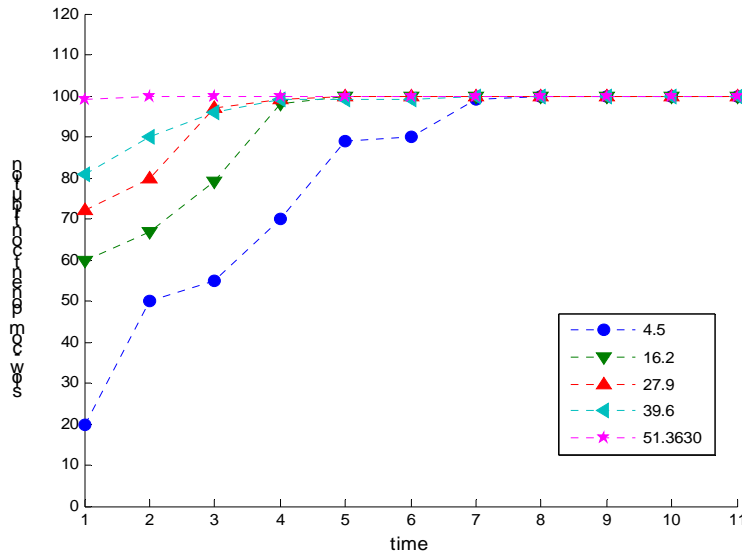

Fig. 4. Axial profile of slow-component   contribution when arterial oxygen tension changes from normal to 50% with time constant 0.1 second.

near the capillary and near arterial end. A single exponential function is used to express the time course of changing the oxygen at all locations excepting points near arterial end and near the capillary end, for these excluding points, a biexponential function is used.

There is a small variation in figure 1 and figure 2, due to the first order chemical kinetics. If we take k=1 then pervious results occurs smoothly. This changed reaction gives good results numerically. Figure 3 shows an axial

profile of fast rate constant for various capillary centres when arterial oxygen tension changes from normal to 50% with time constant 0.1 second. Here fast rate constant decreases with increasing radial and axial distance up to an abrupt transition point at which the oxygen-tension profiles become monoexponential.

From figure 4 and figure 5, it is clear that an increase in the arterial oxygen tension rate of change increases the fast rate constant but has little effect on either the slow
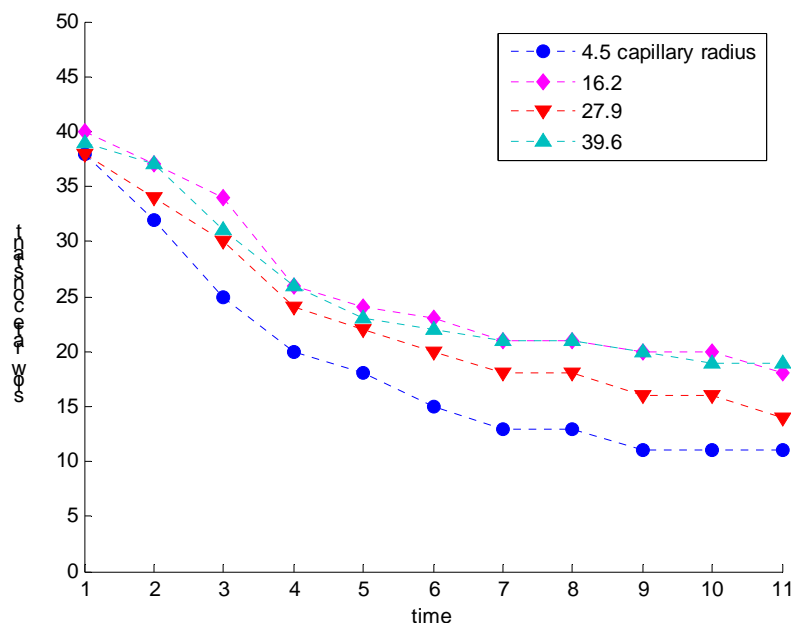
Fig. 5. Axial profile of slow rate contribution when arterial oxygen tension changes from normal to 50% with time constant 0.1 second.

rate constant or the slow-component contribution. As soon as flow velocity increases slow rate and fast rate constant decreases.

CONCLUSION

A Solution of Mathematical Model for Transport of Oxygen in Peripheral nerve with first-order chemical kinetics using finite-difference technique during Pranayama is obtained in this study. The transport of oxygen in peripheral nerve with forward and backward chemical reactions is time-dependent, analyzed using finite difference technique. The chemical reactions as well as new factor (K) (in first order chemical kinetics) were observed to affect the time profiles of tissue oxygen tension in the body with a time step 0.1 second.

REFERENCES

Kreuzer, F. 1982. Oxygen supply to tissue: The Krogh model and its assumptions. Experientia. Birkhauser verlag, CH-4010 Basel/Switzerland. 38:1415-1426.

Krogh, A. 1919. The number and Distribution of capillaries in muscles with calculations of the oxygen pressure head necessary for supplying the tissue. Journal of Physiology. 52(6):409-415.

Low, PA., Schemlzer, JD. and Ward, KK. 1986. The effect of age on energy metabolism and Resistance to ischaemic conduction failure in rat peripheral nerve. Journal of Physiology. 374:263-271.

Low, PA., Ward, K., Schmerzer JD. and Brimijon, S. 1986. Ischemic conduction failure and energy metabolism in experimental diabetic neuropathy. American Journal of Physiology. 248:E457-E462.

Lagerlund, TD. and Low, PA. 1993. Mathematical Modeling of time-dependent oxygen transport in rat peripheral nerve. Journal of Computational Biology Medicine. 23:29-47.

Reneau, DD., Bruley, DF. and Knisely, MH. 1967. A mathematical simulation of oxygen release, diffusion and consumption in the capillaries and tissue of the human brain, proceedings of the 33rd Annual chemical Engg. Symposium. Plenum press, Cincinnati. 135-241.

Reneau, DD., Bruley, DF. and Knisely, MH. 1969. A digital Simulation of transient oxygen transport in capillary tissue systems: development of a numerical method for solution of transport equations describing coupled convection-diffusion systems. AICHE Journal. 15:916-925.

Sharan, M. Singh, B. and Kumar, P. 1997. A two layers model for studying the effect of plasma layer on the delivery of oxygen to tissue using a finite element method. Journal of Applied Mathematical Modeling. 21:419-426.

Sharma, GC. and Jain, M. 2004. A Computational solution of Mathematical model for oxygen transport in peripheral nerve. Journal of Computers in Biology and Medicine. 34:633-645.

DESIGN SLIDING MODE CONTROLLER FOR ROBOT MANIPULATOR WITH ARTIFICIAL TUNEABLE GAIN

*Farzin Piltan, Alireza Salehi, Amin Jalali, Alireza Zare, Marzie Zare,
Farhad Golshan and Ali Roshanzamir
Industrial Electrical and Electronic Engineering SanatkadeheSabze Pasargad Co.,
16 Dena Apr., Seven Tir Ave., Shiraz - 71347-66773, Iran

ABSTRACT

One of the most active research areas in the field of robotics is robot manipulators control, because these systems are multi-input multi-output (MIMO), nonlinear, and uncertainty. At present, robot manipulators are used in unknown and unstructured situation and caused to provide complicated systems, consequently strong mathematical tools are used in new control methodologies to design nonlinear robust controller with satisfactory performance (e.g., minimum error, good trajectory, disturbance rejection). Robotic systems controlling is vital due to the wide range of application. Obviously stability and robustness are the most minimum requirements in control systems; even though the proof of stability and robustness is more important especially in the case of nonlinear systems. The strategies of robotic manipulators control are classified into two main groups: classical and non-classical methods, where the conventional control theory uses the classical method and the artificial intelligence theory (e.g., fuzzy logic, neural network, and neuro fuzzy) uses the non-classical methods. However both of classical and non-classical theories have applied successfully in many applications, but they also have some limitations. One of the best nonlinear robust controllers which can be used in uncertainty nonlinear systems is sliding mode controller (SMC). Sliding mode controller has two most important challenges: chattering phenomenon and nonlinear dynamic equivalent part. This paper is focused on the applied non-classical method (e.g., Fuzzy Logic) in robust classical method (e.g., Sliding Mode Controller) in the presence of uncertainties and external disturbance to reduce the limitations. Applying the Mamdani's error based fuzzy logic controller with 7 rules is the main goal that causes the elimination chattering phenomenon with regard to the variety of uncertainty and external disturbance; as a result this paper focuses on the sliding mode controller with artificial tuneable gain (SMCAT) to adjusting the sliding surface slope coefficient depends on applying fuzzy method.

Keywords: Uncertain nonlinear systems, classical control, non-classical control, fuzzy logic, robot manipulator, sliding mode controller with artificial tuneable gain and chattering phenomenon.

INTRODUCTION

Controller (control system) is a device that can sense data from plant (e.g., robot manipulator) to improve the plants behavior through actuation and computation (Ogata, 2009). SMC is one of the influential nonlinear controllers in certain and uncertain systems which are used to present a methodical solution for two main important controllers' challenges, which named: stability and robustness. Conversely, this controller is used in different applications; sliding mode controller has subsequent drawback i.e. chattering phenomenon. To reduce or remove this challenge, one of the best techniques is applying non-classical method in robust classical such as sliding mode controller method (Kurfess 2005; Siciliano and Khatib, 2008).

A robot is a machine which can be programmed as a reality of tasks which it has divided into three main categories i.e. robot manipulators, mobile robots and hybrid robots. PUMA-560 robot manipulator is an articulated 6 DOF serial robot manipulator. This robot is widely used in industrial and academic area and also dynamic parameters have been identified and documented in the literature (Armstrong *et al*., 1986). From the control point of view, robot manipulator divides into two main sections i.e. kinematics and dynamic parts. Estimate dynamic parameters are considerably important to control, mechanical design and simulation (Siciliano and Khatib, 2008).

In order to solve the uncertain and complicated systems with a set of IF-THEN rules, fuzzy logic teach should be applied so beginning able to recommended and approximate model in the main motivation (Reznik, 1997). Conversely fuzzy logic method is constructive to control complicated mathematical models; the design quality may not always be so high. Besides using fuzzy logic in the main controller of a control loop, it can be used to design adaptive control, tuning parameters, working in a parallel with classical controllers (e.g., sliding mode controller) and design sliding mode fuzzy or

*Corresponding author email: SSP.ROBOTIC@yahoo.com

fuzzy sliding mode controller (Lee, 1990).

As mentioned above to reduce a fuzzy logic and sliding mode limitations one of the significant method is design fuzzy logic in a parallel with sliding mode controller (Shahnazi *et al.* 2008; Hsueh *et al.*, 2009). AFGSMC is sliding mode controller where adjusted by fuzzy logic technique to simple implement, most excellent stability and robustness. AFGSMC has the following advantages; reducing the number of fuzzy rule base and increasing robustness and stability (Hsu and Fu, 2002; Hsu and Malki, 2002; Hsueh *et al.*, 2009).

This paper is organized as, in section 1, main subject of sliding mode controller and formulation are presented. This section covered the following details, classical sliding mode controller for robotic manipulator, equivalent control and chatter free sliding control. In section 2, modelling of robotic manipulators is presented. Detail of fuzzy logic controllers and fuzzy rule base is presented in section 3. In section 4, design Adaptive Fuzzy Gain scheduling sliding mode controller (AFGSMC); this method is used to reduce the uncertainty and variation in dynamic parameter. In section 5, the simulation results and discussion are presented.

1. Classical sliding mode control for robot manipulator
The control law for six degrees of freedom PUMA-560 robot manipulator is written as (Kurfess, 2005; Siciliano and Khatib, 2008):

$$\tau = \tau_{eq} + \tau_{sat} \tag{1}$$

Where, the model-based component τ_{eq} is compensated the nominal dynamics of systems. Therefore τ_{eq} can calculate as follows:

$$\tau_{eq} = \left[M^{-1}(B + C + G) + \dot{S} \right] M \tag{2}$$

Where

$$\tau_{eq} = \begin{bmatrix} \tau_{eq1} \\ \tau_{eq2} \\ \tau_{eq3} \\ \tau_{eq4} \\ \tau_{eq5} \\ \tau_{eq6} \end{bmatrix},$$

$$M^{-1} = \begin{bmatrix} M_{11} & M_{12} & M_{13} & 0 & 0 & 0 \\ M_{21} & M_{22} & M_{23} & 0 & 0 & 0 \\ M_{31} & M_{32} & M_{33} & 0 & M_{35} & 0 \\ 0 & 0 & 0 & M_{44} & 0 & 0 \\ 0 & 0 & 0 & 0 & M_{55} & 0 \\ 0 & 0 & 0 & 0 & 0 & M_{66} \end{bmatrix}^{-1}$$

$$B + C + G = \begin{bmatrix} b_{112}\dot{q}_1\dot{q}_2 + b_{113}\dot{q}_1\dot{q}_3 + 0 + b_{123}\dot{q}_2\dot{q}_3 \\ 0 + b_{223}\dot{q}_2\dot{q}_3 + 0 + 0 \\ 0 \\ b_{412}\dot{q}_1\dot{q}_2 + b_{413}\dot{q}_1\dot{q}_3 + 0 + 0 \\ 0 \\ 0 \end{bmatrix} + \begin{bmatrix} c_{12}\dot{q}_2^2 + c_{13}\dot{q}_3^2 \\ c_{21}\dot{q}_1^2 + c_{23}\dot{q}_3^2 \\ c_{31}\dot{q}_1^2 + c_{32}\dot{q}_2^2 \\ 0 \\ c_{51}\dot{q}_1^2 + c_{52}\dot{q}_2^2 \\ 0 \end{bmatrix} + \begin{bmatrix} g_1 \\ g_2 \\ g_3 \\ 0 \\ g_5 \\ 0 \end{bmatrix}$$

$$S = \begin{bmatrix} S_1 \\ S_2 \\ S_3 \\ S_4 \\ S_5 \\ S_6 \end{bmatrix} \quad \text{and}$$

$$M = \begin{bmatrix} M_{11} & M_{12} & M_{13} & 0 & 0 & 0 \\ M_{21} & M_{22} & M_{23} & 0 & 0 & 0 \\ M_{31} & M_{32} & M_{33} & 0 & M_{35} & 0 \\ 0 & 0 & 0 & M_{44} & 0 & 0 \\ 0 & 0 & 0 & 0 & M_{55} & 0 \\ 0 & 0 & 0 & 0 & 0 & M_{66} \end{bmatrix}$$

Suppose that τ_{sat} is computed as ;

$$\tau_{sat} = K.sat\left(S/\emptyset\right) \tag{3}$$

where

$$\tau_{sat} = \begin{bmatrix} \tau_{dis1} \\ \tau_{dis2} \\ \tau_{dis3} \\ \tau_{dis4} \\ \tau_{dis5} \\ \tau_{dis6} \end{bmatrix}, K = \begin{bmatrix} K_1 \\ K_2 \\ K_3 \\ K_4 \\ K_5 \\ K_6 \end{bmatrix}, \left(S/\emptyset\right) = \begin{bmatrix} S_1 \\ \emptyset_1 \\ S_2 \\ \emptyset_2 \\ S_3 \\ \emptyset_3 \\ S_4 \\ \emptyset_4 \\ S_5 \\ \emptyset_5 \\ S_6 \\ \emptyset_6 \end{bmatrix}, \quad S = \lambda e + \dot{e}$$

and $Sat\left(S/\emptyset\right)$ can be defined as

$$sat\left(S/\emptyset\right) = \begin{cases} 1 & (S/\emptyset > 1) \\ -1 & (S/\emptyset < 1) \\ S/\emptyset & (-1 < S/\emptyset < 1) \end{cases} \tag{4}$$

Moreover by replace the formulation (3) in (1) the control output is written as ;

$$\tau = \tau_{eq} + K.sat\left(S/\emptyset\right) = \begin{cases} \tau_{eq} + K.sgn(S) & ,|S| \geq \emptyset \\ \tau_{eq} + K.S/\emptyset & ,|S| < \emptyset \end{cases} \tag{5}$$

Figure 1 shows the position classical sliding mode control for PUMA-560 robot manipulator. By (5) and (2) the sliding mode control of PUMA-560 robot manipulator is calculated as;

$$\tau = \left[M^{-1}(B + C + G) + \dot{S} \right] M + K.sat\left(S/\emptyset\right) \tag{6}$$

2. Modeling of robotic manipulator

It is well known that the equation of a multi degrees of freedom (DOF) robot manipulator governed by the following equation (Siciliano and Khatib, 2008):

$$M(q)\ddot{q} + N(q,\dot{q}) = \tau \tag{7}$$

Where τ is $n \times 1$ vector of actuation torque, M (q) is $n \times n$ symmetric and positive define inertia matrix, $N(q,\dot{q})$ is the vector of nonlinearity term, and q is $n \times 1$ position vector. In equation 2.8 if vector of nonlinearity derive as Centrifugal and Coriolis and Gravity terms, consequently robot manipulator dynamic equation can also be written in a following form:

$$N(q,\dot{q}) = V(q,\dot{q}) + G(q) \tag{8}$$
$$V(q,\dot{q}) = B(q)[\dot{q}\ \dot{q}] + C(q)[\dot{q}]^2 \tag{9}$$
$$\tau = M(q)\ddot{q} + B(q)[\dot{q}\ \dot{q}] + C(q)[\dot{q}]^2 + G(q) \tag{10}$$

Where,

$B(q)$ is matrix of coriolis torques, $C(q)$ is matrix of centrifugal torque, $[\dot{q}\ \dot{q}]$ is vector of joint velocity that it can give by:

$[\dot{q}_1.\dot{q}_2, \dot{q}_1.\dot{q}_3, \dots, \dot{q}_1.\dot{q}_n, \dot{q}_2.\dot{q}_3, \dots]^T$, and $[\dot{q}]^2$ is vector, that it can given by: $[\dot{q}_1^2, \dot{q}_2^2, \dot{q}_3^2, \dots]^T$.

To derive the dynamic modeling of the robot manipulators, some researchers introduced the kinetic energy matrix and gravity vector symbolic elements by performing the summation of either Lagrange's or the Gibbs-Alembert formulation (Kurfess, 2005; Siciliano and Khatib, 2008).

$$\ddot{q} = M^{-1}(q).\{\tau - N(q,\dot{q})\} \tag{11}$$

From a control point of view this technique is very attractive since the nonlinear and coupled robot manipulator dynamics is replaced by a linear and decoupled second order system. The first step to determine the dynamic equation of robot manipulator by the formulation of (11) is finding the kinetic energy matrix (M) parameters by used of Lagrange's formulation. The second step is finding the Coriolis and Centrifugal matrix which they can calculate by partial derivatives of kinetic energy. The last step to determine the dynamic equation of robot manipulator is to find the gravity vector by performing the summation of Lagrange's formulation.

Therefore the kinetic energy matrix in n DOF is a $n \times n$ matrix that can be calculated by the following matrix

$$M(q) = \begin{bmatrix} M_{11} & M_{12} & \dots & \dots & \dots & M_{1n} \\ M_{21} & \dots & \dots & \dots & \dots & M_{2n} \\ \dots & \dots & \dots & \dots & \dots & \dots \\ \dots & \dots & \dots & \dots & \dots & \dots \\ \dots & \dots & \dots & \dots & \dots & \dots \\ M_{n,1} & \dots & \dots & \dots & \dots & M_{n,n} \end{bmatrix} \tag{12}$$

The Coriolis matrix (B) is a $n \times \frac{n(n-1)}{2}$ matrix that can be calculated by the following matrix;

$$B(q) = \begin{bmatrix} b_{112} & b_{113} & \dots & b_{11n} & b_{123} & \dots & b_{12n} & \dots & \dots & b_{1n-1,n} \\ b_{212} & \dots & \dots & b_{21n} & b_{223} & \dots & \dots & \dots & \dots & b_{2n-1,n} \\ \dots & \dots & \dots & \dots & \dots & \dots & \dots & \dots & \dots & \dots \\ \dots & \dots & \dots & \dots & \dots & \dots & \dots & \dots & \dots & \dots \\ b_{n12} & \dots & \dots & b_{n1n} & \dots & \dots & \dots & \dots & \dots & b_{nn-1,n} \end{bmatrix} \tag{13}$$

The Centrifugal matrix (C) is a $n \times n$ matrix that can be calculated by the following matrix;

$$C(q) = \begin{bmatrix} C_{11} & \dots & C_{1n} \\ \vdots & \ddots & \vdots \\ C_{n1} & \dots & C_{nn} \end{bmatrix} \tag{14}$$

The Gravity vector (G) is a $n \times 1$ vector that can be calculated by the following vector;

$$G(q) = \begin{bmatrix} g_1 \\ g_2 \\ \vdots \\ g_n \end{bmatrix} \tag{15}$$

3. Design Fuzzy logic controller

After the invention of fuzzy logic theory in 1965 by Zadeh (1997), this theory was used in wide range area. Fuzzy logic controller (FLC) is one of the most important applications of fuzzy logic theory. This controller can be used to control of nonlinear, uncertain, and noisy systems. Fuzzy logic control systems, do not use complex mathematically models of plant for analysis. This method is free of some model-based techniques that used in classical controllers. It must be noted that application of fuzzy logic is not limited only to modelling of nonlinear systems (Reznik, 1997)but also this method can help engineers to design easier controller.

The fuzzy inference mechanism provides a mechanism for referring the rule base in fuzzy set. There are two most commonly method that can be used in fuzzy logic controllers, namely, Mamdani method and Sugeno method, which Mamdani built one of the first fuzzy controller to control of system engine and Michio Sugeno suggested to use a singleton as a membership function of the rule consequent. The Mamdani fuzzy inference method has four steps, namely, fuzzification, rule evaluation, aggregation of the rule outputs and defuzzification. Sugeno method is very similar to Mamdani method but Sugeno changed the consequent rule base that he used the mathematical function of the

input rule base instead of fuzzy set. The following define can be shown the Mamdani and Sugeno fuzzy rule base;

Mamdani $F.R^1: if$ $x\, is\, A\, and\, y\, is\, B$ then $z\, is\, C$
Sugeno $F.R^1: if$ $x\, is\, A\, and\, y\, is\, B$ then $f(x,y)\, is\, C$

Fuzzification is used to determine the membership degrees for antecedent part when x and y have crisp values. Rule evaluation focuses on operation in the antecedent of the fuzzy rules. This part can used AND/OR fuzzy operation in antecedent part after that the output fuzzy set can be calculated by using individual rule-base inference. There are several methodologies in aggregation of the rule outputs that can be used in fuzzy logic controllers, namely, Max-Min aggregation, Sum-Min aggregation, Max-bounded product, Max-drastic product, Max-bounded sum, Max-algebraic sum and Min-max. In this paper we used Max-min aggregation. Max-min aggregation defined as below:

$$\mu_U(x_k, y_k, U) = \mu_{\cup_{i=1}^r FR^i}(x_k, y_k, U) = \max\left\{min_{i=1}^r\left[\mu_{R_{pq}}(x_k, y_k), \mu_{p_m}(U)\right]\right\}$$

where r is the number of fuzzy rules activated by x_k and y_k and also $\mu_{\cup_{i=1}^r FR^i}(x_k, y_k, U)$ is a fuzzy interpretation of $i-th$ rule. The last step in the fuzzy inference in any fuzzy set is defuzzification. This part is used to transform fuzzy set to crisp set, therefore the input for defuzzification is the aggregate output and the output is a crisp number. There are several methodologies in defuzzification of the rule outputs that can be used in fuzzy logic controllers but this paper focuses on Center of gravity method (COG), which COG method used the following equation to calculate the defuzzification:

$$COG(x_k, y_k) = \frac{\sum_i U_i \sum_{j=1}^r \mu_u(x_k, y_k, U_i)}{\sum_i \sum_{j=1}^r \mu_u(x_k, y_k, U_i)}$$

where $COG(x_k, y_k)$ illustrates the crisp value of defuzzification output, $U_i \in U$ is discrete element of an output of the fuzzy set, $\mu_{U'}(x_k, y_k, U_i)$ is the fuzzy set membership function, and r is the number of fuzzy rules.

4. Design Adaptive Fuzzy Gain scheduling sliding mode controller (AFGSMC)
Adaptive control used in systems whose dynamic parameters are varying and need to be training on line. In general states adaptive control classified in two main groups: traditional adaptive method and fuzzy adaptive method, that traditional adaptive method need to have some information about dynamic plant and some dynamic parameters must be known but fuzzy adaptive method can training the variation of parameters by expert knowledge. Combined adaptive method to sliding mode controllers can help to controllers to have better performance by online tuning the nonlinear and time variant parameters.

For any plants (e.g., robot manipulators) whose have variation in parameter, adaptive control can learn the dynamic parameter to design an acceptable controller. All pure classical and fuzzy controllers have common difficulty, which they need to find several scale factors. Therefore, adaptive method can adjust and tune parameters (Hwang and Chao, 2005; Mohan and Bhanot, 2006; Hsueh *et al*., 2009).

The addition of adaptive methodology to a sliding mode controller caused to improve the tracking performance by online tuning the parameters. The adaptive sliding mode controller is used to estimate the unknown dynamic parameters and external disturbances.

Design supervisory FIS for classical SMC has five steps:
1. Determine inputs and outputs: This controller has one input (S) and one output (α). The input is sliding surface (S) and the output is tuning coefficient (α).   (17)

2. Find membership function and linguistic variable: The linguistic variables for sliding surface (S) are; Negative Big(N.B), Negative Medium(N.M), Negative Small(N.S), Zero(Z), Positive Small(P.S), Positive Medium(P.M), Positive Big(P.B), and it is quantized in to thirteen levels represented by: -1, -0.83, -0.66, -0.5, -0.33, -0.16, 0, 0.16, 0.33, 0.5, 0.66, 0.83, 1, and the linguistic variables to find the tuning coefficient (α) are; Negative Big(N.B), Negative Medium(N.M), Negative Small(N.S), Zero(Z), Positive Small(P.S), Positive Medium(P.M), Positive Big(P.B), and it is quantized in to thirteen levels represented by: -1, -0.83, -0.66, -0.5, -0.33, -0.16, 0, 0.16, 0.33, 0.5, 0.66, 0.83, 1.   (18)

3. Choice of shape of membership function: In this part the researcher select the triangular membership function that it is shown in figure 1.
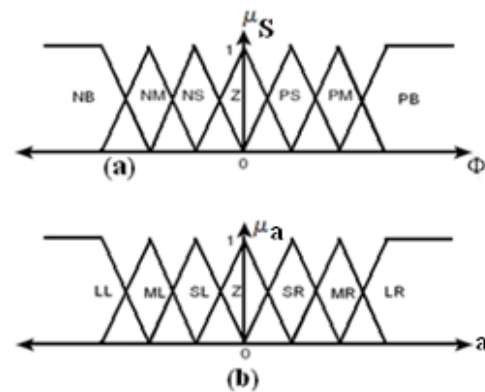

Fig. 1. Membership function: a) sliding surface b) Tuning coefficient.

4. Design fuzzy rule table: design the rule base of fuzzy logic controller can play important role to design best performance AFGSMC, suppose that two fuzzy rules in this controller are:

F.R^1: *IF S is Z, THEN α is Z.*

F.R^2: *IF S is (P.B) THEN α is (L.R).*

The complete rule base for this controller is shown in table 1.

Table 1. Fuzzy rule table.

S	**N.B**	**N.M**	**N.S**	**Z**	**P.S**	**P.M**	**P.B**
α	**N.B**	**N.M**	**N.S**	**Z**	**P.S**	**P.M**	**P.B**

The control strategy that deduced by table 1 are
➢ If sliding surface (S) is N.B, the control applied is N.B for moving S to S=0.
➢ If sliding surface (S) is Z, the control applied is Z for moving S to S=0.

5. Defuzzification: The final step to design fuzzy logic controller is deffuzification, in this controller the COG method will be used.

The block diagram of AFGSMC controller is shown in figure 2.

RESULTS AND DISCUSSION

Adaptive Fuzzy Gain scheduling sliding mode controller (AFGSMC), Adaptive Fuzzy Inference System (AFIS), and Sliding Mode Controller (SMC) were tested for step response trajectories. In this simulation the first, second, and third joints move from home to final position without and with external disturbance. The simulation was implemented in Matlab/Simulink environment. Tracking performance, error, robustness (disturbance rejection), and chattering rejection are compared.

Tracking performances: From the simulation for first, second, and third trajectory without any disturbance, it was seen that AFGSMC and SMC have the same performance. This is primarily because the manipulator robot parameters do not change in simulation. The AFGSMC and SMC give significant trajectory good following when compared to FLC. Figure 3 shows tracking performance without any disturbance for AFGSMC, AFIS and SMC.

Disturbance rejection: An unknown output disturbance is applied in different time. Figure 4 shows disturbance rejection for AFGSMC, AFIS and SMC. However the AFGSMC gives the better performance than AFIS but AFIS also has an acceptable performance.

Errors in the model: However the AFIS gives significant
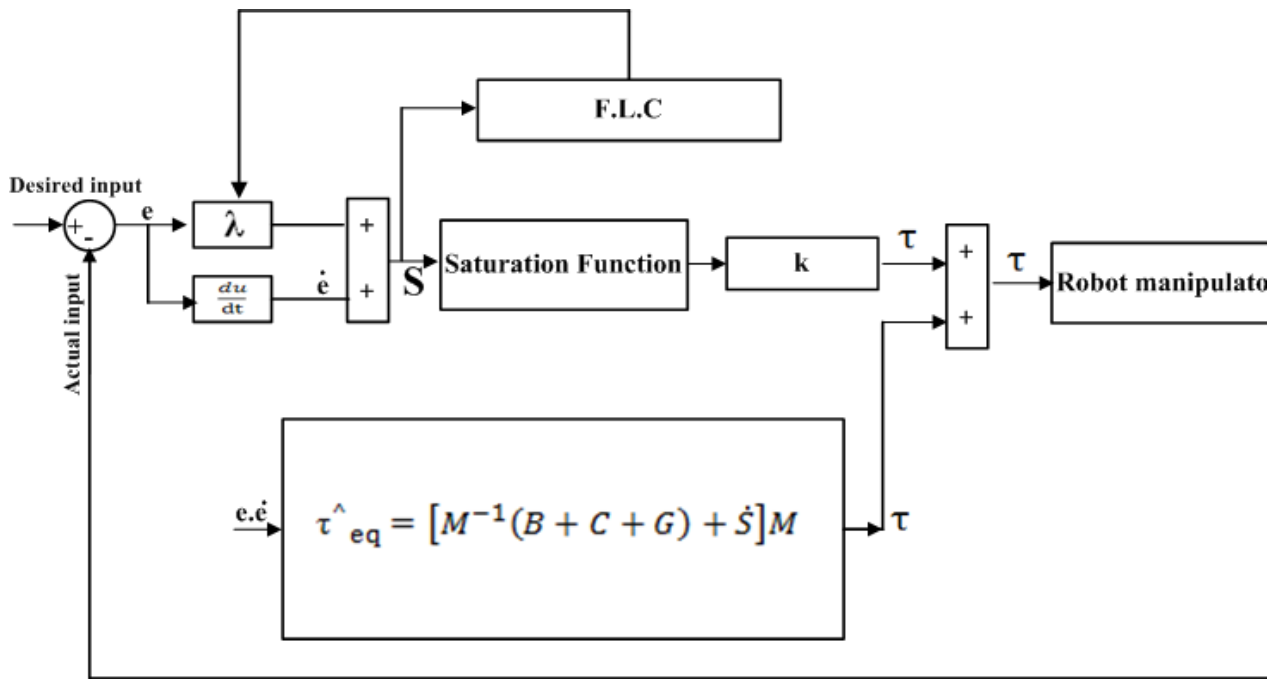
Fig. 2. Block diagram of an adaptive fuzzy gain scheduling sliding mode controller is too big and not readable at current position.
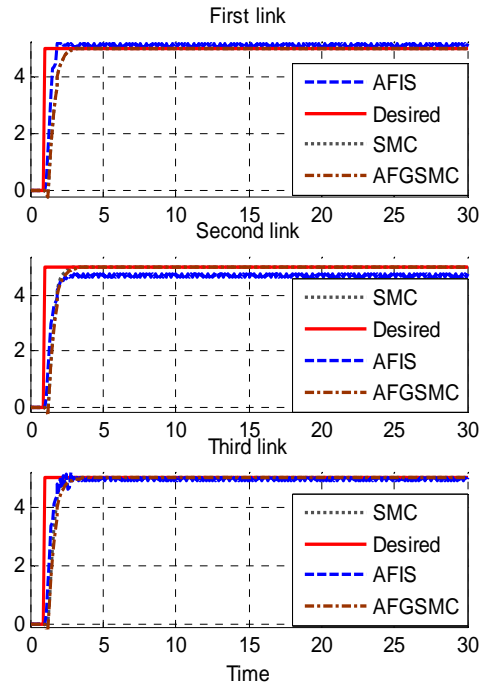
Fig. 5. Step SMC, AFIS, and AFGSMC for first, second and third link errors with external disturbance.



Fig. 6. Step SMC and AFGSMC for first, second and third link chattering rejection with external disturbance.

error reduction when compared to pure FLC, but it is not as good as AFGSMC. The error profile for AFGSMC is smoother compared to the other controllers. Figure 5 shows a comparison of error performance for all three controllers that study in this paper.

Chattering phenomenon: An unknown output disturbance is applied in different time. Figure 6 shows the chattering rejection for step AFGSMC and SMC.

CONCLUSION

This paper presents a new methodology for designing an adaptive fuzzy gain scheduling sliding mode controller for PUMA robotic manipulator. From the simulation, it was seen that AFGSMC has 7 rule base because it has one input for supervisory controller but AFIS has 49 rules for supervisory and 49 rules for main controller therefore implementing of AFIS most of time has many problems and expensive and also the AFGSMC performance is better than SMC and AFIS in most of time, Because this controller can auto tune as SMC with change the robot arm parameters, but pure SMC cannot do it.

The pure sliding mode controller has some problems in parameter variations. In the worst case, the adaptive controller has the potential to perform as well as a sliding mode controller. In AFGSMC, the fuzzy supervisory controller can changed the λ to achieve the best performance and in AFIS the supervisory controller can

changed the gain updating factor of main FIS to have the best performance.

REFERENCES

Armstrong, B., Khatib, O. and Burdick, J. 2002. The Explicit Dynamic Model and Inertial Parameters of the PUMA 560 Arm. IEEE. 510-518.

Hsu, FY. and Fu, LC. 2002. Nonlinear Control of Robot Manipulators Using Adaptive Fuzzy Sliding Mode Control. IEEE. 156-161.

Hsu, YC. and Malki, HA. 2002. Fuzzy Variable Structure Control for MIMO Systems. IEEE. 280-285.

Hsueh, YC., Su, SF et al. 2009. Self-tuning sliding mode controller design for a class of nonlinear control systems. IEEE. 2337-2342.

Hwang, CL. and Chao, SF. 2005. A Fuzzy-model-based Variable Structure Control for Robot Arms: Theory and Experiments. IEEE. 5252-5258.

Kurfess, TR. 2005. Robotics and Automation Handbook, CRC.

Lee, CC. 1990. Fuzzy Logic in Control Systems: Fuzzy Logic Controller. I. IEEE Transactions on Systems, Man and Cybernetics. 20(2):404-418.

Mohan, S. and Bhanot, S. 2006. Comparative Study of Some Adaptive Fuzzy Algorithms for Manipulator

Control. International Journal of Computational Intelligence. 3(4):303-311.

Ogata, K. 2009. Modern Control Engineering, Prentice Hall.

Reznik, L. 1997. Fuzzy Controllers, Butterworth-Heinemann.

Shahnazi, R., Shanechi, HM. and Pariz, N. 2008. Position Control of Induction and DC Servomotors: a novel adaptive fuzzy PI sliding mode control. Energy Conversion. IEEE Transactions on. 23(1):138-147.

Siciliano, B. and Khatib, O. 2008. Springer Handbook of Robotics. Springer-Verlag Inc., New York, USA.

Zadeh, LA. 1997. Toward a Theory of Fuzzy Information Granulation and its Centrality in Human Reasoning and Fuzzy Logic. Fuzzy Sets and Systems. 90(2):111-127.

Canadian Journal of
pure&applied
sciences

SHORT COMMUNICATION

COMPARISON OF ATMOSPHERIC CO$_2$ LEVELS
WITH A NATURAL PHENOMENON

Scott McNeil
SAIC-Frederick, 1050 Boyles Street, PO Box B, Frederick, MD 21702, USA

The rise in global temperature is due to the increase in greenhouse gases, primarily in the form of carbon dioxide (CO$_2$) - which has a rate of increase five times larger than before the pre-industrial era (Jansen *et al*., 2007). Historical atmospheric levels of CO$_2$ obtained from glacial ice cores (Etheridge *et al*., 1998) can be combined with atmospheric CO$_2$ levels collected on Mauna Loa in Hawaii (Keeling *et. al*., 2004; Pales and Keeling, 1965) to provide a record dating from the geologic past. Monthly readings at Mauna Loa since 1958, and now expanded to a network of worldwide sampling stations, provide essentially real-time monitoring of atmospheric CO$_2$ levels.

Concurrent with this rise in atmospheric CO$_2$ has been a decrease in the intensity of the Earth's protective shield: the geomagnetic field. Historical ship logs and magnetic observatories offer a record of geomagnetic intensity from the 1600's to the present (Jackson *et al*., 2000; Gubbins *et al*., 2006). These records show that the intensity of the geomagnetic field (**F**) was relatively stable prior to the late-1800s and then began a sharp decrease; in the last hundred years **F** decreased approximately 5% (USGS, 2011). A plot comparing the global average in magnetic field strength (i.e. the geomagnetic coefficient, "g10") with the increase in atmospheric CO$_2$ from the 17th century to the present reveals an inverse association (Fig. 1), with notable divergence starting in the mid-nineteenth century.
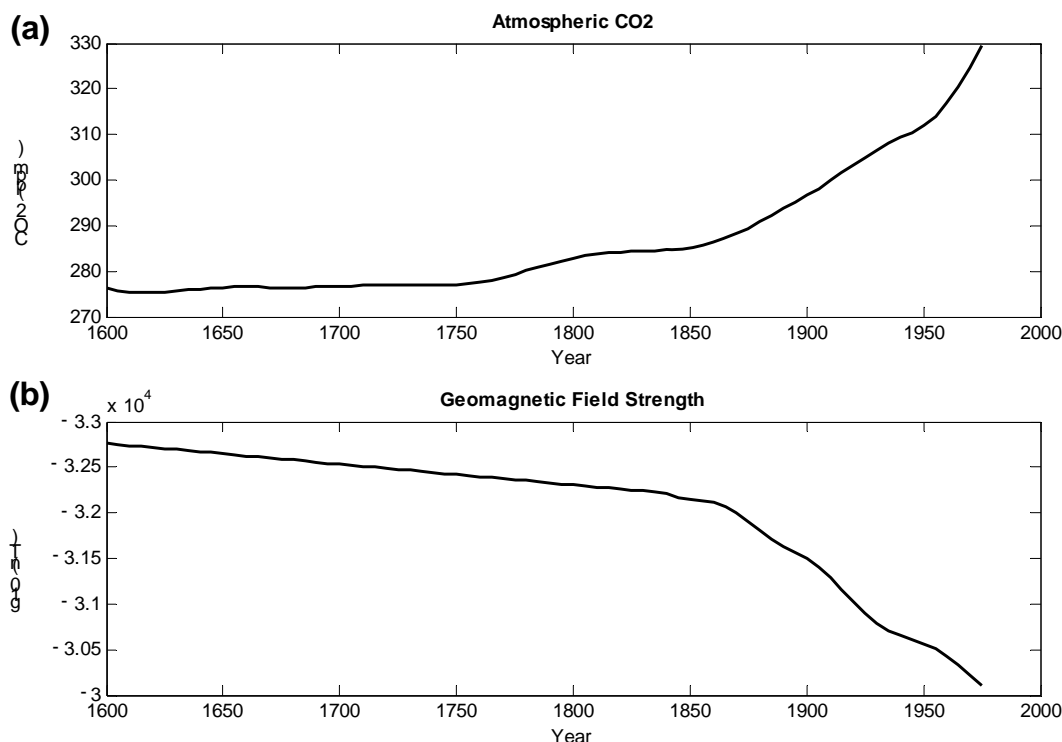
Fig. 1. Historical comparison of CO$_2$ levels with the geomagnetic field strength. Atmospheric CO$_2$ levels (**a**) mirror the global geomagnetic field strength (**b**) from the 16th century to present day [data source: (Gubbins *et al*., 2006; Etheridge *et. al*., 1998)].

Corresponding author email: mcneils@saic.com

The use and worldwide distribution of magnetometers starting in the late-1800's has generated an continuous record of **F** for the last hundred years, with nanoTesla (nT) accuracy. The World Data Center (WDC) for Geomagnetism in Edinburgh houses this comprehensive set of precise geomagnetic data which is supplied from a worldwide network of magnetic observatories (World Data Center, 2011). Using data archived at WDC, globally distributed ground-based magnetometer stations were identified that had continuous recordings in **F** from the start of the twentieth century to the present, with non-linear trends in the mid-1900's similar to those obtained by other methods (Gubbins *et al.*, 2006; Fig. 1b). Scatter plot analysis of **F** vs. CO_2 for this timeframe (Fig. 2) reveals a strong negative correlation ($R^2 = -0.94$). This relationship is conserved well in the time derivative, which shows concurrent local maxima/minima and inflection points (Fig. 3).

The observations reported here demonstrate that the increase in atmospheric CO_2 exhibits strong temporal correlation with a natural phenomenon, namely the decrease in intensity of the geomagnetic field. This association is conserved in the time derivative, arguing against an incidental trend. A model that accounts for this inverse association is not straightforward. The global CO_2 cycle involves interaction between the atmosphere, biosphere and hydrosphere; a relationship between **F** and this cycle has not been established. Recently Pazur *et al.* (2008) presented evidence that microTesla (μT) changes in a magnetic field could influence the solubility constant of CO_2 in seawater (Pazur and Winklhofer, 2008). In their study, a controlled decrease in **F** resulted in an increase in released CO_2. This work was met with skepticism, however, due to potential flaws in the experimental design (Köhler *et al.*, 2009). An alternative association between **F** and CO_2 may be found in the influence of **F** on photosynthesis itself. Several reports in the field of biomagnetics have now observed differences in plant growth and CO_2 uptake following exposure to μT strength magnetic fields (Yano *et al.* 2004; Huang and Wang, 2008). Although these studies were for relatively short time periods ($\sim$ 2 weeks), the trend in the CO_2 response tracked inversely with **F** -- consistent with the observations reported here. These analyses suggest a possible interaction between **F** and atmospheric CO_2. This putative relationship appears to be limited to the last few centuries, however, as paleomagnetic intensity reconstructions do not correlate with ice core CO_2 records over geologic timescales (Köhler *et al.*, 2009).
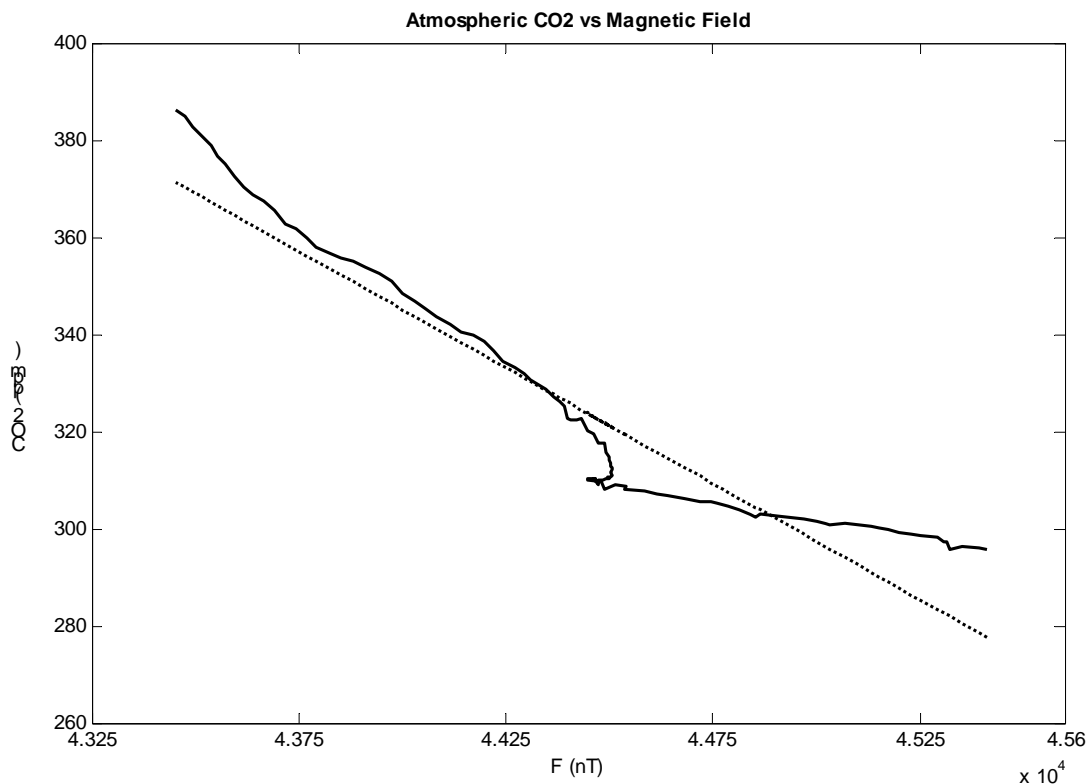

Fig. 2. Correlation of Atmospheric Carbon Dioxide with Global Magnetic Field. Scatterplot analysis of yearly global CO_2 concentration versus the relative global magnetic field intensity (**F**) for years 1900 to 2007. Dotted line is best fit using linear regression; correlation coefficient is shown, $\rho < .001$ using a matched pair t-test (MATLAB, R2008b).

Atmospheric CO2

Field Intensity
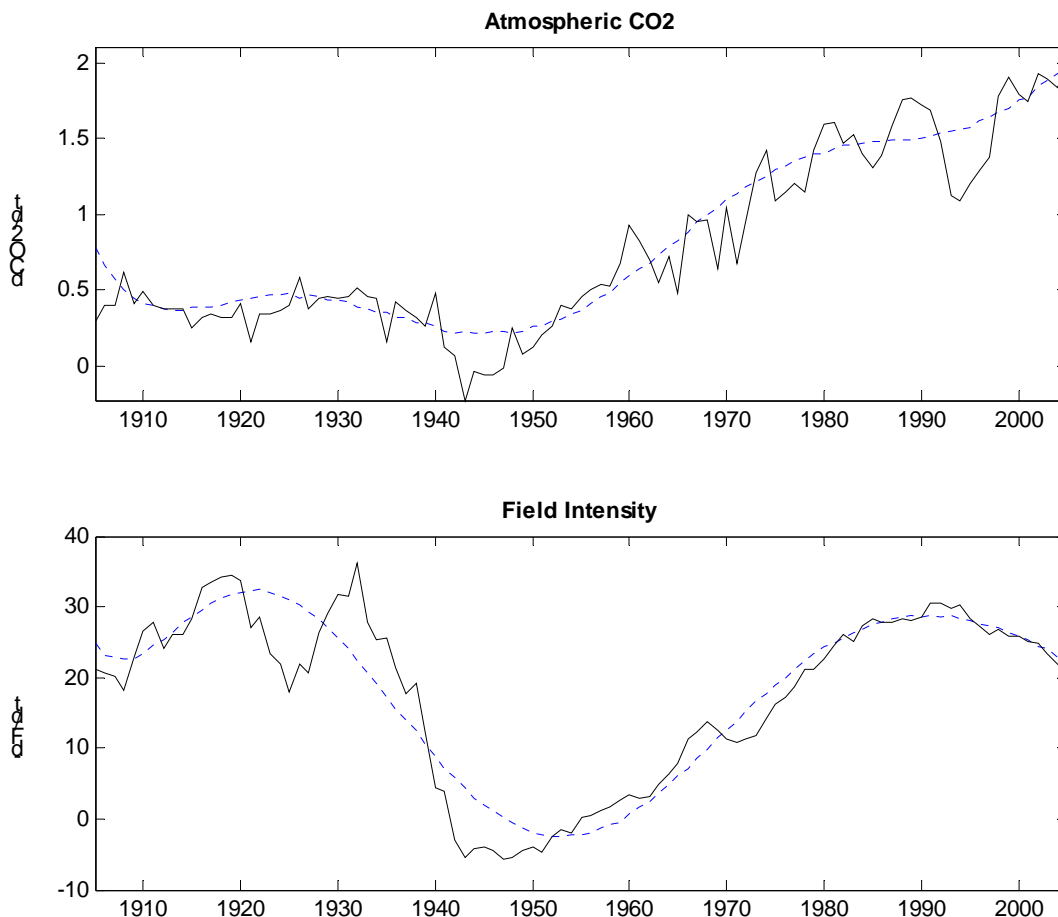
Fig. 3. Time derivative for CO_2 and geomagnetic field. (a) dCO_2/dt and (**b**) dF/dt; **F** is presented as negative (-) values to show the inverse relationship. Solid line in graphs is empirical data smoothed using a 5-year moving average; dotted line is curve of best fit.

REFERENCES

Etheridge, DM., Steele, LP., Langenfelds, RL., Francey, RJ., Barnola, JM. and Morgan, VI. 1998. Historical CO_2 records from the Law Dome DE08, DE08-2, and DSS ice cores. In Trends: A Compendium of Data on Global Change. Carbon Dioxide Information Analysis Center, Oak Ridge National Laboratory, US. Department of Energy, Oak Ridge, Tenn., USA., http://cdiac.esd.ornl.gov/

Gubbins, D., Jones, AL. and Finlay, CC. 2006. Fall in Earth's magnetic field is erratic. Science. 312:900-902.

Huang, HH. and Wang, SR. 2008. The effects of inverter magnetic fields on early seed germination of mung beans. Bioelectromagnetics. 29:649-657.

Jackson, A., Jonkers, ART. and Walker, MR. 2000. Four centuries of geomagnetic secular variation from historical records. Philosophical Transactions: Mathematical, Physical and Engineering Sciences. Geomagnetic Polarity Reversals and Long-Term Secular Variation. 358(1768):957-990.

Jansen, E., Overpeck, J., Briffa, KR., Duplessy, J.-C., Joos, F., Masson-Delmotte, V., D. Olago, D., Otto-Bliesner, B., Peltier, WR., Rahmstorf, S., Ramesh, R., Raynaud, D., Rind, D., Solomina, O., Villalba, R. and Zhang, D. 2007. Paleoclimate. In: Climate Change 2007: The Physical Science Basis. Contribution of Working Group I to the Fourth Assessment Report of the Intergovernmental Panel on Climate Change. Contribution of Working Group I to the Fourth Assessment Report of the Intergovernmental Panel on Climate Change. Eds. Solomon, S., Qin, D., Manning, M., Chen, Z., Marquis, M., Averyt, KB., Tignor, M. and Miller, HL. Cambridge University Press, Cambridge, United Kingdom and New York, NY, USA.

Keeling, CD. and Whorf, TP. 2004. Atmospheric CO_2 concentrations derived from flask air samples at sites in the SIO network. In Trends: A Compendium of Data on Global Change. Carbon Dioxide Information Analysis Center, Oak Ridge National Laboratory, US Department of Energy, Oak Ridge, Tennessee, USA, http://cdiac.esd.ornl.gov/.

Köhler, P., Muscheler, R., Richter, KU., Snowball, I. and Wolf-Gladrow, DA. 2009. Comment on "Magnetic effect on CO_2 solubility in seawater: A possible link between geomagnetic field variations and climate" by Alexander Pazur and Michael Winklhofer. Geophys. Res. Lett. 36:L03705.

MATLAB version R2008[b]. The Mathworks, Inc. 2008. Natick, Massachusetts, US.

Pales, J. C. and Keeling, CD. 1965. The concentration of atmospheric carbon dioxide in Hawaii. J. Geophys. Res. 70:6053-6076.

Pazur, A. and Winklhofer, M. 2008. Magnetic effect on CO_2 solubility in seawater: A possible link between geomagnetic field variations and climate. Geophys. Res. Lett. 35:L16710.

United States Geological Survey (USGS), National Geomagnetism Program. 2011. http://geomag.usgs.gov/

World Data Centre for Geomagnetism (Edinburgh). 2011. http://www.wdc.bgs.ac.uk/. Magnetic observatories used for this analysis were ABG, API, COI, OTT, SIT and VSS.

Yano, A., Ohashi, Y., Hirasaki, T. and Fujiwara, K. 2004. Effects of a 60 Hz magnetic field on photosynthetic CO_2 uptake and early growth of radish seedlings. Bioelectromagnetics. 25:572-581.

Canadian Journal of
pure & applied
sciences

SHORT COMMUNICATION

ANTI GRAVITY - IS IT ALREADY UNDER OUR NOSE?

C K Gamini Piyadasa
Department of Physics, University of Colombo, Colombo - 03, Sri Lanka

ABSTRACT

Particles which undergo a change of state or phase transition to gaseous form by acquiring latent heat have shown a movement against the gravitational field. In this regard, upward mobility of iodine molecules under different conditions and geometries has been studied. No adequate explanation to this observation can be given with conventional laws in physics and hence a novel way of thinking is needed to explicate the behavior.

Keywords: Gravity, anti-gravity, latent heat.

INTRODUCTION

Newton (1687) was the first to realize that the force of attraction, gravity is exerted by all objects in the universe. He then showed how these objects, small or big behave under gravity and came to the conclusion that any two objects in the Universe exert gravitational attraction on each other, with the force, $F_{gravity}$ having a universal form

$$F_{gravity} = G m_1 m_2 / r^2$$

where m_1 and m_2 are masses and r is the distance between two objects. The proportionality constant G is known as universal gravitational constant. The force acting between two particles in space in both electric (E) and magnetic (H) fields have the similar form of expression as the one describing the gravitational field. There is one fundamental difference existing in gravity compared to the electromagnetic field properties: there are two types of properties existing in both E and M fields, called positive and negative or north and south respectively. These entities (charge particles/magnetic poles) also behave in a similar manner: likes repel each other and unlikes attract each other; but such a dual property is not seen in gravity or in the other two fundamental forces of weak and strong interactions.

General relativity (Einstein, 1920) does not specifically recognize anti gravity as a concept. However, both general relativity and Newtonian gravity appear to predict that negative mass would produce a repulsive gravitational field. From the inception, several efforts have been underway in studying potential situations that subscribed to anti gravity type effects. From the past, scientists have been searching for a possible clue, hypothetically known as negative mass that would result

_____

Corresponding author email: gamini@phys.cmb.ac.lk

in anti gravity.

There have been several attempts at interpreting the cause of gravity (Einstein, 1916; Einstein, 1920; Hawking and Israel, 1989; flandern, 1996; Qyvind and Sigbjorn, 2007) but no successful attempt has yet been made to show the opposite, the existence of anti-gravity. The object of this paper is not an interpretation of anti gravity but to demonstrate an experiment that could provide some information about particle behavior against the gravitational pull when they undergo a change of state or phase transition to gaseous form by acquiring latent heat.

We generally observe that particles move against the direction of gravitational attraction such as water vapor rising to form clouds. Although Archimedes law can be conveniently used in explaining the buoyancy of water vapor, one could ask a plausible question as to whether the Archimedes principle could strictly govern the rising of water vapor or the motion against the gravitational field. Could this be due to the motion created by a repulsive force originating at the molecules with expense of its internal energy that absorbed at the change of phase as latent heat?

This experiment was designed in order to investigate the rising of particles of a similar situation as water vapor in air but having excluded factors which were are generally believed to be the reason for the upward movement of particles: viz – buoyancy and the convection lift.

EXPERIMENTAL

A layer of iodine (126.9 amu) was slowly heat-evaporated in a vacuum $\sim 10^{-5}$ mbar so that the evaporated iodine should be projected downwards. Then the pattern of iodine vapor deposited on a roll of paper surrounding the iodine source was observed (Fig. 1a,b).
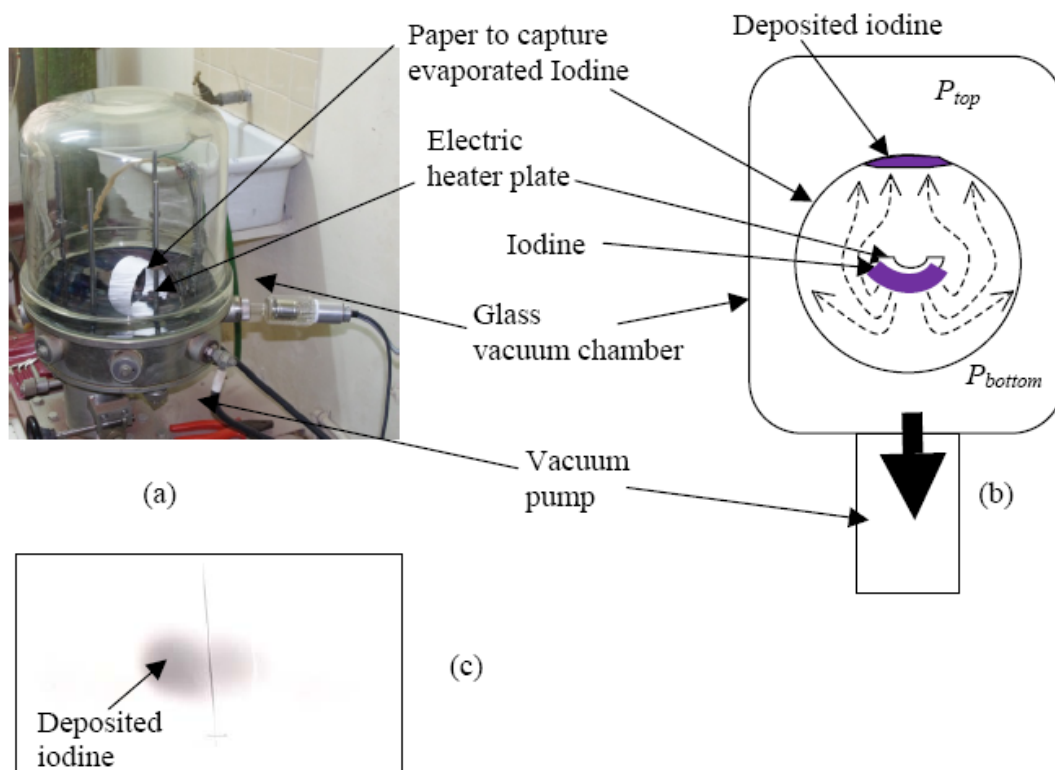
Fig. 1.   Experimental set-up to observe movement of heat-evaporated iodine vapor in vacuum. (a). Vacuum deposition chamber (b). A layer of iodine was slowly heat evaporated in downward direction inside the vacuum chamber. A paper was surrounded along the iodine source in order to capture the deposition geometry of iodine. The paper was placed 50 mm radially away from the iodine source. Pressure in the chamber was ~ 1×10^{-5} mbar, average mean free path of an air molecule is greater than 6.6 m and air density is approximately 12.6ng m^{-3}. Pressure at the top (P_{top}) of the chamber is higher than the bottom (P_{bottom}), $P_{top} > P_{bottom}$ (c) Photograph of deposited iodine on inner top part of the paper.

OBSERVATION

Though the vaporized iodine molecules were ejected downward with a certain initial kinetic energy, interestingly, it is found that the molecules have moved upward and deposited on top surface of the encircled paper (see Fig. 1b,c). We expect gravity to act on the molecules and pull them downwards (and not up), especially as the molecules are in a vacuum, which should make the molecules deposit themselves on the lower part of the encircled paper.   However, when rapid heating/evaporation of the iodine was attempted, a deposition of iodine on the lower part of the paper was observed. This could be explained by the fact that the blast heating results in a much higher kinetic energy/initial velocity of molecules and hence the downward projection and deposition.

The above experiment was performed under several geometries for further clarification.

Viz: Evaporation of iodine (a) projecting the vapor upward,   (b) projecting the vapor downward under atmospheric pressure,   (c) projecting vapor downward within a grounded mu-metal shield

However, the altered geometries did not affect the direction of the upward thrust (movement) of iodine molecules.

DISCUSSION

The buoyancy force causing the upward drift of iodine vapor has to be discarded due to: -
At the pressure 1×10^{-5}mbar, the system is in molecular flow region where Knudson number, Kn>1. At this region only gas – wall collisions dominate and molecules move independently of one another

The average mean free path of an air molecule (at 28^{0}C) is ~ 6.6 m and air density is approximately 12.6 ng m^{-3}; the probability of an air molecule encountering an iodine molecule is far remote. The density of iodine molecule
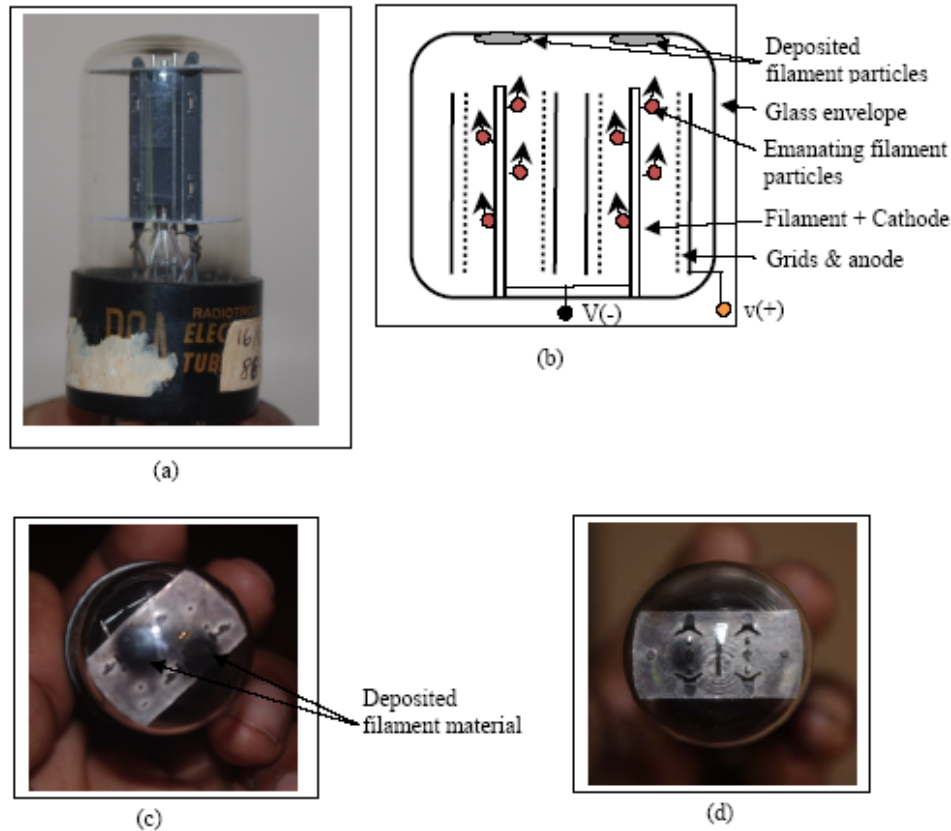
Fig. 2. Thermionic valve (a). Side view of an old thermionic valve 6SN7GTB Duo triode with two filaments (b) basic components and their placement inside the thermionic valve (c). Top view of the same old valve. The valve has been mounted in a tube audio amplifier (EICO Model HF 87) vertically as in Fig. a. It is clearly seen that thin two circular patches have been observed on top inside the glass body above the filaments. The valve was used from 26/01/71 to 16/01/88. (d) Top view of a similar type of valve. This valve is fairly new, it has only been used for several months. A mild deposit of filament material is seen on top of the left hand side filament.

(126.9 amu with atomic radius 1.4 Å) is greater than the density of average air molecule (28.57 amu with atomic radius ~1.5Å). Any lift force due to convection of moving air-molecules on iodine vapor too has to be discredited, due to the fact that no convection current could exist on such low-pressure air.

Pressure gradient ($P_{top} > P_{bottom}$) inside the vacuum chamber also doesn't support this upward movement because the vacuum pump is situated under the chamber and hence the lowest pressure occurs at the bottom as shown in figure 1.

We also considered the effect of ionization and space charge formation. These effects could be expected to have an influence on the net movement of iodine molecules due to the possible barrier formation. But such a barrier-effect could be ruled out as the upward mobility of iodine was observed in both geometries of upward and downwardly projected evaporation.

A thermionic valve (see Fig. 2a) in use affords us further evidence of molecules moving upward in a pressure around 10^{-7}mbar – 10^{-9}mbar. There are valves with clear glass tops in which the gutter (material which is used to keep the vacuum inside) is placed at the bottom. In such valves, when the valve is in use for a period of time, we could observe detached filament particles (Fonda, 1926) (usually tungsten/thorium, 183.84/232.04 amu respectively) on the upper region of the glass envelope (Figs. 2c and 2d). Convection currents cannot exist in such a low pressure and hence cannot be expected to carry the metal particles upward (Fig. 2b) in a valve filament placed in a vacuum. If such convection currents occur, the operation of the valve would be erratic due to the noise which is created by the bombardment of gas particles on electrodes. Furthermore the thin electron cloud surrounding the filament too cannot provide a buoyancy effect for the metal atom to move upwards. The electric field (Fig. 2b) existing between the filament and the other electrodes (anode) being perpendicular to the filament axis, cannot drift metal particles (even if the particles are

ionized) upwards. Hence the electric field is also not responsible for the observed effect.

It has to be emphasized that this upward mobility of particles against gravity has been observed by us only in situations (Figs. 1b and 2b) where a change of state of the particles or phase transition to gaseous form by acquiring heat of evaporation (latent heat) in question is involved.

CONCLUSION

Now that the buoyancy force and convection force are untenable, we have to speculate the driving force behind the upward movement of particles against the gravity under vacuum conditions.

Buoyancy force and convection force being ruled out the cause of the upward mobility in the particles observed strongly suggest an unknown force, it could be Antigravity: perhaps, an avenue for further research.

ACKNOWLEDGEMENT

REFERENCES

Einstein, A. 1916. The foundation of the General theory of relativity. Annalen der Physik. 49(7):769-822.

Einstein, A. 1920. Relativity: The Special and General Theory. H. Holt and Company, New York, USA. 74-83.

Fonda, RG. 1926. Evaporation of Tungsten under various pressure of Argon. Physical Review. 31:260-266.

Flandern, TV. 1996. Possible new properties of gravity. Astrophysics and Space Sci. 244:249-261.

Hawking, SW. and Israel, W. 1989. Three Hundred Years of Gravitation. Eds. Penrose, R., Cook, AH., Will, CM., Damour, T., Blandford, RD., Thorne, KS., Rees, MJ., Vilenkin, A., Blau, SK., Guth, AH., Linde, A., Schwartz, JH., Crnkowic, C. and Witten, E. Cambridge Univ. Press. 34-127.

Newton, I. 1687. Mathematical Principles of Natural Philosophy. pp. 177.

Øyvind, G. and Sigbjørn. H. 2007. Einstein's general theory of relativity: with modern applications in cosmology. Springer. 201-210.

SHORT COMMUNICATION

A POLYNOMIAL COLLOCATION METHOD FOR A CLASS OF NONLINEAR SINGULAR INTEGRAL EQUATIONS WITH A CARLEMAN SHIFT

Samah M Dardery
Mathematical Department, Faculty of Science
Zagazig University, Zagazig, Egypt

ABSTRACT

The paper is concerned with the applicability of the polynomial collocation method to a class of nonlinear singular integral equations with a Carleman shift preserving orientation on simple closed smooth Jordan curve in the generalized Holder space $H_\varphi(L)$. The method is illustrated by considering some simple examples.

INTRODUCTION

Nonlinear singular integral equations are widely used and connected with applications in several field of engineering mechanics like structural analysis, fluid mechanics and aerodynamics. This leads to the necessity to derive solutions for the nonlinear singular integral equations arising in applications, by using some approximate and constructive methods, (Ladopoulous, 2000). The theory of nonlinear singular integral equations with Hilbert and Cauchy kernel and its related Riemann-Hilbert problems have been developed in works of Pogorozelski (1966), Guseinov and Mukhtarove (1980), Wolfersdorf (1985) and Ladopoulous (2000).

The successful development of the theory of singular integral equations (SIE) naturally stimulated the study of singular integral equations with shift (SIES). The Noether theory of singular integral operators with shift (SIOS) is developed for a closed and open contour (Kravchenko and Lebre, 1995; Kravchenko and Litvinchuk; 1994). Existence results and approximate solutions have been studied for nonlinear singular integral equations (NSIE) and nonlinear singular integral equations with shift (NSIES) by many authors among them we mention (Amer and Dardery (2004, 2005, 2009), Amer and Nagdy (2000), Amer (2001, 1996), Jinyuan (2000), Junghanns and Weber (1993), Ladopoulous and Zisis (1996), Ladopoulous (2000), Nguyen (1989) and Saleh and Amer (1992).

The classical and more recent results on the solvability of NSIE should be generalized to corresponding equations

with shift (Wolfersdorf, 1992). The theory of SIES is an important part of integral equations because of its recent applications in many field of physics and engineering (Baturev *et al*., 1996; Kravchenko *et al*., 1995; Kravchenko and Litvinchuk, 1994).

We consider a simple closed smooth Jordan curve L in the complex plane with equation $t = t(s)$, $0 \le s \le l$ where s-arc coordinate accounts from some fixed point, l-length of the curve L. Denote by D^+ and D^- the interior and exterior domain of L respectively and let the origin be $0 \in D^+$. Denote by L_0 the unite circle with the center at the origin and let $L_0{}^+$ and $L_0{}^-$ the interior and exterior domain of L_0 respectively. Consider the conformal mappings $A(r)$ from $L_0{}^-$ onto D^- such that $A(\infty) = \infty$, $\lim_{r \to \infty} A(r) r^{-1} > 0$ and $B(r)$ from $L_0{}^-$ onto D^+ such that $B(\infty) = 0$.

Now, consider the following NSIES:

$$(P(u))(t) = \Psi_1(t, u(t)) + \Psi_2(\alpha(t), u(\alpha(t))) -$$
$$- \frac{1}{\pi i} \int_L \left[\frac{\Psi_3(\tau, u(\tau))}{\tau - t} + \frac{\Psi_4(\tau, u(\tau))}{\tau - \alpha(t)} \right]$$
$$d\tau = f(t), \quad \text{for all } t \in L \qquad (0.1)$$

Under the following conditions

*Corresponding author email: sd.1974@hotmail.com

$\psi_{1u}(t,u_o(t)) = \psi_{3u}(t,u_o(t)) = a(t)$,

$\psi_{2u}(\alpha(t),u_o(\alpha(t))) = -\psi_{4u}(\alpha(t),u_o(\alpha(t))) = b(t)$.   (0.2)

for initial value u_0, in the generalized Holder space $H_\varphi(L)$, $u(t)$ is unknown function, $f(t)$ and $\Psi_r(t,u(t))$, $r = 1,...,4$, are continuous functions on L and on the domain

$$D = \{(t,u): t \in L, u \in (-\infty,\infty)\},$$

respectively, and the homeomorphism $\alpha: L \to L$ is preserving orientation, satisfying the Carleman condition

$$\alpha(\alpha(t)) = \alpha_2(t) = t, \quad t \in L,   (0.3)$$

and the derivative $\alpha'(t) \neq 0$ satisfies the usual Holder condition.

The equation (0.1) in case $f(t) = 0$ without shift has been studied in Amer and Nagdy (2002) by modified Newton-Kantorovich method in the generalized Holder space $H_{\varphi,m}[a,b]$.

In this paper the polynomial collocation method has been applied to NSIES (0.1) under condition (0.2), with zero index, in the generalized Holder space $H_\varphi(L)$.

1. Some auxiliary results.

Definition 1.1. We denote by $H_{\varphi,1}(D)$ to be the space of all functions $\Psi_r(t,u(t))$, $r = 1,...,4$, which have partial derivatives up to second order with respect to u and satisfy the following condition

$$\left|\psi_{ru^j}(t_1,u_1) - \psi_{ru^j}(t_2,u_2)\right| \le c_j^r \{\varphi(|t_1 - t_2|) + |u_1 - u_2|\}$$
,   (1.1)

where $(t_i,u_i) \in D$, $i = 1,2$, $\varphi \in \Phi$ and c_j^r are constants; $j = 0,1,2$.

Definition 1.2 (Guseinov and Mukhtarov, 1980; Mikhlin and Prossdorf, 1986). We denote by $c(L)$ the space of all continuous functions $u(t)$ defined on L with the norm:

$$\|u\|_{c(L)} = \max_{t \in L} |u(t)| .   (1.2)$$

Definition 1.3 (Amer, 2001; Guseinov and Mukhtarov, 1980). We denote by $H_\varphi(L)$ the space of all functions

$u(t) \in c(L)$ such that $\omega_u(\delta) = o(\varphi(\delta))$, $\varphi \in H\Phi$, with the norm:

$$\|u\|_\varphi = \|u\|_{c(L)} + \|u\| ;   (1.3)$$

$$\|u\| = \sup_{\delta > 0} \frac{\omega_u(\delta)}{\varphi(\delta)} ;$$

$$H\Phi = \left\{\varphi \in \Phi : \int_0^\delta \frac{\varphi(\xi)}{\xi} d\xi + \delta \int_\delta^l \frac{\varphi(\xi)}{\xi^2} d\xi \le \tilde{c}\, \varphi(\delta)\right\},$$

$\tilde{c}$ is a positive constant.

Definition 1.4 (Amer, 2001; Kravchenko and Litvinchuk, 1994). Let $S : H_\varphi(L) \to H_\varphi(L)$ denotes to the operator of singular integration

$$(Su)(t) = \frac{1}{\pi i} \int_L \frac{u(\tau)}{\tau - t} d\tau ,   (1.4)$$

to which we associate the Cauchy projection operators

$$P_\pm = \frac{1}{2}(I \pm S), \quad S^2 = I ,   (1.5)$$

where I is the identity operator on $H_\varphi(L)$. The Carleman shift operator

$W : H_\varphi(L) \to H_\varphi(L)$, is given by $(Wv)(t) = v(\alpha(t))$.

Lemma 1.1 (Amer, 2001). The singular operator S is a bounded operator on the space $H_\varphi(L)$ and satisfies the inequality

$$\|Su\|_\varphi \le \rho_0 \|u\|_\varphi,   (1.6)$$

where ρ_0 is a constant defined as follows :

$$\rho_0 = c_1 \left(\int_0^\delta \frac{\varphi(\xi)}{\xi} d\xi + 1\right) + c_2 \tilde{c} ,$$

where c_1, c_2, $\tilde{c}$ are constants.

Lemma 1.2 (Amer, 2001). The shift operator W is a linear bounded continuously invertible operator on the space $H_\varphi(L)$ and satisfies the inequality

$$\|Wu\|_\varphi \le \gamma_0 \|u\|_\varphi ,   (1.7)$$

where $\gamma_0 = \max\{1,\alpha_0\}$ and α_0 is a constant given by

$$\alpha_0 = \sup_{\delta\phi 0} \frac{\omega_{\tilde{u}}(\delta)}{\omega_u(\delta)}, \quad \tilde{u}(t) = u(\alpha(t)).$$

Lemma 1.3 (Amer and Dardery, 2009) Let the functions $\psi_r(t,u)$, $r = 1,...,4$, belong to $H_{\varphi,1}(D)$. Then the

operator $P(u)$ is Frechet differentiable at every fixed point $u \in H_\varphi(L)$, moreover

$$P^{'}(u)h = \psi_{1u}(t,u(t))h(t) + \psi_{2u}(\alpha(t),u(\alpha(t)))h(\alpha(t)) -$$
$$-\frac{1}{\pi i}\int_L\left\{\frac{\psi_{3u}(\tau,u(\tau))}{\tau - t} + \frac{\psi_{4u}(\tau,u(\tau))}{\tau - \alpha(t)}\right\}h(\tau)\,d\tau, \qquad (1.8)$$

satisfies Lipschitz condition

$$\left\|P^{'}(u_1) - P^{'}(u_2)\right\|_\varphi \le \rho_1\left\|u_1 - u_2\right\|_\varphi, \qquad (1.9)$$

in the sphere $S_\varphi(u_0,r) = \left\{u \in H_\varphi(L): \left\|u - u_0\right\|_\varphi \le r\right\}$,

where

$$\rho_1 = \left(c_1^1 + \gamma_0 c_1^2 + \rho_0 c_1^3 + \gamma_0\rho_0 c_1^4\right).$$

Under condition (0.2), the equation (1.8) reduces to the following SIES, for the unknown function $h(t)$:

$$\Gamma_0 h = a(t)h(t) + b(t)h(\alpha(t)) - \frac{a(t)}{\pi i}\int_L\frac{h(\tau)}{\tau - t}d\tau +$$
$$+\frac{b(t)}{\pi i}\int_L\frac{h(\tau)}{\tau - \alpha(t)}d\tau + \frac{1}{\pi i}\int_L R(t,\tau)h(\tau)\,d\tau = f(t), \qquad (1.10)$$

for initial value u_o and the arbitrary function $f(t)$ belong to the space $H_\varphi(L)$,

where

$$R(t,\tau) = \frac{\psi_{3u}(t,u_o(t)) - \psi_{3u}(\tau,u_o(\tau))}{\tau - t}$$
$$+\frac{\psi_{4u}(\alpha(t),u_o(\alpha(t))) - \psi_{4u}(\tau,u_o(\tau))}{\tau - \alpha(t)}.$$

Using Definition 1.4 the dominant equation of equation (1.10) reduces to the following singular integral operator with shift :

$$M = 2a(t)P_- + 2b(t)WP_+. \qquad (1.11)$$

Theorem 1.1 (Amer and Dardery, 2009; Kravchenko and Litvinchuk, 1994). The singular integral functional operator M is Noetherian on $H_\varphi(L)$ if and only if

$$\inf|e(t)| > 0 \ and \ q(t) \ne 0, \ on\, L,$$

where

$$e(t) = 2b(t), q(t) = \frac{a(t)}{b(t)}; b(t) \ne 0 \ on\, L.$$

The index of a Noetherian operator M is given by

$$\chi = ind\, M = \frac{1}{2\pi}\{\arg q(t)\}_L. \qquad (1.12)$$

Theorem 1.2 (Amer 2001; Saleh and Amer, 1992). Let the conditions of Lemma 1.3 and Theorem 1.1 be satisfied

and $u_0 \in H_\varphi(L)$ is the initial approximation for equation (0.1) under conditions (0.2), $\left\|(P'(u_0))^{-1}\right\|_\varphi \le \varepsilon_0$ and $\left\|(P'(u_0))^{-1}P(u_0)\right\|_\varphi \le \varepsilon_1$. Then if $m = \varepsilon_0\rho_1\varepsilon_1 < \frac{1}{2}$, then equation (0.1) under conditions (0.2) has a unique solution u^* in the sphere $S_\varphi(u_0;r_0)$ of the space $H_\varphi(L)$, $r_0 = \varepsilon_1\left(1 - \sqrt{1 - 2m}\right)m^{-1} \le r$, to which the successive approximations: $u_{n+1} = u_n - (P'(u_0))^{-1}P(u_n)$ of modified Newton method converges and the rate of convergence is given by the inequality:

$$\left\|u_n - u^*\right\|_\varphi \le \frac{B^n}{1 - B}\varepsilon_1; \ B = 1 - \sqrt{1 - 2m}$$

2. Collocation method.

Now, we seek an approximate solution of equation (0.1) under conditions (0.2) in $H_\varphi(L)$ as the form:

$$u_n(\eta,t) = \sum_{k=-n}^{n}\eta_k t^k, \qquad (2.1)$$

where the coefficients η_k are defined from the system of nonlinear algebraic equation with shift (SNAES)

$$\Psi_1(t_j, u_n(\eta, t_j)) + \Psi_2(\alpha(t_j), u_n(\eta, \alpha(t_j)))$$
$$-\frac{1}{\pi i}\int_L\left[\frac{\Psi_3(\tau, u_n(\eta, \tau))}{\tau - t_j} + \frac{\Psi_4(\tau, u_n(\eta, \tau))}{\tau - \alpha(t_j)}\right]d\tau = f(t_j) \qquad (2.2)$$

where $t_j = \exp(2\pi i j/(2n+1))$, $j = \overline{0,2n}$.

Consider $(2n+1)$- dimensional spaces $H_\varphi^{(1)}$ and $H_\varphi^{(2)}$ with the norms:

$$\left\|\eta\right\|_\varphi^{(1)} = \left\|u_n(\eta,.)\right\|_\varphi,$$
$$\left\|u\right\|_\varphi^{(2)} = \max_j|u_j| + \sup_{j \ne k}\frac{|u_j - u_k|}{\varphi(|t_j - t_k|)},$$

respectively, where $\eta = (\eta_{-n},...,\eta_{-1},\eta_0,...,\eta_n) \in H_\varphi^{(1)}$ and $u = (u_0,...,u_{2n}) \in H_\varphi^{(2)}$.

Introduce the operator $P_n(\eta): H_\varphi^{(1)} \to H_\varphi^{(2)}$ where

$$P_{j,n}(\eta) = \Psi_1(t_j, u_n(\eta, t_j)) + \Psi_2(\alpha(t_j), u_n(\eta, \alpha(t_j)))$$
$$-\frac{1}{\pi i}\int_L\left[\frac{\Psi_3(\tau, u_n(\eta, \tau))}{\tau - t_j} + \frac{\Psi_4(\tau, u_n(\eta, \tau))}{\tau - \alpha(t_j)}\right]d\tau, \quad j = \overline{0,2n}$$

We can rewrite SNAES (2.2) in the operator form:

$$P_n(\eta) = f; \ f = f(t_j), \ j = \overline{0,2n}. \qquad (2.3)$$

Consider, the coordinates of the vector $\eta^{(0)}$ from $H_\varphi^{(1)}$ these are the Fourier coefficients of the function $u_0 \in H_\varphi(L)$ that is

$$\eta_j^{(0)} = \frac{1}{2\pi i} \int_{L_0} u_0(B(w))w^{-j-1}dw, \quad j = \overline{0, n} \qquad \text{and}$$

$$\eta_j^{(0)} = \frac{1}{2\pi i} \int_{L_0} u_0(A(w))w^{-j-1}dw, \quad j = \overline{-n, -1}.$$

Analogous to Lemma 1.3 the following lemma is valid.

Lemma 2.1. Amer (1996) Let the conditions of Lemma 1.3 be satisfied. Then the operator P_n is Frechet differentiable at every fixed point $x = (\eta_{-n}, ..., \eta_n) \in H_\varphi^{(1)}$, Moreover

$$P'_{j,n}(x)h = \psi_{1u}(t_j, u_n(x, t_j))u_n(h, t_j)$$
$$+\psi_{2u}(\alpha(t_j), u_n(x, \alpha(t_j)))u_n(h, \alpha(t_j)) -$$
$$-\frac{1}{\pi i}\int_L \left\{ \frac{\psi_{3u_n}(\tau, u_n(x,\tau))}{\tau - t_j} + \frac{\psi_{4u_n}(\tau, u_n(x,\tau))}{\tau - \alpha(t_j)} \right\} u_n(h, \tau)\, d\tau, \quad j = \overline{0, 2n}.$$

where $h = (h_{-n}, ..., h_n) \in H_\varphi^{(1)}$, the derivative $P'_n(x) = (P'_{0,n}(x), ..., P'_{2n,n}(x))$ satisfies Lipschitz condition

$$\left\| P'_n(x_1) - P'_n(x_2) \right\|_{H_\varphi^{(2)}} \le \rho'_1 \left\| x_1 - x_2 \right\|_{H_\varphi^{(1)}},$$

in the sphere $S(\eta^{(0)}; r_1)$ of the space $H_\varphi^{(1)}$, where ρ'_1 is a positive constant.

Now, we show that the system of linear algebraic equations with shift (SLAES):

$$P'_n(\eta^{(0)})h = g, \qquad (2.4)$$

under the conditions

$$\psi_{1u}(t_j, u_o(\eta^{(0)}, t_j)) = \psi_{3u}(t_j, u_o(\eta^{(0)}, t_j)) = a(t_j), \quad (2.5)$$
$$\psi_{2u}(\alpha(t_j), u_o(\eta^{(0)}, \alpha(t_j))) =$$
$$-\psi_{4u}(\alpha(t_j), u_o(\eta^{(0)}, \alpha(t_j))) = b(t_j).$$

has a unique solution $h \in H_\varphi^{(1)}$ for arbitrary $g = (g_0, ..., g_{2n}) \in H_\varphi^{(2)}$.

For this aim, we consider the SALES:

$$a(t_j)u_n(h, t_j) + b(t_j)u_n(h, \alpha(t_j))\tau -$$
$$-\frac{a(t_j)}{\pi i} \int_L \frac{u_n(h, \tau)}{\tau - t_j}\, d\tau + \frac{b(t_j)}{\pi i} \int_L \frac{u_n(h, \tau)}{\tau - \alpha(t_j)}\, d\tau +$$

$$+\frac{1}{\pi i} \int_L R(t_j, \tau)u_n(h, \tau)\, d\tau = g(t_j), \quad j = \overline{0, 2n} \qquad (2.6)$$

corresponding to the SIES:

$$a(t)u(t) + b(t)u(\alpha(t)) - \frac{a(t)}{\pi i} \int_L \frac{u(\tau)}{\tau - t}\, d\tau + \frac{b(t)}{\pi i} \int_L \frac{u(\tau)}{\tau - \alpha(t)}\, d\tau +$$

$$+\frac{1}{\pi i} \int_L R(t, \tau)u(\tau)\, d\tau = g(t), \quad (2.7)$$

According to the collocation method, we seek an approximate solution of equation (1.10) as the form :

$$h_n(t) = \sum_{k=-n}^{n} \beta_k t^k, \quad t \in L, \qquad (2.8)$$

where the coefficients β_k are defined from SLAES:

$$\sum_{k=-n}^{n} A_{jk} \beta_k = g(t_j), \quad j = \overline{0, 2n} \qquad (2.9)$$

where

$$A_{jk} = a(t_j)\left(t_j^k - \frac{1}{\pi i} \int_L \frac{\tau^k}{\tau - t_j}\, d\tau \right) + b(t_j)$$
$$\left((\alpha(t_j))^k + \frac{1}{\pi i} \int_L \frac{\tau^k}{\tau - \alpha(t_j)}\, d\tau \right) + \frac{1}{\pi i} \int_L R(t_j, \tau)h_n(\tau)d\tau$$

The SLAES (2.9) can be rewritten as following form:

$$2a(t_j)\sum_{k=-n}^{-1} \beta_k t_j^k + 2b(t_j)\sum_{k=0}^{n} \beta_k (\alpha(t_j))^k + \frac{1}{\pi i} \int_L R(t_j, \tau)$$
$$\sum_{k=-n}^{n} \beta_k \tau^k d\tau = g(t_j), \quad j = \overline{0, 2n}. \qquad (2.10)$$

Where

$$h_n^+(t) = \sum_{k=0}^{n} \beta_k t^k, \quad h_n^-(t) = -\sum_{k=-n}^{-1} \beta_k t^k,$$

Theorem 2.1. Let $a(t), b(t)$ and $g(t)$ belong to $H_\varphi(L)$, $b(t) \ne 0$ on L, the index $\chi = 0$ and the operator P' has a linear inverse in $H_\varphi(L)$, then for all $n \ge \max(n_0, \chi)$,

$$n_0 = \min\left\{ n \in N : d_1 \varphi\left(\frac{1}{n}\right) \ln n < 1 \right\}, \quad \text{the system}$$

(2.10) has the unique solution $\{\beta_k^*\}_{-n}^{n}$ and the approximate solution $, h_n^*(t) = \sum_{k=-n}^{n} \beta_k^* t^k,$ of equation

(1.10) convergences to its exact solution h^*, moreover

$$\left\| h^*(t) - h_n^*(t) \right\|_\varphi \le d_2 \varphi\left(\frac{1}{n}\right) \ln n ,$$

where d_1 and d_2 are constants do not depend on n.

Proof.

From [Gakhov, 1966], we can write equation (1.10) in the following form:

$$h^+(\alpha(t)) - q(t)h^-(t) + \frac{1}{e(t)\pi i}\int_L R(t,\tau)h(\tau)d\tau = \frac{g(t)}{e(t)},$$

setting

$$q(t) = \frac{\psi^+(\alpha(t))}{\psi^-(t)}.$$

Then we have

$$\Gamma h = Bh + Gh = \tilde{g} . \tag{2.11}$$

Where

$$(Bh)(t) = \psi^-(t)h^+(\alpha(t)) - \psi^+(\alpha(t))h^-(t) ,$$

$$(Gh)(t) = \frac{c(t)}{\pi i}\int_L R(t,\tau)h(\tau)d\tau ,$$

$$\tilde{g}(t) = g(t)c(t), \quad c(t) = \frac{\psi^-(t)}{e(t)},$$

$$\psi(z) = \exp(\theta(z)), \tag{2.12}$$

$$\theta(z) = \frac{1}{\pi i}\int_L \frac{\rho(\gamma(\tau))}{\tau - z}d\tau; \ z \in D^+,$$

$$\theta(z) = \frac{1}{\pi i}\int_L \frac{\rho(\tau)}{\tau - z}d\tau; \ z \in D^- ,$$

where $\gamma(t)$ is the inverse $\alpha(t)$ and $\rho(t)$ is a solution of the Fredholm integral equation of second kind

$$\rho(t) + \frac{1}{\pi i}\int_L \left(\frac{\alpha'(\tau)}{\alpha(\tau) - \alpha(t)} - \frac{1}{\tau - t}\right)\rho(\tau)d\tau = \ln q(t).$$

Moreover, B is linear and G is completely continuous from $H_\varphi(L)$ into itself.

Denote by X_n to be the (2n+1)- dimensional subspace of the space $H_\varphi(L)$, and let Q_n be the projection operator into the set of interpolation polynomial of degree n with respect to the collocation points t_j, $j = \overline{0,2n}$. Then the system (2.10) can be written in X_n as a linear operator

$$\Gamma_n h_n = B_n h_n + G_n h_n = \tilde{g}_n , \tag{2.13}$$

where

$$B_n h_n = Q_n B h_n ,$$

$$G_n h_n = Q_n G h_n, \quad \tilde{g}_n = Q_n \tilde{g} .$$

Now, we determine the difference $\Gamma h_n - \Gamma_n h_n \in X_n$, from (2.11), (2.13) we have

$$(\Gamma - \Gamma_n)h_n(t) = (I - Q_n)[(\psi^-(t) - \psi_n^-(t))h_n^+(\alpha(t)) - (\psi^+(\alpha(t)) - \psi_n^+(\alpha(t)))h_n^-(t)] + (G - G_n)h_n(t) \tag{2.14}$$

where ψ_n is polynomial of the best uniform approximation of the function ψ with degree not exceeding n.

From [Amer, 1996, Gakhov, 1966] and inequality (1.7), we have

$$\left\| h_n^\pm \right\|_\varphi \le d_1 \left\| h_n \right\|_\varphi$$

$$\left\| (\psi^-(t) - \psi_n^-(t))h_n^+(\alpha(t)) - (\psi^+(\alpha(t)) - \psi_n^+(\alpha(t)))h_n^-(t) \right\|_\varphi \le \gamma_0 d_2 \varphi\left(\frac{1}{n}\right)\left\| h(t) \right\|_\varphi ,$$

and

$$\left\| Q_n \right\|_\varphi \le d_3 \ln n .$$

Hence, we get

$$\left\| (I - Q_n)[(\psi^-(t) - \psi_n^-(t))h_n^+(\alpha(t)) - (\psi^+(\alpha(t)) - \psi_n^+(\alpha(t)))h_n^-(t)] \right\|_\varphi \le d_4 \varphi\left(\frac{1}{n}\right)(\ln n)\left\| h_n(t) \right\|_\varphi \tag{2.15}$$

where $d_4 = \gamma_0 d_2 d_3$.

Let $J_n(t)$ be the polynomial of best uniform approximation to the function

$$J(t) = \frac{c(t)}{\pi i}\int_L R(t,\tau)h_n(\tau)d\tau ,$$

Then from Amer (1996), we have

$$\left\| J - J_n \right\|_\varphi \le d_5 \varphi\left(\frac{1}{n}\right)\left\| h_n \right\|_\varphi ,$$

hence for arbitrary $h_n \in X_n$, we get

$$\left\| Gh_n - G_n h_n \right\|_\varphi \le d_6 \varphi\left(\frac{1}{n}\right)(\ln n)\left\| h_n \right\|_\varphi , \tag{2.16}$$

where $d_6 \ln n = d_5 + d_3 d_5 \ln n$. From (2.14)- (2.16), we get

$$\left\| \Gamma h_n - \Gamma_n h_n \right\|_\varphi \le d_7 \varphi\left(\frac{1}{n}\right)(\ln n)\left\| h_n \right\|_\varphi , \tag{2.17}$$

where $d_7 = d_4 + d_6$. From Theorem 1.2 , the operator Γ_0 has a linear bounded inverse operator Γ_0^{-1} , since $\Gamma_0 h = c^{-1}\Gamma h$ then the operator Γ has a linear inverse,

also from Amer (1996) and by virtue of (2.17) the operator Γ_n has a linear bounded inverse.

Now, for the right parts of (2.11) and (2.13), we have

$$\left\| \tilde{g} - \tilde{g}_n \right\|_\varphi \le d_8 \varphi\left(\frac{1}{n}\right) \ln n. \qquad (2.18)$$

From Amer (1996), and inequalities (2.17), (2.18) for the solution h^* of equation (1.10) and the approximate solution h_n^*, we obtain

$$\left\| h^* - h_n^* \right\|_\varphi \le d_9 \varphi\left(\frac{1}{n}\right) \ln n .$$

Thus the theorem is proved.

From Theorem 2.1 there exists the number n_0 such that for arbitrary $n \ge \max(n_0, \chi)$ the SLAES (2.6) has the unique solution h^* and the following inequality is valid:

$$\left\| u_n^*(h^*,.) - u^*(.) \right\|_\varphi \le d_{10} \varphi\left(\frac{1}{n}\right) \ln n \quad ,$$

where $u^* \in H_\varphi(L)$ is the unique solution of (2.7). Let

$$\Gamma_n(u_0)h = \left(\Gamma_{0,n}(u_0)h, ..., \Gamma_{2n,n}(u_0)h\right)$$

where

$$\Gamma_{n,j}(u_0)h = a(t_j)u_n(h,t_j) + b(t_j)u_n(h,\alpha(t_j)) - \frac{a(t_j)}{\pi i}\int_L \frac{u_n(h,\tau)}{\tau - t_j}d\tau +$$
$$+ \frac{b(t_j)}{\pi i}\int_L \frac{u_n(h,\tau)}{\tau - \alpha(t_j)}d\tau + \frac{1}{\pi i}\int_L R(t_j,\tau)u_n(h,\tau)\,d\tau, \quad j = \overline{0,2n}$$

From Amer (1996), we have

$$\left\| \Gamma_n(u_0) - P_n'(\eta^{(0)}) \right\|_{H_\varphi^{(1)} \to H_\varphi^{(2)}} \le d_{11} \varphi\left(\frac{1}{n}\right) \ln n . \quad (2.19)$$

Since for arbitrary $n \ge (n_0, \chi)$, there exists a bounded linear inverse operator, $\Gamma_n^{-1} : H_\varphi^{(2)} \to H_\varphi^{(1)}$ then from (2.19), Banach theorem follows that there exists $n_1 \ge (n_0, \chi)$ such that for arbitrary $n \ge n_1$, the linear operator $P_{j,n}'$ has bounded inverse, that is the SLAES (2.4) under condition (2.5) has the unique solution $h^* \in H_\varphi^{(1)}$ for arbitrary right side $g = g(t_j) \in H_\varphi^{(2)}$, $j = \overline{0,2n}$. Thus the following theorem is proved.

Theorem 2.2 Let the coordinate of the vector $\eta^{(0)} = \left(\eta_{-n}^{(0)}, ..., \eta_{-1}^{(0)}, \eta_0^{(0)}, ..., \eta_n^{(0)}\right)$ be the Fourier coefficients the function $u_0 \in H_\varphi(L)$ and the conditions of Theorem 1.2 are satisfied and for $n \ge n_1$,

$$\left\| \left(P_n'(\eta^{(0)})\right)^{-1} \right\|_\varphi \le \varepsilon_0' \text{ and }$$

$$\left\| \left(P_n'(\eta^{(0)})\right)^{-1} P_n(\eta^{(0)}) \right\|_\varphi \le \varepsilon_1' . \text{ Then if}$$

$m' = \varepsilon_0' \rho_1' \varepsilon_1' < \frac{1}{2}$, then SNAES (2.3) has the unique solution $\eta^* = \left(\eta_{-n}^*, ..., \eta_{-1}^*, \eta_0^*, ..., \eta_n^*\right)$ in the sphere $S_\varphi(\eta^{(0)}; r_0')$ of the space $H_\varphi(L)$,

$r_0' = \varepsilon_1'\left(1 - \sqrt{1 - 2m'}\right)(m')^{-1} \le r'$, to which the following iteration process converges

$$\eta^{(m+1)} = \eta^{(m)} - \left(P_n'(\eta^{(0)})\right)^{-1} P_n(\eta^{(m)}) \text{ and the rate of}$$

convergence is given by the inequality:

$$\left\| \eta^{(m)} - \eta^* \right\|_\varphi \le \frac{B_1^n}{1 - B_1} \varepsilon_1'; \; B_1 = 1 - \sqrt{1 - 2m'} .$$

3. Illustrative examples

We illustrate the above method by some problems.

Example 1.

Consider the following integral equation

$$t^2 h(t) - -\frac{1}{\pi i}\int_L \frac{h(\tau)}{\tau - t}d\tau = t^3 + t \qquad (3.1)$$

Where the contour L is a unit circle in the complex plane.

It is easy to find that the index of equation (3.1) equal to zero and the exact solution takes the form $h(t) = t$.

According to the collocation method the approximate solution of equation (3.1) takes the form (2.8), where the coefficients β_k are defined from SLAE

$$\left(a(t_j) + b(t_j)\right)\sum_{k=0}^{n} \beta_k t_j^k + \left(a(t_j) - b(t_j)\right)\sum_{k=-n}^{-1} \beta_k t_j^k = g(t_j), \; j = \overline{0,2n},$$
$$(3.2)$$

where

$$t_j = \exp(2\pi i j /(2n+1)), \; a(t_j) = t_j^2, \; b(t_j) = -1, \; g(t_j) = t_j^3 + t_j$$
$$(3.3)$$

From relation (3.3) we get

$$\left(t_j^2 - 1\right)\sum_{k=0}^{n} \beta_k t_j^k + \left(t_j^2 + 1\right)\sum_{k=-n}^{-1} \beta_k t_j^k = t_j^3 + t_j, \quad j = \overline{0,2n}$$
$$(3.4)$$

By solving SLAE (3.4) we found the approximate solution takes the form $h_n(t) = t$ for $n \ge 2$.

Example 2.

Consider the following integral equation

$$t\,h(t) - \frac{(t-2)}{\pi i}\int_L \frac{h(\tau)}{\tau - t}\,d\tau = 2\left(t^2 - 1\right) \qquad (3.5)$$

where the contour L is the circle $|z| = 1/2$ in the complex plane.

It is easy to find that the index of equation (3.5) equal to zero and the exact solution takes the form $h(t) = t^2 - 1$. According to the collocation method the approximate solution of equation (3.1) takes the form (2.8), where the coefficients β_k are defined from SLAE (3.2);

$$a(t_j) = t_j, \quad b(t_j) = 2 - t_j, \quad g(t_j) = 2\left(t_j^2 - 1\right) \quad (3.6)$$

From relation (3.6) we get

$$\sum_{k=0}^{n}\beta_k t_j^k + \left(t_j - 1\right)\sum_{k=-n}^{-1}\beta_k t_j^k = t_j^2 - 1, \quad j = \overline{0,2n} \qquad (3.7)$$

By solving SLAE (3.7) we found the approximate solution coincides with the exact solution for $n \geq 2$.

REFERENCES

Amer, SM. and Dardery, S. 2009. The method of Kantorovich majorants to nonlinear singular integral equation with shift. Appl. Math. and Comp. 215:2799-2805.

Amer, SM. and Dardery, S. 2005. On the theory of nonlinear singular integral equations with shift in Holder spaces. Forum Math. 17:753-780.

Amer, SM. and Dardery, S. 2004. On a class of nonlinear singular integral equations with shift on a closed contour. Appl. Math. and Comp. 158:781-791.

Amer, SM. and Nagdy, AS. 2002 On the modified Newton's approximation method for the solution of nonlinear singular integral equations. Hokkaido Mathematical Journal. 29:59-72.

Amer, SM. 2001. On solution of nonlinear singular integral equations with shift in generalized Holder space. Chaos, Solitons and Fractals. 12:1323-1334.

Amer, SM. 1996. On the approximate solution of nonlinear singular integral equations with positive index. Int. J. Math. Math. Sci. 19 (2):389-396.

Baturev, AA., Kravchenko, VG. and Litvinchuk, GS. 1996. Approximate Method for Singular Integral Equation with a non-Carleman shift. Integral Equation App. 8:1-17.

Gakhov, FD. 1966. Boundary Value Problems. Pergamon Press Ltd. 121-138.

Guseinov, AI. and Mukhtarov, KS. 1980. Introduction to the theory of nonlinear Singular integral equations. (in Russian), Nauka Moscow, Russian. 5-55.

Jinyuan, D. 2000. The collocation methods and singular integral equations with Cauchy kernel. Acta Math. Sci. 20 (B3):289-302.

Junghanns, P. and Weber, U. 1993. On the solvability of nonlinear singular integral equations. ZAA. 12:683-698.

Kravchenko, VG., Lebre, AB., Litvinchuk, GS. and Texeira FS. 1995. Fredholm theory for a class of singular integral operators with Carleman shift and unbounded coefficients. Math. Nach. 172:199-210.

Kravchenko, VG. and Litvinchuk, GS. 1994. Introduction to the Theory of Singular Integral Operators with Shift. Kluwer Academic Publishers, London, UK. 60-73.

Ladopoulous, EG. and Zisis, VA. 1996. Nonlinear singular integral approximations in Banach spaces. Nonlinear Analysis, Theary, Methods Appl. 26(7):1293-1299.

Ladopoulous, EG. 2000. Singular integral equations linear and nonlinear theory and its applications in science and engineering. Springer, New York, USA. 409-528.

Mikhlin, SG. and Prossdorf, S. 1986. Singular integral operator; Academy-Verleg, Berlin, Germany. pp 66.

Nguyen, DT. 1989. On a class of nonlinear singular integral equations with shift on complex curves. Acta Math. Vietnam. 14 (2):75-92.

Pogorzelski, W. 1966. Integral equations and their applications. (vol. 1), Oxford Pergamon Press and Warszawa, PWN. pp 591.

Saleh, MH. and Amer, SM. 1992. On a class of nonlinear singular integral equations with Cauchy kernel. AMSE Review. 22(1):15-26.

Wolfersdorf, LV. 1992. On the theory of nonlinear singular integral equations; TU Bergakde-min Freiberg, Fakultat fur Mathematik und Informatik; lecture presented on the international symposium "Operator Equations and Numerical Analysis", September 28-October 2, 342-355.

Wolfersdorf LV. 1985. On the theory of nonlinear singular integral equations of Cauchy type. Math. Meth. In the Appl. Sci. 7:493-517.